NASA CR-66732-II

31 JANUARY 1969

MARS SPINNING SUPPORT MODULE STUDY

BY J. J. RIBARICH,
PROJECT MANAGER
SYSTEMS LABORATORIES

VOLUME II
ANALYSIS

PREPARED UNDER CONTRACT NAS 1-8638 BY
HUGHES AIRCRAFT COMPANY,
AEROSPACE GROUP
SPACE SYSTEMS DIVISION
EL SEGUNDO, CALIFORNIA, 90009
FOR
NATIONAL AERONAUTICS AND SPACE ADMINISTRATION—
WASHINGTON, D.C.

CONTENTS

ILLUSTRATIONS

TABLES

1. INTRODUCTION

The Mars Spinning Support Module (MSSM) Study conducted by the Hughes Aircraft Company Space System Division for the National Aeronautics and Space Administration's Langley Research Center (NASA/LRC) is summarized in Volume I of this final report. The background information and analysis that the study results are based on is presented in this document, Volume II. Volume III presents program planning and cost estimates for a MSSM 1973 Program. The three volumes satisfy the requirement for a MSSM study final report.

The MSSM study was conducted in three phases during a 2-month period. A brief phase I effort resulted in the selection of a support module (SM) - aeroshell/lander (A/L) concept wherein the total spacecraft spin axis is approximately in the ecliptic plane while en route to Mars in 1973-74. The SM is separated from the A/L near Mars and relays entry data to earth from the A/L during the descent phase (Flyby - Entry Data design). This concept was selected because of its advantages of light weight and simplicity over alternate concepts with spin axis orientations normal to the ecliptic plane. The phase II effort provided a detailed analysis of the Flyby - Entry Data design, including configuration drawings, detailed weight statement, subsystem/component definition, hardware status, and trajectory control accuracy.

The phase III effort produced a modified phase II SM concept which has the added capability to relay lander video data during its post-landing flyby phase (Flyby - Video Data). The modifications in the Entry Data design necessary to accommodate the video data requirement were not major and were provided for during the phase II effort by the inclusion of an adequate growth margin into the Entry Data design. This results in a high degree of similarity between the two SM designs.

In addition, an Orbiter SM concept was studied during phase III. The Orbiter design includes a capability for insertion into a Mars orbit after performing the initial relay function. The Orbiter while in Mars orbit relays scientific data from the lander for its lifetime. Phase III was concluded with a cost estimate and comparison of the three SM concepts.

The guidelines followed during the MSSM study were either initially specified by LRC or defined by a joint Hughes-LRC agreement during the study. Volume I contains a complete set of the guidelines which, though not repeated as such in this volume, are included as required for the presentation of information in each section of this volume.

The order of presentation of the study material in this volume is based on the significance attached to the SM design concepts with respect to the Mars 1973 Program rather than chronological order of the study. The Flyby - Video Data design is presented first, giving detailed trajectory/navigation, structural, attitude and velocity control, reaction control, telecommunication, power, and mission sequence of events background data. Next, the same aspects of the Flyby - Entry Data design are presented, but mainly in terms of differences between it and the Video Data design. The Orbiter design is then presented with advantage taken of its commonality to the Flyby designs and emphasis placed on its unique features. Volume II is completed with a discussion of the alternate designs considered during the initial phase I period. The program plan and cost supporting data is presented in Volume III.

2. FLYBY - VIDEO DATA DESIGN

TRAJECTORY/NAVIGATION

Transit Trajectory Characteristics

The Mars 1973 mission, based on the use of a Flyby support module (SM) design, will employ the direct entry mode of flight. This mode results in the spacecraft (SM plus aeroshell/lander) being placed on a Mars impacting trajectory and the SM being deflected near encounter to flyby Mars and relay aeroshell/lander (A/L) data to earth. Two spacecraft will be sent to Mars by separate Titan III-C launch vehicles. The launch and arrival dates, based on a 2080-pound payload capability, 30-day minimum period, and at least a 2-hour window per day, are:

	Spacecraft 1	Spacecraft 2
Launch:	July 12 to Aug. 9, 1973	July 12 to Aug. 11, 1973
Arrival:	January 12, 1974	January 22, 1974

These launch and arrival dates result in sun-spacecraft ranges which are used primarily to design the SM solar panels and specify their performance characteristics (see Figure 1). The solar panels must be designed to supply the required power at the maximum sun-spacecraft range, at Mars encounter, of 232×10^6 km.

The transit phase earth-spacecraft telecommunications subsystem design and performance is dependent upon the range data given in Figure 2. The limiting cases of the specified launch and arrival periods are shown. The maximum earth-spacecraft communications distance is less than 160×10^6 km.

The earth-spacecraft (probe)-sun (EPS) angle during the mission is shown plotted in Figure 3. This data is of concern because it influences the narrow beam antenna pointing direction, spacecraft attitude and the number of attitude corrections required, and the power and thermal performance.

The minimum corresponds to earth-spacecraft conjunction and marks the point where the earth starts to "lead" the spacecraft as they both rotate about the sun. The 40-degree EPS angle that is approached asymptotically near Mars encounter, along with the range, is of primary importance to the solar panel design.

Spacecraft Attitude Corrections

Since earth-to-spacecraft communications is maintained via the narrow beamwidth antenna after approximately 90 days from injection, spacecraft attitude torquing is required to keep the earth within the antenna beamwidth. The attitude correction time and number of corrections is dependent on many factors. Degradation of the orbit determination accuracy process should be minimized. This can be achieved by minimizing the total number of corrections, performing maneuvers during noncritical tracking phases, and by combining the attitude correction sequence with the required midcourse corrections. Continuous pointing at the earth is not required because of the finite beamwidth of the antenna. Also, the reduced earth-spacecraft range during the early portion of the flight will increase the communications capability (bit rate) for a given angle off of the antenna boresight. Figures 4 and 5 illustrate a typical strategy. The mission has a total flight time of 194 days, with a launch date of July 12, 1973. Midcourse corrections are planned at injection (I) + 5 days, encounter (E) –30 days, and at E–5 days. Plotted in Figure 4 is the right ascension and declination of the earth-spacecraft line with time points spaced at 5-day intervals. At some time early in the mission, the spacecraft axis is oriented antiparallel to its estimated coordinates at I + 157 days. As a result, the earth will be within 8 degrees of the beam center from approximately I + 100 days to I + 177 days. At approximately E –30 days, and in conjunction with the midcourse maneuver sequence, the spin axis is torqued to the spacecraft - earth direction at I + 174 days. The attitude remains in this position during the critical tracking period, prior to the final midcourse correction, from E –30 to E –5 days. Immediately following the final correction, the axis is precessed to the required position that will maximize the gain at encounter.

The bit rate capability over the entire mission, using the above scheme, is presented in Figure 5. Shown is the maximum bit rate available, for RF power output of 3 and 20 watts, as a function of range and angle off the antenna boresight. The range-boresight angle "trajectory" with re-orientation at 164 and 189 days is superimposed to show the overall capability. The minimum capability occurs at 189 days and is greater than 200 bits per second (bps) at low power and 1500 bps at high power.

Figure 6 illustrates the pointing strategy for the Flyby - Video Data SM design where angles 4 to 5 degrees off the antenna boresight are acceptable.

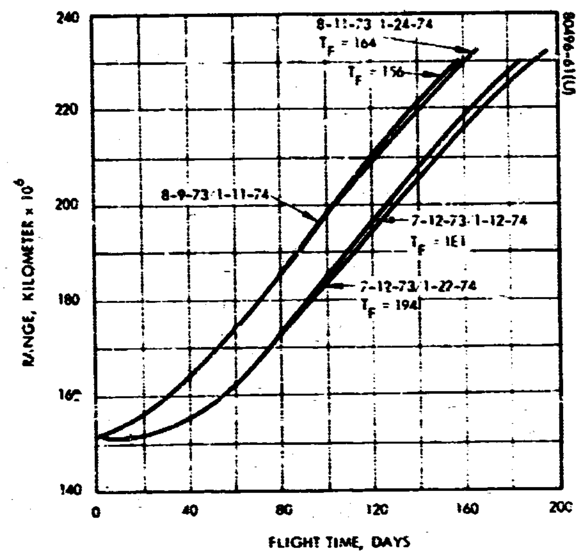

Figure 1. Sun-Probe Range Versus Flight Time

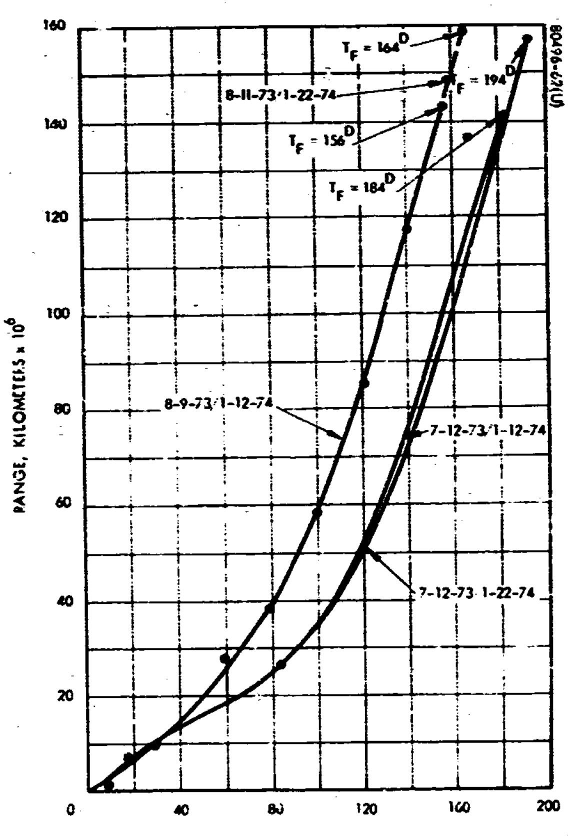

Figure 2. Earth-Probe Range Versus Flight Time

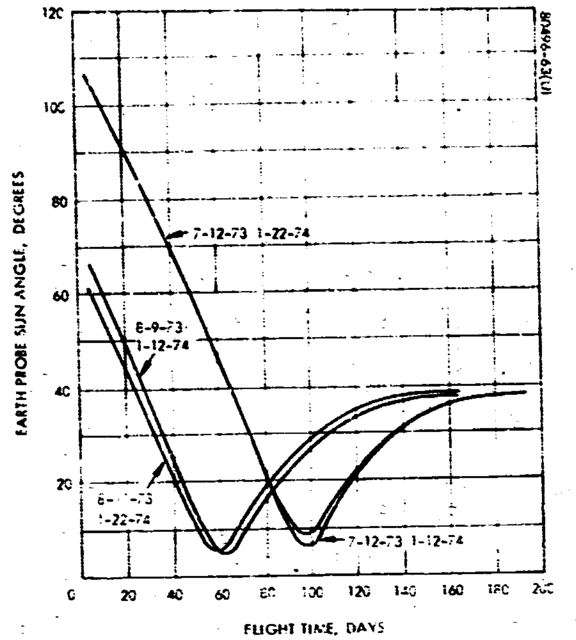

Figure 3. Earth-Probe-Sun Angle Versus Flight Time

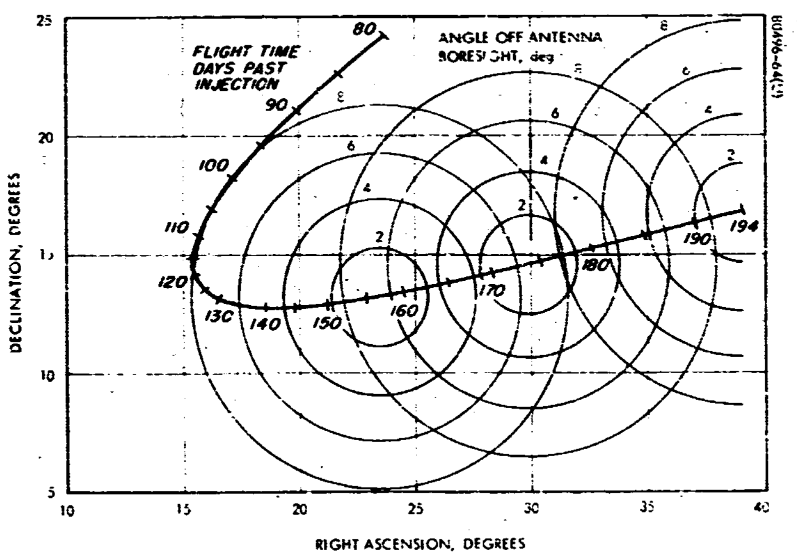

Figure 4. Earth-Probe Direction and High-Gain Antenna Pointing Requirements

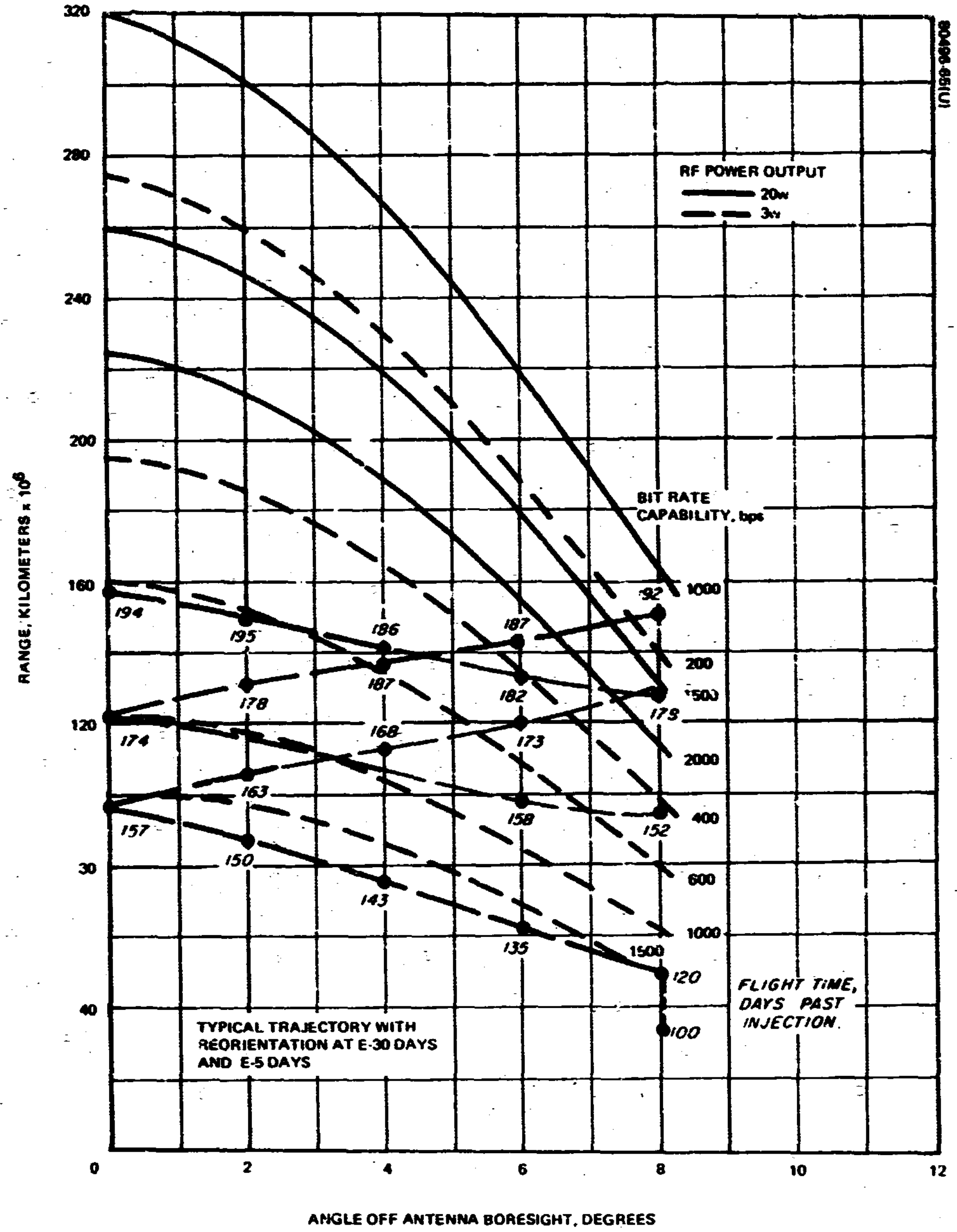

Figure 5. Typical High-Gain Antenna Bit Rate Capability for Fixed Orientation

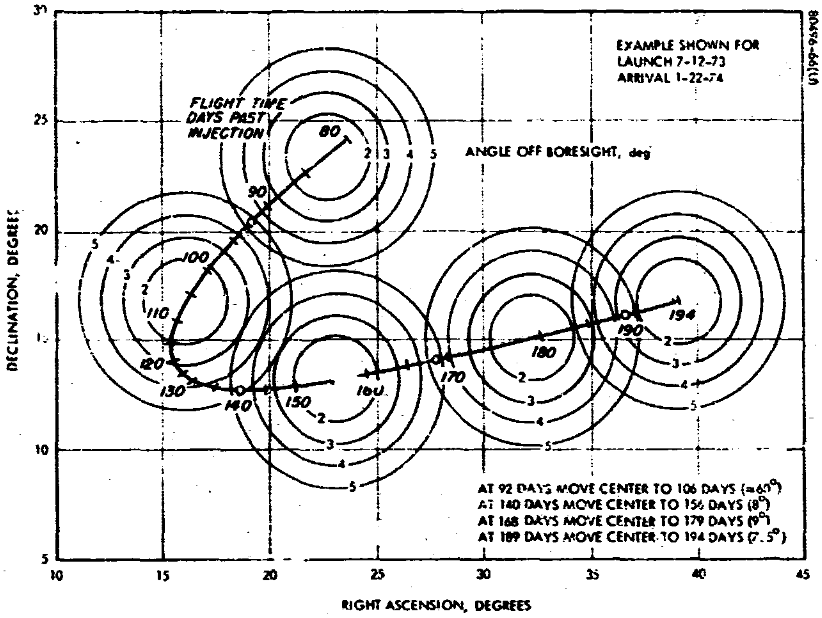

Figure 6. Earth-Probe Direction and High-Gain Antenna Pointing Requirements

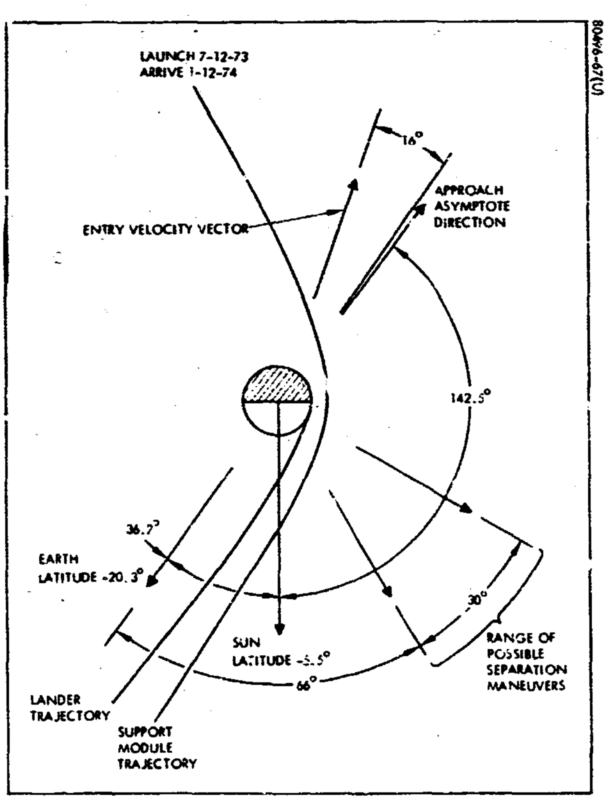

Figure 7. Typical Arrival Geometry

Arrival Geometry

Typical arrival geometry for the 1973 mission is shown in Figure 7, where SM and entry vehicle trajectories for direct approach are shown. The nominal entry angle as illustrated is -27.4 degrees. The expected uncertainty in the magnitude of the miss parameter for the entry vehicle will result in variations in the entry angle of between -19.8 and -33.4 degrees.

For the direct approach (with the rotation of the planet), landing will occur in daylight, but with only a short time remaining until earthset and sunset.

The relative relation between the nominal entry velocity vector and the Mars-earth direction is also shown. The latitude and longitude differences are about 20.3° and 16°, respectively, assuming a near equatorial landing. These angles are significant because they determine the orientation maneuver required, prior to SM-A/L separation, to place the aeroshell in its entry attitude. Also shown is the approximate range of SM deflection maneuvers and their relation to the approach trajectory. The magnitude and direction of the deflection maneuver is determined primarily by the SM-A/L post-landing visibility requirements.

Midcourse Maneuver Analysis

Let δx_o be the perturbation in the state vector at injection as a result of boost vehicle guidance errors. Let U be the matrix of partials relating perturbations in the initial state to perturbations in the terminal state. Then the error in the terminal state is given by

$$\delta m = U \delta x_o$$

where

$$\delta m_i = m_i \qquad i = 1, 2, 3$$

$$U = \frac{\delta m_i}{\delta x_j} \qquad i = 1, 2, 3 \qquad j = 1, 2, 3, 4, 5, 6$$

Given the covariance matrix of injection errors $\Lambda_o = E(\delta X_o \; \delta X_o^T)$, the covariance matrix of the terminal error is obtained from

$$\Lambda m = U \Lambda_o U^T \tag{2}$$

TABLE 1. TYPICAL UNCORRECTED TRAJECTORY DISPERSIONS OF ATLAS/CENTAUR INJECTION ERRORS

Launch Date	Arrival Date	Flight Time, days	Uncorrected Miss (1σ)			
			Semi-Major Axis, kilometers	Semi-Minor Axis, kilometers	Flight Time, minutes	Theta, degrees
7/12/73	1/12/74	184	74,507	10,612	607	-43.4
7/12/73	1/22/74	194	33,748	13,932	340	-68.0
8/ 9/73	1/12/74	156	24,610	7,582	259	-36.1
8/11/73	1/22/74	164	26,814	8,340	337	-47.8

It is desirable to define the terminal error vector in terms of a two-dimensional impact parameter vector, $\delta b = (\delta b_t, \delta b_r)$*, and the error in flight time, δt_f. The covariance matrix of the impact parameter (Λ_b) and the flight time variance can be obtained by partitioning Equation 2. That is

$$\Lambda_m = \left[\begin{array}{c|c} \Lambda_b & \sigma_{b,\ t_f} \\ \hline \sigma_{b,\ t_f} & \sigma_{t_f}^2 \end{array}\right]$$

Assuming that δx_o is gaussian, then δb is also gaussian, and the contours of constant probability density specified by $\delta b^t \Lambda_b \delta b$ = constant are therefore ellipses. The eigenvectors of Λ_b satisfy the equation

$$\Lambda_b \epsilon_i = \sigma_i^2 \epsilon_i \qquad i = 1, 2$$

where the ϵ_i's are the normalized eigenvectors and the σ_i^2 are the eigenvalues. It is well known that the eigenvectors define the principal directions of the equi-probability density ellipses in an orthogonal coordinate system in which the errors are uncorrelated. The eigenvalues, σ_i^2, are the variances of the uncorrelated error and the probability of δb being within the ellipse with semi-axes $k\sigma_i$ where k = 1, 2, 3 is P = 0.4, 0.86, 0.99, respectively.

Table 1 presents typical uncorrected dispersions in terms of the 1σ semi-axes values using Atlas/Centaur guidance errors. Also shown is the 1σ flight time uncertainty and the angle θ measured positive clockwise from the Mars orbital plane to the principal axis. Data is presented for each of the four specified launch and arrival dates.

In order to null the above error at a specified midcourse maneuver time t_1, it is necessary to apply a correction

$$\delta v_1 = k_1^{-1} (-\delta m) \tag{3}$$

---

*The miss at the target is specified in terms of the conventional miss parameter, or b-vector, in the r, s, t coordinate system. Where b is defined from the target center perpendicular to the asymptote of the approach hyperbola, t is a unit vector along the intersection of the Martian orbital plane and a plane normal to the asymptote, and r is a unit normal to both t and a unit vector s along the incoming asymptote. The b vector is therefore specified by its components b_t and b_r in the r and t directions.

The matrix k_1 depends upon a specification of the terminal constraints to be controlled. For miss plus flight time corrections

$$k_1 = \frac{\partial m_i}{\partial v_j} \quad i = 1, 2, 3 \quad j = 1, 2, 3$$

However, if only δb_t and δb_r are to be specified, it is necessary to impose an additional constraint such as requiring the magnitude of the velocity to be a minimum. For this case

$$k_1 = \begin{bmatrix} a_{11} & a_{12} & a_{13} \\ a_{21} & a_{22} & a_{23} \\ a_{31} & a_{32} & a_{33} \end{bmatrix} \tag{4}$$

where

$$a_1 = \partial b_t / \partial v_1, \quad a_2 = \partial b_r / \partial v_1, \quad \text{and} \; a_3 = (a_1 \times a_2) / \left| a_1 \times a_2 \right| .$$

Furthermore

$$\delta m = (\delta b_t, \; \delta b_r, \; 0)^{z}.$$

For miss plus flight time corrections, the midcourse velocity covariance matrix is given by

$$\Lambda v_1 = k_1^{-1} \, U \, \Lambda_o \, U^T \, (k_1^{-1})^T \tag{5}$$

The modifications for miss only corrections are obvious: k_1 is given by Equation 4 and the last row of U is set equal to zero.

The rms value of the required correction is sometimes referred to as the figure of merit (FOM) and is obtained by taking the square root of the trace of Equation 5. It should be pointed out that although δv_1, satisfies a joint gaussian distribution, the distribution of the FOM is <u>not</u> gaussian. Assignment of probabilities to specific values of the FOM requires consideration of the relative values of the eigenvalues of Equation 5.

Table 2 presents the rms midcourse maneuver magnitude to correct miss only and miss plus flight time for the four trajectories as a function of the midcourse maneuver time. It is significant that the required maneuver magnitude is essentially independent of the maneuver strategy and time for the first 16 days of the mission. Adequate tracking can therefore be obtained without propellant requirement penalty.

Figure 8 is an additional presentation of the midcourse maneuver sensitivity as a function of maneuver time. Each contour was obtained by mapping a unit sphere to the r-t, or impact parameter, plane. Note that the sensitivity is essentially circular from E -64 days and is proportional to the remaining flight time.

The accuracy with which the impact parameter, and therefore the entry angle, can be controlled depends upon a number of factors. Of primary concern is the ability to accurately predict the trajectory of the spacecraft through the processing of tracking data. The uncertainty associated with the determination of spacecraft trajectories via earth-based tracking is a complex function of many parameters. The hardware and computational uncertainties of the Jet Propulsion Laboratory (JPL) Deep Space Network (DSN), data type and weighting, station location uncertainties, imperfect knowledge of physical constants, and nominal flight trajectory, all contribute to limiting the available accuracy. The data shown in Table 3, which was taken from previous Voyager studies, specifies the accuracy that will be available for the 1973 mission. Although studies performed at Hughes indicate that this data is somewhat conservative, it is used for illustrative purposes.

It has been shown that the midcourse maneuver control system has a basic error of about 5 percent. In order to minimize the final approach error, a number of midcourse corrections will be performed. The execution time and maneuver magnitude for each correction will depend to a large extent upon the error to be corrected, the available pre-maneuver tracking accuracy, the possibility of later corrections, and the probability of satisfying the success zone based upon the approach requirements. Two examples are given in Table 4. The first case illustrates the maneuver requirement and overall accuracy for a sequence originating with the worst 3σ Atlas/Centaur injection from Table 1. The maneuver requirements for four times this error is also presented.

The time of the first correction should be based upon propellant and execution accuracy considerations. The uncertainty due to tracking should be small when compared to the estimated error, and the miss due to spacecraft mechanization should be about the same order of magnitude as the tracking error. The latter condition is the obvious result of considering the reduction in tracking uncertainty without significantly decreasing the overall execution error at the expense of increased propellant requirement. As previously noted, the first maneuver could be performed as late as I + 16 days without increasing the maneuver magnitude. Postponing the

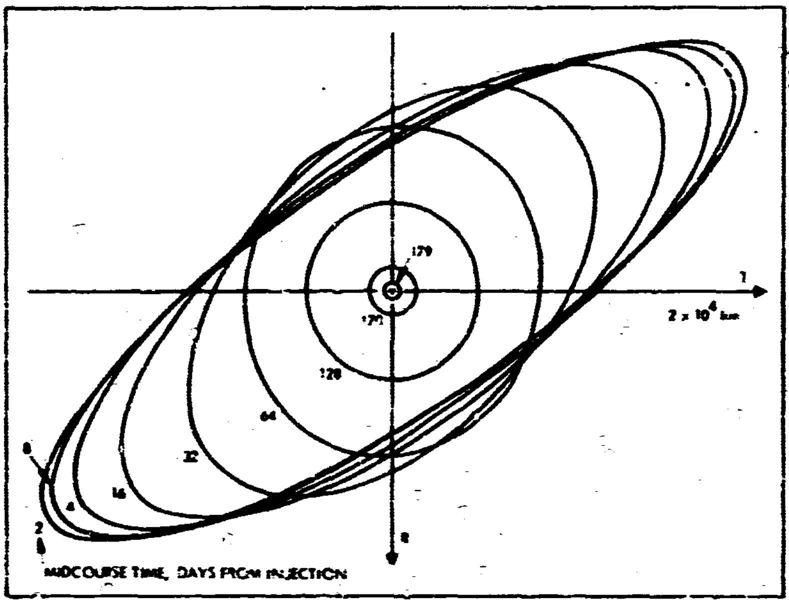

Figure 8. Midcourse Maneuver Sensitivity

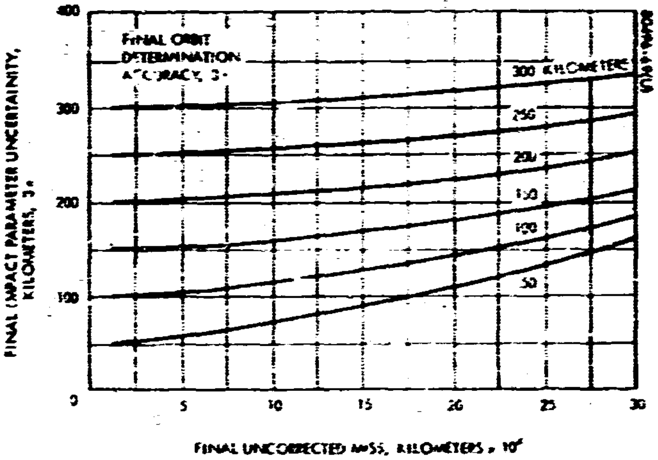

Figure 9. Final Impact Parameter Uncertainty Versus Uncorrected Miss

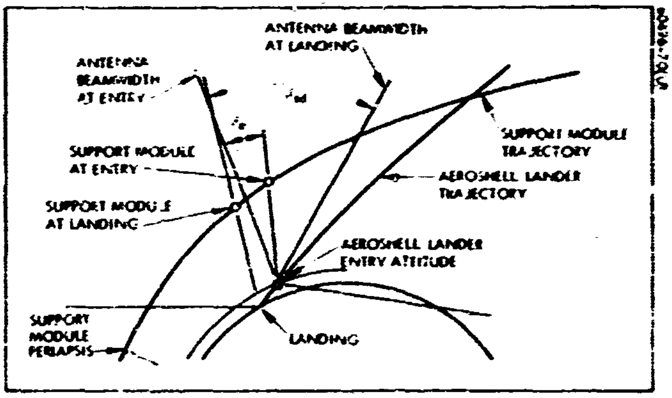

Figure 10. Geometry of Aeroshell Lander and Support Module Trajectories

correction will not reduce the execution error, however, and may jeopardize reestablishment of the trajectory if an additional correction is required at I + 30 days. For large injection errors, the first maneuver should be made as soon as the tracking constraint permits.

Successive maneuvers are made when the above constraints are satisfied. Use of 3σ execution errors in conjunction with the 3σ maneuver requirement in computing the post-maneuver residual error results in values which are far too pessimistic. Monte Carlo analysis has shown that a 2σ maneuver magnitude will yield errors which are conservative when compared to the actual 99 percent dispersions. This technique was used to compute the values shown. The correction at approximately E -30 days should be made when the tracking uncertainty is reduced to the point where the total execution error is no more than about 500 km (3σ). By reducing the uncorrected miss to less than 500 km, the approach conditions, after a final correction at E -5 days, will essentially be a function of the tracking accuracy alone. Figure 9 shows that this is true for tracking uncertainties down to 50 km (3σ).

Deflection/Relay Phase Characteristic

The launch and arrival dates considered are tabulated below, along with the resulting range of approach velocities corresponding to the range of launch dates.

Launch date	July 12 to August 9, 1973	July 12 to August 11, 1973
Arrival date	January 12, 1974	January 22, 1974
Approach velocity range	3.7 - 4.1 km/sec	3.4 - 3.6 km/sec

The maximum approach velocity of 4.1 km/sec was selected for this study. This corresponds to worst-case launch and arrival dates of August 9, 1973 and January 12, 1974, respectively.

In the case of the Flyby designs, the nominal approach trajectory is an impact trajectory. At some point prior to atmospheric entry the SM is deflected from the A/L into a hyperbolic flyby trajectory. The separation maneuver must be made so that the SM will be in view of the A/L UHF antenna throughout entry and for at least 12 minutes past lander touchdown, to obtain 10^7 bits of video data. The 12 minutes includes 2 minutes to initiate video operations. Figure 10 shows a typical geometry indicating the A/L and SM trajectories, the A/L at entry in its entry attitude (aligned with the velocity vector), the landing point, and the relative positions of the SM at the time of entry and landing. In order that communications at entry be maintained, the angle between the A/L antenna beamwidth and the SM (β_e) must be greater than zero. Similarly, at touchdown, $0 \leq \beta_{td} \leq 120$ degrees (see Figure 10).

TABLE 2. RMS MIDCOURSE MANEUVER MAGNITUDE OF TYPICAL ATLAS/CENTAUR INJECTION ERRORS

Launch Arrival Flight Time	7/12/73 1/12/74 184 Days		7/12/73 1/22/74 194 Days		8/ 9/73 1/12/74 156 Days		8/11/73 1/22/74 164 Days	
Midcourse Maneuver Time, days	Miss Only, mps	Miss and Flight Time, mps	Miss Only, mps	Miss and Flight Time, mps	Miss Only, mps	Miss and Flight Time, mps	Miss Only, mps	Miss and Flight Time, mps
2	4.1	4.1	2.5	2.7	2.1	2.8	2.3	2.8
4	4.1	4.2	2.6	2.7	2.1	2.8	.23	2.8
8	4.2	4.3	2.5	2.7	2.2	2.9	2.4	2.9
16	4.6	4.7	2.5	2.7	2.4	3.1	2.6	3.1
32	5.7	5.9	2.7	2.9	2.8	3.9	3.0	4.0
64	8.7	10.5	3.7	4.4	3.7	6.7	3.8	6.8
128	16.2	30.7	6.6	12.5	10.4	27.	8.8	23.5
151					51.4	140.4		
170	61.	63.8	16.8	35.9				
179	163	357.						
189			68.	156.				

TABLE 3. MAXIMUM ALLOWABLE 3σ ORBIT DETERMINATION UNCERTAINTIES

Time at Which Orbit Estimates are Calculated	Magnitude and Time of Prior Orbit Corruptions*	Uncertainty in Magnitude of Impact Parameter Vector, km	Uncertainty in Aiming Plane Normal to Nominal Impact Parameter Vector, km	Uncertainty in Time of Encounter, minutes
I +2 days	Planetary vehicle injection	2000 (1000)	2000 (1000)	15 (7)
I +30 days	150 m/sec arrival data adjustment and interplanetary trajectory correction at I + 5 days	1000 (500)	1500 (750)	10 (5)
E - 30 days	5 m/sec interplanetary trajectory correction at I +30 days	500 (300)	750 (500)	4 (3)
E - 2 days	1 m/sec interplanetary trajectory correction at E - 30 days	400 (150)	500 (200)	3 (1)
E - 4 hours	Same as above	300 (100)	500 (150)	2 (0.5)

*For purposes of error analysis only.

Numbers not in parentheses are maximum allowable uncertainties.
Numbers in parentheses are design goals.

TABLE 4. MIDCOURSE MANEUVER REQUIREMENTS

Uncorrected Miss	225,000 km	900,000 km
Midcourse Maneuver		
I + 5 days		
Magnitude, mps	15	60
Execution error (5 percent of $2\sigma\,\delta v$), kilometers	7500	30,000
Orbit determination error*, kilometers	2000	2,000
Total, kilometers (rss)	7750	30,000
I + 30 Days		
Magnitude, mps	----	3
Execution error, kilometers	----	1000
Orbit determination errors, kilometers	----	1000
Total, kilometers	----	1400
E - 30 DAYS		
Magnitude, mps	3	0.6
Execution error, kilometers	260	35
Orbit determination error, kilometers	500	500
Total, kilometers	560	500
E - 5 DAYS		
Magnitude, mps	1.3	1.2
Execution error, kilometers	20	20
Orbit determination error, kilometers	300	300
Total, kilometers	301	301
Total maneuver magnitude, mps	19.3	64.8

*Orbit determination errors from JPL 1973 Voyager mission performance and design requirements.

The nominal A/L impact trajectory will have 3σ dispersions in the miss parameter (assumed 3σ dispersion of ± 300 km) which will result in 3σ dispersed A/L entry angles, γ_e, ranging from -33.4 to -19.8 degrees, with γ_e = -27.4 degrees nominally. These entry angles must be considered over the range of Martian atmospheres specified by LRC as minimum, mean, and maximum. From Figure 11 it can be seen that the shallow entry angle of -19.8 degrees results in maximum A/L downrange travel from entry. If the descent is made in a minimum time (minimum atmosphere), the SM, having traversed a minimum distance on its flyby trajectory, will be at a minimum value of β_{td}. Similarly, the steep entry angle of -33.4 degrees results in minimum A/L downrange travel from entry. If the descent is made in a maximum time (maximum atmosphere), the SM, having traversed a maximum distance on its flyby trajectory, will be at a maximum value of β_{td}. Therefore, for the shallow entry angle of -19.8 degrees, the worst case corresponds to the minimum atmosphere; and for the steep entry angle of -33.4 degrees, the worst case corresponds to the maximum atmosphere.

Figure 12 presents, for a separation time of 5 hours before A/L atmospheric entry, separation maneuver requirements (ΔV magnitude and direction) for the 3σ dispersed entry angles and SM periapsis altitudes of 1000, 2000, and 3000 km. Also shown are contours of constant β_e, β_{td}, and post-landing visibility time, t_{pl}. In order to simultaneously satisfy all of the constraints, the allowable ΔV-θ region must be bounded by β_e = 0, β_{td} = 15 degrees (allowing 15 degrees for adverse landing slopes) and t_{pl} = 12 minutes for entry angles of -33.4, -19.8 and -33.4 degrees, respectively. The design point indicated on the figure (ΔV = 250 m/sec, θ = 60°) was chosen to maximize the post-landing visibility with a minimum separation maneuver magnitude. The tabulation below lists, for this design point, the characteristics of the nominal and 3σ dispersed trajectories.

Entry Angle, degrees	SM Periapsis Altitude, km	β_e, degrees	β_{td}, degrees	Post-Landing Visibility Time, t_{pl}, minutes
-19.8	4000	25.2	16.3	23.9
-27.4	3725	23.2	32.3	17.6
-33.4	3425	21.7	47.4	13.2

The SM periapsis altitudes vary from 3425 to 4000 km, while the postlanding visibility time varies from 13.2 to 23.9 minutes.

The magnitude of the separation maneuver is substantially larger for a 5-hour separation time than previous studies indicated. The increase may be attributed to two primary factors. First, the constraints bounding the allowable ΔV-θ region include a minimum post-landing visibility time of 12 minutes in the present study, while the previous study was bounded in part

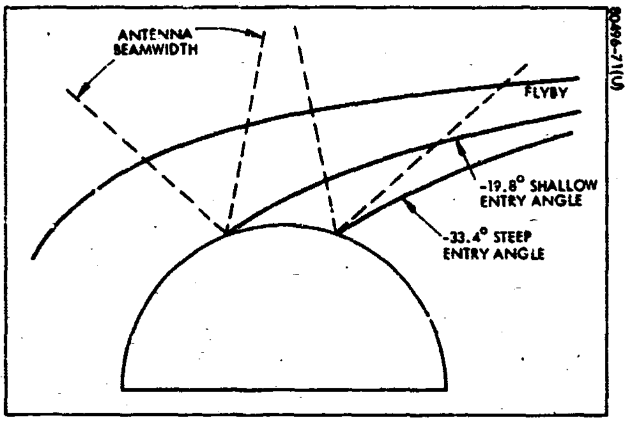

Figure 11. 3σ Dispersed Entry Angle Geometry

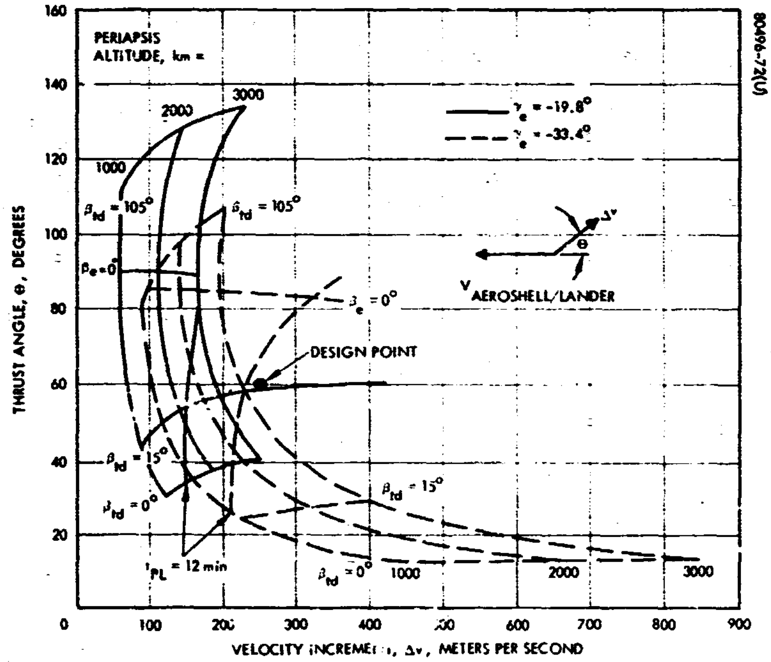

Figure 12. Aeroshell Lander/Support Module Visibility for 5-Hour Separation Maneuver

by a minimum periapsis altitude. Second, the arrival date in the present study is earlier than that assumed for the previous study. This leads to larger approach velocities and, therefore, larger separation velocities.

Figure 13 shows separation maneuver requirements for separation times of 12 and 24 hours. This figure indicates that the separation maneuver magnitude may be decreased by increasing the time before entry at which the maneuver is made. Figure 13a shows that the ΔV magnitude would decrease to approximately 105 m/sec if the separation maneuver was performed 12 hours before entry. In general, the ΔV magnitude decreases or increases with the time to go. For example, if the 5-hour separation magnitude is 250 m/sec, then the separation magnitude for a 12-hour separation time would be approximately 5/12 of 250 or 105 m/sec. 100 m/sec at 12 hours was assumed for the Flyby design.

Post-landing visibility and range conditions were determined for the design point indicated in Figure 12. The results are shown in Figures 14 and 15. Figure 14 shows, for the 3σ entry angles, time past landing versus angle from vertical, α. There are two interpretations of this figure. First, one may consider α as being the angle between vertical and a line of sight from the lander to the SM. Figure 14 is then a history of the SM angular position as a function of time past landing. Second, one may consider α as being the angle between vertical and the edge of the lander antenna beam. Figure 14 then indicates post-landing visibility time versus landing slope. For example, if the antenna field of view is 120 degrees (60 degrees on either side of the antenna boresight) and there is no landing slope, the SM will be visible (within the antenna field of view) until α = 60 degrees. This indicates a post-landing visibility time of approximately 17 or 31.5 minutes for γ_e = -33.4 or -19.8 degrees, respectively. If there is a 15-degree adverse slope, the SM will be visible until α = 45 degrees, indicating a post-landing visibility time of approximately 13 or 24 minutes for γ_e = -33.4 or -19.8 degrees, respectively. (Recall that the design point in Figure 12 of ΔV = 250 m/sec, θ = 60 degrees was chosen to give a minimum post-landing visibility time of 12 minutes for an adverse slope of 15 degrees by bounding the allowable ΔV-θ region by t_{pl} = 12 minutes and β_{td} = 15 degrees for entry angles of -33.4 and -19.8 degrees, respectively.)

Figure 15 shows, for the 3σ entry angles, the relative distance between lander and SM as a function of time past landing. These results are also for the design point of Figure 12. By using Figures 14 and 15, one may determine the position of the SM relative to the lander (in terms of angle and range) as a function of time past landing.

The relative trajectories of the A/L and SM are presented in Figure 16. Using a 5-hour separation maneuver of ΔV = 250 m/sec, θ = 60 degrees, the trajectories were generated for a nominal entry angle of -27.4 degrees. The A/L is held in its entry attitude for the entire post-separation trajectory. The line-of-sight from the A/L antenna boresight to the SM (ϕ) varies from approximately 43.5 to 36.8 degrees during transit from separation to entry, indicating that the SM is well within the A/L

120-degree field of view. The maximum relative range occurs at entry and is approximately 5366 km. Similar trajectories generated for the 3σ dispersed trajectories showed a variation of less than 3 degrees in the line-of-sight angles from nominal.

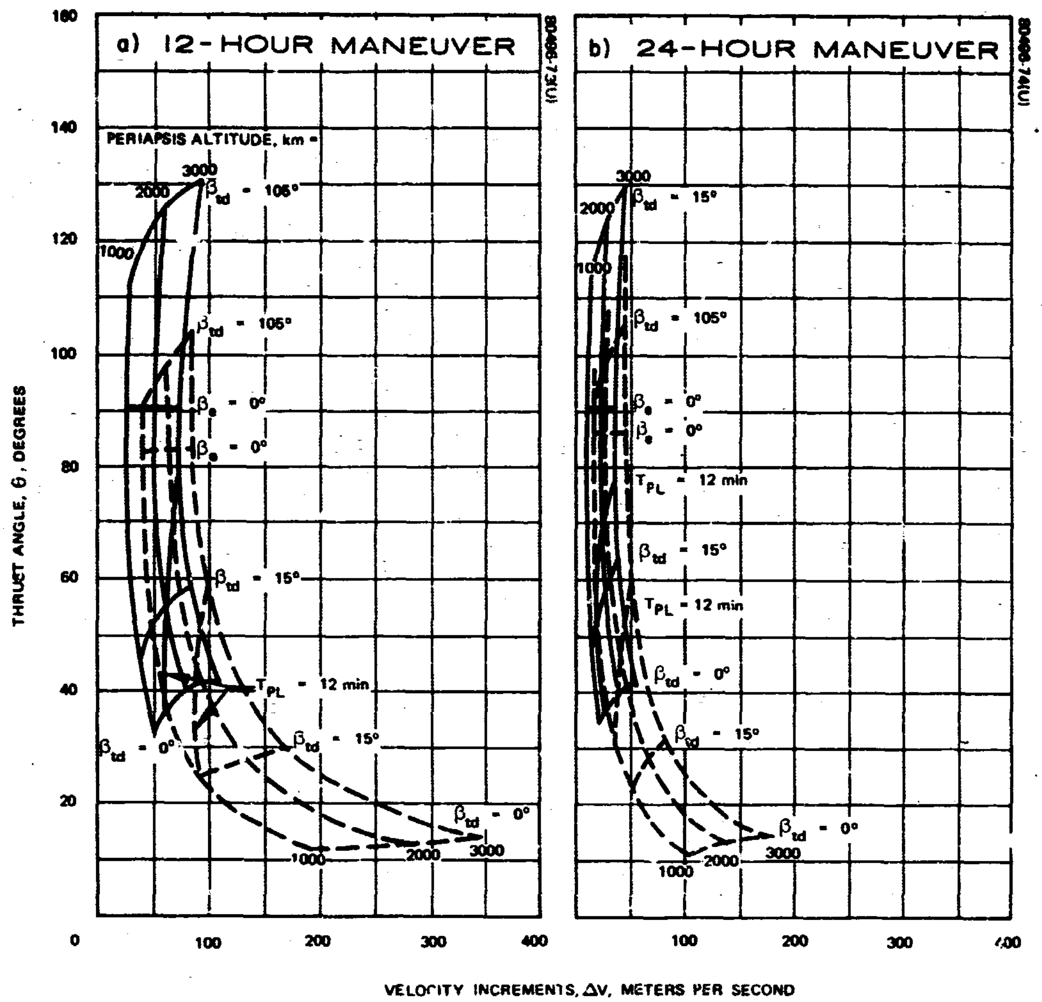

Figure 13. Aeroshell Lander/Support Module Visibility for Separation

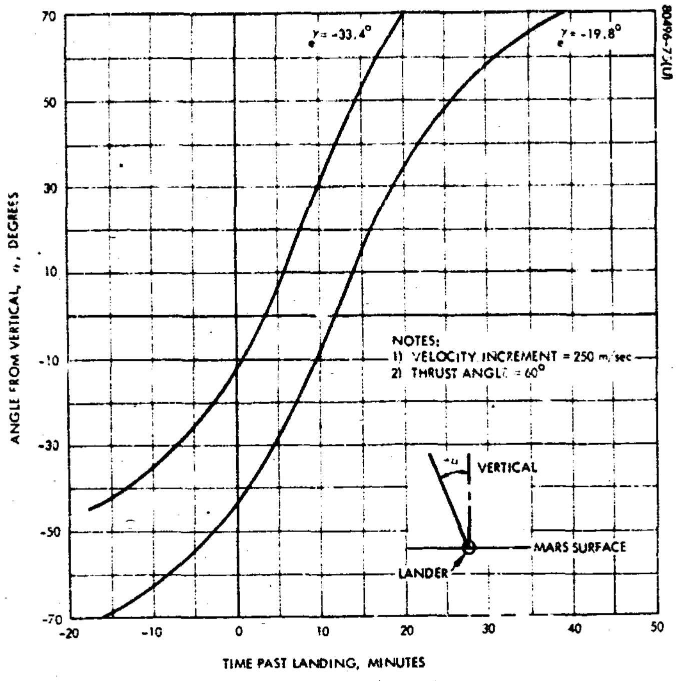

Figure 14. Angular Position Versus Time Past Landing

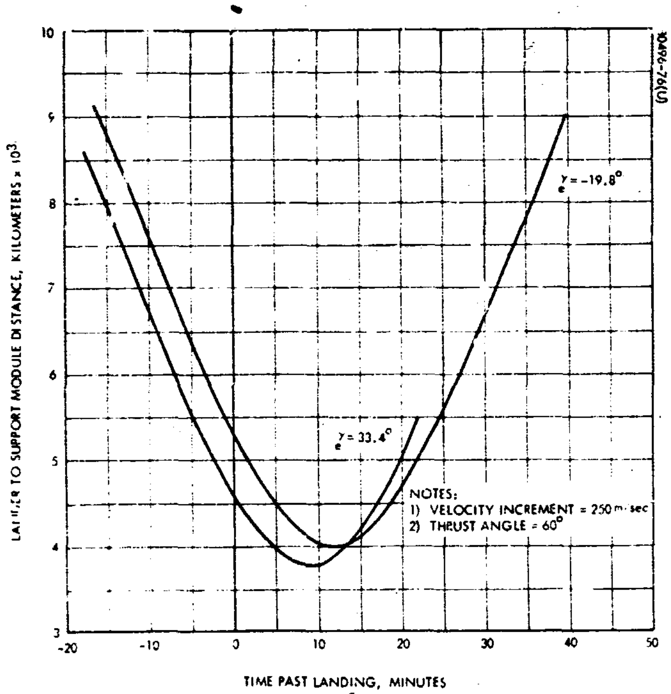

Figure 15. Aeroshell Lander/Support Module Range Versus Time Past Landing

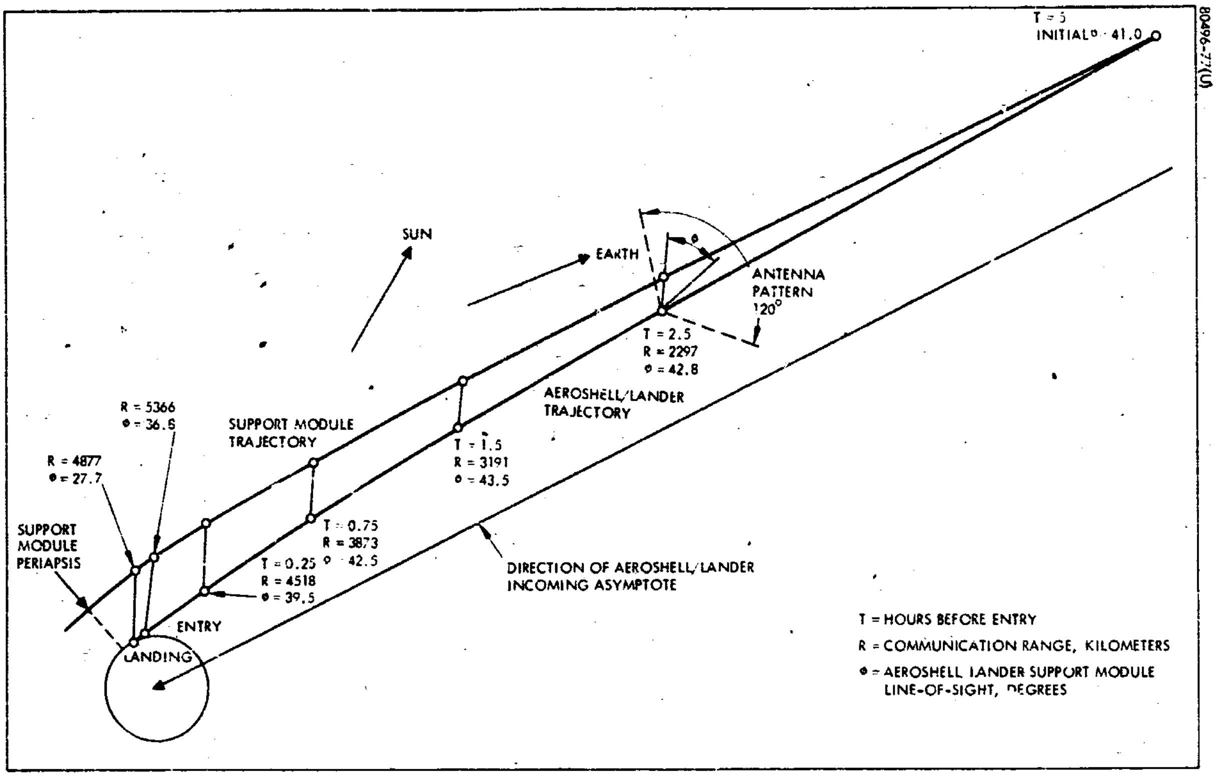

Figure 16. Descent Communication Geometry

VEHICLE CONFIGURATION/WEIGHTS

General Design Considerations

The mechanization and general configuration of the Flyby - Video Data SM is strongly dependent on the incorporation of similar hardware used in subsystems on Hughes earth communications satellites and the Surveyor spacecraft. In addition, the Mars 1973 mission profile, use of the Titan III-C booster with its payload and interface specifications, the A/L interface requirement, and sterilization canister/environment aspects all place constraints and requirements on the SM total configuration. Also, the need to manufacture, assemble, test, and integrate at a total systems level has a major influence on the overall design and layout. Although the SM design is of primary concern, the study did include a modification of the initially specified A/L, canisters, and Titan III-C adapter. These items are briefly considered in this section, but the section is primarily concerned with the SM structural design, arrangement rational, and the resulting mass properties.

A/L, Canister, and Adapter Redesign

The A/L and canister configuration specified by LRC at the initiation of the MSSM study is shown on Figure 17. This hardlander configuration was intended to be interfaced with a nonsterilized Orbiter SM design. To accommodate the Flyby - Video Data design concept and incorporate a new communications system into the lander design, a series of minor modifications were made.

The solid propellant deflection engine was removed from the A/L, since the SM, not the A/L performs the deflection maneuver near Mars encounter. The A/L weight was increased from 978 to 1100 pounds to accommodate the communications system and the change in the aeroshell diameter to 121 inches required to maintain the same mass to area ratio. The A/L-to-SM interface ring diameter was changed to match the SM central cylinder diameter of 67.5 inches. The ring height was changed to minimize A/L-to-SM separation, which enhanced spin stability and minimized canister and ring weight. The ring is part of the A/L and is included in the 1100 pounds.

The A/L diameter increase resulted in an increase in the canister diameter (and weight) to provide adequate clearance. The diameter was set at 125 inches to provide 1.5 inches of A/L - canister clearance. The weight of the forward section of the canister was estimated at 69 pounds. The aft canister weight was increased by the diameter change and also a height increase required for encapsulation of the total spacecraft plus adequate clearance. The aft canister structural weight, 128.8 pounds, plus an allowance for a pressure and vent system, 50 pounds, and canister separation cable, 3 pounds, yields a total of 181.8 pounds. The end of the aft canister is removable to allow access during assembly and testing.

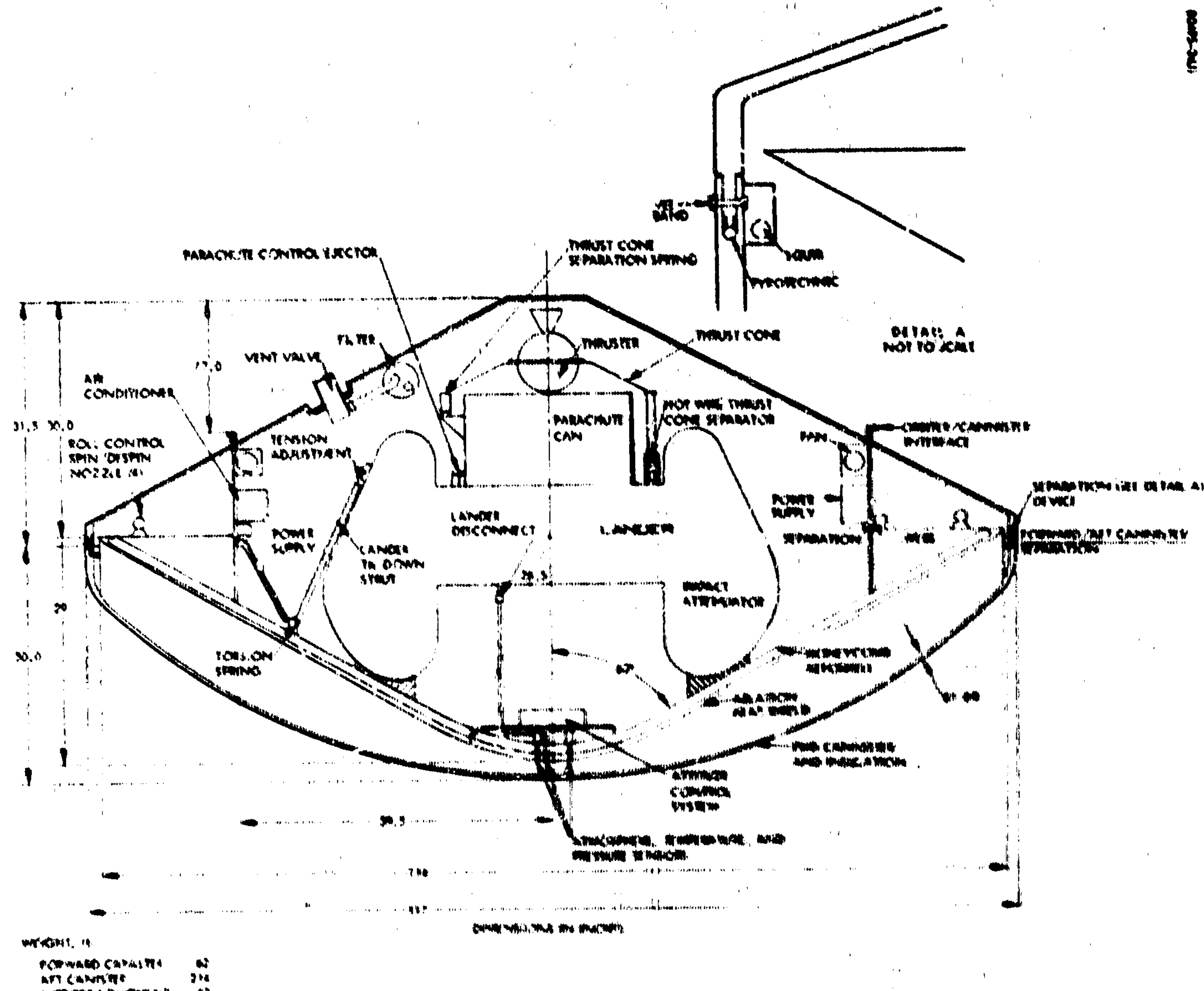

Figure 17. Aeroshell/Lander and Canister Configuration

The function of the capsule - Titan III-C adapter is to provide a mechanical coupling that is capable of withstanding the booster and capsule loads during the boost phase. One end of the adapter is hard-bolted to the 120-inch diameter transtage at eight points. The other end is attached to the 67.5-inch diameter central ring of the SM at four points. The SM attachment uses explosive separation bolts because the spacecraft is detached from the adapter at earth injection. The adapter must pass through the aft canister, and this is mechanized with a firm field joint. The height of the adapter is chosen to minimize weight and still provide adequate load bearing and stiffness.

The adapter structural weight of 77.2 pounds is based on the use of aluminum semimonoque construction, end stiffening rings, and the capsule and booster loads. The capsule weight at launch is approximately 1909 pounds, and Titan III-C booster dynamic characteristics are those used in the design of current Hughes communication satellite systems. The adapter also includes an umbilical line (35 pounds) for post-sterilization testing and Titan III-C to SM communications and canister pyrotechnique separation logic (5 pounds). The total adapter weight is 11[illegible].2 pounds.

Figure 18 illustrates the arrangement of the A/L, SM (with arms extended), canisters, and adapter with respect to the Titan III-C transtage. This general configuration and the dimensions given are applicable to the remaining Flyby design presentation.

The possibility of mounting the capsule other than shown in Figure 18 was briefly explored. The weight of the SM design can be reduced if the A/L, rather than SM, is mated with the adapter. This approach was not pursued because of the reluctance to pass a load bearing structure through the aeroshell. The adapter weight can be reduced if the SM attach points diameter were increased because the height of the adapter can be reduced. A severe SM solar panel interface problem and increase in SM structural weight results; therefore, this possibility was excluded. Another possibility is to interface the adapter between the A/L and SM, but the associated adapter structural weight increase, shroud diameter increase, and separation problems did not warrant further investigation.

<u>SM Structure and Configuration</u>

The SM subsystem equipment is mounted to a structure which provides a central location and, thereby independent module, isolation from the A/L loads, stiffening to withstand boost phase forces, and thermal properties to enhance subsystem temperature control. In providing these and other features, the previously mentioned considerations and constraints are applicable. Figure 19 is an inboard profile of the Flyby - Video Data SM which illustrates the structural and subsystem aspects of the design.

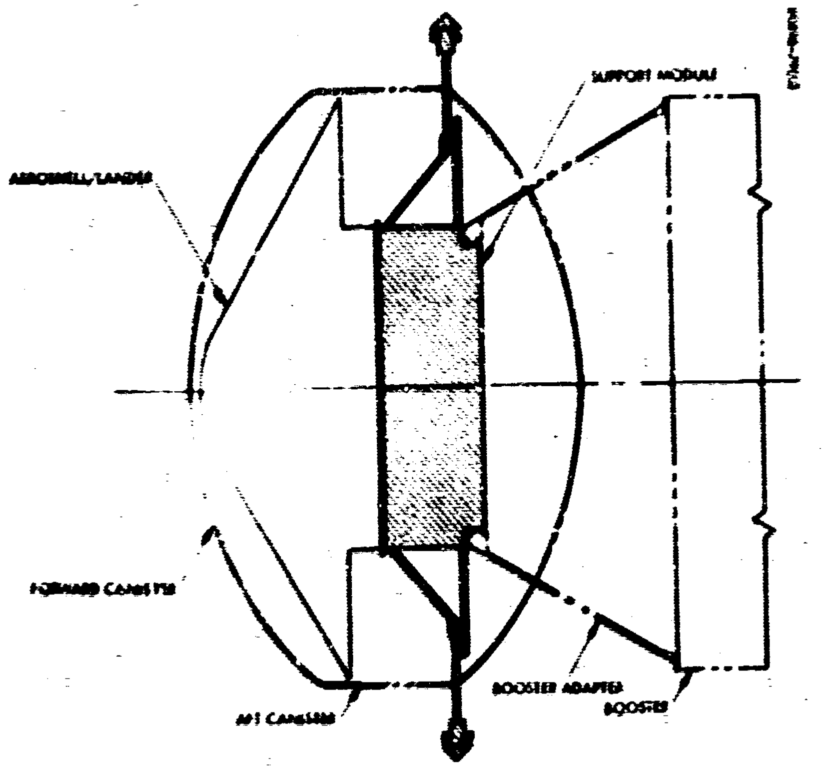

Figure 18. MSSM Arrangement for Titan III-C Transtage

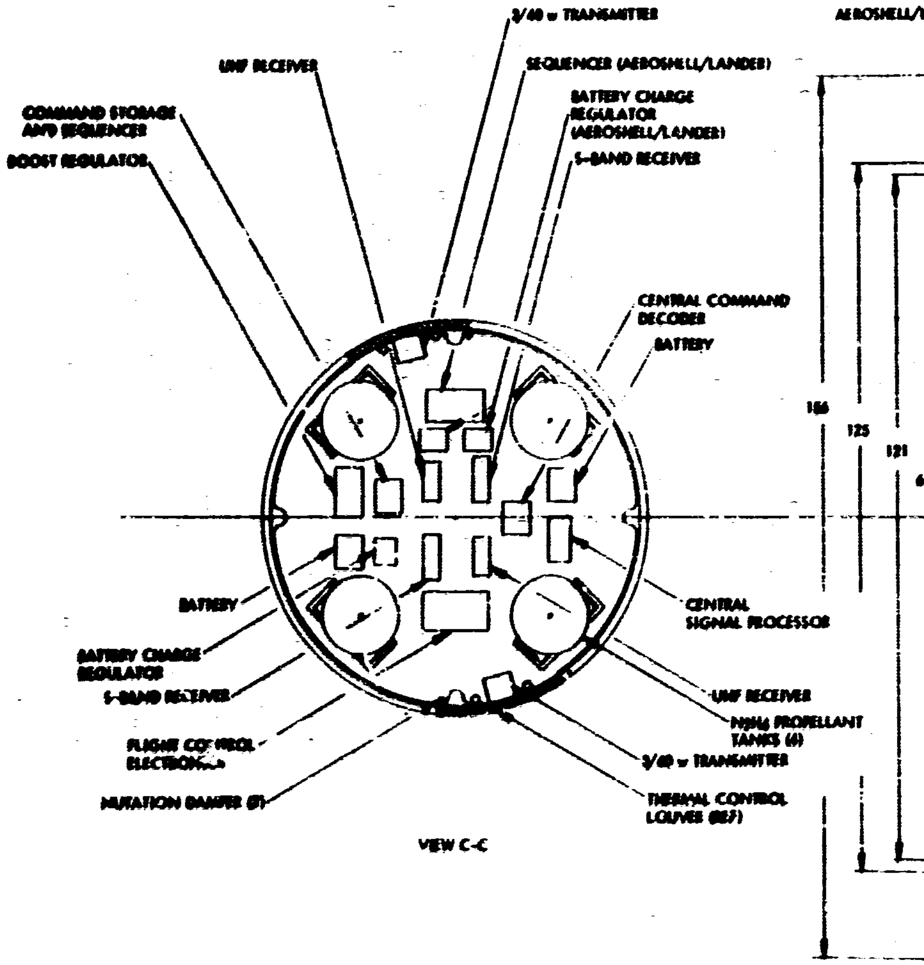

VIEW C-C

DIMENSIONS IN INCHES

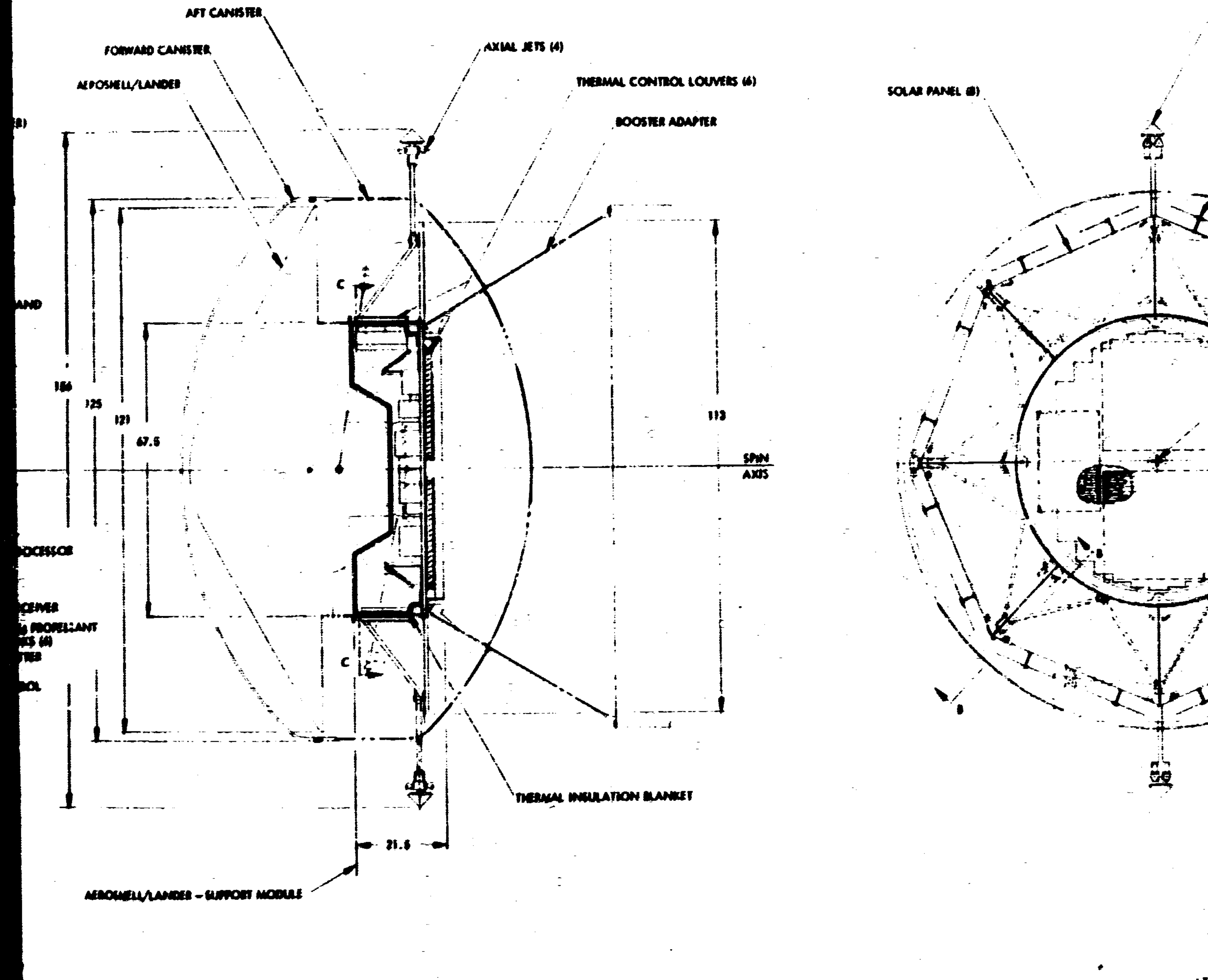
AFT CANISTER
FORWARD CANISTER
AEROSHELL/LANDER
AXIAL JETS (4)
THERMAL CONTROL LOUVERS (6)
BOOSTER ADAPTER
SOLAR PANEL (8)
186
125
121
67.5
113
SPIN AXIS
THERMAL INSULATION BLANKET
21.5
AEROSHELL/LANDER – SUPPORT MODULE

Figure 19.

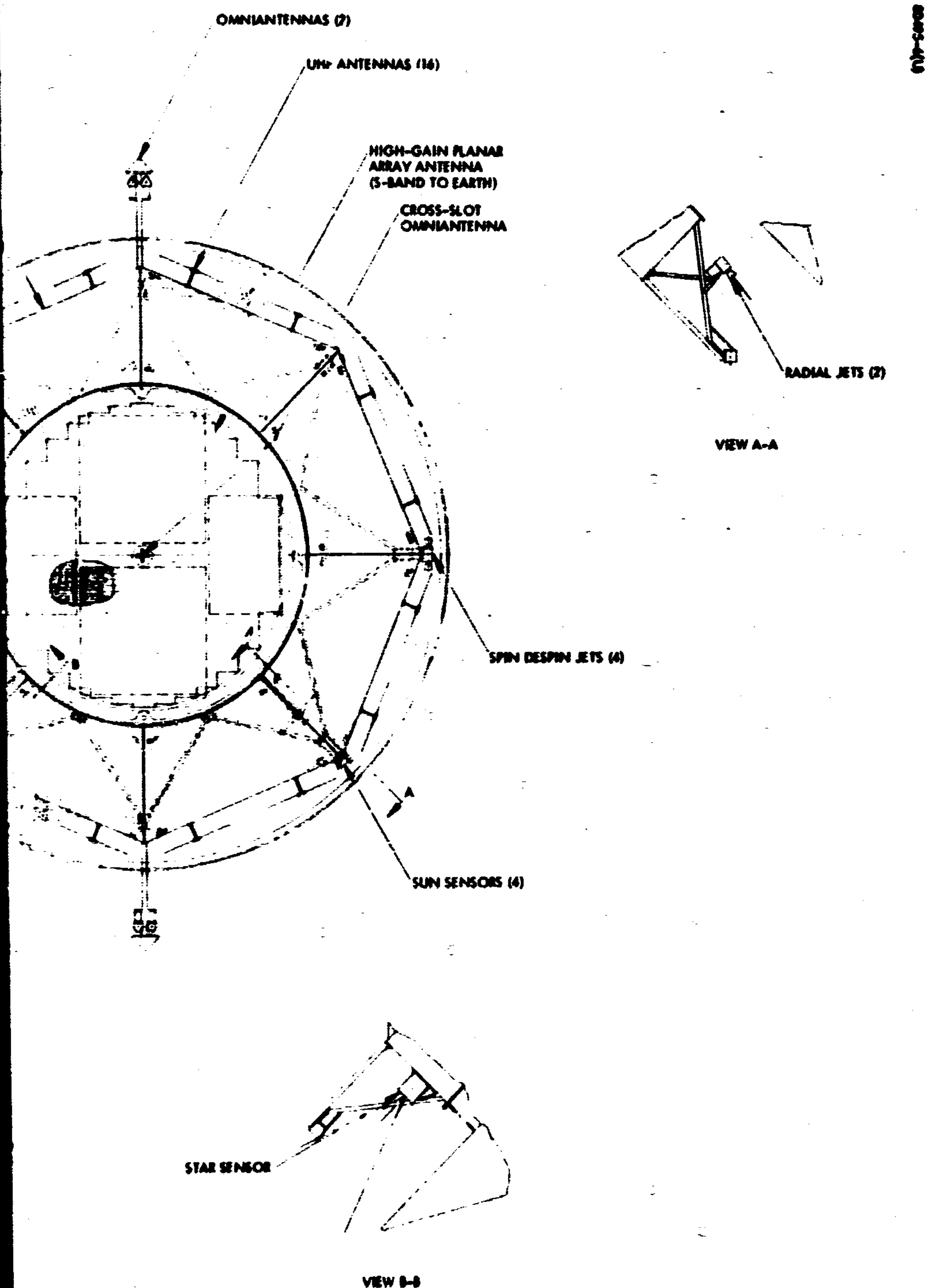

Figure 19. Inboard Profile of Flyby-Video Data Support Module

Upper Cylinder

A simple cylindrical section, 67.5 inches in diameter, interfaces with the A/L and adapter and provides a central mounting location for the equipment. The diameter satisfies the A/L interface structure diameter limits, ±6 inches about that given in Figure 17, and passes conveniently between the high gain antenna and solar panels to mate with the adapter. The minimum cylinder height, 21.5 inches, is fixed mainly by the internal height required for the reaction control system propellant tanks and A/L configuration limits. In general, it is desired to minimize the height to reduce SM and canister weight and increase the spin axis moment of inertia to enhance spin axis stability. The cylinder weight, 21.1 pounds, is based on aluminum-monocoque construction with a strength judged as adequate for support of anticipated loads. An upper and central ring are used to attach the cylinder to the A/L interface and adapter, respectively, along with squib activated separation bolts. The rings weigh 11.7 and 11.6 pounds, respectively, and the bolts weigh 11.6 pounds. The cylinder volume is more than ample to house the subsystems and provide for easy accessibility.

Attached to the outside of the cylinder are two thermal louvers for internal compartment temperature control, two radial jet supports (1.2 pounds), and a star sensor positioned such that stray light from the structure presents no problem and nominal viewing is perpendicular to the spin axis. Two mercury tube nutation dampers and 4 pounds of balance weights are attached to the inside of the cylinder. The communication transmitter drivers and traveling-wave tubes (TWT) are attached directly behind the louvers.

Solar Panels

Eight trapezoidal solar panels are attached to the cylinder at the adapter interface in a plane normal to the spin axis. This orientation achieves the minimum panel weight consistent with the requirement of supplying 85 watts of electrical power at the sun-to-Mars distance and 40-degree sun incidence angle. In addition, shadowing problems are eliminated. The outer 113-inch diameter bounding the panels is set by the aft canister dimension, UHF antenna and spin jet positions, and margin required to achieve spacecraft separation at earth injection. The inner dimension of the panels allows for the maximum planar array diameter and clearance for the SM-to-adapter interface while maintaining 37.4 square feet of panel area required to produce the 85 watts. A series of sixteen support tubes, with a total weight of 7.0 pounds, attached behind the panels and to the cylinder provide support during the boost phase.

Planar Antenna

The S-band high-gain planar antenna is mounted at the adapter end of the SM with its nominal electrical axis along the spacecraft spin axis. It is attached to four thermal louvers that support and radiate heat energy through it. The planar antenna outer diameter, 60 inches, has been maximized consistent with solar panel/adapter interface constraints. A lower cover or ring weighing 2 pounds constrains the antenna. The antenna plane location relative to the solar panel plane enables solar energy incidence angles of 40 degrees to be used without shadowing the panels. The antenna is constructed from rectangular cross slot cavity sections, and is energized by a waveguide running from the transmitters, between the louvers, to its backside.

Equipment Shelf

Most of the SM equipment, electronics, batteries, and propellant tanks, are attached to one side of a shelf that is fastened to the cylinder in the plane of the solar panels. The four louvers and planar antenna are attached to the opposite side. Its weight of 21 pounds and aluminum construction are adequate to sustain boost loads and conduct heat energy from the equipment to the louvers. The shelf concept enhances accessibility, testing, and installation while the SM is in development. In addition, the equipment on the shelf, as well as the other SM items, is arranged to achieve static and dynamic balance. The equipment sizes are based on similar Hughes unit dimensions unless the items, such as tanks, are specified.

Axial Jet Deployment Arms

Two arms which are pivoted about an attachment to the solar panel struts are extended immediately after spacecraft separation from the Titan III-C. These arms have the axial reaction control jets and backup semi-omnidirectional antennas attached to them. The arms place the jets far enough outboard the spacecraft such that jet impingement on the A/L is insignificant. The use of coiled propellant lines to supply the axial jets will eliminate internal line flaking, trapping potential valve-jamming materials, and will provide a spring action for arm deployment. The design allows for mission completion even if both arms should fail to extend, since two of the axial jets protrude past the panels while in the stowed position. In addition to the centrifugal force keeping the arms extended, a positive lock will assure permanent arm extension. The flexible coaxial cables for the antennas present no special problems. The estimated weight for two axial jet deployment arms is 3.2 pounds.

Peripheral Equipment

Four spinup/spindown reaction control jets are attached in pairs to struts just below the solar panels. They are positioned to eliminate significant jet impingement on the panels and sensors, and provide a large moment for spin control.

Two radial jets are mounted to struts and are in a plane near the SM-A/L interface. Their position eliminates significant jet impingement on the panels. One jet produces thrust through the spacecraft cg and the other through the SM cg. It is desirable to keep their thrust axes as normal to the spin axis as possible and passing through the cg to eliminate axial components of velocity when only radial components are required.

The four sun sensors are attached to struts just below the solar panels. Two have nominal viewing directions normal to the spin axis and the other two 45 degrees from the spin axis.

Sixteen half-wavelength dipole antennas are mounted outboard of the solar panels. Their orientation is chosen to yield a satisfactory receiving pattern for collecting A/L scientific data, and provide adequate clearance for spacecraft separation from the canister. Antenna feed lines are mounted below the solar panels and run to the UHF receivers inside the cylinder.

A thermal blanket is placed around the equipment and tied down to the cylinder, shelf, and upper fiberglass support which encloses the cylinder at the A/L end. The thermal blanket and tie-downs weigh 4.5 pounds, and the upper thermal blanket support weighs 6.5 pounds.

An 11-pound weight is included in the SM design to account for electrical wires and associated harnesses needed for interconnection of the units.

Separation Analysis

During separation of the spacecraft from the aft canister, the two bodies will be in near contact for approximately 30 inches of motion, with approximately 4 inches of minimum clearance available. Consequently, a preliminary analysis was made, assuming existing separation hardware. This indicated that the use of the simplest, uncalibrated system is acceptable, and that the use of calibrated springs would further increase the margin. The parameters which were used in the analysis are:

Mass of spacecraft	40 slugs
Mass of booster	143 slugs
Transverse inertia of spacecraft	255 slug-ft^2
Relative separation velocity	2 fps

The use of six springs was assumed (spring constant = 30.5 lb/in. deflection = 3 inches). This provided a separation velocity of 2.1 fps. Using uncalibrated springs, tipoff rates and clearance changes were calculated to be as shown in Table 5. The spacecraft lateral velocity due to separation forces was calculated to be 0.08 fps, worst case, and 0.03 fps rss. This results in a clearance loss of 1.08 inches per foot of axial motion. The configuration has a 4-inch clearance available as compared to 2.7-inch minimum clearance requirement. A separation analysis, assuming that the separation springs were used in calibrated sets, reduces the clearance loss per foot from 1.08 to 0.43 inch. This is the present procedure for many spacecraft, and is a readily available technique if the additional margins are needed. Although the Flyby-Video Data SM design only uses four springs, it can be assumed they produce the effect of six springs; therefore, the analysis is valid for the Video design.

TABLE 5. SEPARATION VERTICAL VELOCITY 2 FPS, UNCALIBRATED SYSTEM

Type of Disturbance Assumed	3σ Tolerance Limit	Contributed Tipoff Rate, degrees/second	Clearance R uction per 12 inches of Axial Travel
Spring constant mismatch (10 percent)	± 3 pounds/ inch	0.95	
Initial deflection mismatch	± 0.02 inch	0.09	
Spring length mismatch	± 0.03 inch	0.05	
Lateral center of gravity to spring centroid mismatch	± 0.05 inch	0.62	
Separation devices hangup to form temporary hinge	0.007 second	0.68	
Lateral force in springs (i.e., nonvertical force)	4.5 pounds	0.46	
Σ		2.85	1.13
RSS		1.40	0.62
Lateral velocity (rss) 0.03 fps			0.46
Total rss			1.08
Available clearance 4.0 inches			

Jet Impingement Analysis

The axial jet operations prior to A/L separation constitute a potential interface problem. In this configuration, a problem of far field impingement upon the A/L heat shield may exist because the aft heat shield of the A/L is approximately 36 exit diameter from the exit. This configuration was selected for a first-order analysis of the temperature rise that might be expected in the heat shield, and the possible loss in net force of the thruster.

Rocket Research Corp. engine performance and dimensions were assumed and are summarized below:

Propellant (liquid)	Hydrazine (N_2H_4)	
Thrust	5 pounds	
Chamber pressure, p_c	120 psia (maximum)	
Chamber temperature, T_c	2260° R	
Nozzle area ratio, ϵ	40	
Nozzle exit radius, r_e	0.575 inch	
Nozzle semicone angle, θ	6 degrees	
Decomposition products (50 percent)	Specie	Mole fraction K_i
	N_2	0.28
	H_2	0.44
	NH_3	0.28

This composition was assumed frozen in flowing through the nozzle from chamber to exit plane. Therefore, at the exit plane the gas mean molecular weight m = 13.5, and the gas constant R = (1714)(29)/13.5 = 3680 ft^2/sec^2 °R. The mixture specific heat ratio, γ_{max}, was computed as 1.26. This value of γ was fixed for all plume calculations. Exit plane static pressure, temperature, and Mach number were computed from isentropic nozzle flow equations as p_e = 0.198 psi, T_e = 604°R, M_e = 4.6.

These exit plane conditions were input to an axisymmetric, inviscid method of characteristics computer program. At each computed flowfield point, the Mach number, pressures, temperature, density, velocity, and stream angle, θ, were obtained with respect to jet axis.

Jet impingement pressures and heat transfer were desired at X ≅ 36 r_e. This is sufficiently far downstream so that Newtonian hypersonic

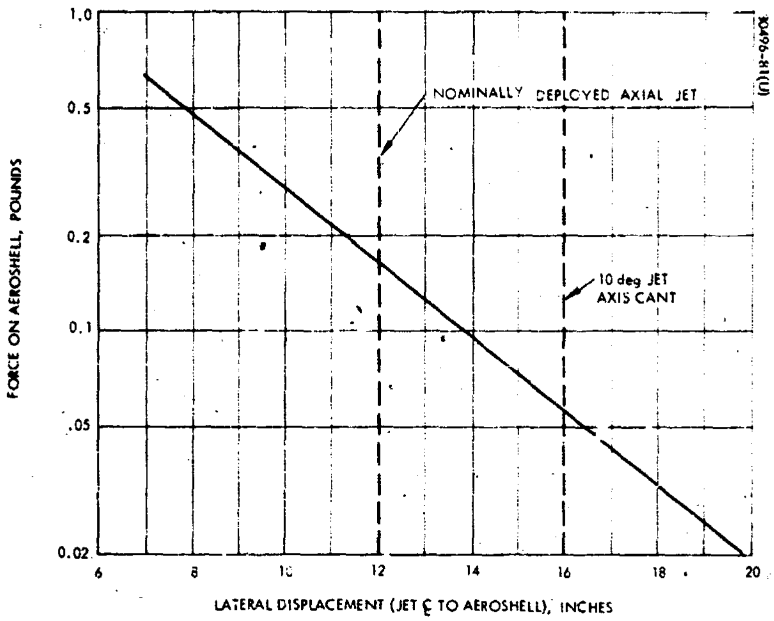

Figure 20. Reaction Force on Aeroshell Due to Axial Jet Impingement

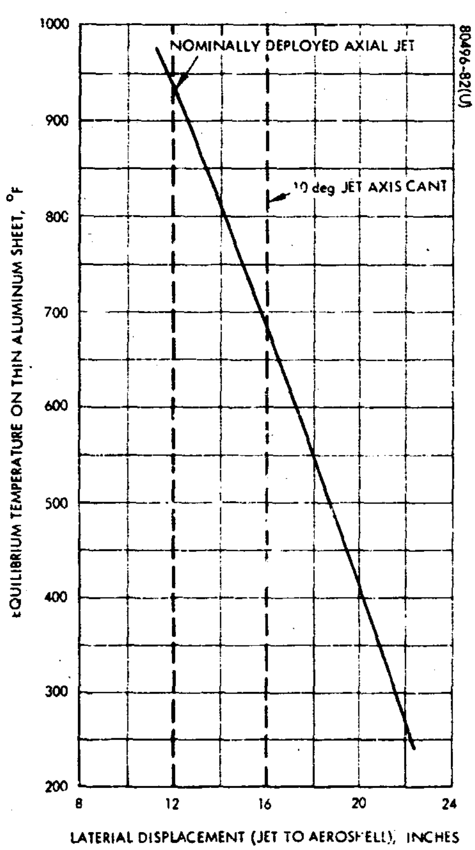

Figure 21. Aeroshell Base Heating Due to Axial Jet

aerodynamic theory is applicable. Hence, pressure on a surface normal to ℄ was calculated by the equation

$$P_{newt.} = p_e \left(1 + \gamma \; M_e^{\,2} \cos^2 \theta_e\right)$$

where $(\;)_e$ is the local free jet property which would exist at the point in the absence of any impingement surface.

These pressures were integrated over the back of the A/L configuration (assuming the back face normal to the flow), and the results are presented in Figure 20. With the configuration as drawn, the jet deploys with the thrust line parallel to the vehicle axis. In this position, the reaction force on the lander caused 0.16 pound of thrust, or 3.2 percent of the nominal thrust. Canting the nozzle 10 degrees to the axis decreases this loss to 1.5 percent. This does cause an additional loss in effective thrust of $(1 - \cos 10^\circ)$ - 1.5 percent. In either event, a loss of the 3 percent level in the effectiveness of the forward firing axial jet is to be expected. Heat transfer rates were calculated using the equation

$$\left(\frac{dQ}{dA}\right)_{JM} = \frac{\alpha \rho R V \cos\theta}{(1556)\,(32.2)} \left[\frac{V^2}{R} - \frac{\gamma}{\gamma - 1}\, T_w\right] \frac{Btu}{ft^2\ sec}$$

and converted to temperature by assuming that the heat was applied to a very thin, space viewing aluminum sheet (Figure 21). This will yield a very conservative heat rate and temperature. Even so, the indicated effect upon the aft heat shield would be small since only small areas would be involved. The effect should, however, be considered in the A/L aft heat shield design.

Mass Properties

Weights

[illegible]

TABLE 6. MSSM SUBSYSTEM WEIGHT ALLOTMENT

Item	Weight, pounds	
RF Subsystem		80.7
[illegible]-watt transmitter (2)	41.[illegible]	
40-watt transmitter (2)		
High-gain antenna (1)	14.0	
UHF antennas (16)	[illegible].0	
Turnstile antenna (2)	1.4	
S-band receiver (2)	8.0	
UHF receiver (2)	4.7	
RF switches (5)	1.5	
Coaxial cables and attach clips	5.5	
Crossed-slot omnidirectional antenna	0.5	
Diplexer (5)	3.3	
Signal Processing		36.7
Central command decoder (2)	5.7	
Central signal processor	10.0	
Command storage and sequencer (S/M)	5.0	
Sequencer (S/C)	10.0	
Propulsion		160.6
1-pound thrusters (10)	11.0	
4.7-inch diameter tanks (4)	21.6	
Valves, lines, filters, and pressurant	8.0	
Propellant (includes 11 pounds contingency)	120.0	
Flight Control		[illegible]
Flight control electronics	17.0	
Sun sensors (1)	5.1	
[illegible] sensors (4)	1.0	
Interconnect cables, connectors, and clips	4.4	
Nutation damper	2.5	
[illegible] and acceleration switch	1.0	
Structure		117.[illegible]
Upper ring	11.[illegible]	
Upper cylinder	21.[illegible]	
Central ring	11.[illegible]	
[illegible]	7.6	
Equipment wall	21.0	
[illegible] brackets and [illegible]	4.[illegible]	
[illegible] support	6.[illegible]	
Flanges	[illegible]	
[illegible] support tubes	7.6	

TABLE [illegible]. MSSM SUBSYSTEM WEIGHT ALLOTMENT - Concluded

Item	Weight, pounds	
Balance weights	4.0	
Thermal control louver (4)	1[illegible]	
Radial jet supports (2)	1.7	
Mechanisms		14.8
Separation mechanism	11.[illegible]	
SM lander 4.6		
SM adapter [illegible].8		
Axial jet deployment (2)	[illegible]	
Electrical Power		[illegible]
Solar panel (substrate, cells, interconnections)	[illegible].8	
Shunt regulator	8.5	
Battery charge regulator (1 SM, 2 [illegible])	10.[illegible]	
Battery (2)	28.3	
Total	[illegible]18.1	
Contingency	[illegible].8	
Total SM weight	[illegible]	

Table 7 lists the SM, A/L, adapter, and canister weights which sum to a total launch weight of 2025.9 pounds [illegible]. The SM weight includes the [illegible] pounds for contingencies. The difference between the [illegible] payload capability and total launch weight is [illegible] pounds. [illegible] weight [illegible] 105 pounds [illegible] allowable for SM, adapter, and canister contingencies.

Moments of Inertia

Table 8 presents the [illegible] moments of inertia (MOI) [illegible] loading conditions. The spin [illegible] (roll) to pitch MOI ratio is [illegible] 1.0 for all conditions [illegible] spinning [illegible] during the entire mission.

TABLE [illegible]. MSSM - LAUNCH WEIGHT DISTRIBUTION, FLYBY - VIDEO DESIGN

Item		Weight, pounds
Aeroshell/lander		1100.0
SM weight (includes 51 pounds contingency)		557.9
SM/booster adapter		117.2
Structure	77.2	
Umbilical	[illegible]	
Pyrotechnic separation logic	[illegible]	
[illegible]		[illegible]
[illegible]	128.8	
[illegible]	30.0	
[illegible]	[illegible]	
[illegible]		[illegible]
[illegible]		[illegible]
[illegible]	2000	
[illegible] for SM, adapter, and canisters		[illegible]

TABLE 8. MOMENTS OF INERTIA,
FLYBY-VIDEO DESIGN

Vehicle State	Slug – ft^2
A/L and SM	
Full fuel	
I_{roll}	390.9
I_{pitch}	295.2
40 percent fuel	
I_{roll}	362.2
I_{pitch}	269.2
SM	
40 percent fuel	
I_{roll}	72
I_{pitch}	57.6
Zero percent fuel	
I_{roll}	64.8
I_{pitch}	54.6

ATTITUDE AND VELOCITY CONTROL

Spacecraft stabilization and attitude control of the Mars spinning support module - aeroshell/lander (MSSM-A/L) combination and of the MSSM alone are implemented by a direct application of the components, subsystems, and techniques which have undergone extensive flight experience in spin-stabilized missions, including Syncom II and III, Intelsat I and II, and Applications Technology Satellites (ATS) I and 3. Additional flight experience for the type of stabilization and control described below is in the offing on ATS-E, AF MILCOMSAT, and Intelsat IV. The objective of the analyses and considerations presented below is to define the design and performance of the stabilization and control system with sufficient detail to establish overall mission feasibility and adequate performance margins. Specifically omitted are the mathematical derivations and theoretical background material related to subsystems, techniques, and procedures which have been flight proven or which have been extensively reported in the open literature.

Stabilization Requirements and Performance/Implementation Considerations

The stabilization requirements and the implementation and performance of the stabilization system are quite simple and straightforward. Specifically, to establish an angular momentum with adequate gyroscopic stiffness, one needs a thruster system controllable to some accuracy, a means of orienting the angular momentum to the desired attitude, and a damping system to eliminate the nutational motion caused by various maneuvers, such as spinup, despin, and re-orientation. In addition, certain design parameters such as jet alignment, thrust mismatch, and thrust level must be controlled to ensure satisfactory dynamical performance during periods of spinup or despin.

Spinup/Despin Requirements For Mission Profile

The spinup of the spacecraft is initiated by a switch which is actuated by separation of the spacecraft from the booster. The dynamical performance of the spinup process is not critical in that the induced nutation, final attitude error, and final spin error may be reasonably large without any effect on the mission performance. A 20 percent error in final spin would impose no serious limitation on stabilization performance, but significantly better accuracy is readily available from the system described below. Deviation in final attitude immediately after spinup may be as large as 7.5 degrees, and a nutation angle of several degrees would not be objectionable, since there is adequate time after spinup for nutation to be damped and for measurement and adjustment of attitude. A reasonable (several degrees) attitude error is actually to be preferred after initial spinup so that the attitude measurement subsystem and the re-orientation subsystem and procedures may be adequately checked out and exercised early in the mission. This is not to say that such a large attitude error is allowable during despin, and indeed the despin attitude performance is significantly better because of the different initial conditions.

During the cruise mode there is no change in spacecraft spin except when the propulsion system is exercised for attitude adjustment or spacecraft velocity change. Spin change resulting from control jet misalignment should not exceed 20 percent in order to preclude making spin changes during critical mission times, i.e., after the deflection maneuver, when "off-nominal" possibilities should be minimized. Nominal alignment, design, and fabrication procedures are adequate for ensuring acceptable thrust misalignment tolerances.

The second spin maneuver consists of a despin to 5 ± 1/2 rpm after re-orientation to the entry attitude. Although the spin accuracy is not critical (± 10 percent), the attitude change during despin must be kept within specific limits because this error is part of the encounter maneuver error budget which should result in a final attitude error of less than the -3 dB half-beamwidth of the high-gain antenna (2.6 degrees). An attitude error of 1.5 degrees has been alloted to the despin maneuver. All maneuvers subsequent to the entry attitude re-orientation maneuver are initiated by the on-board command sequencer. No adjustment or correction of performance is planned, all necessary command and control functions being implemented through appropriate sensors and control logic on board. The nominal value of 5 rpm for A/L entry is based entirely on lander requirements. This spin should be as high as possible in order to minimize deviations from the nominal cruise attitude upon return to that orientation.

After despin and separation from the lander, spinup to 60 ± 6 rpm is required. Again, the spin speed accuracy is not particularly significant, but attitude deviation is important. The 60 rpm value is adequate for maintaining stable pointing of the high-gain antenna while permitting re-orientation within reasonable time.

Since spinup/despin is monitored by inertial sensors, thrust level is not a significant parameter. The major components used in the spin control system should, of course, be redundant, particularly the inertial devices (accelerometer, centrifugal switch). The primary performance requirements for spinup/despin are tabulated below.

	Spin Rate, rpm	Allowable Attitude Error, degrees	Allowable Nutation Angle, degrees
MSSM A/L spinup	20 to 40	5 to 10	20
MSSM A/L despin	5 ± 0.5	1.5	10
MSSM spinup	55 to 100	0.5	1

Selection of Nominal Spin

The performance parameter to which mission success is least sensitive is probably the spin of the spacecraft. Tabulated below are the spin angular momenta of several successful spin stabilized missions.

Spacecraft	Typical Spin Angular Momentum, ft - lb - sec
Tiros I, II	8
Syncom II	24
Syncom III	34
Intelsat I	34
Intelsat II	160
Vela Hotel	480
ATS-B	900
ATS-C	780
MSSM	955

The absence of a boost rocket on the MSSM (Flyby design) eliminates one of the factors which would be instrumental in establishing a minimum spin rate. The disturbing torques sometimes encountered in earth orbit (gravity gradient, magnetic) are essentially absent in the MSSM mission, leaving only solar radiation torque to be considered. A reasonable estimate of the solar radiation torque is 3×10^{-6} ft-lb, which results in a precession rate of about 0.02 degree per day at 25 [illegible], requiring a 1-degree attitude change every 50 days or so.

The most significant parameter involved in selection of spin speed for the MSSM is the necessity of placing the axial jets at relatively large (75 inches) radii in order to preclude impingement on the aeroshell. In addition to operating at a relatively large moment arm, the axial jets operate in pairs to produce a pure couple for re-orientation so that negligible velocity is imparted to the spacecraft. The other "invariant" is the use of off-the-shelf thrusters which have a thrust range of 3 to 5 pounds. The net result is an attitude control torque of 37 to 61 ft-lb, 55 percent full tanks, at the beginning of the mission. The spin should be high enough to provide satisfactory resolution (minimum attitude increment) during re-orientation maneuvers in the presence of the relatively high control torque. A pulse width of at least 0.075 second should be used to ensure good impulse and centroid calibration data. A nominal spin consistent with the above considerations is in the range of 20 to 40 rpm for the MSSM/AL combinations, and 60 to 100 rpm for the MSSM alone. Quantitative details of the resulting performance are considered later under Re-orientation Maneuvers-Execution and Performance.

Spin Performance/Implementation

The performance of several types of spinup systems has been extensively investigated at Hughes in connection with various spin-stabilized spacecraft projects. From a flight experience standpoint, the cold gas (nitrogen) blowdown system has yielded excellent results, having been used on all Hughes satellites to date. Other systems have been considered for various missions but none has been considered superior to the cold gas system when all facts, including cost, have been considered. One of the significant factors is attitude error after spinup when starting from zero rpm. In general, the faster the angular momentum is imparted to the spacecraft, the smaller will be the attitude error after spinup. Using a low thrust system for spinup (like MSSM) results in a long spinup time, and initial transverse axis rates integrate up to much larger attitude errors. For the MSSM, the attitude error after spinup is easily corrected and does not present any problem; thus the hydrazine, low thrust spinup jets are acceptable, and no additional hardware is required other than to include the spin jets in the basic reaction control system (RCS). Existing computer programs have been utilized in this study to evaluate the dynamic performance of the proposed spinup/despin system, the results being summarized in the following pages. As expected, the initial spinup yields the largest attitude error. Despin to 5 rpm, and subsequent spinup to 60 rpm yield relatively small errors in final attitude as a result of the fact that the spacecraft angular momentum never gets too close to zero. The selection of 5 rpm for the lander spin was somewhat arbitrary and eventually will depend upon lander requirements, inasmuch as any higher value would improve despin and subsequent spinup performance, and a lower value (down to about 3 rpm) would not seriously degrade spin performance.

The design parameters affecting spin performance are summarized for each case, although the actual MSSM design may, in a few instances, differ slightly from the indicated values. These differences are not significant in overall results, and, in any event, are only representative of what a final design might be.

Some additional clarification of the terminology may be in order for the parameters summarized in the spin performance data, as follows:

β = principal axis tilt angle between principal axis of maximum moment of inertia (MOI) and the normal to the plane containing the spin jets, said plane being normal to the geometric longitudinal axis of the spacecraft

L = distance from spin nozzle plane to cg plane, both planes being normal to the geometric longitudinal (roll) axis of the spacecraft

φ = thrust vector misalignment normal to the transverse plane

γ = thrust vector misalignment in transverse plane

<u>Flyby-Video Data; Mars Lander and Module Spinup After Booster Separation</u>

<u>Typical parameters:</u>

A = roll MOI = 390 slug-ft^2

B = pitch-yaw MOI = 294 slug-ft^2

N = numbers of nozzles = 2

β = principal axis tilt = 1 degree

L = distance from nozzles to cg = 20 inches

ΔL = tolerance on L = 0.1 inch

D = nozzle position diameter = 108 inches

ϕ = angular nozzle misalignment normal to roll plane = 0.25 degree

γ = angular nozzle misalignment in roll plane = 0.25 degree

ω_t = initial tipoff rate = 1.4 deg/sec

F = thrust level per nozzle = 5 pounds

ΔF = thrust tolerance per nozzle = 4 percent

Spinup (thrusting) interval ≈ 25.4 seconds

Spin rate at end of spinup ≈ 25 rpm

RSS body fixed transverse torque (due to various error sources above) as a percentage of the available spinup torque ≈ 2 percent

Nutation angle resulting from spinup ≈ 0.8 degrees (body nutation rate = 9.2 rpm)

Attitude error resulting from spinup ≈ 6.0 degrees (inertial nutation rate 37.4 rpm)

Time delay between separation start and spinup start ≈ 2 seconds

Attitude error resulting from time delay and tipoff rate ≈ 2.8 degrees

Total attitude error ≈ 7.5 degrees

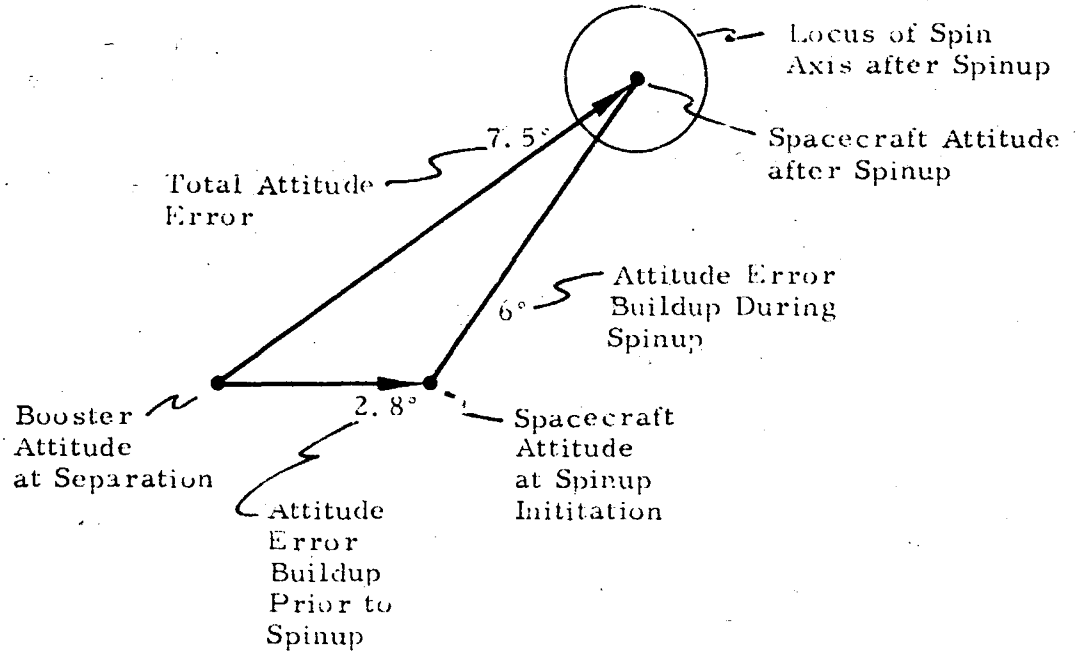

Flyby-Video Data; Mars Support Module Spinup After Lander Separation

Typical parameters:

A roll MOI = 71.5 slug-ft^2

B = pitch-yaw MOI = 37.4 slug-ft^2

N = number of nozzles = 2

β = principal axis tilt - 0.5 degree

L = distance from nozzles to cg = 10 inches

ΔL = tolerance on L = 0.1 inch

D = nozzle position diameter = 108 inches

ϕ = angular nozzles misalignment normal to roll plane = 0.25 degree

γ = angular nozzle misalignment normal to roll plane = 0.25 degree

ω_s = initial spin rate = 5 rpm

θ_o = initial nutation angle - 1 degree

F = thrust level per nozzle = 4 pounds

ΔF = thrust tolerance per nozzle = 0.16 pound (4 percent)

Spinup (thrusting) interval = 11.4 seconds

Spin rate at end of spinup = 60 rpm

RSS body fixed transverse torque (due to various error sources above) as a percentage of the available spin torque = 1.1 percent

Nutation angle after spinup = 0.25 degree (body nutation rate = 54 rpm)

Attitude change resulting from spinup < 0.2 degree (inertial nutation rate = 114 rpm)

Flyby-Video Data; Mars Lander and Module Despin Prior to Separation

Typical parameters:

A = roll MOI = 381 slug-ft^2

$B \equiv$ pitch-yaw MOI = 289 slug-ft^2

$N \equiv$ number of nozzles = 2

$\beta \equiv$ principal axis tilt - 1 degree

$L \equiv$ distance from nozzles to cg = 20 inches

$\Delta L \equiv$ tolerance on L = 0.1 inch

$D \equiv$ nozzle position diameter = 108 inches

$\phi \equiv$ angular nozzle misalignment normal to roll plane = 0.25 degree

$\gamma \equiv$ angular nozzle misalignment in the roll plane = 0.25 degree

$\omega_s \equiv$ initial spin rate = 25 rpm

$\theta_o \equiv$ initial nutation angle = 0.9 degree

$F \equiv$ thrust level per nozzle - 4 pounds

$\Delta F \equiv$ thrust tolerance per nozzle = 0.16 pound (4 percent)

Spindown (thrusting) interval ≈ 26.6 seconds

Spin rate at end of spindown ≈ 5 rpm

RSS body fixed transverse torque (due to various error sources above) as a percentage of the available spindown torque = 2 percent

Nutation angle resulting from spindown ≈ 6.2 degrees (body nutation rate = 1.54 rpm)

Attitude change resulting from despin ≈ 1.5 degree (inertial nutation rate = 6.4 rpm)

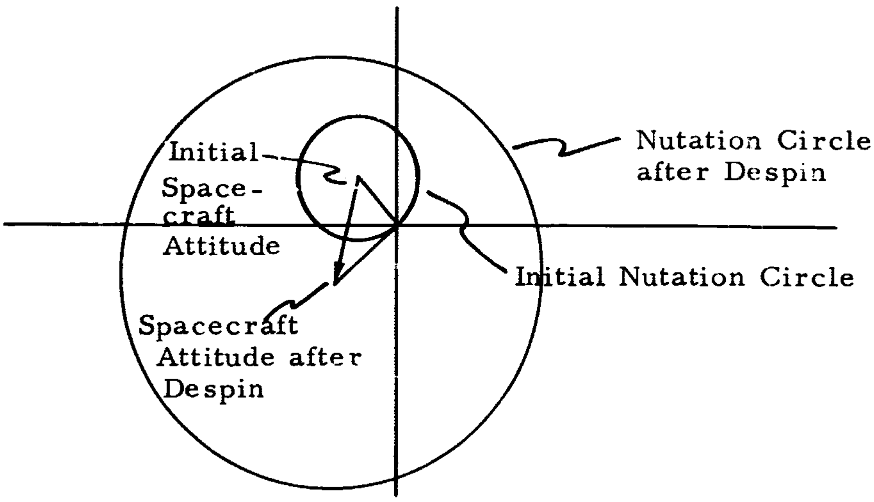

The spin control electronics are shown in Figure 22. At the separation switch signal, spinup is initiated. Command backup is available if needed. Spinup is terminated by an accelerometer signal, and command backup is also available. The despin command changes the accelerometer gain to 60 rpm and initiates the despin to 5 rpm, which is sensed by a centrifugal switch. Module separation is delayed after despin to provide nutation damping, and spinup of the module is delayed to ensure clearance from the lander. The "enable separation" command comes from the SM sequencer.

Nutation Damping Requirements/Implementation

The application of the passive, mercury tube nutation damper to stable, spin-stabilized configurations has been so successful it should pose no problem for the MSSM mission. A nutation damper will be required, and the time constant may be in the range of 5 to 20 minutes for the MSSM/AL combination and the MSSM alone. That a single damper may not be adequate for both configurations has been established by a computer program utilized for the design of such dampers. The time constants are 5 minutes and 40 minutes for the MSSM/AL combination and the MSSM, respectively. Further parametric studies would be required here. In any event, satisfactory performance could be obtained by using two dampers approximately 18 inches long, 1-inch in diameter, and weighing 1.2 pounds each.

Attitude Control System Design and Performance

The use of control jets pulsed in synchronism with the spin to re-orient the spin axis has accumulated many satellite years of flight experience. The application of these proven components, techniques, and procedures to the MSSM mission is a design exercise consisting primarily of the selection of a satisfactory combination of design and performance parameters within the framework of existing hradware wherever possible. From the standpoint of system design, there is no sharply defined optimum such as minimum weight, minimum power, minimum size, and so forth, and the great flexibility in performance afforded by the variable pulse width capability allows much latitude in design requirements. A basic aspect of spin stabilization performance is that the spin axis is never very far from where it was the last time its attitude was known – a fact which often permits a relaxed confidence in mission operations. Furthermore, failure modes in the attitude control system are inherently less disastrous for spin-stabilized spacecraft than they are for three-axis stabilized spacecraft. An open or leaking jet or the saturation of a reaction wheel can play havoc with a three-axis stabilization system, whereas an open jet hardly perturbs a spin-stabilized vehicle. The spin-stabilized versus three-axis stabilized comparison has been made many times with varying conclusions depending upon the mission, the payload, the point of view, ground rules, and so on. A detailed comparison here would require a specific design study of a three-axis system, which is not available for this mission. Quantitative comparisons of the two approaches are, therefore, not considered in this discussion. It should be noted that the specific design parameters discussed below might be altered somewhat were it necessary to meet specific performance requirements in several areas. Lacking definitive specifications, the design effort was centered around meeting somewhat broadly defined mission objectives and included adequate flexibility for particular performance variations without affecting hardware design, cost, or mission operations.

Functional Description and Overall System Design Characteristics

Attitude control for a spin-stabilized spacecraft is a matter of providing transverse torque pulses in a desired average inertial direction to "precess" the angular momentum vector. This precession of the angular momentum vector is accompanied by a bounded nutational motion (i.e., a coning of the spin axis about the angular momentum vector). The attitude control system design must consider this nutational motion as well as the precession of the angular momentum vector, while minimizing the velocity imparted to the spacecraft. The heart of the attitude control system (and the velocity control system) is a propulsion system capable of being electronically controlled and having a predictable accuracy in flight, as defined by calibration data taken during flight acceptance tests. Specific design and performance of the propulsion system are presented in more detail, but for the present, only the control aspects are considered. Attitude and velocity control, while operationally similar from the control aspect, are functionally different for the mission, and are thus treated separately.

In view of its mission-critical role, the attitude control system (and velocity control system) are redundantly implemented, for the most part. For attitude maneuvers, an axial jet pair is operated in opposing directions to produce a couple which does not contribute to translational velocity, except for a small mismatch in thrust. There are two pairs of axial jets, as illustrated in Figure 23, which is a schematic of jet arrangement and alignment. All axial jets are aligned with their thrust axes parallel to the nominal spin axis of the spacecraft and are radially positioned so that there is no difficulty with plume impingement on the A/L.

Control of the axial jets for attitude maneuvers is effected by an electronic system which has been flight proven many times, and since its inception at Hughes in 1959, has been known as the JCE (jet control electronics). The heart of this electronic control system is a synchronous controller that provides control jet pulses of any desired duration, spaced one spin period apart, and starting at any desired point in the spin cycle relative to a plane containing the spin axis and the sun. This "start angle" remains constant during any particular maneuver, even though the plane containing the spin axis and the sun line is moving during the maneuver. Such a mode of precession is called rhumb line precession, and is considered in greater detail. The operational essence of the precession maneuver is that a given initial attitude and a desired final attitude explicitly define the "start angle" for the jet control pulses.

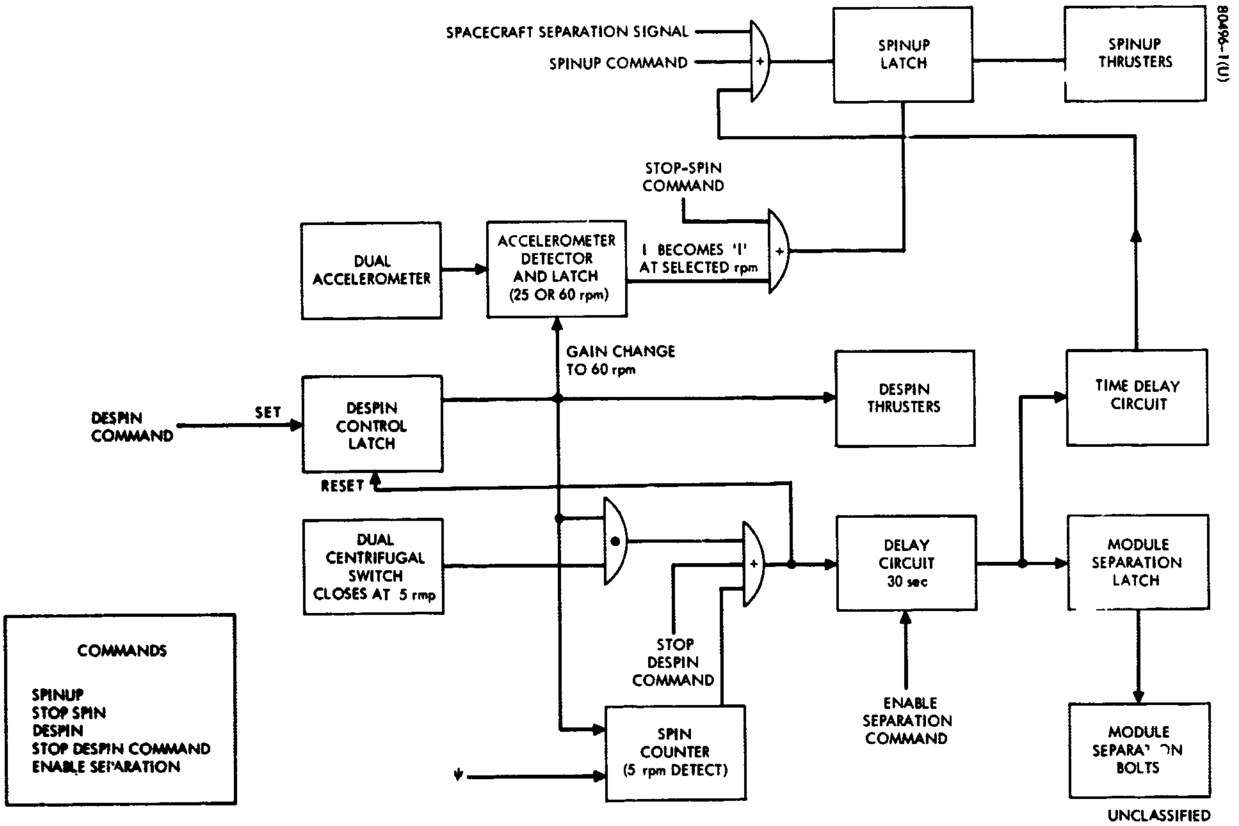

Figure 22. Spinup/Despin System

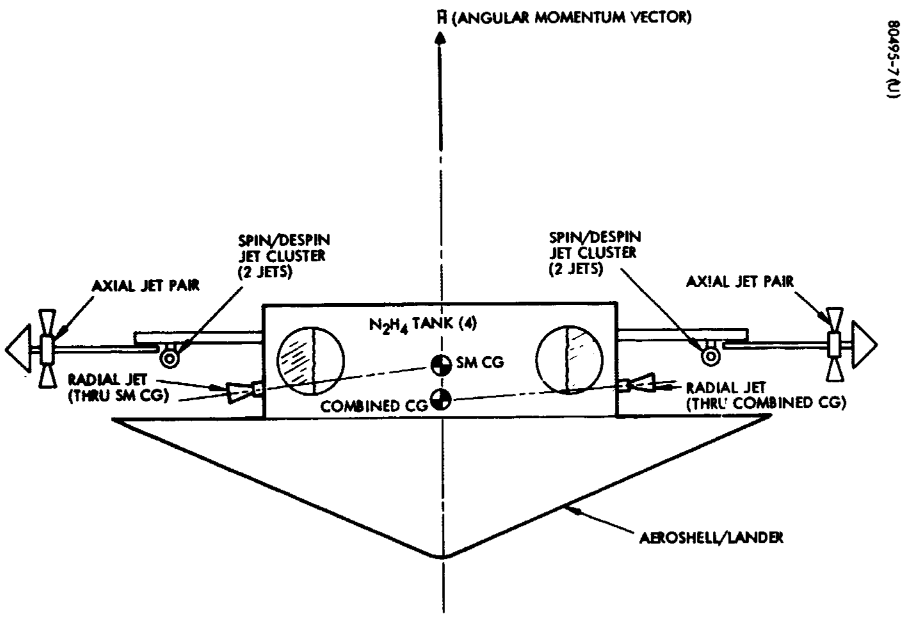

Figure 23. General Arrangement of Reaction Control Subsystem

Jet Control Electronics. The electronic circuitry associated with the orientation control and velocity control subsystem includes signal amplifiers for the sun sensors, power switches for the jet control valves, and data processing circuits for selecting and operating the various control modes. JCE for spin-stabilized spacecraft, as defined herein, have experienced many satellite years of trouble-free operation in eight satellites launched over the period 1961 to 1968. Although the details of the command and control circuitry for the MSSM differ slightly from previous systems, the basic circuits remain unchanged.

The primary control element is a phase-locked loop containing a counter synchronized with the spin. The counter is reset to zero each revolution by a sun sensor pulse (ψ-pulse). Beginning with the ψ-pulse, the counter (controlled by the voltage-controlled oscillator (VCO) proceeds to count 512 pulses (nominally) before the next ψ-pulse occurs. If more or less than 512 pulses are counted during the spin period, the error is detected by an analog error detector that adjusts the oscillator frequency so that the synchronous counter is never more than one count in error out of 512 counts. When the counter counts exactly 512 pulses between successive Ψ-pulses, the loop is in lock. Operations which depend on the phase-locked loop synchronous signals will operate only if the loop is in lock. In addition to providing a synchronous reference frequency for pulse mode operation of control jets, the JCE provides for starting a jet pulse at any desired angle from a sun pulse and terminating the jet firing at any desired angle. The jet firing angle register and the pulse width controller (Figure 24) accept commands for axial jet operation. In addition to the jet start angle and jet pulse width, the control circuitry accepts a pulse number command which results in the enable jet latch being reset when the selected jet has fired the commanded number of pulses. (See "Reset A" signal in Figure 24.) Note that the pulse width controller operates with the axial jets only, the radial jet pulse width being fixed at 90 degrees. The firing angle (start angle) command may, of course, apply to any jet, depending upon the condition of the enable jet latches. Angular resolution for jet fire start angle is $360 \div 512$ or 0.7 degree, and the start angle error is a maximum of ± 0.35 degree.

For continuous mode operation of the axial jets, the firing duration "clock" is the satellite spin, whose period is precisely known from ground station processing of Ψ-pulse data. The number of spin periods of continuous firing to produce the desired axial ΔV is stored by command in the spin period counter, which resets the enable axial jet latch after the required number of periods. (See "spin reset" on Figure 24.) The resolution on axial jet continuous firing is one spin period, which corresponds to a ΔV resolution of 0.05 fps. Note that axial jets always operate in pairs which are selected by the control mode circuit logic — two jets firing in opposite directions to produce a pure couple for re-orientation without ΔV, and two jets firing in the same direction to produce ΔV with no transverse torque. The latter capability is not essential, but is convenient for the circuitry needed to fire jet pairs for re-orientation.

Nominal operation of the jets is controlled by the phase-locked loop (for pulse mode operation) and by the spin period counter for continuous mode operation (axial jets only). The function of the JCE (nominal mode) may be summarized by the following list of commands which operate the system:

1) ≡ jet start angle magnitude

2) ≡ pulse number

3) ≡ pulse width (axial jets only)

4) ≡ jet select

5) ≡ continuous fire (axial jets only)

6) ≡ spin period count

7) ≡ enable axial jets

8) ≡ enable radial jets

Given the above system, a simple, reliable, inexpensive back-up mode of operation is available in the event of failure in the phase-locked loop or in some other particular components of the JCE system. This back-up system, called the quadrant mode system, requires some additional logic circuitry and two additional sun sensors (Ψ-pulse only), and is essentially independent of the nominal JCE system. The quadrant mode system requires fewer commands to operate, has significantly fewer parts and less complexity, is less expensive, and has also had successful flight testing (Syncom II). It was discarded as the primary mode of control mainly because of reduced accuracy in re-orientation and ΔV maneuvers, but was considered adequate for a back-up mode. An alternate approach would be to simply use two of the primary JCE described above.

The Ψ-simulator represents a rate memory mode which, when the spin axis is within 10 to 15 degrees of the sun line, is switched into the system to provide pseudo Ψ-pulses until more favorable sun angle geometry is again established.

Quadrant Mode Control. Given the primary jet control system described above, a back-up mode of synchronous pulsing operation is readily available with the addition of two sun sensors and some logic circuitry. This back-up mode would be utilized only in the event of failure in the synchronous controller and is called the quadrant mode, a simple technique which requires less complexity on-board and allows for reduced command and control requirements. Figure 25 defines the basic attitude control geometry. A cone of half-angle ϕ is defined by the sun line and the spacecraft angular momentum vector, H. A transverse torque pulse of magnitude M and duration Δt is applied, the effective center of the torque pulse occurring

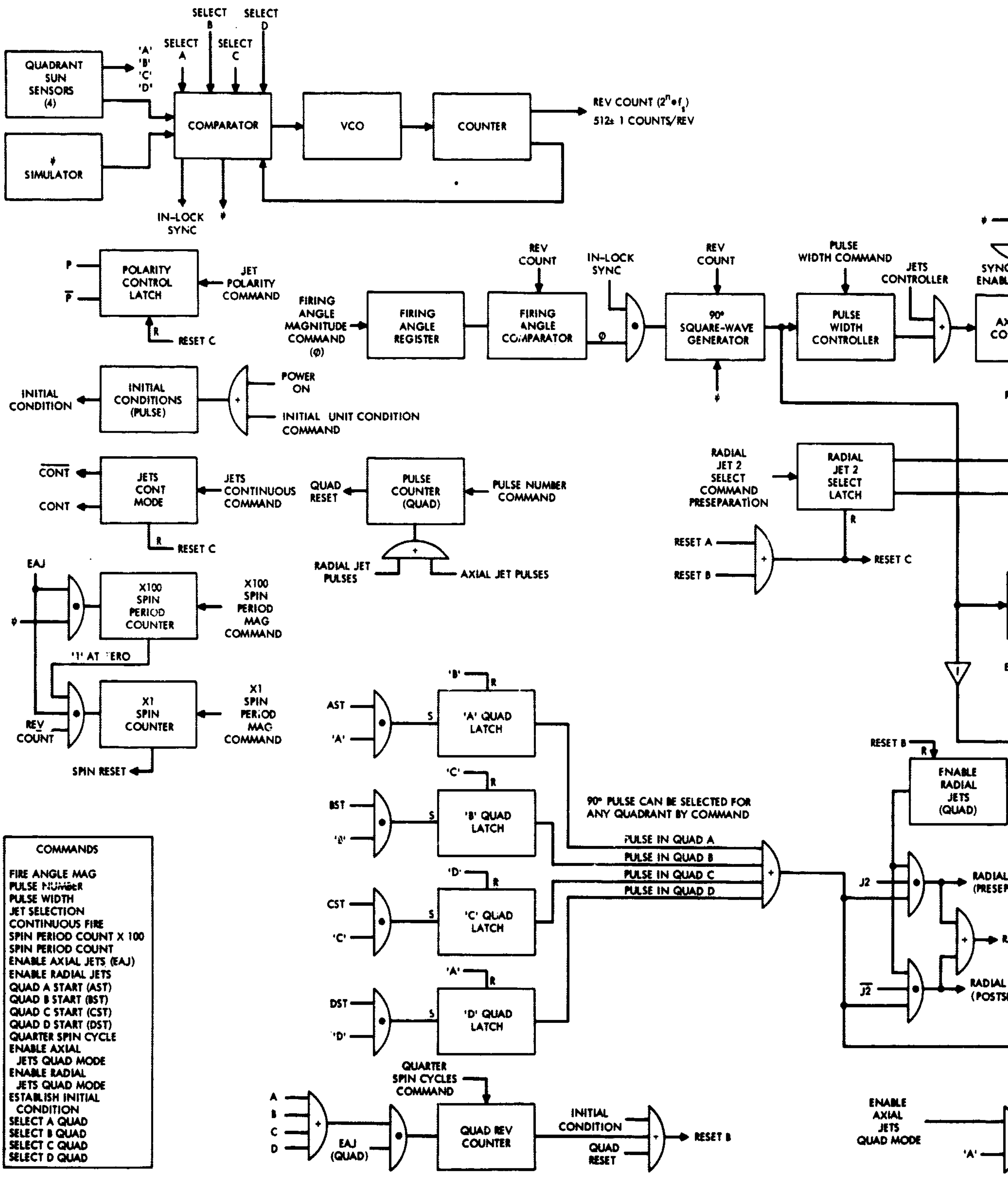
QUADRANT SUN SENSORS (4)
'A' 'B' 'C' 'D'
SIMULATOR
SELECT A
SELECT B
SELECT C
SELECT D
COMPARATOR
VCO
COUNTER
REV COUNT
512± 1 COUNTS/REV
IN-LOCK SYNC
POLARITY CONTROL LATCH
JET POLARITY COMMAND
RESET C
FIRING ANGLE MAGNITUDE COMMAND (φ)
FIRING ANGLE REGISTER
FIRING ANGLE COMPARATOR
90° SQUARE-WAVE GENERATOR
PULSE WIDTH COMMAND
PULSE WIDTH CONTROLLER
JETS CONTROLLER
INITIAL CONDITION
INITIAL CONDITIONS (PULSE)
POWER ON
INITIAL UNIT CONDITION COMMAND
CONT
JETS CONT MODE
JETS CONTINUOUS COMMAND
QUAD RESET
PULSE COUNTER (QUAD)
PULSE NUMBER COMMAND
RADIAL JET PULSES
AXIAL JET PULSES
RADIAL JET 2 SELECT COMMAND PRESEPARATION
RADIAL JET 2 SELECT LATCH
RESET A
RESET B
EAJ
X100 SPIN PERIOD COUNTER
X100 SPIN PERIOD MAG COMMAND
X1 SPIN COUNTER
X1 SPIN PERIOD MAG COMMAND
SPIN RESET
AST
BST
CST
DST
'A' QUAD LATCH
'B' QUAD LATCH
'C' QUAD LATCH
'D' QUAD LATCH
90° PULSE CAN BE SELECTED FOR ANY QUADRANT BY COMMAND
PULSE IN QUAD A
PULSE IN QUAD B
PULSE IN QUAD C
PULSE IN QUAD D
ENABLE RADIAL JETS (QUAD)
J2
QUARTER SPIN CYCLES COMMAND
QUAD REV COUNTER
EAJ (QUAD)
ENABLE AXIAL JETS QUAD MODE
COMMANDS
FIRE ANGLE MAG
PULSE NUMBER
PULSE WIDTH
JET SELECTION
CONTINUOUS FIRE
SPIN PERIOD COUNT X 100
SPIN PERIOD COUNT
ENABLE AXIAL JETS (EAJ)
ENABLE RADIAL JETS
QUAD A START (AST)
QUAD B START (BST)
QUAD C START (CST)
QUAD D START (DST)
QUARTER SPIN CYCLE
ENABLE AXIAL JETS QUAD MODE
ENABLE RADIAL JETS QUAD MODE
ESTABLISH INITIAL CONDITION
SELECT A QUAD
SELECT B QUAD
SELECT C QUAD
SELECT D QUAD

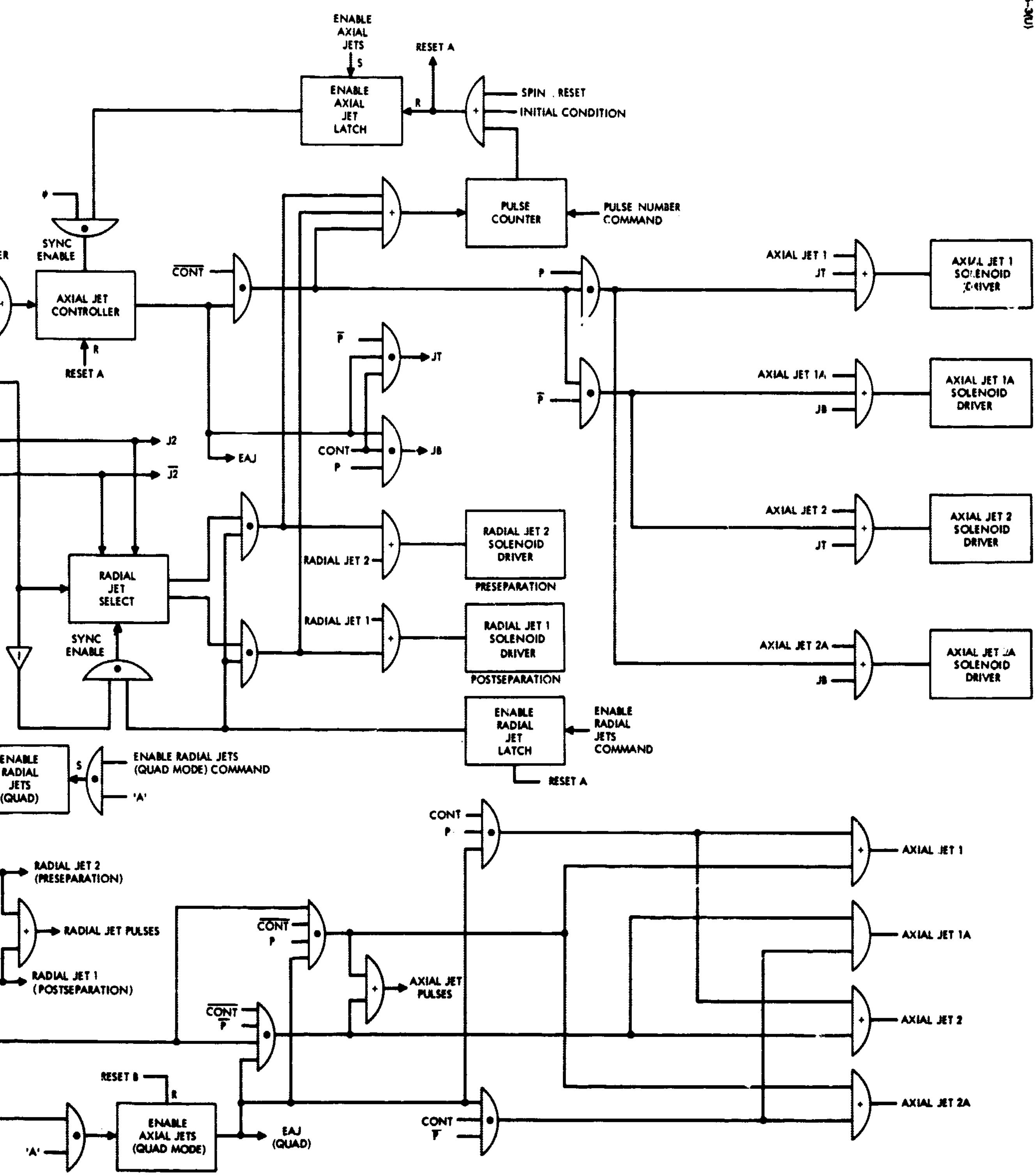

Figure 24. Jet Control Electronics

PRECEDING PAGE BLANK NOT FILMED.

at an angle Ψ from the plane containing the spin vector and the sun line (see figure). The result is a change, dP, in angular momentum vector orientation and a corresponding change, $d\phi$, in the "sun angle" ϕ.

For reasons explained later, the torque pulse angle, Ψ, is restricted to the following fixed values:

$$\Psi = \pm \frac{\pi}{2}$$

and

$$\Psi = 0, \pi$$

If $\Psi = 0$, the H vector will precess toward the sun line. If $\Psi = \pi$, the H vector will precess away from the sun line. Thus, no matter what the attitude of the spin axis, it will precess either toward or away from the sun line, depending upon Ψ being 0 or π.

If a series of torque pulses are applied at constant $\Psi = \pi/2$, the H vector will generate a cone around the sun line at constant ϕ. For $\Psi = -\pi/2$, the direction of travel of H is simply reversed, but again ϕ is constant. Figure 25 contains all of the spin axis precessing geometry necessary for the mission. Only two modes of precession are available for the back-up quadrant mode, and all "maneuvers" are made by an appropriate combination of the two modes.

Figure 26 illustrates a typical attitude maneuver. It is clear that there is a preferred order of the precession mode which minimizes maneuver time. If ϕ_2 is smaller than ϕ_1, the $\Psi = 0$ mode is performed first, then the $\Psi = \pi/2$ or $\Psi = -\pi/2$ mode is executed. The converse is true if ϕ_2 is larger than ϕ_1; then the $\Psi = \pm \pi/2$ mode is executed first, followed by the $\Psi = \pi$ mode. The torque pulse width is 90 degrees of spin, allowing four simple sun sensors to easily control any desired maneuver.

Consider four Ψ-pulse sensors symmetrically placed around the periphery of the spacecraft as indicated in Figure 27. The jet control function of the sensors is very simple. Depending upon which of the four modes of precession is desired, <u>one</u> of the sensors is selected to <u>start</u> the jet pulse each revolution. The succeeding sun sensor pulse always turns the jet off. Thus, there is available a 90-degree pulse which produces a torque in one of four possible directions. For example (using jet No. 1), if sensor "a" turns the jet on, sensor "b" will turn it off. The result is a torque pulse whose average direction during its 90 degrees of rotation is away from the sun ($\Psi = \pi$ mode). To precess toward the sun, sensor "c" would turn the jet on and sensor "d" would turn it off ($\Psi = 0$ mode). The $\Psi = \pi/2$ mode would use sensor "d" for jet initiation and sensor "a" would cause turn-off. The following tabulation lists all possible modes.

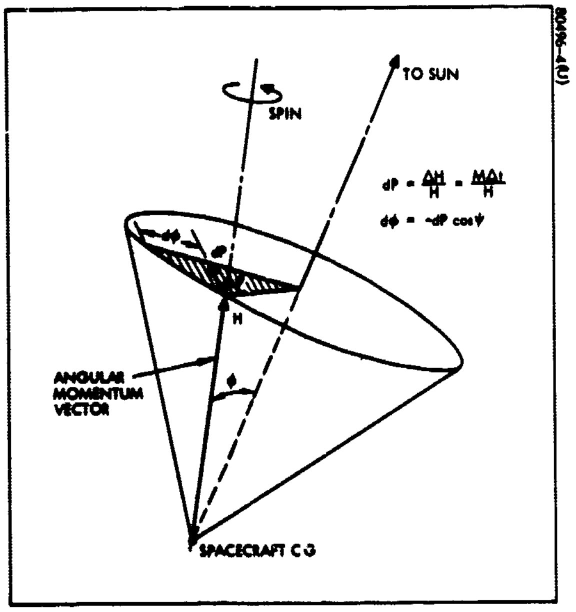

Figure 25. Spin-Axis Attitude Control Geometry

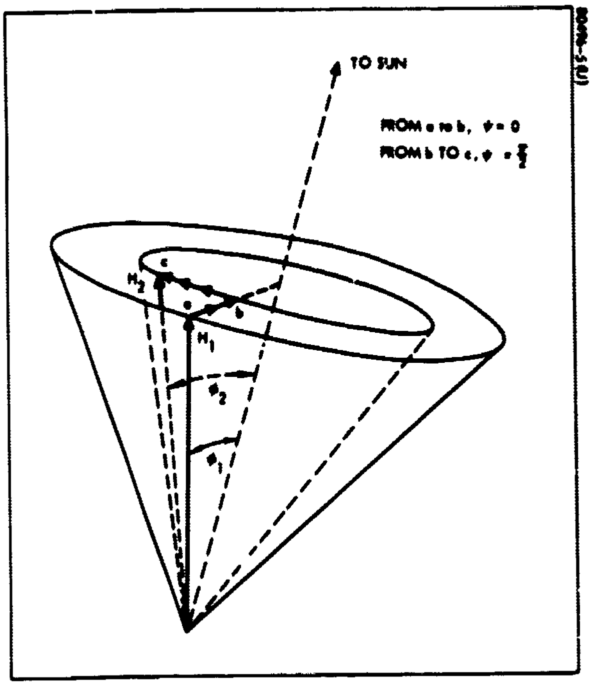

Figure 26. Reorientation Maneuver Using Two Modes of Precession

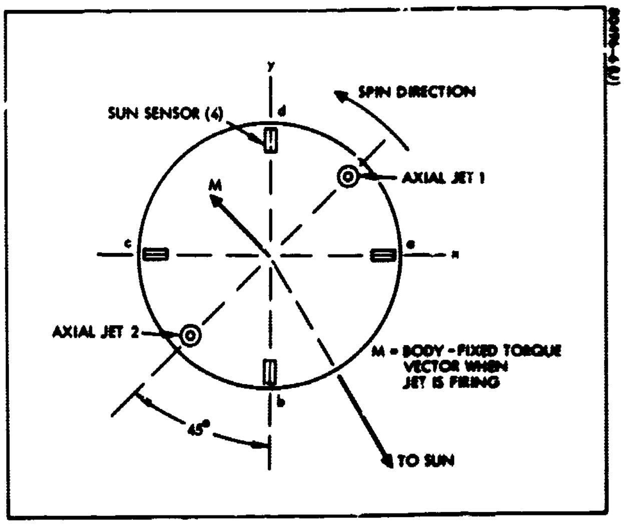

Figure 27. Quadrant Mode Arrangement of Sun Sensors and Jets

	$\Psi = 0$		$\Psi = \pi$		$\Psi = \pi/2$		$\Psi = -\pi/2$	
Jet number	1	2	1	2	1	2	1	2
Sun sensor	c	a	a	c	d	b	b	d

The on-board command and control logic would be set up to receive the following commands:

1) Select jet for attitude maneuver
2) Select mode (Ψ- mode) for first precession
3) Select jet start sun sensor
4) Select number of pulses for first precession
5) Select Ψ - mode for second precession
6) Select jet start sun sensor
7) Select number of pulses for second precession

The above simple commands are stored and verified prior to a maneuver, and the execute command is then sent at the appropriate time, taking into account the long delay time in propagation. The seven commands above may be retained for re-execution (reverse the order of the Ψ - modes) to return the spin axis to very nearly the original attitude (cruise attitude) which existed prior to the maneuver, at which point the star sensor would be available for precise determination of attitude, after which a "touch-up" maneuver may be made if desired.

An alternative to the quadrant mode is to simply provide complete redundancy in the JCE. In this case, only two sun sensors would be used, one for each JCE. Whether to use two JCE or one JCE and one quadrant mode system is a design choice which may be made in a subsequent phase of the study.

Attitude Determination – Sensors and Performance

The spacecraft attitude is determined by finding the angle between a spacecraft reference axis (the spin axis) and two celestial bodies. The sun and the star Canopus have been selected for this mission. The star Canopus is a particularly desirable navigation star because it is very bright (-0.9 magnitude), it is close to the ecliptic south pole, and is in a sector of the heavens where there are few bright bodies.

The spacecraft attitude is not explicitly required for implementing the on-board control function. The output of the sun sensors and the star sensor

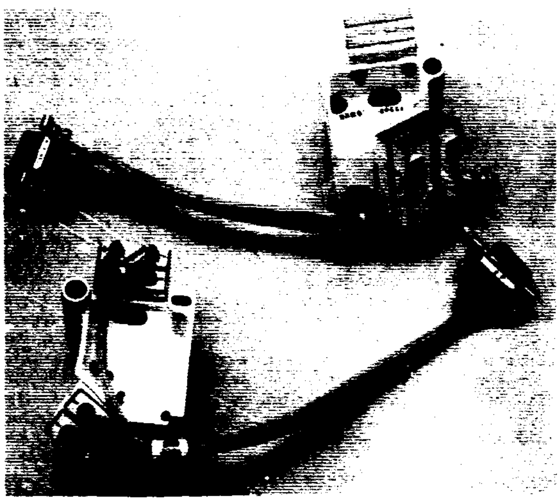

Figure 28. Sun Sensor Assemblies (Photo A11836)

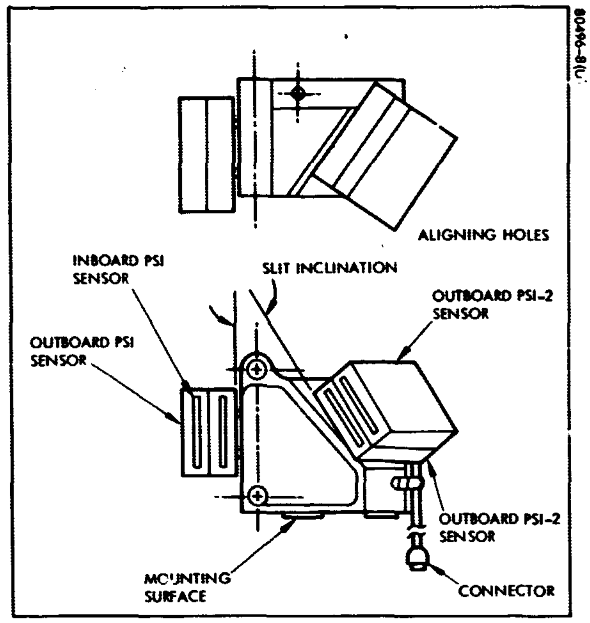

Figure 29. Sun Sensor Assembly Details

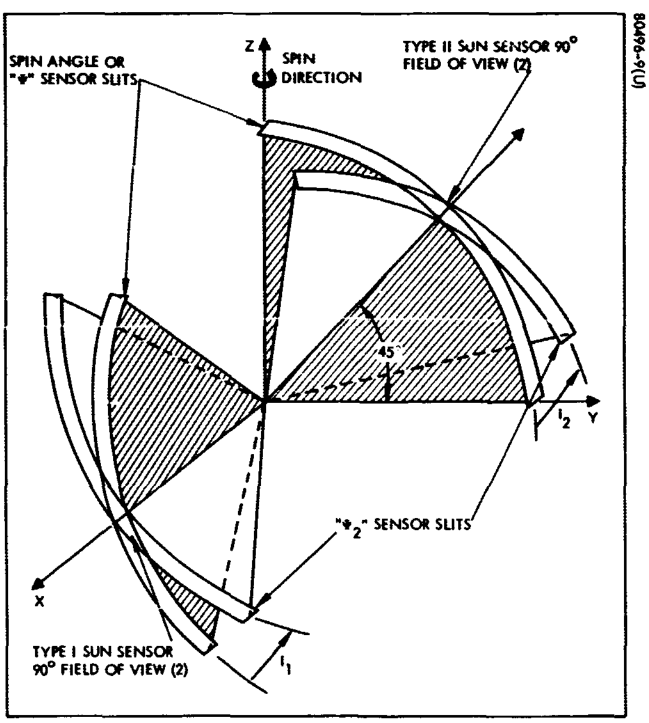

Figure 30. Sun Sensor Geometry

are telemetered to mission control where the attitude is computed. Necessary attitude correction commands (jet start angle and number of pulses) are then transmitted to the spacecraft. The on-board timing cycle is based on the spin period, which is simply the time between sun pulses from a given sun sensor.

The attitude of the spacecraft can be determined, provided the spin axis is no less than 15 degrees from the sun and is no more than 5 degrees out of the ecliptic plane, based on a 20-degree field of view for the star sensor. If either or both of these conditions is violated, a programmed search maneuver is initiated until the sun and Canopus are visible.

The attitude of the spacecraft can be determined to better than 0.5 degree.

Sun Sensors. The sun sensor assembly consists of four identical units mounted on a precision bracket (Figures 28 and 29). Two sensors are mounted 90 degrees with respect to the spin axis, and two are mounted at 45 degrees with respect to the spin axis (Figure 30). The bracket and sensor assemblies are painted with a special white paint which has low absorptivity in the solar spectral range and high emissivity in the infrared spectral range to ensure that sensor temperatures do not rise above 100° F. Each sensor consists of an n/p silicon photovoltaic cell, a load resistor, and two clam-like aluminum shells (Figure 31). The cells are bonded to the housing with an epoxy-fiberglass combination used to bond solar cells to the solar panel substrates on the Early Bird and ATS satellites.

A narrow gap between the clam shells defines the fan-shaped field of view of the sensor. The shims placed between the two aluminum sensor halves at the three screw locations determine the width of the sensor slit, which is 0.007 to 0.008 inch. This width, in conjunction with the 32-minute angular size of the sun, results in a nominal pulse width of approximately 1.25 degree (Figure 32). The field of view of each cell is ±75 degrees from the normal to the cell surface.

Each unit produces pulse pairs once per revolution (Ψ and Ψ_2 pulses). The Ψ and Ψ_2 pulses are telemetered to ground (after appropriate shaping). With both prelaunch and in-flight calibration of the unit, and by smoothing the data over a number of measurements, the sun angle uncertainty can be reduced to 0.2 degree.

The equation which relates the Ψ, Ψ_2 pulses to the sun angle Φ for a sensor mounted 90 degrees from the spin axis is

$$\cot \Phi = \cot I \sin (\Psi - \Psi_2 - 35 \text{ degrees}) \qquad (6)$$

where Φ is the angle between the spin axis and the sun sensor.

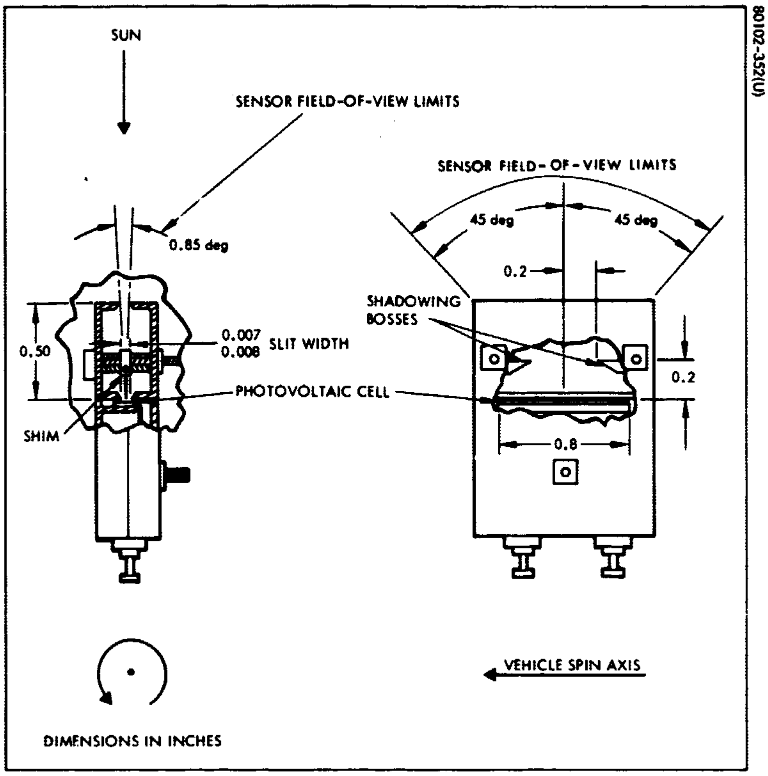

Figure 31. Schematic Diagram of Sensor Unit

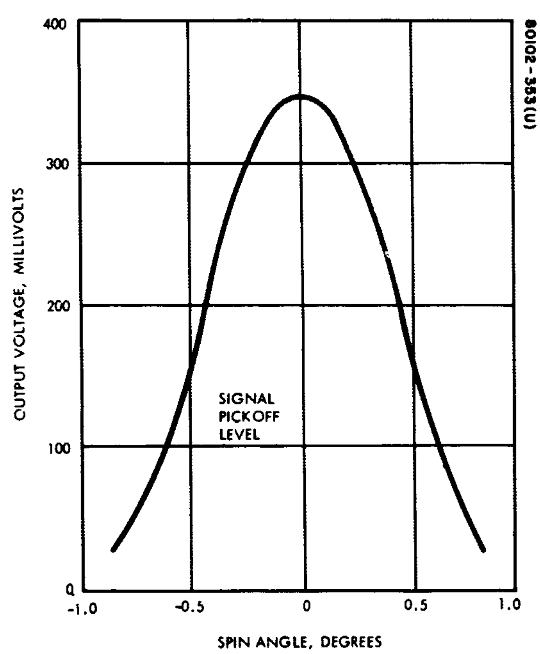

Figure 32. Typical Sun Sensor Output Pulse

I is the inclination of the Ψ_2 sensor half with respect to the Ψ sensor half, and 35-degrees is the angular separation, in a spin sense, to preclude the Ψ and Ψ_2 pulses coinciding when ϕ = 90 degrees.

Inspection of Equation 6 indicates that the minimum sun angle detectable is equal to the slit inclination angle, I. Hence, if a minimum sun angle of 15 degrees is desired, the slit inclination angle must be reduced to at least 15 degrees. This is considered undesirable because the error in sun angle increases sharply as slit inclination decreases (Figure 33).

This problem can be alleviated by mounting sun sensors at 45 degrees as well as 90 degrees with respect to the spin axis.

The minimum detectable sun angle is plotted as a function of slit inclination on Figure 34 for both the 45- and 90-degree mounting case. It is seen that some benefit is obtained for the 45-degree mounting case. For a minimum detectable sun angle of 15 degrees, a slit inclination angle of 21 degrees is required.

The principal physical characteristics of the sensor assembly are tabulated below. High reliability is obtained, since only two components with relatively low failure rates are used, and two sensor assemblies are incorporated in the spacecraft design.

Weight	0. 25 pound assembly
Power	None
Reliability	0. 9999 per Ψ and Ψ_2 pair (7 years)
Accuracy	0. 5 degree unsmoothed data
	0. 2 degree smoothed and calibrated data
Slit inclination	21 degrees

Figure 33 shows plots of the sun sensor error coefficients for the 45- and 90-degree mounting cases.

The error coefficient curves are used in determining the total error in apparent sun angle which results from errors in Ψ - Ψ_2 pulse and slit inclination

The following example gives typical sun sensor attitude errors.

Sun angle = 60 degrees; Sensor mounting = 45 degrees; I = 21 degrees

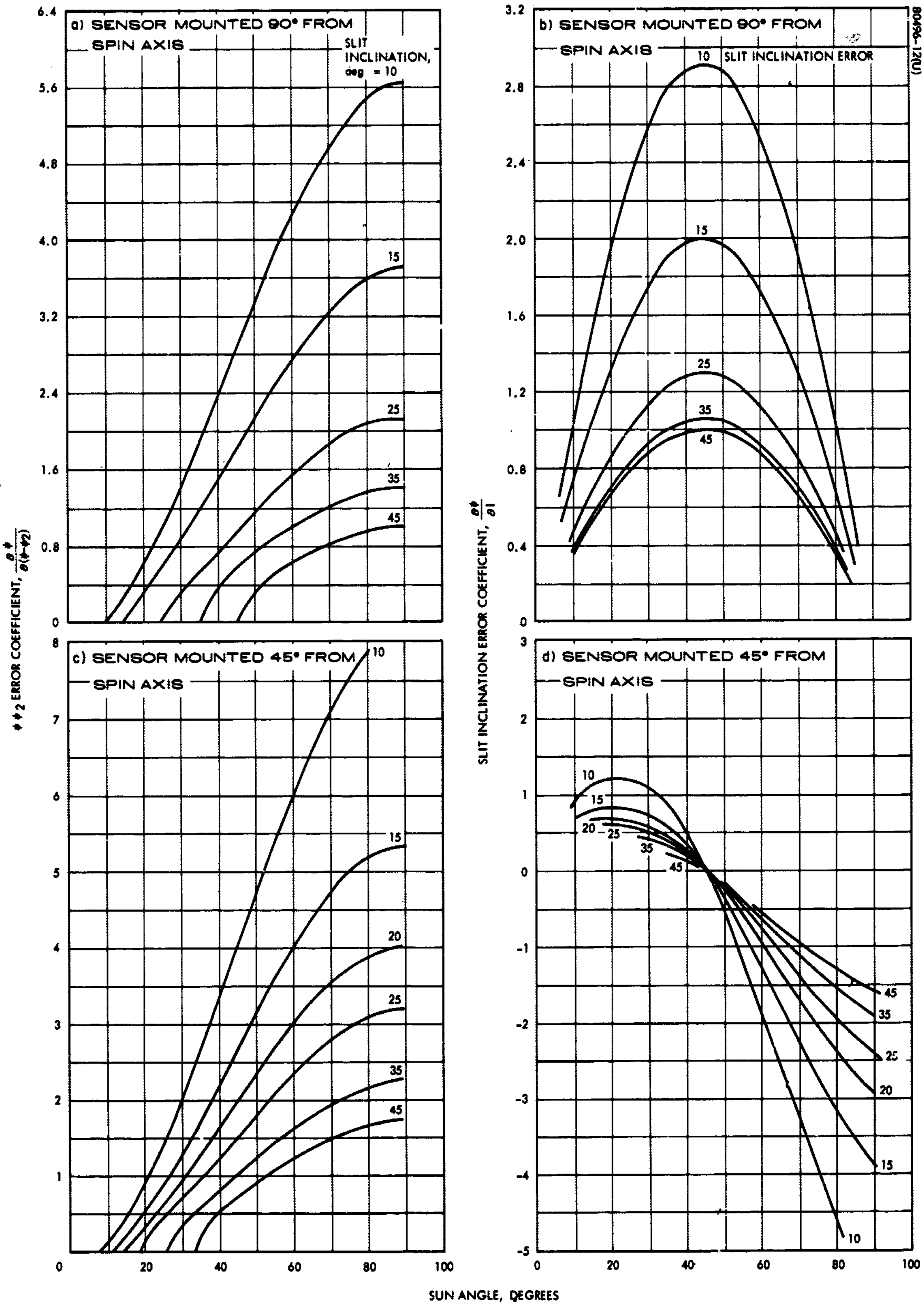

Figure 33. Sun Sensor Error Coefficient

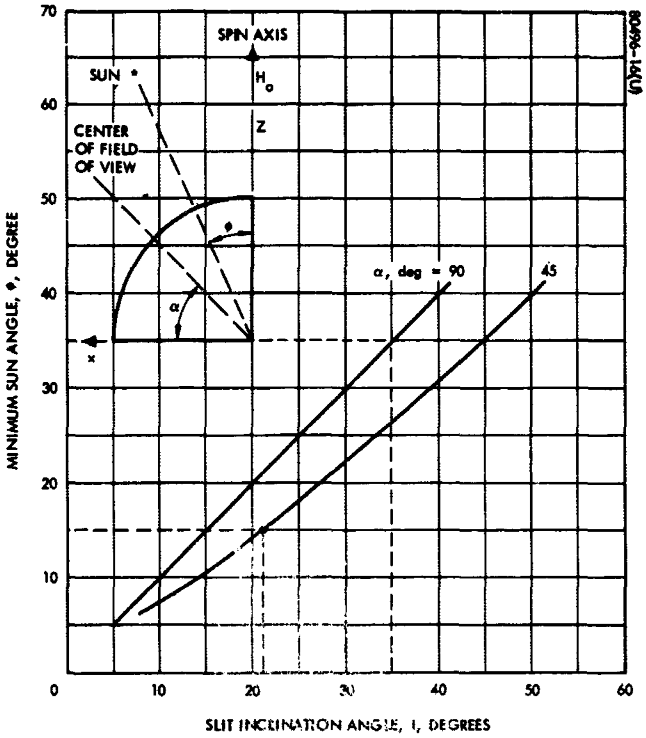

Figure 34. Minimum Sun Angle as Function of Slit Inclination

Sun sensor 45 degrees from spin axis

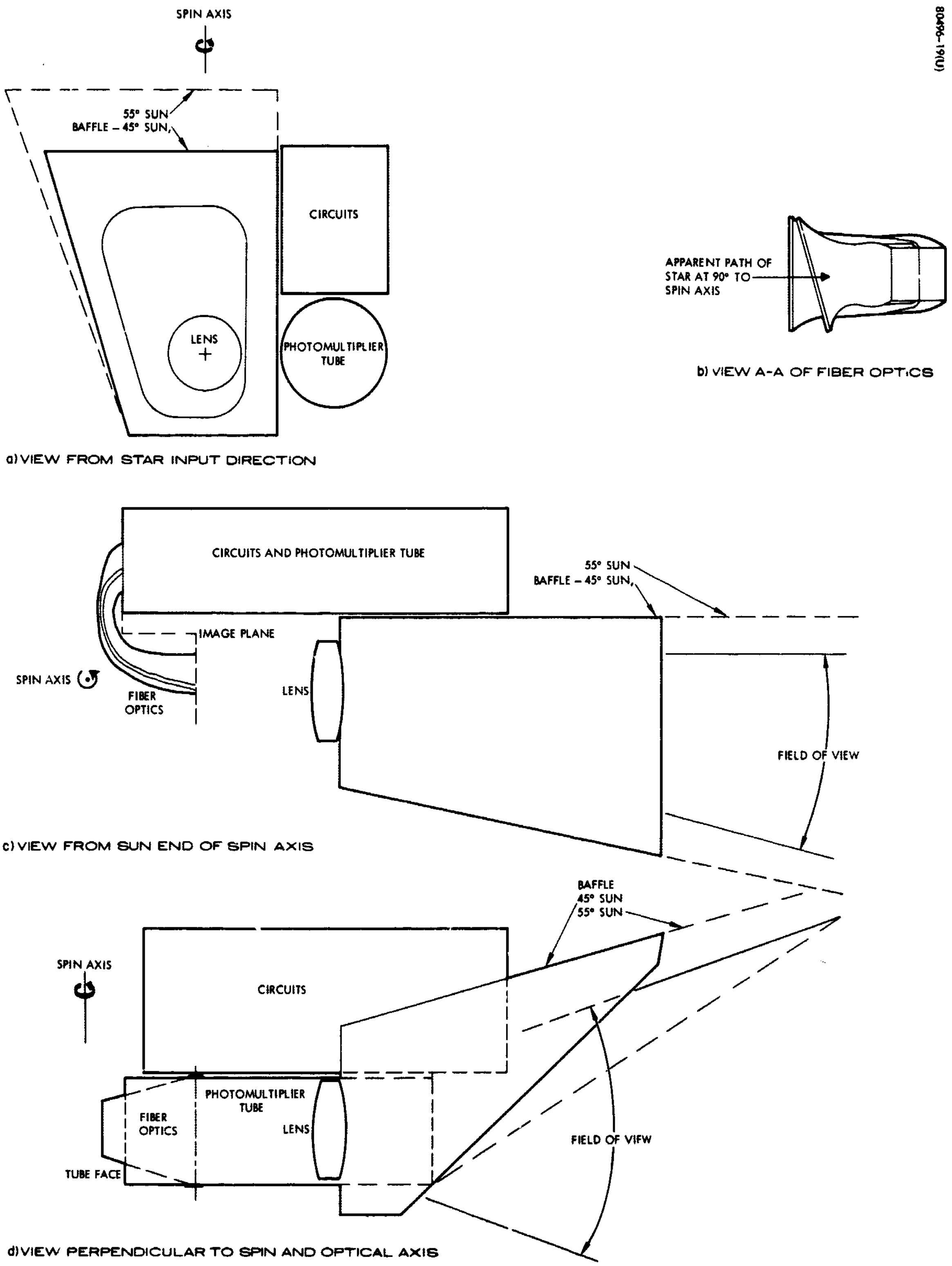

Figure 35. Star Sensor

Error Source	Error Magnitude	Error Coefficient	Error in Sun Position
$\delta(\Psi - \Psi_2)$	0.1	2.9	0.29
δI	0.1	-0.9	-0.09
RSS error			0.302

The errors contributed by the sun sensor are seen to be relatively small and are consistent with the overall attitude control pointing accuracy.

Star Sensor. This sensor is intended to allow the identification of Canopus and measure the angle between Canopus and the spin axis of the vehicle, for a vehicle with spin axis within 5 degrees of the ecliptic plane. Canopus is a logical space navigation choice because of its brightness and its nearness to the pole of the ecliptic.

The instantaneous field of view of the sensor consists of two fans of approximately 0.5 by 40 degrees each. The centers of the fans are at 90 degrees to the spin axis, and the long dimension of one fan is parallel to the spin axis. The long dimension of the other fan is at a small angle to this axis. Thus during a spin, the fans will each view any star briefly, with a time between views depending upon distance along the fan, which corresponds to the angle desired. Figure 35 shows a possible layout of such a sensor.

The angle of Canopus from the ecliptic pole is close to 14 degrees. Then, with the maximum angle of spin axis to ecliptic of 5 degrees, the angle of Canopus to spin axis normal can reach 19 degrees in either direction. A fan dimension of ±20 degrees has been chosen for preliminary design considerations. A larger angle may be selected to provide for larger excursion of the spin axis, or additional stars may be considered. The signals produced by the fans crossing stars are telemetered to the ground, where a map of star intensity versus angle can be used to identify Canopus and measure the delay between fan crossings to determine the Canopus - spin axis angle. Knowing the angle of spin axis to sun line and the date, computer programs are available from the Surveyor program to generate the sequence of star and planet signals which would be produced during a spin cycle.

It is believed feasible to identify Canopus automatically if sun sensor signals can be used to indicate spin angle phase, as then gating can be used to restrict the view to avoid all of the most confusing objects (planets and brighter stars). The sun sensor can provide a signal indicating the time of passage of the ecliptic plane by the star sensor field of view whenever the sun is not less than 15 degrees from the spin axis. Then, Canopus is bound to appear in the region of 90 ± 14 degrees or 270 ± 14 degrees after this time (with the addition of errors in locating the time of passage). As the gated region is widened about the poles to allow for errors, the first object reached brighter than Canopus (when not very near a planet) would be Sirius, at 50 degrees from the ecliptic pole. Thus, it is apparent that quite large errors can be tolerated by an automatic identification scheme which selects the brightest object in regions which have been angle-selected by the sun sensor. With such a scheme, a telemetered signal sequence during a spin cycle could be used for verification of Canopus selection. The star nearest in intensity to Canopus which might be seen would be Vega. The Canopus/ Vega ratio is 1.7.

The photomultiplier to be chosen for this sensor is the Electromechanical Research (EMR) 541N-01-14, which has been determined to be sterilizable. It is stated by EMR that the quantum efficiency drops to 0.12 to 0.14, from the 0.18 to 0.20 presterilization value. (The lower range is approximately the same as the tube used in the Surveyor Canopus sensor.)

Sensitivity. The noise bandwidth for a spinning sensor can be shown to be $\Delta f = nf_s/(\delta k_f)$ where f_s is spin frequency (60 Hz worst case), δ is angular field of view (0.5 degree), and k_f is the ratio of information bandwidht to noise bandwidth (0.6 for single RC), or Δf = 600 Hz.

This is coincidentally the same as for the Surveyor Canopus sensor, although the modulating scheme was different. Because the same light collecting area was chosen, the signal-to-noise ratio will be the same; approximately 10.

Baffle. Stray light entering the field of view by multiple reflections has been a problem in the past, necessitating a fairly extensive development program on the Surveyor Canopus sensor. That experience has been drawn upon in the design of the light baffle illustrated in Figure 35d. It should be noted that before final design, any portion of the spacecraft falling outside the plane defined by the front of the baffle must be evaluated as a source of reflected light. In the first Lunar Orbiter moon flight, the Canopus sensor (made by ITT) was unusable because of stray light. The solar panels may assist in shading the sensor, but this would need further evaluation.

Image Dissector Star Sensor. The image dissector basically allows an electronically produced scan. The spinning vehicles provide a built-in scan, making such a device with its added coamplifications unnecessary.

The JPL Mariner Canopus Tracker used a Columbia Broadcasting System (CBS) image dissector with a modulation scheme facilitating closed-loop tracking, which is not contemplated for this mission.

The International Telephone and Telegraph (ITT) Lunar Orbiter Canopus tracker program was unable to obtain a suitable CBS image dissector, and redesigned to use an ITT image dissector rather late in the program.

Failure Mode Consideration. The spacecraft carries four sun sensors and one star sensor. These sensors are highly reliable, and the chance of a failure is considered remote. The sun sensors are used for both attitude determination and control of the thrusters. For attitude determination only, one sensor is required; so, if three should fail, the attitude determination function would not be inhibited.

Thruster control in the back-up quadrant mode is accomplished by turning on the thruster with one sun sensor and turning it off with the next sun sensor. Thus, four sun sensors are needed to perform all necessary maneuvers in the quadrant mode. The capability to perform all necessary maneuvers in the primary mode exists so long as one sun sensor and the phase-locked loop are operational. This is true because in the synchronous mode only one sun pulse is used as a timing reference, and selected thrusters can be turned on and off at arbitrarily selected angles in the spin cycle.

The star sensor is used only for attitude determination and not in a control loop. If the star sensor should fail, the attitude determination task is made more difficult and the attitude accuracy is somewhat degraded, but the control function is not impaired.

Several methods have been considered for attitude determination if the star sensor fails. The high gain antenna could be used to give attitude information to within 1 or 2 degrees. This involves rotating the spacecraft to point at earth to find the direction of maximum gain.

Another method that does not involve rotation of the spacecraft is to use sun angle data gathered over a period of weeks or even a month. Knowledge of the trajectory and the change in measured sun angle can be used to determine attitude to within a degree or two.

Re-Orientation Maneuvers – Execution and Performance.

The preferred mode of jet operation results in a particular performance for various items, including change in orientation per pulse, nutation angle, maneuver time, and fuel weight. This section presents the equations needed in evaluating the re-orientation system performance. Also presented are performance curves for the range of expected system parameters.

System Performance - Parameter Relationships. In Figure 36, jets 1 and 2A are firing, producing the indicated torque. The figure indicates that for a constant thrust, the torque, M, produced by the jet varies in direction as it rotates about the spin axis. At the time the thrust is turned on, the torque is at M_1. When the jet has moved through the firing angle, θ, the torque has moved to M_2. It is apparent that some energy is wasted since at the start of thrust a component of torque about an orthogonal axis exists. This is cancelled during the second half of the pulse. The bigger the firing angle, the less efficient the pulse. It can be shown that the pulse efficiency is

$$\text{Efficiency} = \frac{\sin \theta/2}{\theta/2} \tag{7}$$

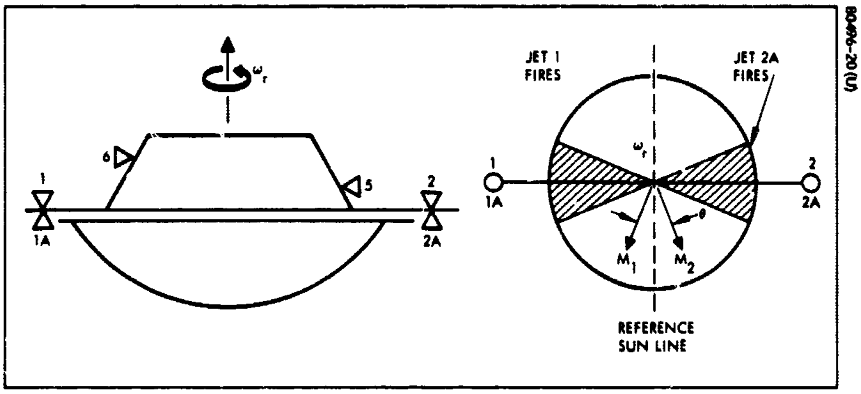

Figure 36. Thruster Configuration
Jets 1 and 2A firing

This is plotted in Figure 37. It is seen from the Figure that for a 45-degree pulse the efficiency is ov r 97 percent. Even if the pulse is 90 degrees wide, the efficiency is still 90 percent.

Rotation magnitude: The re-orientation angle per pulse (2 jet firing) is

$$\phi/\text{pulse} = \frac{183\ F\ \ell\ \theta}{I_r\ (w_s)^2} \cdot \left[\frac{\sin\theta/2}{\theta/2}\right] \qquad (8)$$

where

	Nominal A/L Plus SM	Nominal SM Only
F = thrust per jet, pounds	(4 to 5)	(4 to 5)
ℓ = lever arm, feet	(6. 08	(6. 08)
I_r = moment of inertia about spin axis, slug-ft.^{2}	390	72
w_s = spin speed, rpm	25	60
θ = firing angle, degrees	45	45

For a thrust pulse of 45 degrees, Equation 8 becomes

$$\phi/\text{pulse} = \frac{8.04 \times 10^{3} \; F\ell}{I_r \, (w_s)^2} \tag{9}$$

Figure 38 is a plot of angular rotation per pulse as a function of axial jet thrust for both 45- and 90-degree thrust pulses. During the mission the thrust will decrease from 5 pounds to about 3 pounds because of the nature of the blow-down system.

Maneuver time: The total elapsed time required to re-orient through each degree of the maneuver is

$$\Delta t/\text{degree} = \frac{.328 \, I_r \, (w_s)}{F\ell \, \theta \left[\frac{\sin \theta/2}{\theta/2}\right]} \tag{10}$$

For a 45-degree thrust pulse, Equation 6 becomes

$$\Delta t/\text{degree} = \frac{7.48 \times 10^{-3} \; I_r \, (w_s)}{F\ell} \tag{11}$$

Figure 39 is a plot of re-orientation time per degree as a function of axial jet thrust for both 45 and 90-degree pulses.

Fuel weight: The fuel weight required to re-orient the vehicle 1 degree is

$$W_f/\text{degree} = \frac{1.83 \times 10^{-3} \; I_r \, (w_s)}{I_{sp} \, \ell \left[\frac{\sin \theta/2}{\theta/2}\right]} \tag{12}$$

For a 45-degree thrust pulse, Equation 12 becomes

$$W_f/\text{degree} = \frac{1.88 \times 10^{-3} \; I_r \, (w_s)}{I_{sp} \, \ell} \tag{13}$$

Figure 40 is a plot of fuel weight per degree of rotation as a function of specific impulse for both the 90- and 45-degree cases.

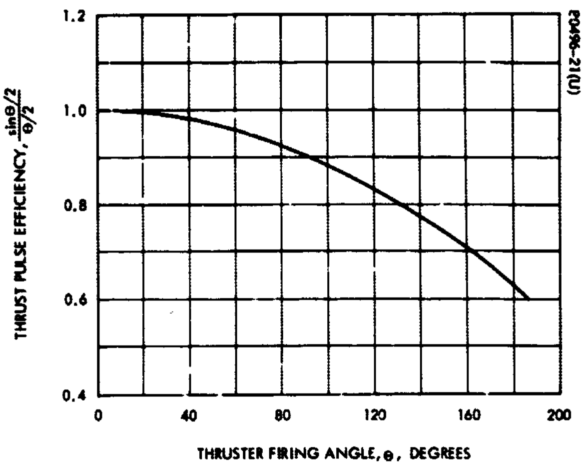

Figure 37. Thrust Pulse Efficiency Versus Firing Angle

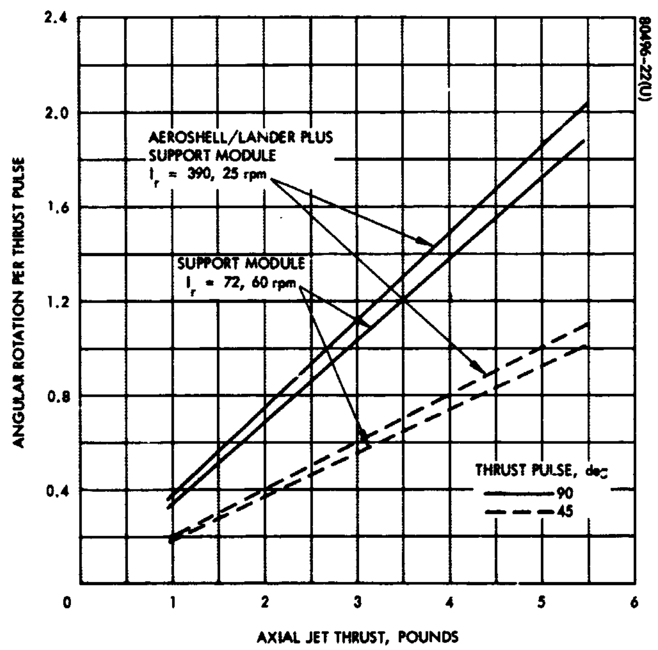

Figure 38. Rotation Per Thrust Pulse With Two Jets Firing

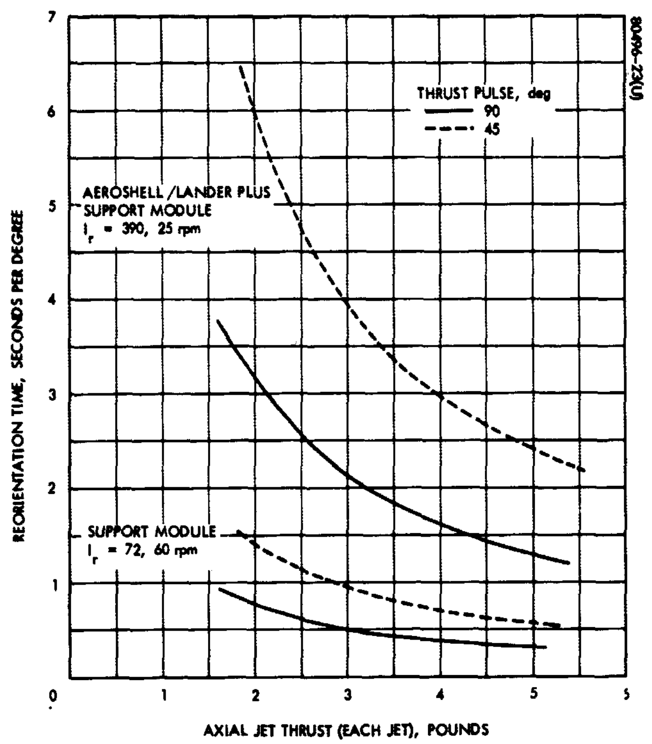

Figure 39. Time Required to Reorient Spacecraft With Two Jets Firing

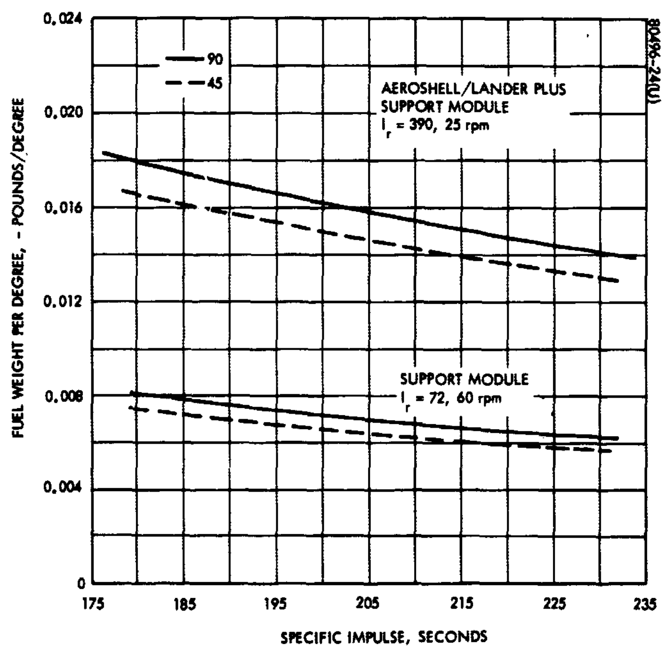

Figure 40. Fuel Weight Required for Reorientation

Imparted ΔV: In the nominal system as described above, there is no net velocity increment imparted to the spacecraft because the two opposed jets fire simultaneously. If a malfunction occurs and only one axial jet can be fired at a time, some ΔV is imparted to the vehicle.

The velocity increment imparted per degree of re-orientation is

$$\frac{\Delta V}{\phi} = \frac{5.88 \times 10^{-2} \; I_r \; (w_s)}{w\ell \quad \left[\frac{\sin \theta/2}{\theta/2}\right]} \tag{14}$$

For a 45-degree thrust pulse, Equation 10 becomes

$$\frac{\Delta V}{\phi} = \frac{6.04 \times 10^{-2} \; I_r \; (w_s)}{w\ell} \tag{15}$$

where w is the spacecraft weight.

Figure 41 is a plot of velocity increment per degree of re-orientation as a function of roll moment of inertia for a family of rotation speeds.

Point Design Performance. The nominal firing angle to be used for re-orientation maneuvers is 45 degrees. Figure 37 indicates that the pulse efficiency is 97.5 percent.

The average thrust available for re-orientation of the cruise vehicle is about 4.5 pounds. The spin axis re-orientation per 45-degree thrust pulse with two jets firing is 0.9 degree. For the SM alone, the average thrust is about 4.0 pounds. The spin axis re-orientation per 45-degree pulse with two jets firing is 0.74 degree. These minimum values are consistent with the overall mission pointing requirements. If pulses smaller than 45 degrees are used, a corresponding reduction in minimum angular rotation is achieved.

The maneuver time for each degree of rotation for the nominal system is 2.7 seconds for the total vehicle, and 0.7 second for the SM alone. The nominal rotation speed for the total vehicle is 25 rpm, and for the SM alone is 60 rpm. Maneuver time can be decreased if firing angle is increased. Figure 42 is a plot of re-orientation time as a function of firing angle for the total vehicle. It is apparent that increasing the firing angle above 90 degrees is relatively ineffective.

The fuel weight per degree of re-orientation is 0.014 pound for the total vehicle with a 45-degree pulse, and 0.006 pound per degree for the SM alone.

Another performance factor of some importance is the nutation angle buildup during re-orientation maneuvers, the maximum nutation angle being given by

$$\eta = \frac{M\,\Delta t}{I w_s} \cdot \frac{1}{\sin\pi\ (\sigma - 1)}$$

where

M = torque

Δt = pulse width

w_s = spin, rad/sec

I = spin MOI

σ = roll-to-pitch MOI ratio

For the parameters of the mission under consideration, we have

η = 1.3 degrees for the MSSM-A/L combination

η = 2.5 degrees for the MSSM alone

Re-Orientation Maneuver Execution. To execute a re-orientation maneuver, one of the two following sequences is selected, depending on whether the synchronous mode or the quadrant mode is selected.

Subsequence A: re-orientation:

1) Synchronous mode

   a) Select firing start angle magnitude

   b) Select pulse width

   c) Select number of pulse

   d) Select thruster pair number

   e) Enable axial jet pair

2) Quadrant mode

   a) Quadrant select command

   b) Select number of pulses

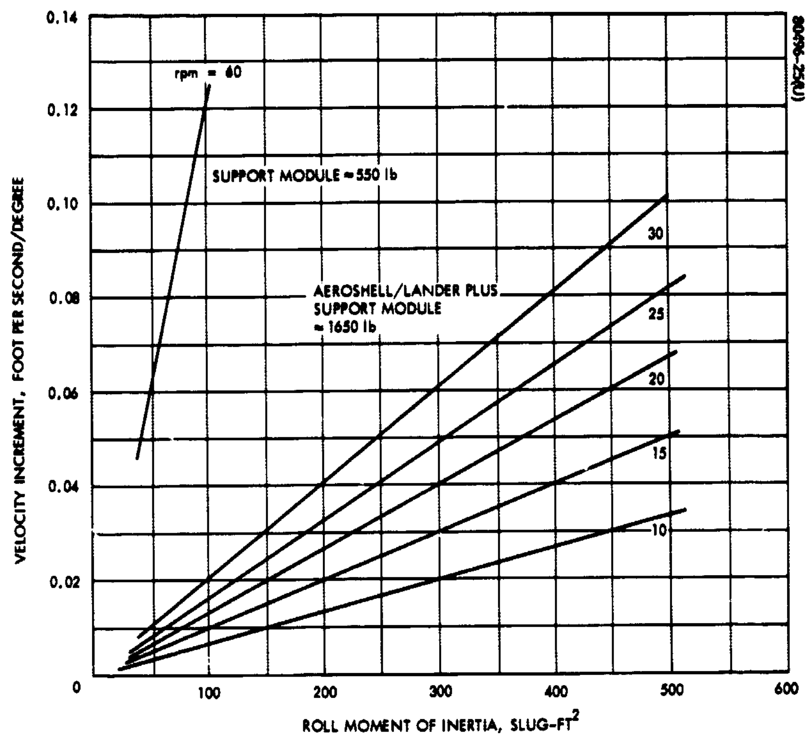

Figure 41. Velocity Increment Per Degree of Reorientation - One Axial Jet Firing

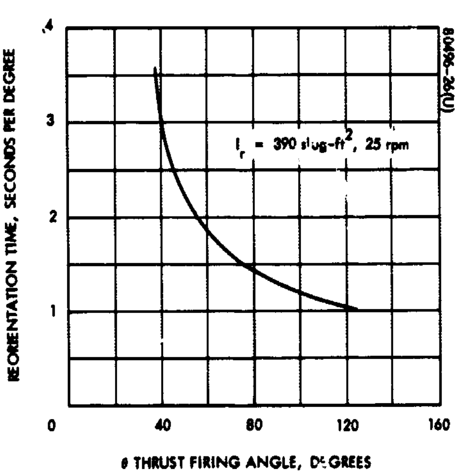

Figure 42. Time Required to Reorient Spacecraft — Two Jets Firing

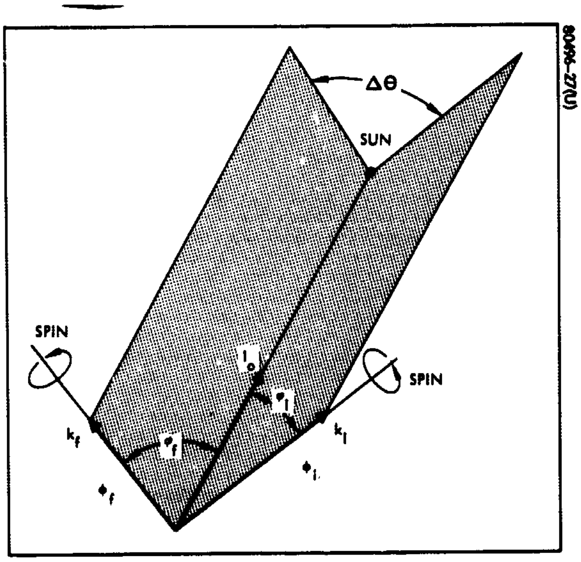

Figure 43. Reorientation Variables

c) Select thruster pair number

d) Enable axial jet quadrant mode

e) Quadrant select command

f) Select number of pulses

g) Select thruster number

h) Enable axial jet quadrant mode

The re-orientation commands may be sent, verified, and executed individually, or they may be stored on board, verified, and executed automatically in sequence. The former approach would be the nominal mode during the cruise portion of the trajectory, while the latter procedure would be used just prior to encounter.

Re-Orientation Maneuver Error Analysis. The most stringent attitude maneuver accuracy requirement is placed on the final re-orientation of the SM which directs the planar antenna toward earth after A/L separation. All other attitude maneuvers have relaxed requirements on accuracy and, in addition, there is always ample time for attitude adjustment by earth station command. In view of the importance of the final re-orientation prior to relaying data back to earth, a definitive analysis of the error sources will be included.

For this error analysis, the attitude maneuver may be defined in terms of two convenient angles - ϕ in the plane containing the spin axis and the sun, and θ about the sun line (see Figure 43). Errors in ϕ are called in-plane errors, and errors in θ are called out-of-plane errors. A re-orientation maneuver may be analyzed in terms of the following variables;

ϕ_i = initial sun angle

ϕ_f = final (desired) sun angle

$\Delta\theta$ = total nominal (desired) rotation about the sun line

ψ = nominal phase angle between sun pulse and torque pulse centroid.

Error sources are defined as follows:

$\delta\theta$ = error in the attitude of the spin axis (out-of-plane component)

$\delta\phi_i$ = error in initial attitude of spin axis (in-plane component)

$\delta\psi_1$ = error in torque pulse phase angle due to centroid error and electronic error

$\delta\psi_2$ = error in torque pulse phase angle due to initial error in ϕ

δH = per unit error in total impulse of control jet

An attitude error, $\delta\theta$, in rotation about the sun line affects pointing accuracy directly as the sine of the sun angle ϕ_i

$$\epsilon_i = \sin\phi_i \, \delta\theta$$

After precession, the attitude error is

$$\epsilon_f = \sin\phi_f \, \delta\theta$$

$$= \frac{\sin\phi_f}{\sin\phi_i} \, \epsilon_i \quad \text{(out-of-plane error)}$$

In other words, the final out-of-plane error in spin axis attitude is a function of the initial error ϵ_i, and the final and initial sun angles, provided there is no error in the torque phase angle, ψ. If an error $\delta\psi$ exists, the total precession angle remains nominally the same, but there is now a rotation error, $\delta\theta_f$, around the sun line, given by

$$\delta\theta_f = \Delta\theta \, \frac{\sec^2\psi}{\tan\psi} = \frac{\Delta\theta}{\sin\psi\cos\psi} \cdot \delta\psi$$

In this case, the final attitude error (for ψ error only) is

$$\epsilon_f = \Delta\theta \, \frac{\sin\phi_f \, \delta\psi}{\sin\psi \, \cos\psi} \quad \text{(out-of-plane)}$$

The error in ψ arises as a result of error in ϕ_i, so that the wrong value of ψ is computed. Also, ψ is in error due to pulse centroid error and electronic error. The error in ψ as a result of error in ϕ_i is

$$\delta\psi_2 = \frac{\sin^2\psi}{\Delta\theta \sin\phi_i} \, \delta\phi_i$$

and the total error in ψ is

$$\delta\psi = \left(\delta\psi_1^{\ 2} + \delta\psi_2^{\ 2}\right)^{1/2}$$

The resulting final attitude error in spin axis orientation (out-of-plane) is

$$\epsilon_f = \left(\Delta\theta \frac{\sin \phi_f}{\sin \psi \cos\psi}\right)\left(\frac{\sin^4 \psi}{\overline{\Delta\theta}^2 \sin^2 \phi_i} \overline{\delta\phi}_i^{\,2} + \overline{\delta\psi_1}^{\,2}\right)^{1/2}$$

The following values are chosen for the first maneuver

$\Delta\theta$ = 20 degrees

ϕ_i = 40 degrees

ϕ_f = 25 degrees

$\delta\phi_i$ = 0.5 degree

$\delta\psi_1$ = 2 degrees

δH = 5 percent of total impulse

The angle ψ is computed from

$$\psi = \tan^{-1}\left[\Delta\theta/\ln \frac{\tan 1/2\ \phi_f}{\tan 1/2\ \phi_i}\right]$$

Substituting numerical values (in radians) in the above equations, we have

$$\psi = \tan^{-1}\left[0.35/\ln \frac{0.222}{0.364}\right] = \tan^{-1} 0.707$$

$= 0.615$ radians

= angle to center of torque pulse, measured from the sun line

$$\epsilon_f = \left(0.35 \frac{0.423}{\sin \psi \cos \psi}\right) \left(\frac{0.111}{0.0505} \times 0.758 \times 10^{-4} + 1.22 \times 10^{-3}\right)^{1/2}$$

$$= (0.314)\ (0.0373) = 0.0117 \text{ radians}$$

$$= 0.671 \text{ degree (out-of-plane)}$$

Thus, the re-orientation from cruise attitude to the entry attitude will have a 0.671-degree rss error, neglecting jet impulse error. The total error in the direction of precession due to jet impulse errors is

$$\delta p = 15 \text{ degrees} \times \delta H$$

$$= 15 \text{ degrees} \times 0.05$$

$$= 0.30 \text{ degree}$$

This error divides between the in-plane and out-of-plane errors as follows

$$\delta\phi = 0.3 \cos 20 \text{ degrees} = 0.282$$

$$\theta = 0.3 \sin 20 \text{ degrees} = 0.102$$

The rss out-of-plane error is 0.68 degree.

Despin and spinup add 1.5 degrees and 0.2 degree, respectively, so that the initial error prior to the second re-orientation may be

$$\phi_i = \left[\left((0.68)^2 + (1.5)^2 + (0.28)^2\right)\right]^{1/2}$$

$$= 1.75 \text{ degrees (worst case)}$$

Re-orientation to the cruise attitude then uses the following values:

$\Delta\theta$ = 20 degrees

ϕ_i = 25 degrees

ϕ_f = 40 degrees

$\delta\phi_i$ = 1.75 degreee

$\delta\psi\ i$ = 2 degrees

The final error in attitude after return to the cruise attitude, computed from the above procedure, is

$$\epsilon_f = \left(0.35 \frac{0.643}{0.472}\right)\left(\frac{0.111}{0.021} \times 9.38 \times 10^{-4} + 1.22 \times 10^{-3}\right)^{1/2}$$

$$\simeq (0.475)\ (0.0785) = 0.0373 \text{ radian}$$

$$= 2.14 \text{ degrees}$$

The error, δp, remains the same as above (0.3 degree), so that the total rss error for all maneuvers, beginning with re-entry attitude maneuver, is

$$\text{Total error} = \left[\left((2.14)^2 + (0.282)^2 + (0.102)^2 + (1.7)^2\right)\right]^{1/2}$$

$$= 2.75 \text{ degrees,}$$

which agrees reasonably well with the summary of encounter maneuver errors generated early in the study which estimated the encounter maneuver error by the rss of despin/spinup errors and precession errors without taking into account errors in ψ and ϕ_i.

Failure Mode Analysis. Excluding catastrophic failures, one may postulate various failures and then describe specific procedures and maneuvers for continuing the mission. Such an exercise would not be particularly productive at this time because of the redundancy and operational flexibility already described. However, a typically difficult failure situation may be considered as follows. It is 12 hours before encounter, and all commands for the encounter maneuvers have been stored on board and verified. The encounter maneuver sequence has been initiated, as evidenced by loss of the high-gain antenna signal, and more than sufficient time has elapsed for the SM to re-orient itself to the cruise attitude, but no signal of any kind is apparent. In other words, telemetry contact is lost, and the encounter maneuver sequence has not proceeded as planned. The question now is: How should the mission proceed?

It must be assumed that command contact is available; otherwise, under the above conditions, the mission will fail. The first consideration is to arrive at what might be called the most probable failure, which in this case may be an interruption of the encounter maneuver sequence. Since the initial re-orientation was actually observed to start, it would be reasonable to assume that the spacecraft at least reached the entry attitude. This is the key question in re-orientation failure — namely, in what attitude did the maneuver terminate? Prior to encounter, the spin axis does not leave the ecliptic plane, so that a starting point for failure mode operations is much easier to postulate. For the more difficult situation under consideration here, one must postulate a crude attitude from which to begin operations. First, one would exercise any redundancy features of the telecommunications system. Now the spin axis-earth angle must be greater than 60 degrees, because the 120-degree beamwidth telecommunications system cross-slot antenna cannot be picked up. The earth-MSSM-sun angle is about 40 degrees, leaving at least 20 degrees between the spin axis and the sun line, as shown in Figure 44, which defines:

Region A - spin axis is not in this region.

Region B - if spin axis were in this region, a rotation about the sun line would result in contact with the earth.

Region C - rotation about the sun line would not result in contact.

Thus, one would first ascertain if the spin axis were in Region B by commanding a quadrant mode ($\psi = \pi/2$) precession about the sun line. This would be done in several steps to preclude passing up the contact attitude and having to return. If contact is established during this precession, attitude data becomes available, and further maneuvers may then be planned. If no contact is made, it may be assumed that the spin axis is in Region C. Quadrant mode precession would then be initiated, using either a series of pulses commanded directly from the ground station, or employing the ψ simulator if applicable. The $\psi = 0$ or π mode would be used to get the spin axis out of Region C, after which a rotation about the sun line would result in contact. The above maneuvers would require a maximum of 8 minutes actual maneuver time (worst cases assumed throughout) and possibly 2 to 3 hours of planning and decision making in the ground station.

Although single axial jet re-orientation maneuvers are highly improbable in view of the redundancy available, an analysis was made of the ΔV resulting from a re-orientation maneuver with a single axial jet. Figure 45 shows the results, which indicate a significant ΔV if large re-orientation is required. Note that a complete (360-degree) rotation results in nominally zero ΔV.

Spacecraft Velocity Control System Design and Performance

The addition of a radial jet(s) to the propulsion system provides for spacecraft velocity control without re-orientation of the spacecraft. Synchronous pulse mode operation of a radial jet provides for a lateral or radial increment of velocity in the average direction of radial thrust, while continuous firing of an axial jet produces a velocity increment in the direction of the angular momentum vector. Vector combination of the two velocity increments is employed to achieve any desired velocity maneuver.

Functional Description and Overall Design Considerations

Three approaches were considered for obtaining a particular vector velocity increment. One approach was to re-orient the spin axis to the desired ΔV direction and then fire the axial jet(s) continuously until the desired ΔV was obtained. This re-orientation approach to ΔV implementation has several disadvantages, depending upon how many jets are actually used. If the axial jets are positioned to thrust in one direction only, rather large attitude maneuvers may be required (up to 180 degrees) to obtain the desired direction of ΔV. If both directions of axial thrust are provided for (see Figure 23), two additional jets are required, and they must be placed at a radius large enough to preclude impingement on the A/L. With only two axial jets thrusting in a single direction, one jet is redundant, and all attitude maneuvers result in a velocity being imparted to the spacecraft. This velocity due to re-orientation is objectionable, being difficult to accommodate on large maneuvers and requiring excessively complex maneuver tactics, to say nothing of the residual error in ΔV, said error being excessive for the small, third mid-course maneuver (see Figure 45). After due consideration, this re-orientation approach to ΔV was discarded in favor of the fixed attitude ΔV maneuver, thus eliminating the other major disadvantages of the first approach; namely, degraded communications capability in the latter stages of the mission, additional command storage and flight control complexity at encounter, and increased probability of failure to reacquire the high-gain antenna. The fixed attitude ΔV approach was selected, for which there are two specific schemes for achieving the desired ΔV.

Without change in attitude, the nominal mode for ΔV maneuvers is to first fire the appropriate axial jets to obtain the desired axial component of ΔV. Two forward thrusting or two aft thrusting jets are fired simultaneously

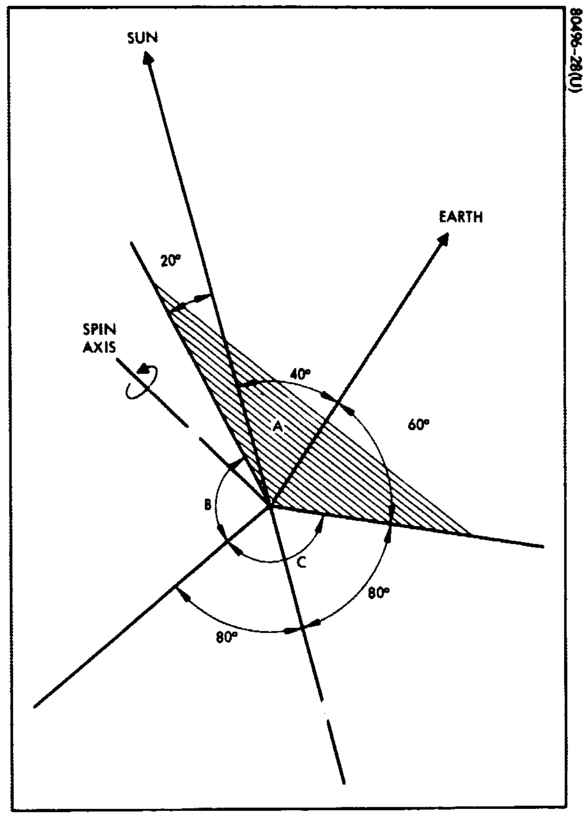

Figure 44. Regions of Interest for Failure Mode Maneuvers at Encounter

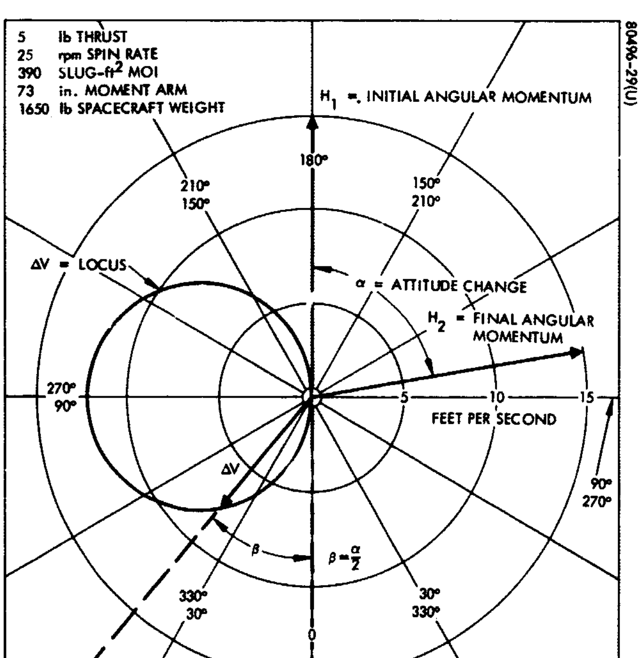

Figure 45. Polar Plot of Velocity Change (ΔV) Resulting From Attitude Change and Return to Initial Attitude, Using Only One Axial Jet (a Failure Mode)

to preclude attitude perturbation and nutation. A radial jet is next fired in the synchronous, pulsed, mode to impart the desired radial component of ΔV. One method of obtaining the correct magnitude of each ΔV component is to use linear, integrating accelerometers appropriately placed (on the spin axis) which terminate the maneuver when the stored ΔV is reached. Some difficulties accompany this approach, including accelerometer output bias due to misalignment and spacecraft cg off-set, and extraneous acceleration due to small nutational motion. Command and control functions also become more complex. However, without making a detailed, quantitative tradeoff study, the metered or closed-loop ΔV approach was rejected in favor of an open-loop approach based on jet calibration data. In this approach, the ΔV is determined on the basis of propellant tank temperature and pressure and total "on" time in a particular mode (pulsed or continuous). Adequate accuracy is available from the jet acceptance tests, which would include comprehensive testing over the entire range of pressure and temperature for both modes of operation. The above approach greatly simplifies the on-board circuit complexity and the maneuver execution while providing suitable accuracy both in magnitude and direction. Later in this section, the subject of ΔV errors is discussed in greater detail under Velocity Maneuver Error Analysis.

The control of the radial jets is accomplished by the JCE in the same manner as axial jet control for re-orientation. In order for radial jet operation not to produce attitude change, the thrust direction should pass through the spacecraft cg, which has one location for the combined configuration and another location for the SM alone. Thus, one of the radial jets is aligned to thrust through the combined cg, this jet being used for all radial ΔV mid-course maneuvers. The shift in cg due to propellant consumption is small enough (less than 1 inch) so that when the jet is aligned through the average location of the cg, the moment arm never becomes large enough to seriously affect attitude during ΔV maneuvers. The reason for performing the axial maneuver first is to preclude the entire attitude perturbation from the radial maneuver directly affecting the axial maneuver. Maximum change in attitude during radial jet operation would not exceed 0.06 degree per foot per second at radial ΔV. There are several ways of handling this attitude perturbation. For example, the attitude change for a given radial ΔV is known a priori, so that part of the axial ΔV may be done in the pulsed mode to adjust the attitude to compensate for the change in attitude when the radial ΔV is performed. For the small angles involved here, the spin axis attitude change does not affect maneuver accuracy. Another possibility is to utilize both radial jets aligned in a manner to produce attitude torques of opposite sign (but not necessarily equal) and to program the radial jet maneuver between jets so that the net attitude change is zero. Another solution is to correlate thrust level, cg position, and alignment so the overall attitude perturbation is minimized. (i.e., since thrust level decreases as propellant is consumed, a larger moment arm may be allowed.)

The fixed attitude approach to ΔV maneuvers offers the greatest operational flexibility and the least complexity in on-board circuitry and command logic, while providing adequate accuracy for mission requirements.

Velocity Maneuver Execution and Performance

In all likelihood, several velocity corrections will be required prior to the encounter phase. The midcourse correction capability is 65 m/sec. There will probably be three or four velocity corrections during the transit phase. After separation of the A/L, the SM must be placed on the proper flyby trajectory. The maximum ΔV required for this maneuver is 100 m/sec.

The spacecraft is not re-oriented prior to performing a ΔV correction. The ΔV vector is made up of a velocity increment in the axial direction, ΔV_a, and a velocity increment in the radial direction, ΔV_R (see Figure 46).

The angle, α, is the angle the radial jet is canted with respect to the perpendicular to the spin axis, in order that the jet thrust direction passes through the cg.

System Design and Performance. A midcourse velocity correction is computed from spacecraft tracking data and the desired Mars encounter conditions, and this vector is then broken into two components: along the axial direction and along the direction of the radial jet. The appropriate set of axial jets is selected, either the forward firing or aft firing pair. The axial jets are always fired two at a time in a continuous mode for an integral number of spin periods. The number of spin periods required is determined from the calibration curves for the particular jets involved.

The radial corrections are performed with one jet firing in the pulsed mode once each revolution. A 90-degree firing angle is nominally selected. Once the radial component of ΔV is found, it is necessary to select the delay angle (point in spin cycle at which the jet is turned on). The total number of radial jet pulses is then determined from the jet calibration curves.

In general, the required ΔV will not be in the direction of either the axial or radial jet. Thus, some penalty in expended fuel must be paid because the ΔV correction is made up of the vector sum of the two available thrust vectors. Figure 47 is a plot of the ΔV expended to obtain one unit of ΔV correction. The parameter is radial engine cant angle. If the desired ΔV is in the direction of the axial jet (in the direction of the spin axis or opposite the direction of spin), one unit of correction is obtained for one unit expended. The same is true in the radial direction. If one unit of correction is desired in a direction 45 degrees from H_0, for example, then 1.414 units are expended for every unit desired for a cant angle of zero. The penalty can be found from Figure 47 by drawing a line from the origin in the direction of desired correction and out to the appropriate cant angle.

The cant angle for the total vehicle is 3 degrees. If it is assumed that the direction of ΔV is random, then the average penalty is 28 percent.

Axial jet performance: The time required to perform a ΔV maneuver in the direction of the axial jet is given by

$$\Delta t = \frac{w \, \Delta V_a}{2g \, F} \tag{16}$$

where

Δt is total elapsed maneuver time, seconds

w is vehicle weight, pounds

F is thrust per engine, pounds

ΔV_a is velocity increment in axial jet direction, fps

g is earth's gravitational acceleration, fps^2

The axial jet firing is continuous in this mode. Figure 48 is a plot of time required per foot per second of axial ΔV.

The number of spin periods required to complete the axial maneuver is given by

$$N = \left(\frac{1}{2g(60)}\right) \frac{w \, (\Delta V_a) \, w_s}{F} \tag{17}$$

where

w_s = spin, rpm

The number of spin periods is transmitted to the spacecraft, followed by a start command. The number of spin periods is counted down to zero to complete the maneuver.

The fuel weight required to perform an axial ΔV is approximated by

$$w_f = \frac{w \, \Delta V_a}{g I_{sp}} \tag{18}$$

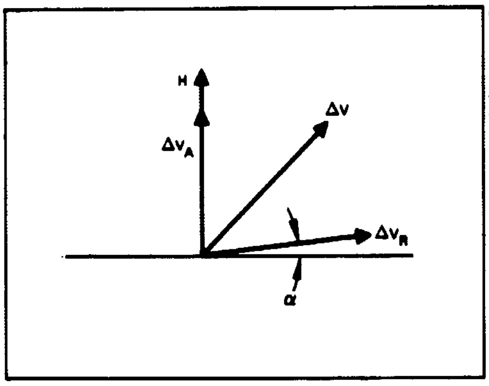

Figure 46. ΔV Correction Vector

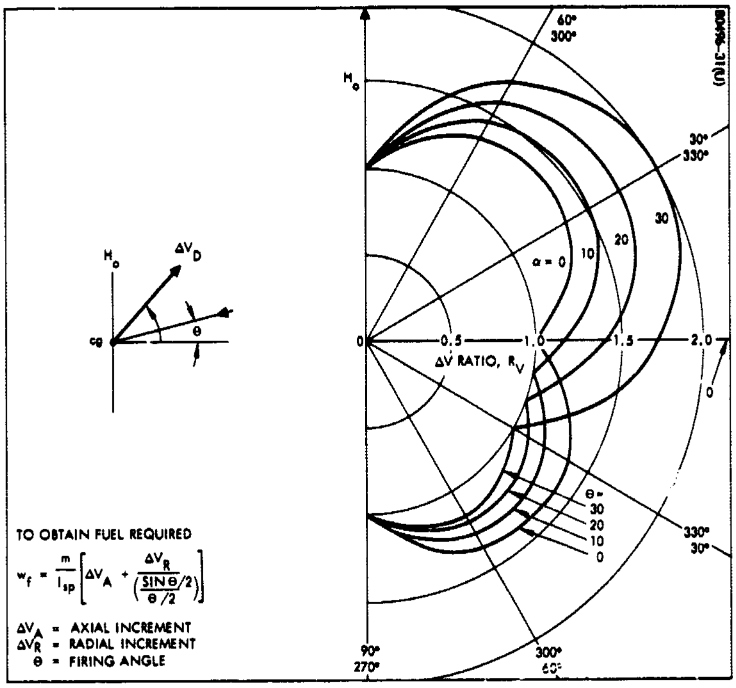

Figure 47. R_V = ΔV Expended to Obtain One Unit of ΔV Correction With No Vehicle Rotation

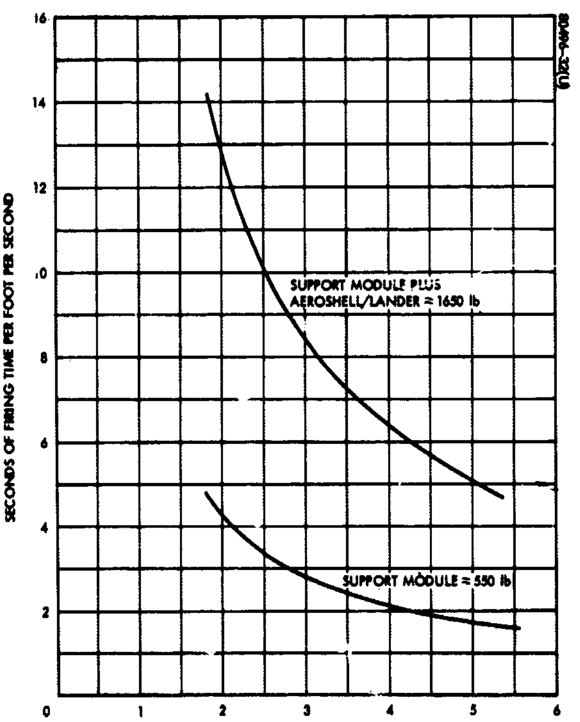

Figure 48. Time Required Per Foot Per Second for Axial Velocity Correction – Two Jets Firing Continuously

where

I_{sp} is the specific impulse of the fuel, seconds.

Figure 49 is a plot of fuel weight per foot per second as a function of vehicle weight.

Radial jet performance: The radial jet system consists of two jets. One jet is mounted so that its thrust line passes through the cg of the combined A/L plus SM. This jet alone is used to perform ΔV corrections in the radial direction (ΔV_r) prior to lander separation. The other jet is mounted so that its thrust line passes through the cg of the SM alone. This jet is used for ΔV_r maneuvers after lander separation. This system allows for ΔV_r maneuvers to be performed with no re-orientation for the combined vehicle, and also for the SM after separation with a minimum number of jets. The nominal firing angle is 90 degrees for all radial velocity correction maneuvers.

Once the magnitude of the radial velocity increment is determined, it is necessary to determine the total number of radial jet pulses required for the maneuver. The velocity increment per pulse is given by

$$\Delta V_{pulse} = \left(g \frac{60}{360}\right)\frac{F\theta}{w(\omega_s)} \left(\frac{\sin \theta/2}{\theta/2}\right) \tag{19}$$

Figure 50a is a plot of ΔV per pulse as a function of radial jet thrust for the A/L plus SM. Spin speed is the parameter. Figure 50b is a similar plot for the SM alone spinning at 60 rpm.

Figure 51a is a plot of the number of pulses required per foot per second of radial correction. The figure is for the total vehicle and for several spin speeds. Figure 51b is a similar plot for the SM spinning at 60 rpm.

The total elapsed time to perform a radial correction is given by

$$t_r = \frac{11.2\ w\ \Delta V_r}{F\theta\ \left[\frac{\sin \theta/2}{\theta/2}\right]} \tag{20}$$

Figure 52 is a plot of the time required for each foot per second of radial correction. Both the combined vehicle and the SM alone are plotted on this figure. The maneuver time required for a 50 fps radial correction for the cruise vehicle would be about 37 minutes and require 950 pulses.

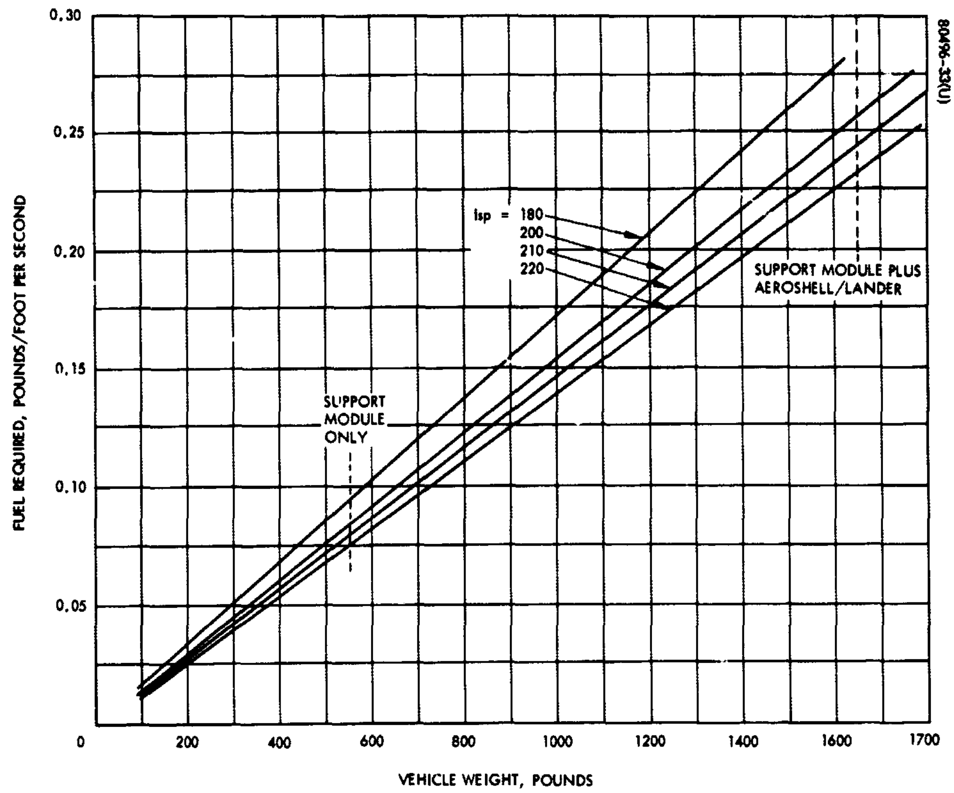

Figure 49. Fuel Weight Required for Axial Jet Velocity Change

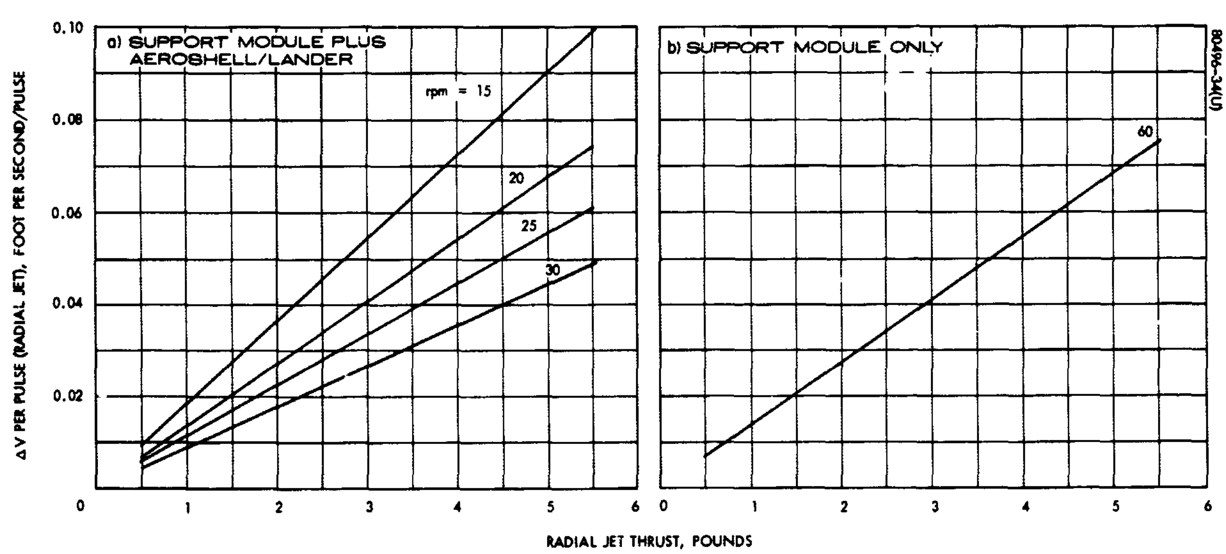

Figure 50. Radial Jet Velocity Change Per Pulse

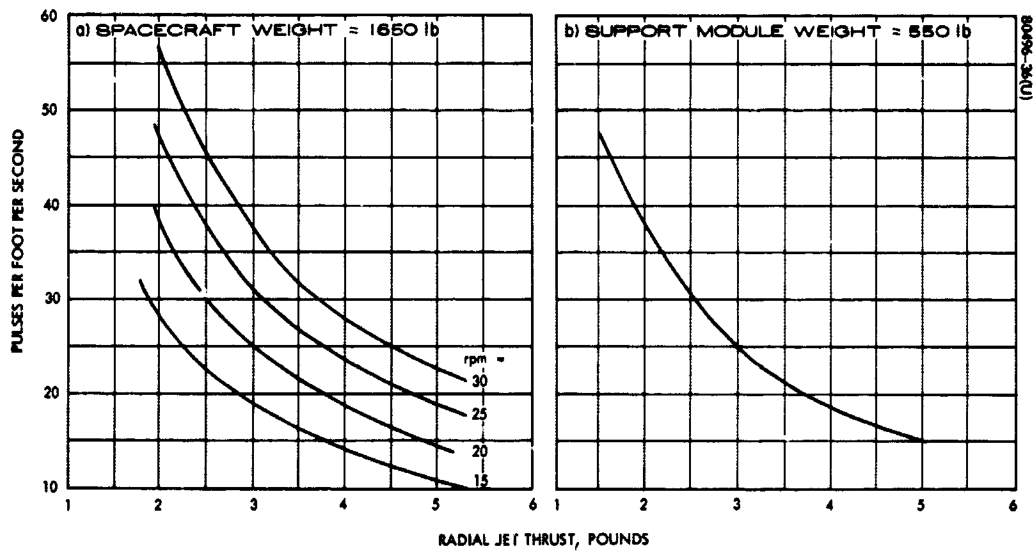

Figure 51. Number of Radial Jet Pulses Required for Velocity Change

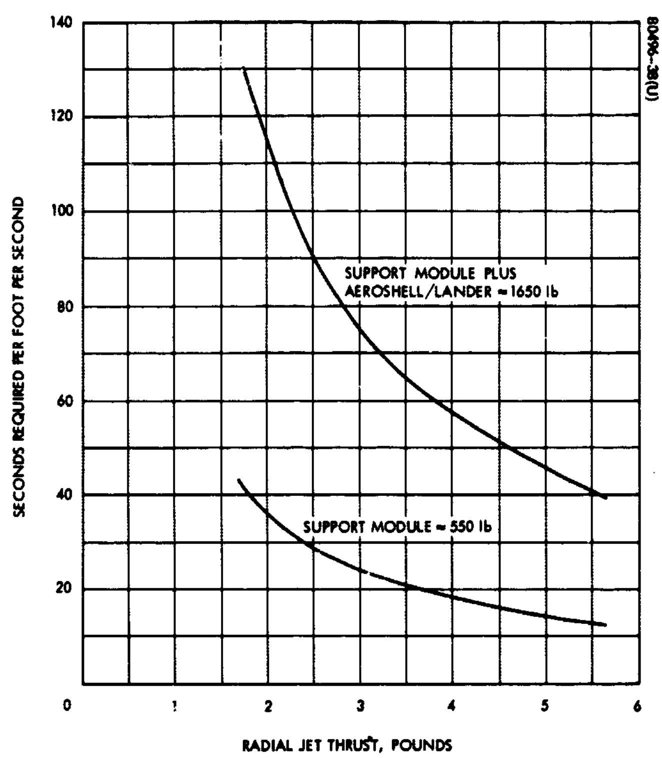

Figure 52. Time Required to Perform
ΔV Correction With Radial Jet

The fuel consumed per radial jet pulse is given by

$$w_{f_{\text{pulse}}} = \frac{F\theta}{I_{sp}(\text{rpm})} \frac{60}{360} \tag{21}$$

Figure 53 is a plot of fuel weight per pulse for the combined vehicle and for the SM only.

The fuel weight required for a radial maneuver is given by

$$w_f = \frac{w\, \Delta V_r}{g\, I_{sp} \left(\frac{\sin \theta/2}{\theta/2} \right)} \tag{22}$$

The fuel weight per foot per second is plotted on Figure 54 as a function of spacecraft weight for several specific impulses.

Point Design Performance. Table 9 is a summary of the point design velocity and attitude control capability for the SM attached to the A/L, and for the SM alone.

Velocity Maneuver Execution. In order to execute a velocity maneuver, a series of commands must be transmitted to the spacecraft. For an axial ΔV, the number of spin periods for continuous thrusting and thruster to be fired must be determined. In commanding a radial maneuver, the total number of thrust pulses must be determined and also the thrust start time (thrust start angle) in the period. The thrust on time or firing is fixed at 90 degrees. The complete sequence of commands is given below.

Continuous thrusting:

1) Synchronous mode

   a) Select number of spin periods x 100 (MAG)
   b) Select number of spin periods (MAG)
   c) Jet continuous command
   d) Polarity control command
   e) Enable axial jets

2) Quadrant mode

   a) Select number of quarter spin cycles x 100 (MAG)
   b) Select number of quarter spin cycles (MAG)
   c) Jet continuous command
   d) Polarity control command
   e) Enable axial jets quadrant mode

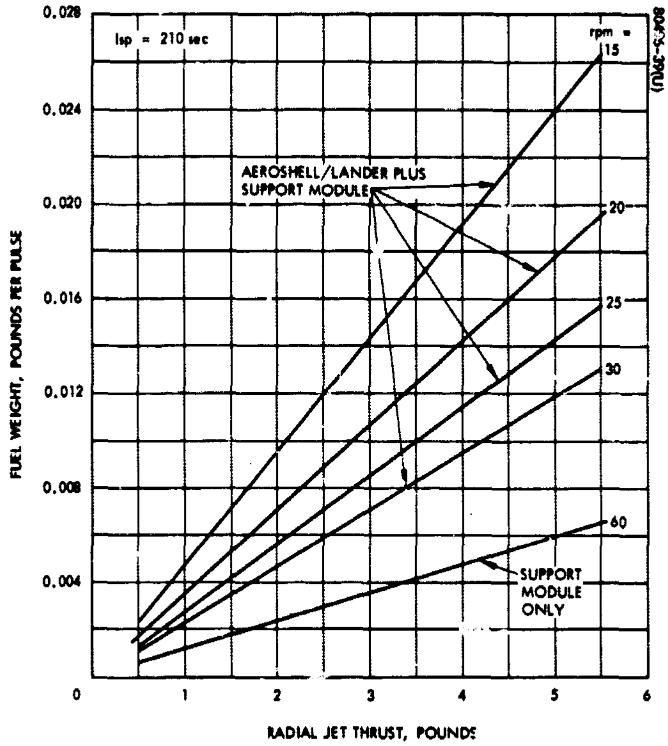

Figure 53. Radial Jet Fuel Weight Required Per Pulse

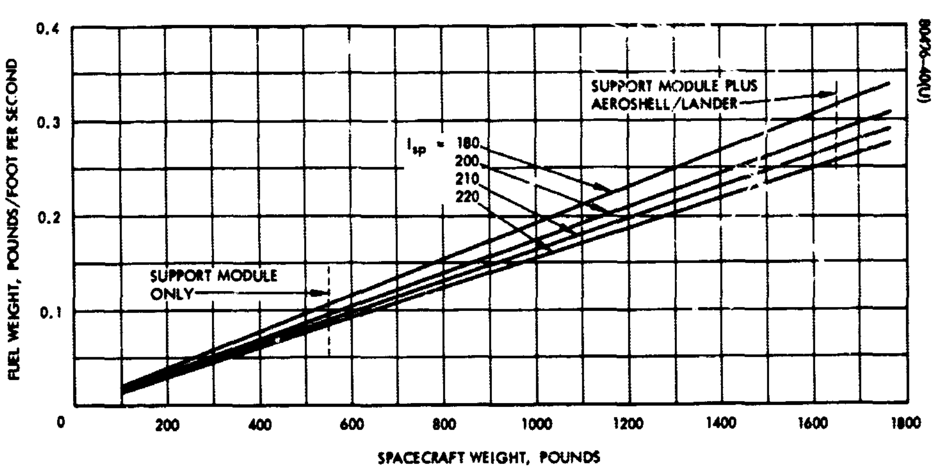

Figure 54. Radial Jet Fuel Weight Required to Make Velocity Change Versus Spacecraft Weight

TABLE 9. VELOCITY AND ATTITUDE CONTROL CAPABILITY

	SM Attached to A/L	SM Alone
ΔV per continuous axial jet firing per spin period (one jet)	0.210 fps/rev (25 rpm, 4.5-pound thrust)	0.123 fps/rev (60 rpm, 4.0-pound thrust)
Axial jet continuous firing time per fps ΔV	11.3 seconds/fps (one jet) 5.65 seconds/fps (two jets)	8.14 sec/fps (one jet) 4.07 sec/fps (two jets)
Weight of propellant per fps ΔV (axial jet)	0.245 lb/fps	0.081 lb/fps
Attitude change per pulse (two jets)	1.63 deg/pulse (90-degree pulse) 0.876 deg/pulse (45-degree pulse)	1.39 degree (90-degree pulse) 0.754 degree (45-degree pulse)
Propellant weight per degree attitude change	0.0154 lb/deg	0.0068 lb/deg
ΔV per 90-degree pulse of radial jet	0.0478 fps/pulse	0.0534 fps/pulse
Propellant weight per radial jet pulse, 90-degree pulse	0.014 lb/pulse	0.00476 lb/pulse
Number of radial jet pulses per fps	20.9	18.7 pulse/fps
Propellant weight per fps (radial jet)	0.267 lb/fps	0.089 lb/fps
Time required per fps (radial jet)	49.3 seconds (one jet)	18.9 seconds (one jet)
Spacecraft ΔV per degree of attitude change	0 (nominally, using two axial jets)	0 (two jets produce pure couple)
Maximum nutation angle during reorientation	2 degrees	2 degrees

Radial jet thrusting:

1) Synchronous mode

   a) Select thrust start angle magnitude (MAG)
   b) Select number of pulses x 100 (MAG)
   c) Select number of pulses (MAG)
   d) Select jet
   e) Enable radial jet

2) Quadrant mode

   a) Quadrant select command
   b) Select number of pulses x 100 (MAG)
   c) Select number of pulses (MAG)
   d) Select jet
   e) Enable radial jet quadrant mode
   f) Quadrant select command
   g) Select number of pulses x 100 (MAG)
   h) Select number of pulses (MAG)
   i) Enable radial jet quadrant mode

Velocity Maneuver Error Analysis. A detailed consideration of error sources and their effect on velocity maneuver accuracy has been made to show that the open loop approach to maneuver execution is feasible. The primary source of error is the uncertainty in total impulse delivered by a particular jet. Other contributions to ΔV error are almost insignificant insofar as the MSSM mission is concerned. Specific consideration of jet impulse error is treated earlier in this section, the analysis here being primarily a parametric study. All previous missions involving Hughes-built satellites have been controlled directly from a ground station in a quasi-closed loop fashion. That is, a maneuver would be made and then evaluated by ground-based measurement. Thus, accuracy has not been a significant factor to date in view of the particular mission operations. Conditions are different for the MSSM mission; and thus, a more definite analysis of maneuver accuracy has been undertaken.

Analysis: The effects of the following error sources on the accuracy of performing a ΔV maneuver are determined:

$\delta\Psi$ = error in Ψ-sun sensor pulse location

$\delta\Psi_2$ = error in Ψ_2-sun sensor pulse location

$\delta\alpha_1$, $\delta\alpha_2$ = errors in star pulse locations

$\delta\beta$ = error in radial jet pulse centroid location

δm = error in spacecraft mass

δI_a = error in magnitude of axial jet impulse

δI_r = error in magnitude of radial jet impulse

δz = error in spacecraft cg location

μ_a = axial jet misalignment

μ_r = radial jet misalignment

ϵ = spin-axis tilt due to dynamic unbalance

δw = spin speed error

Assuming that the axial jet is firing in a continuous mode and the radial jet is firing in a pulsed mode the total axial ΔV and radial ΔV combine to produce a resultant ΔV as shown in Figure 55.

ΔV_a = total ΔV in axial direction.

ΔV_r = total ΔV in radial direction

ΔV_t = resultant ΔV

η = cant angle of radial jet

The error sources listed previously will contribute to two types of errors in ΔV_t: either an error in the magnitude of ΔV_t or an error in the direction of ΔV_t. This is shown in Figure 56.

ΔV_{td} = desired ΔV_t

ΔV_{ta} = actual ΔV_t

δ = directional error in ΔV_t

ΔV_{tm} = magnitude error in ΔV_t

However, directional and magnitude errors in ΔV_t are equivalent in the sense that a directional error (with no magnitude error) can be reduced to some equivalent magnitude error in the axial jet and some equivalent magnitude error in the radial jet. This relationship is shown next. The purpose in doing this is the following. It will be shown that the individual effects of the error sources (whether they produce magnitude or directional errors in ΔV_t) can be determined directly or from a single family of parametric curves. These individual errors can be rss to produce a resultant error on the magnitude of ΔV_t and an indication of the maximum directional error in ΔV_t.

Equivalence of magnitude and directional errors in V_t: Suppose that there is only an attitude error in the spacecraft but no impulse magnitude errors in the axial or radial jets. Then, at worst, as in Figure 57, there is only a directional error in ΔV_t equal to the attitude error, but no error in the magnitude of ΔV_t, i.e., $|\Delta V_{ta}| = |\Delta V_{td}|$.

It is desired to find an equivalent magnitude error in ΔV_a and an equivalent magnitude error in ΔV_r to produce the actual ΔV_t, ΔV_{ta}. This is illustrated in Figure 58.

δ = attitude error (for example, of spin axis)

$\left.\begin{array}{l}\Delta V_{ad},\\ \Delta V_{rd},\\ \Delta V_{td}\end{array}\right\}$ = desired axial, radial, and total ΔV, respectively

ΔV_{ta} = actual ΔV_t due to attitude error

Φ = angle ΔV_{td} makes with axial or spin direction

δa_e = equivalent magnitude error in axial jet

δr_e = equivalent magnitude error in radial jet

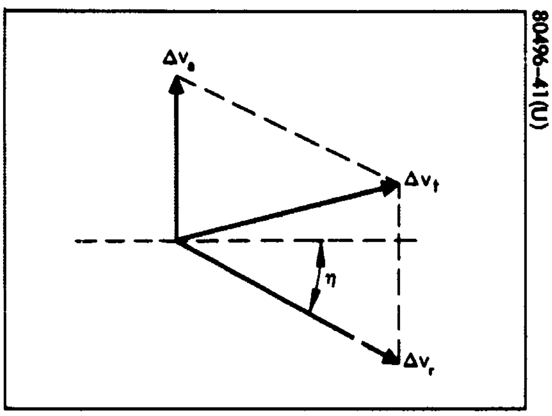

Figure 55. Total Axial and Radial ΔV

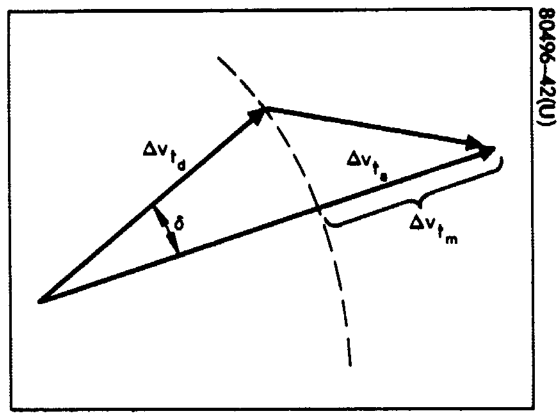

Figure 56. Magnitude and Direction Errors

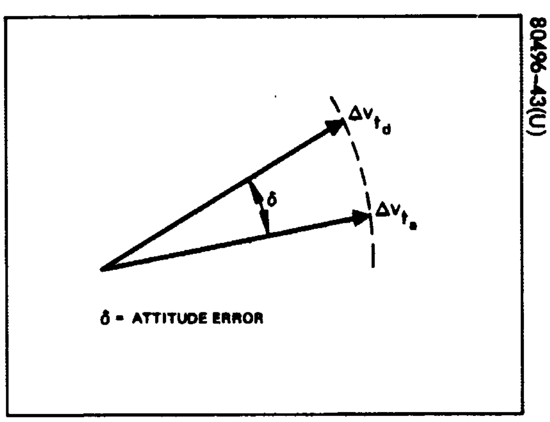

Figure 57. Directional Error in ΔV_t

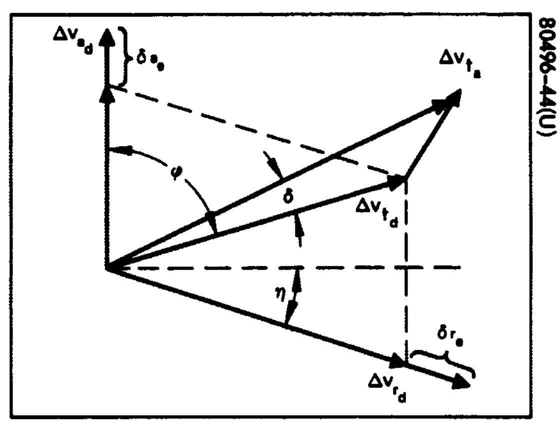

Figure 58. Magnitude Errors in ΔV_a and ΔV_r

Nominally (i.e., with no attitude error), there is

$$\Delta V_{ad} - \Delta V_{rd} \sin \eta = \Delta V_{td} \cos \Phi \tag{23}$$

$$\Delta V_{rd} \cos \eta = \Delta V_{td} \sin \Phi \tag{24}$$

However, with the errors, there is

$$(\Delta V_{ad} + \delta a_e) - (\Delta V_{rd} + \delta r_e) \sin \eta = \Delta V_{td} \cos (\Phi + \delta) \tag{25}$$

$$(\Delta V_{rd} + \delta r_e) \cos \eta = \Delta V_{td} \sin (\Phi + \delta) \tag{26}$$

Using

$$\cos (\Phi + \delta) \approx \cos \Phi - \delta \sin \Phi$$

$$\sin (\Phi + \delta) \approx \sin \Phi + \delta \cos \Phi$$

and subtracting Equations 23 and 24 from 25 and 26 results in

$$\delta a_e - \delta r_e \sin \eta = -\delta \Delta V_{td} \sin \Phi$$

$$\delta r_e \cos \eta = \delta \Delta V_{td} \cos \Phi$$

Hence,

$$\delta r_e = \frac{\delta \Delta V_{td} \cos \Phi}{\cos \eta} \tag{27}$$

$$\delta a_e = \delta \Delta V_{td} \left[\cos \Phi \tan \eta - \sin \Phi\right] \tag{28}$$

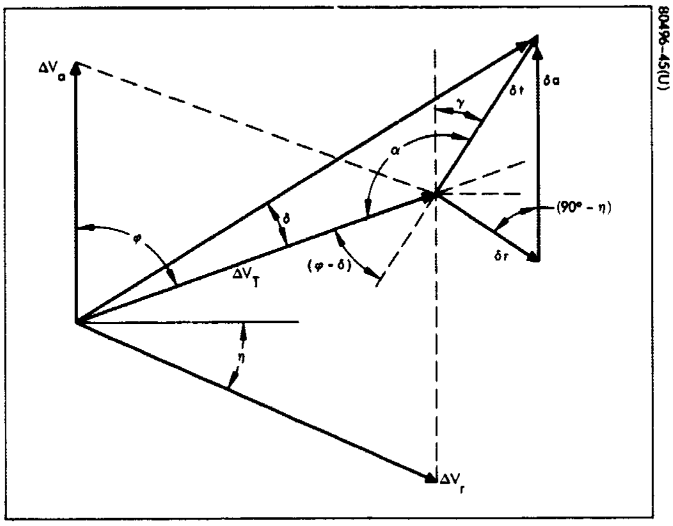

Figure 59. Effect of Magnitude Errors in ΔV_a and ΔV_r on ΔV_t

Equations 27 and 28 give the equivalent magnitude errors in ΔV_a and ΔV_r so as to produce the same error in ΔV_t as an attitude error of "δ".

It should be noted that an attitude error in the spacecraft produces only a directional error in ΔV_t; but magnitude errors in ΔV_a and/or ΔV_r will produce both a magnitude and a directional error in ΔV_t.

Effect of magnitude errors in ΔV_a and ΔV_r on ΔV_t: The next step is to parameterize the effect on ΔV_t of the individual magnitude errors in ΔV_a and ΔV_r. The situation is shown in Figure 59, where

δa = impulse magnitude error of axial jet

δr = impulse magnitude error of radial jet

δt = error in ΔV_t, which is not necessarily parallel with ΔV_t

From the cosine law,

$$\begin{aligned}(\delta t)^2 &= (\delta a)^2 + (\delta r)^2 - 2(\delta a)(\delta r)\cos(90^\circ - \eta) \\ &= (\delta a)^2 + (\delta r)^2 - 2(\delta a)(\delta r)\sin\eta\end{aligned} \tag{29}$$

Define the following parameters

$$k = \frac{\Delta V_a}{\Delta V_r} \tag{30}$$

$$p_a = \text{percentage error in magnitude of } \Delta V_a = \frac{\delta a}{\Delta V_a} \times 100 \tag{31}$$

$$p_r = \text{percentage error in magnitude of } \Delta V_r = \frac{\delta r}{\Delta V_r} \times 100 \tag{32}$$

$$\rho = \frac{p_a}{p_r} \tag{33}$$

Thus,

$$\delta_a = p_a \, \Delta V_a \times 100 \quad \text{and}$$
$$\delta_r = p_r \, \Delta V_r \times 100 \tag{34}$$

Equation 29 then becomes

$$\delta_t = \Delta V_r p_r \sqrt{1 + k^2 \rho^2 - 2 k \rho \sin \eta} \tag{35}$$

Also, from Figure 59

$$(\Delta V_t)^2 = (\Delta V_r \cos \eta)^2 + (\Delta V_a - \Delta V_r \sin \eta)^2 \tag{36}$$

Using the parameters defined as before, Equation 36 becomes

$$\Delta V_t = \Delta V_r \sqrt{1 + k^2 - 2 k \sin \eta} \tag{37}$$

Define p_t = percentage error in magnitude of ΔV_t

then

$$p_t = \frac{\delta_t}{\Delta V_t} \times 100 \tag{38}$$

where

$$\frac{\delta_t}{\Delta V_t} = \frac{p_r \sqrt{1 + k^2 \rho^2 - 2 k \rho \sin \eta}}{\sqrt{1 + k^2 - 2 k \sin \eta}} \tag{39}$$

Define a normalized parameter, F, to be

$$F = \frac{\delta_t}{p_r \Delta V_t} = \frac{\sqrt{1 + k^2 \rho^2 - 2 k \rho \sin\eta}}{\sqrt{1 + k^2 - 2 k \sin\eta}} \tag{40}$$

Equation 40 is plotted in Figure 60, and is to be used as follows: It will be shown that all of the error sources can be reduced to either equivalent magnitude errors in ΔV_a and ΔV_r or directional errors in ΔV_t. In the first case, for a given p_a, p_r, k, and η, the percent error in magnitude of ΔV_t, p_t, can be determined from the curve. In the second case, the attitude error gives $\delta_t / \Delta V_t$ directly as seen by Figure 61.

If ϵ_a is the attitude error of the spin axis, for example:

$$\delta_t \cong \epsilon_a \Delta V_{td} = \epsilon_a \Delta V_{ta} = \epsilon_a \Delta V_t \tag{41}$$

or

$$p_t = \frac{\delta_t}{\Delta V_t} = \epsilon_a \tag{42}$$

Thus, the effect of each of the error sources on the parameter, p_t, defined by Equation 38 can be determined either from using Figure 60 or Equation 42. These can then be rss to produce an rss "p_t", which is a measure of the combined error in ΔV_t.

Define this rss "p_t" to be

$$P_t = \text{rss } "p_t" \tag{43}$$

It should be pointed out that knowing P_t will give the rss magnitude error in ΔV_t but does not give the directional error in ΔV_t directly. However, the maximum directional error in ΔV_t can be determined from P_t. This can be seen from Figure 62.

Assuming the desired ΔV_t is known, the radius of the dotted circle is $P_t \Delta V_t$, and the actual ΔV_t can be anywhere on the circle. Three cases are illustrated in Figure 62, where the actual ΔV_t's are ΔV_{t1}, ΔV_{t2}, and ΔV_{t3}. In each case, the magnitude error is the same; viz, $P_t \Delta V_t$; but the

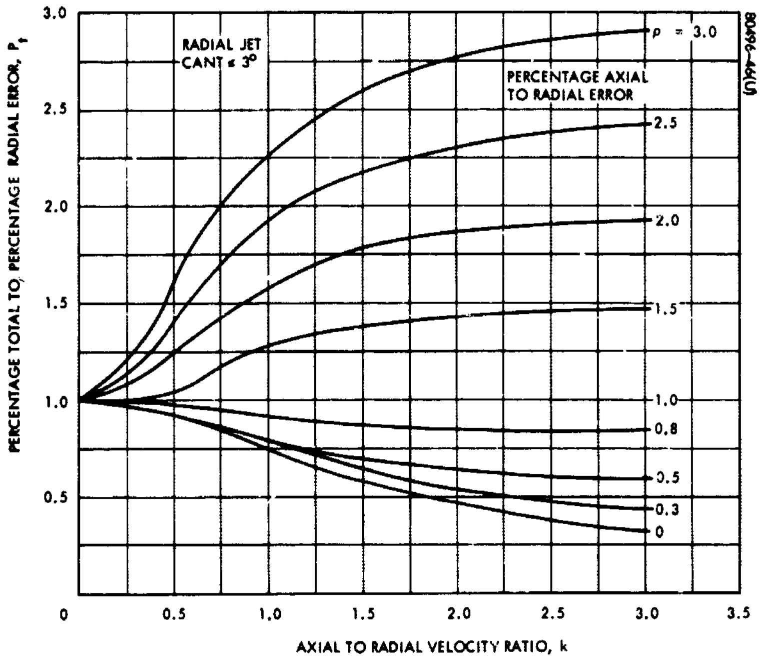

Figure 60. Normalized Error Parameters

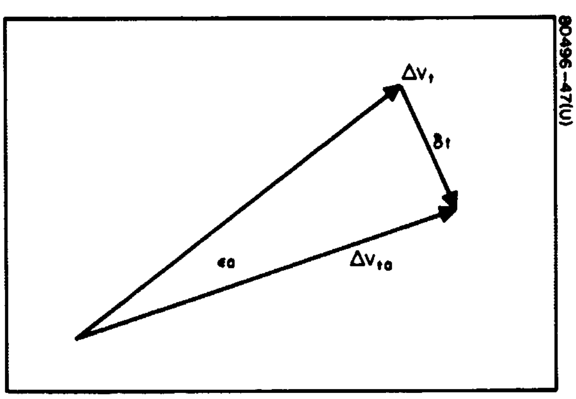

Figure 61. Attitude Errors

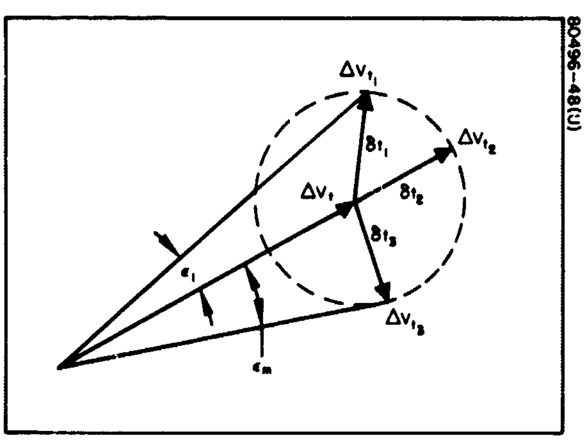

Figure 62. Maximum Directional Error in ΔV_t

directional error in the first case is shown as ϵ_1. There happens to be no directional error in the second case, whereas the maximum directional error, ϵ_m, is shown in the third case. But

$$\epsilon_m \cong \frac{\delta_{t3}}{\Delta V_t} = P_t \text{ (converted to radians)} \tag{44}$$

so that the magnitude error and the maximum directional error is contained in P_t.

The contribution to ΔV_t of each of the error sources is discussed next. In each case, the object is to minimize the amount of computation by normalizing and/or transforming the problem in such a way as to take advantage of Equation 40 (or Figure 60) or Equation 42, i.e., to find an equivalent p_a, p_r, ρ, and ϵ_a defined by Equations 31, 32, 33, and 42, for each error source.

Magnitude errors in ΔV_a and ΔV_r: If the percent error in the axial jet, p_a, and the percent error in the total ΔV, P_t, as a function of "k" can be found directly from Equation 40 or Figure 60 by using the following parameters:

$$\rho = \frac{p_a}{p_r}$$

$$p_r = \text{given}$$

Error in sun pulse and star pulse locations: The sensor configuration consists of two slits: one in a plane containing the spin axis, and the other in a plane inclined with respect to the spin axis by an angle ξ, as shown in Figure 63.

It can be shown that the relationship between Ψ, Φ, and ξ is

$$\sin\Psi = \frac{\cot\Phi}{\cot\xi} \tag{45}$$

Differentiating Equation 45,

$$\delta\Psi\cos\Psi = \frac{\csc^2\Phi\,\delta\Phi}{\cos\xi}$$

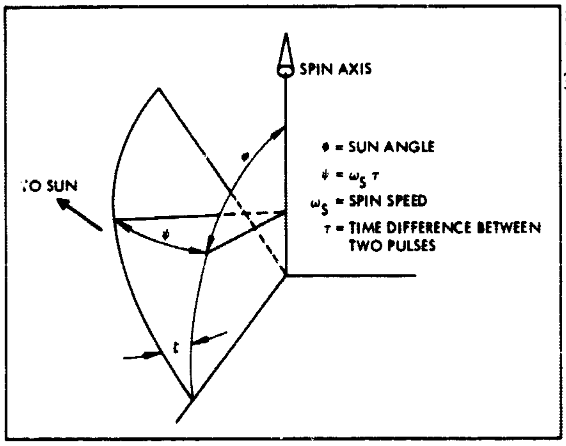

Figure 63. Sensor Configuration

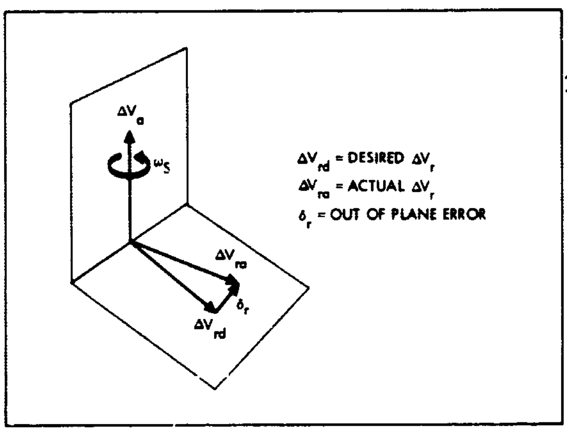

Figure 64. Directional Error in ΔV_t

or

$$\delta\Phi = \frac{-\omega_s \cot \xi \cos \Psi}{\csc^2 \Phi} \delta\tau \qquad (46)$$

For a given error in Ψ-pulse location of $\delta\tau$ (sec), Equation 46 gives the spin axis attitude error, which in turn gives p_t directly from Equation 42. The same procedure can be used for the error due to the star sensor, since it will operate in the same manner.

Error in radial jet pulse centroid location: Assuming the radial jet fires in a pulsed, synchronous mode, a centroid error in the radial jet will produce a directional error in ΔV_t out of the ΔV_a - ΔV_r plane. This directional error in ΔV_t can be computed from Figure 64. $\delta_r = \omega_s \Delta V_r \delta\tau_c$, where $\delta\tau_c$ = error in centroid jet location (seconds).

$$\therefore p_t = \frac{\delta_r}{\Delta V_t} = \frac{\omega_s \Delta V_r \delta\tau_c}{\Delta V_t}$$

or using Equation 37, we get

$$p_t = \omega_s \delta\tau_c \left[\frac{1}{\sqrt{1 + k^2 - 2 k \sin \eta}} \right]$$

where the expression in the bracket can be computed from Equation 39 by setting $\rho = 0$ and $p_r = 1$. Hence, Figure 60 can be used to determine p_t using these values for ρ and p_r.

Error in spacecraft mass: The ΔV's produced by firing the axial jet continuously and the radial jet in a pulsed mode are

$$\Delta V_a = \frac{F_a \Delta_{ta}}{M} \qquad (47)$$

$$\Delta V_r = \frac{G F_r \Delta_{tr}}{M} \qquad (48)$$

where

Δ_{ta} = duration of axial jet burn

Δ_{tr} = duration of radial jet burn

G = geometry factor

An error in the spacecraft mass will produce magnitude errors in ΔV_a and ΔV_r since

$$\delta(\Delta V_a) \equiv \delta_a = \frac{-F_a \Delta_{ta}}{M^2} \delta M \tag{49}$$

$$\delta(\Delta V_r) \equiv \delta_r = \frac{-G F_r \Delta_{tr}}{M^2} \delta M \tag{50}$$

where δM = mass uncertainty.

Now, in order to use Figure 60, we must compute ρ and p_r for this case

$$\delta_r = -\Delta V_r \frac{\delta M}{M} \quad \text{from Equations 48 and 50}$$

$$\therefore \; p_r = \left| -\frac{\delta_r}{\Delta V_r} \right| = \frac{\delta M}{M} \tag{51}$$

Similarly, $p_a = \frac{\delta M}{M}$

$$\therefore \; \rho = \frac{p_a}{p_r} = 1 \tag{52}$$

Hence, for a given percent error in mass, Figure 60 can be used to compute p_t with these values for ρ and p_r.

Error in spacecraft cg location: The shift in the cg will be due to the burning of the propellant. Since the axial jet is fired continuously, the errors due to a cg error will cancel during one spin period.

The radial jet is fired in a pulsed mode, so there will be a net torque during one spin period if there is a cg error. However, this torque is perpendicular to the radial jet direction and will cause a rotation of the spacecraft about this direction. But this does not affect the magnitude of ΔV_r. There are not effects of a cg error on the magnitude of ΔV_t if the following sequence is used. The axial jet is fired first to produce the desired V_a, and the radial jet is fired next to produce the desired ΔV_r. There will be no ΔV_t magnitude errors, although there will be a net spacecraft attitude error.

Axial and radial jet misalignments: The situation is shown in Figure 65.

If the axial jet is fired alone, there will not be a radial component of velocity, but there will be both an axial and radial component of the error, i.e.,

$$\delta_a = - \mu_r \Delta V_r \cos \eta \tag{53}$$

$$\delta_r = - \mu_r \Delta V_r \sin \eta \tag{54}$$

The errors when firing both jets are then

$$\delta_a = - \mu_r \Delta V_r \cos \eta \tag{55}$$

and

$$\delta_r = - \mu_r \Delta V_r \sin \eta \tag{56}$$

Again, to use Figure 60, an equivalent ρ and p_r must be found for this case.

$$p_r = \frac{\delta_r}{\Delta V_r} = - \mu_r \sin \eta \tag{57}$$

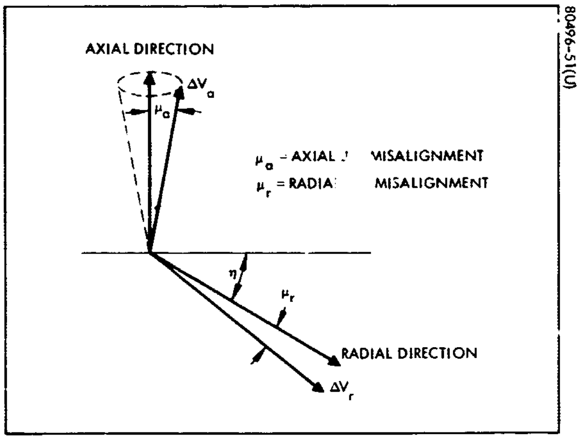

Figure 65. Axial and Radial Jet Misalignments

$$p_a = \frac{\delta_a}{\Delta V_a} = \frac{-\mu_r \cos \eta}{k}$$

$$\therefore \; \rho = \frac{p_a}{p_r} = \frac{\mu_r \cos \eta}{k \, \mu_r \sin \eta} = \frac{1}{k} \cot \eta \qquad (58)$$

Hence, P_t can be computed from Figure 60 by using the values for ρ and p_r computed from Equations 57 and 58.

Spin axis tilt: If ϵ is the spin axis tilt, Equation 42 can be used directly to compute p_t, i.e.

$$p_t = \epsilon \qquad (59)$$

Spin speed error: A spin speed error will produce a timing error in the duration of jet firing. Define the following quantities:

ΔV_{ap} = axial ΔV per pulse

ΔV_{rp} = radial ΔV per pulse

N_a = number of axial pulses

N_r = number of radial pulses

Δ_{ta} = duration axial jet is fired during one spin period

Δ_{tr} = duration radial jet is fired during one spin period

Note that here, one pulse pertains to the duration either jet is on during one spin period.

If ω_s = spin speed,

$\Delta_{ta} = \frac{2\pi}{\omega_s}$ since the axial jet is fired continuously and

$\Delta_{tr} = \frac{2\pi}{\omega_s}$, λ = some fraction, since the radial jet is pulsed

For example, if the radial jet is fired for 90 degrees of spin, $\lambda = 1/4$

Now,

$$\Delta V_a = N_a \ \Delta V_{ap} = \frac{N_a F_a \Delta_{ta}}{M} = \frac{N_a F_a \ 2\pi}{M \ \omega_s} \tag{60}$$

$$\Delta V_r = N_r \ \Delta V_{rp} = \frac{N_r F_r \Delta_{tr}}{M} = \frac{N_r F_r \lambda \ 2\pi}{M \ \omega_s} \tag{61}$$

$$\therefore \ \delta_a = \text{error in } \Delta V_a = \frac{- N_a F_a \lambda 2\pi}{M \ \omega_s^2} \ \delta\omega_s \tag{62}$$

and

$$\delta_r = \text{error in } \Delta V_r = \frac{- N_r F_r \ \lambda \ 2\pi}{M \ \omega_s^2} \ \delta\omega_s \tag{63}$$

Using Equations 60 and 61,

$$\delta_a = - \ \Delta V_a \ \frac{\delta\omega_s}{\omega_s} \tag{64}$$

$$\delta_r = - \ \Delta V_r \ \frac{\delta\omega_s}{\omega_s} \tag{65}$$

Therefore,

$$|p_a| = \frac{\delta\omega_s}{\omega_s} \tag{66}$$

$$|p_r| = \frac{\delta\omega_s}{\omega_s} \tag{67}$$

Again, to use Figure 60, an equivalent ρ and p_r must be determined. From Equations 66 and 67,

$$\rho = 1 \tag{68}$$

$$p_r = \frac{\delta\omega_s}{\omega_s} \tag{69}$$

Summary: The effects on the total ΔV_t due to each of the error sources have been tabulated under each of the sections. The results have been normalized in the sense that the percent error in ΔV_t, p_t, contains both the magnitude error in ΔV_t and the maximum directional error. Furthermore, the errors have been normalized in such a way that p_t can be readily computed as follows. Either the error produces a p_t directly, as in the case of an error in sensor pulse location or spin axis tilt, or Figure 60 can be used, since an equivalent p_a, p_r, and ρ has been computed for each error source. Next, the individual contribution to p_t of each error source can be rss to produce a resultant p_t.

A typical example with the assumptions listed below has been plotted in Figure 66.

Assumptions

Cant angle of radial jet = 3 degrees

Spin rate = 25 rpm

Jet thrust (radial and axial) = 5 pounds

Accuracy of sun sensor and star sensor = 0.5 degree*

Mass uncertainty = ±1 percent

Jet misalignment (radial and axial) = ±0.5 degree

Spin axis tilt = 0.25 degree

Spin speed error = ±1 percent

Impulse magnitude error in radial jet = 5 percent

Impulse magnitude error in axial jet = 4 percent

Spacecraft mass = 1100 pounds

Roll MOI = 312 slug-ft^2

*This number can be related to the actual pulse location error ($\delta\tau$) by Equation 46.

Propellant Budget Analysis. The propellant requirement for the overall mission has been determined by analyzing the requirements for the individual phases of the mission. The maneuvers requiring the expenditure of fuel are: 1) spinup and despin, 2) re-orientation, and 3) velocity corrections.

The fuel used for spin and despin is given by

$$w_{sp} = \frac{2\pi \Delta\omega_s I_r}{60 I_{sp} \ell}$$

where

w_{sp} is the spinup or despin fuel, pounds

Δw_s is change in spin speed desired, rev/min

I_r is moment of inertia about spin axis, slug ft^2

ℓ is perpendicular distance from spin jet to spin axis, feet

Change in spin speed is required several times during the mission as follows:

1) Spinup at booster separation, from zero to 25 rpm

2) Despin prior to lander separation, from 25 to 5 rpm

3) Spinup after lander separation, from 5 to 60 rpm

The re-orientation fuel r· .rement of the spacecraft can be determined from the performance curves or from the point design summary table. Re-orientation is required to accomplish the following:

1) Maintain proper angle between antenna and earth. Total maneuver of approximately 90 degrees.

2) Align lander prior to separation (no greater than 90 degrees).

3) Realign antenna to earth after separation of the lander.

There may be up to four midcourse corrections prior to encounter. The total correction capability is 65 m/sec (213 fps). In computing the fuel required, it is assumed that each velocity correction will be in a random direction. Hence, the 28 percent fuel penalty discussed above applies. Additionally, it was assumed that one-half of the total correction would be performed with the radial jet. Since the radial jet sweeps through an angle of

90 degrees while it is firing, each pulse is only 90 percent efficient. This fuel penalty was assessed.

After lander separation, a ΔV correction must be applied to the SM to place it in the proper Flyby trajectory. The maximum maneuver here is 100 m/sec (329 fps). In order to determine the fuel weight, the same reasoning was applied here as above. The fuel budget summary is presented in Table 10.

Failure Mode Consideration. In a mission of this duration, cost, and complexity, it is necessary to provide a good degree of redundancy. If one-to-one redundancy cannot be provided, then the system must have built into it means by which the functions may be carried out using the remaining operative subsystem. One-to-one redundancy exacts a high price in weight penalty.

In the design of the velocity control system, the thrusters were configured so as to provide a substantial back-up or failure mode capability. Figure 67 shows the placement of the velocity control thrusters. There are four axial and two radial jets.

Table 11 gives the jets used for the several required velocity maneuvers in the normal operating mode. Thruster 5 is mounted so its thrust line passes through the cg of the combined vehicle, and the thrust line of thruster 6 passes through the cg of the SM.

Axial jet failure:

One jet fails – If any single axial jet fails, the axial ΔV maneuver can still be accomplished with the one remaining jet by firing for twice the time.

Two jets fail – If two jets fail that fire in opposite directions such as 2 and 3 or 1 and 4, this is really equivalent to the single jet failure above. Doubling the firing time is all that is required.

If the two jets that fail fire in the same direction such as 2 and 4 or 1 and 3, then the fix is not as simple. To achieve the desired ΔV correction, it would be necessary to rotate the vehicle so that operative jets can be fired in the appropriate direction. Although a nonstandard procedure, the mission would be accomplished. In this case, the pure couple is not available for reorientation, so the ΔV due to the reorientation must be accounted for.

Three jets fail – If three jets fail, the procedure for the double jet failure is instituted. The vehicle is reoriented to point the operative jet in the direction to accomplish the correction. This highly nonstandard procedure would probably be adequate to accomplish the maneuver requirements.

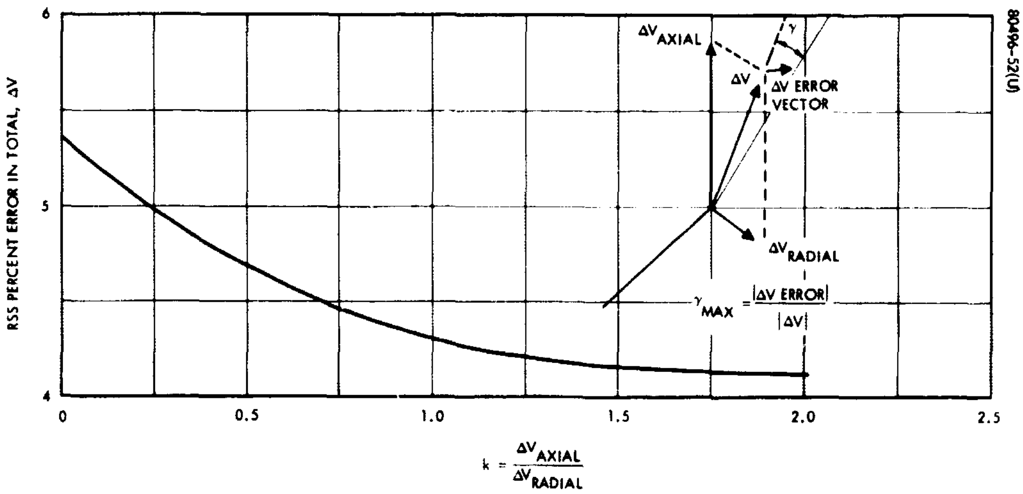

Figure 66. Velocity Error Versus Axial-Radial Ratio

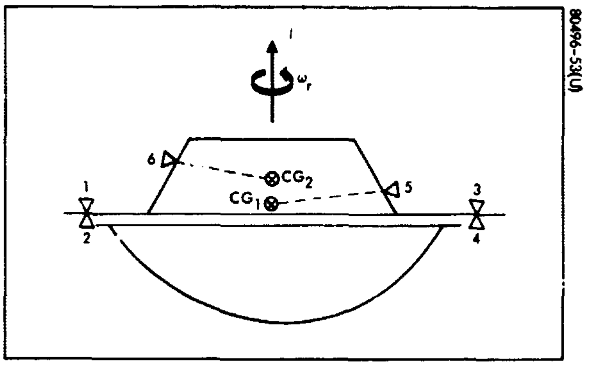

Figure 67. Placement of Velocity Control Thrusters

TABLE 10. MSSM PROPELLANT BUDGET

Maneuvers	Velocity Increment, m/sec	Propellant Weight, pounds
Initial spinup of lander and module to ≈25 rpm	--	1.05
Midcourse corrections typical allocation*	64.8	69.0
1st midcourse	60.0	63.9
2nd midcourse	3.0	3.2
3rd midcourse	0.6	0.6
4th midcourse	1.2	1.3
In-transit attitude corrections to maintain proper angle between boresight and earth (≈90 degrees) high-gain antenna	--	1.38
Attitude maneuver to align lander (≈90 degrees)	--	1.38
Spindown of lander and module to ≈ 5 rpm	--	0.84
Spinup of module to ≈ 60 rpm	--	0.4
Attitude maneuver to align antenna toward earth (≈90 degrees)	--	0.57
Deflection maneuver	100	34.2
Propellant required		108.8
Propellant available		120.0
Contingency		11.2

*A midcourse ΔV correction in an arbitrary direction will, in general, consist of firing a pair of axial jets in the continuous mode as well as pulsing the radial jets in synchronism with spin. Thus, the weight required for a maneuver must be computed using the components of ΔV in the axial and radial jet impulse directions. The weights listed above take into account the vector addition of radial and axial ΔV's to achieve the required spacecraft ΔV.

TABLE 11. NOMINAL JET USAGE

ΔV Maneuver	Jet(s) Fired
Combined Vehicle	
Axial ΔV	
Forward	2 and 4
Aft	1 and 3
Radial ΔV	5
Support Module	
Axial ΔV	
Forward	2 and 4
Aft	1 and 3
Radial ΔV	6

Radial jet:

Aeroshell/lander plus support module — If the nominal radial jet (jet 5) fails, there are two possible courses of action, as follows.

1) Use jet 6. The ΔV correction could be accomplished, but since there is a lever arm between the line of force of jet 6 and the cg of the combined vehicle, an unwanted rotation will result. This can be taken out after the ΔV maneuver is completed.

2) The vehicle could be reoriented so that the maneuver could be performed with the axial jets. If both radial jets fail, the procedure would definitely be used.

Support module alone — Same as 1 and 2 above.

It is apparent from the discussion above that a great deal of flexibility is built into the system, and jet failures, both single and multiple, could be tolerated with little consequence other than initiating a nonstandard procedure.

REACTION CONTROL SYSTEM

In view of the accumulated flight experience of hydrazine thruster systems and the accuracy available from calibrated thrusters, the velocity maneuvers (and some attitude maneuvers, if necessary) may be made in an open loop manner by commanding a specific on time for continous mode thrusting or a particular number of pulses for pulsed mode operation. The essential element of the system design for this study is adequate accuracy rather than feasibility, the latter having been firmly established in extensive design, development, and flight experience. The following discussion defines the Mars spinning support module (MSSM) positioning and orientation system in terms of hardware either existing or under development and, in the light of past and continuing experience, in the application of control thrusters to space vehicles.

Description and Performance

A description of the thruster (propulsion) system selected for the MSSM may be best conveyed by diagrams of the system function and system components. Detail design and assembly are not represented, such details being unwarranted in this preliminary study.

Functional Description of the RCS

Two independent propulsion systems would be arranged on the MSSM to provide thrusters, as indicated in Figure 23. There are two diametrically opposed pairs of axial jets and two radial jets. Each system carries one-half the propellant for the mission, so that complete redundancy may or may not be available, depending upon the amount of propellant actually used and the postulated failure mode. The radial jets are aligned differently, one thrusting through the combined cg of the spacecraft and the other thrusting through the cg of the MSSM alone. Nominally, therefore, utilization of the radial jets is restricted to one jet prior to and the other jet after separation from the lander. However, this situation does not preclude partial redundancy because slightly degraded ΔV performance may readily be obtained utilizing a radial jet operating at some moment arm, as indicated previously under Functional Description and Overall Design Considerations, which also considers the relatively small motion of the combined cg resulting from propellant consumption.

Figure 68 is a schematic of the reaction control system (RCS) arrangement. Each tank contains a temperature transducer and each system has a pressure transducer, these data being necessary for entering the calibration curves to ascertain the number of pulses or duration of firing to achieve a particular velocity increment or attitude change. Re-orientation may, in general, be monitored by the attitude sensors, the calibration curves being required essentially for the ΔV maneuvers.

The spinup/despin jets operate in pairs to produce a pure couple. Note that a spin change requires both tank systems to produce the pure couple about the spin axis. This arrangement simplifies the plumbing,

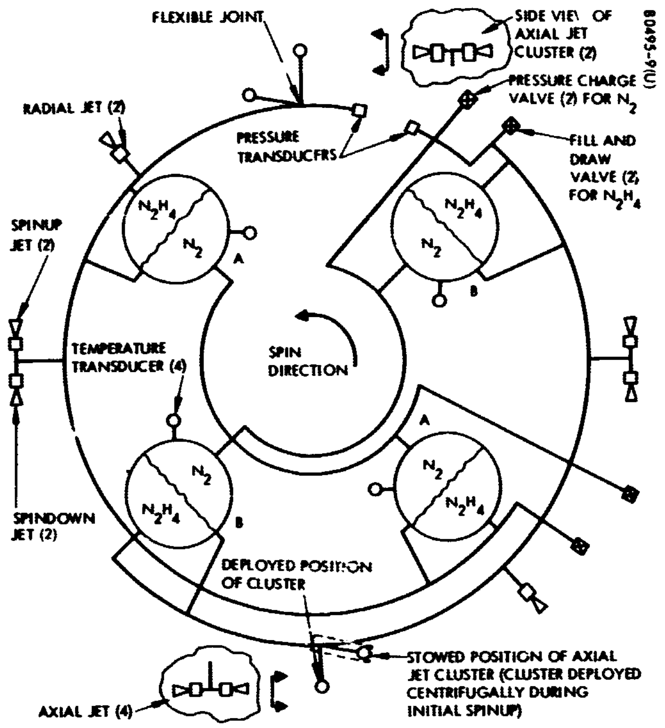

Figure 68. Schematic of Reaction Control Subsystem Arrangement

requiring only one feed line to each spin jet cluster. Should one of the RCS systems be lost, spinup or despin may still be accomplished with a single jet (one jet for spinup, one jet for despin), although the dynamic performance would be somewhat degraded. Loss of one of the RCS systems would not be a serious failure mode for spin changes, provided adequate propellant remained in the other system to effect despin and MSSM spinup. Initial spinup (at zero g) would be assured by one of several approaches. A small flapper valve could be used to prevent propellant loss from the lines, or the use of surface tension screens could be considered. Another possibility is that it may not be possible for the propellant to return to the tanks under zero g. The best approach would be a matter of design study.

The axial jets operate in oppositely directed pairs to produce a pure couple for re-orientation, and in unidirectional pairs to produce axial ΔV. As in the spinup/despin case, almost double redundancy is available in the axial jets because of the specific combinations of failures required before the mission is seriously degraded. (See Failure Mode Analysis and Failure Mode Considerations earlier in this section.)

Deployment of the axial jet clusters may be passively accomplished without the use of electrical signals, squibs, or actuation. This technique was successfully used ontwo Applications Technology Satellite (ATS) missions for deployment of eight VHF antennas. The flexible connection for the hyrazine line would not present any problem. Two approaches would be considered: 1) a flexible bellows line and 2) a coiled line of suitable diameter and number of coils.

The thrusters are controlled through electrically operated valves, there being at least one valve per thruster. Series-redundant valves could be used if desired, as on the Intelsat IV satellite. (Note: Intelsat IV has a design lifetime of 7 years.) The four spin jets attached to the mission-critical propellant supply may possibly not be optimum from a reliability standpoint. Series-redundant valves might be used on these jets, or the spin jets could be separately supplied by their own small propellant tanks for an additional weight of about 2 pounds.

Other elements of the system, including pressure and temperature transducers, pressure charge valve (for nitrogen), and fill and drain valve are items of existing, flight-proven hardware and hardly need consideration in this preliminary study.

Design and Performance

The RCS design and performance are summarized in Table 12. The propellant feed system is of all-welded construction to minimize weight and leakage. Liquid and gas manifolds and all component attachments (except thrusters) use welded joints. High strength titanium is used for the tanks, lines, and gas and propellant fill valves, and the pressure transducers are of stainless steel. Where titanium-to-stainless steel joints are required, diffusion-bonded transition joints are used. A propellant mass fraction of 0.85 is typical as a result of design effort to minimize tankage and fixed hardware weight.

TABLE 12. PROPOSED HYDRAZINE RCS DESIGN AND PERFORMANCE CHARACTERISTICS

Propellant	Monopropellant hydrazine
Pressurant	Gaseous nitrogen
Feed design	Blowdown pressurization and centrifugal force expulsion (spinup is accomplished by using propellant trapped in lines under pressure to supply centrifugal field on propellant in tanks during initial stages of spinup)
Pressure range	275 to 125 psi (typically)
Thrust range	5 to 3 pounds force (typically)
Specific impulse range	225 to 200 lbs-sec/lb (typically)
Pulse width	125 milliseconds to 15 minutes
Total impulse delivered	≈22, 000 lb-sec
Operating temperature range	40° to 120° F
Propellant weight	~120 pounds
Pressurant weight	~2 pounds
Hardware weight	~39 pounds
Tank outer diameter	14. 2 inches
Initial fill fraction	55 percent

Catalytic hydrazine thruster designs are available from several suppliers, including Rocket Research, Walter Kidde, and Hamilton Standard, the latter thruster design having been successfully flown on ATS-3 and subjected to a wide variety of spacecraft maneuvers over the past year.

A Rocket Research thruster design is shown in Figure 69. It is based on the 5-pound engines designed for a Jet Propulsion Laboratory sponsored program for a Ling-Temco-Vought project. Table 13 lists pertinent design characteristics and summarizes component weights of the rocket thrust chamber assembly (TCA). Table 14 presents a performance summary, and Figure 70 gives additional performance data.

A Walter Kidde thruster assembly is shown in Figure 71. The designs referred to here do not necessarily represent the specific design to be used on MSSM, but are presented as typical of the components which could be used. The series-redundant valve selected for Intelsat IV is shown in Figure 72. In view of the relatively short lifetime requirements and the rather low duty cycle required for the MSSM mission, a single valve per thruster would suffice, as in the ATS-3 hydrazine system. The series-redundant valve is shown for the purpose of defining typical component development. Table 15 is a summary of the valve characteristics.

The valve assembly is the most critical component relative to overall mission performance and success. Hughes has placed great emphasis on valve design and performance in all of its RCS system experience, and a company-sponsored valve evaluation program is under way to extensively test several designs obtained from various manufacturers. Any MSSM system design would benefit directly from this program.

The amount of specific design and performance data on typical RCS components is too great to include in this preliminary study. Present RCS technology is more than adequate for the mission requirements, and further discussion of design details would best be left to a more appropriate phase of the program.

Total Impulse Accuracy

Given a state-of-the-art positioning and orientation system, the question most pertinent to the MSSM mission concerns the accuracy with which a maneuver may be made without inertial instruments. The answer hinges directly on predicting the total impulse in a particular sequence of thrust pulses, whether that sequence be one long, continuous pulse or any number of successive pulses of particular duration. In this connection, it should be noted that the Intelsat IV procurement specifications require a total impulse accuracy considerably more stringent than required for the MSSM mission. Factors affecting total impulse, particularly for pulse mode operation, are propellant temperature, tank pressure, number of pulses, length of pulse, and catalyst bed temperature. A specific task of the Intelsat IV thruster development program is a complete mapping of pulse performance as a function of all pertinent variables. The result of such a test program is an extensive set of parametric curves which might be called

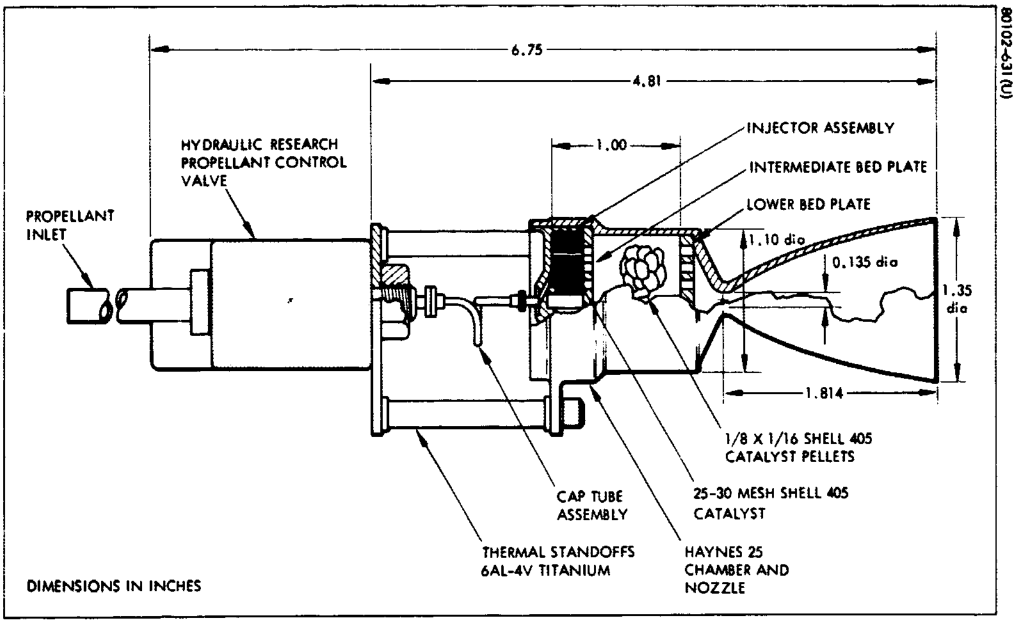

Figure 69. Rocket Research 5-Pound Monopropellant Hydrazine Thruster

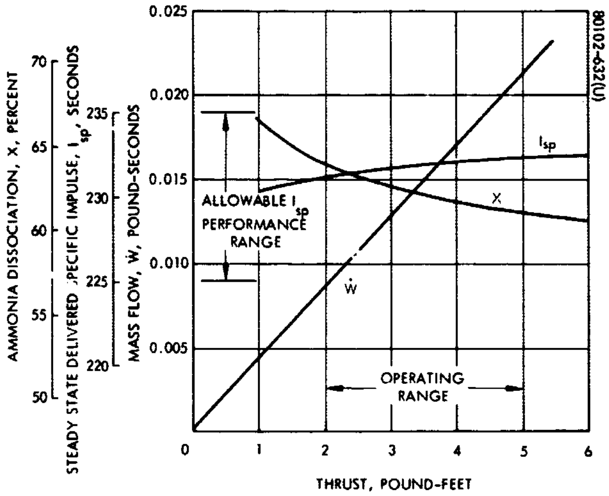

Figure 70. Rocket Research Thrust Chamber Assembly Performance Schedule

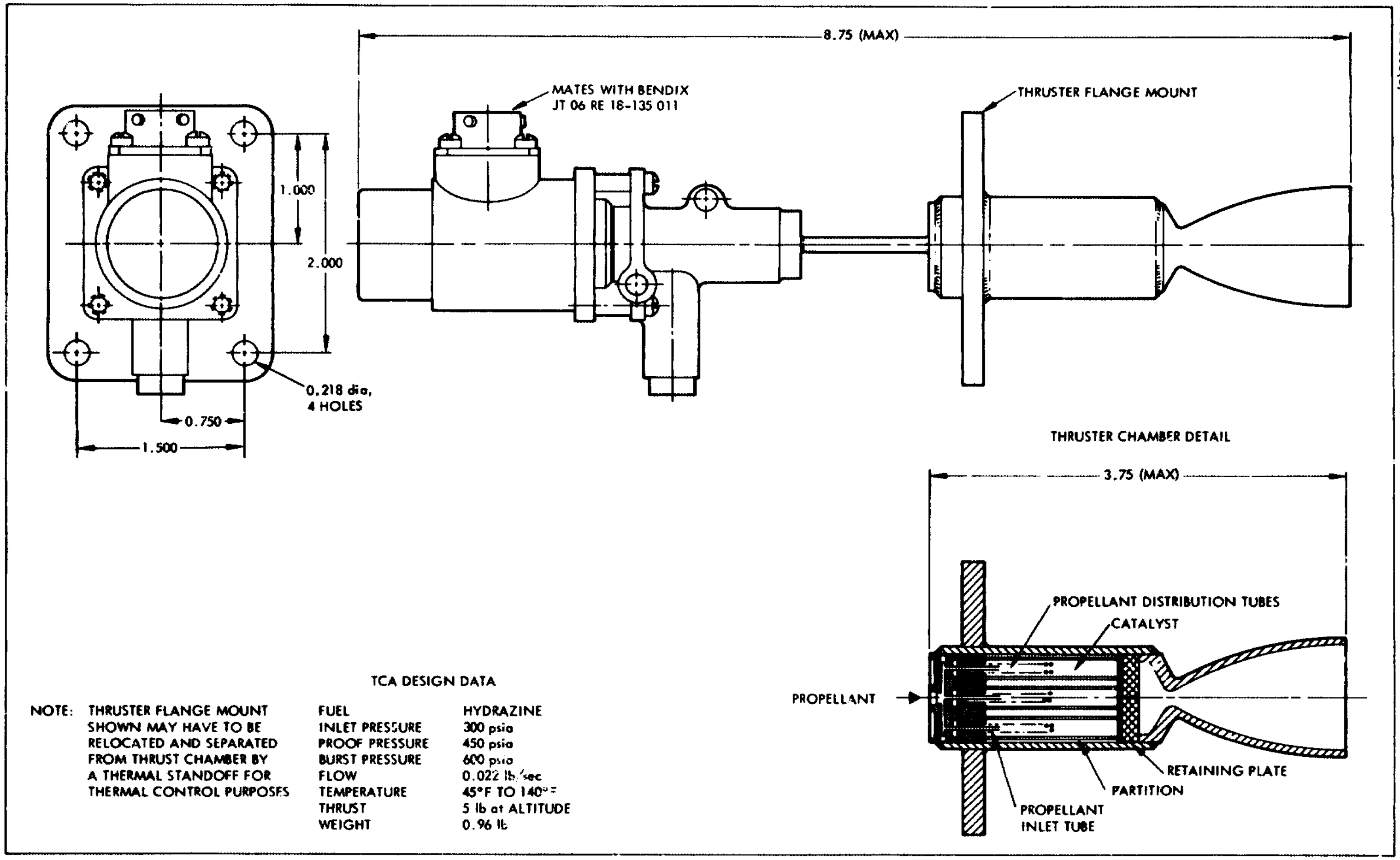

Figure 71. W. Kidde Company 5-Pound Hydrazine Thruster Assembly

TABLE 13. ROCKET RESEARCH TCA DESIGN AND WEIGHT SUMMARY

Design Summary	
Catalyst	Shell 405
Upper bed	25 to 30 mesh granules
Lower bed	1/8- by 1/16-inch pellets
Bed diameter	1.1 inch
Bed length	
Upper bed	0.25 inch
Lower bed	0.75 inch
Total bed length	1.00 inch
Nozzle	80 percent bell contour
Expansion ratio	100:1
Throat diameter	0.135 inch
Exit diameter	1.35 inch
Material selection	
Thrust chamber	Haynes 25 (L605)
Injector	Inconel 600
Capillary feed tube	Inconel 600
Reactor standoffs	Titanium 6A1-4V
Valve mount plate	Titanium 6A1-4B
Weight Summary	
Thrust chamber	0.132
Nozzle	0.042
Catalyst	0.108
Injector	0.075
Feed tube	0.007
Thermal standoff assembly	0.056
Total thrust chamber weight	0.42
Hydraulic research valve weight	0.80
Total thrust chamber assembly weight	1.22

TABLE 14. ROCKET RESEARCH TCA PERFORMANCE SUMMARY

	Initial Condition	Final (3:1 blowdown) Condition
Propellant tank pressure, psia	300	100
Propellant tank temperature, °F	70	70
Valve pressure drop, psia	6[illegible] 7	11.5
Injector and capillary feed tube drop, psia	23.0	3.7
Catalyst bed pressure drop, psia	7.3	3.4
Downstream chamber pressure, psia	200.0	81.4
Delivered thrust, lb-ft	5.00	2.05
Ammonia dissociation, percent	61.2	63.8
Delivered characteristic velocity, fps	4.252	4.136
Delivered thrust coefficient	1.759	1.757
Delivered specific impulse, lb-sec/lb	232.5	231.3
Flow rate, lb/sec	0.0215	0.0091
Bed loading, lb/in^2-sec	0.0264	0.0096

thruster calibration curves. These performance curves are obtained for a particular TCA and its associated valve, lines, and propellant supply under carefully controlled environmental conditions. A typical page of calibration curves for a hydrazine thruster is shown in Figure 73. The variable "impulse bit" is the average impulse per pulse and (for the particular data presented) is applicable only to a specific tank pressure and pulse interval.

The MSSM reaction control system would have a set of calibration curves for each jet (except the spin jets, which do not require any precision). These curves would be in three parts: 1) total impulse (lb-sec) versus "on" time for continuous firing (axial jets only), 2) total impulse versus number of pulses for 45-degree pulse width (all axial and radial jets, at nominal spin of lander plus module), and 3) same as 2), for 90-degree pulse width.

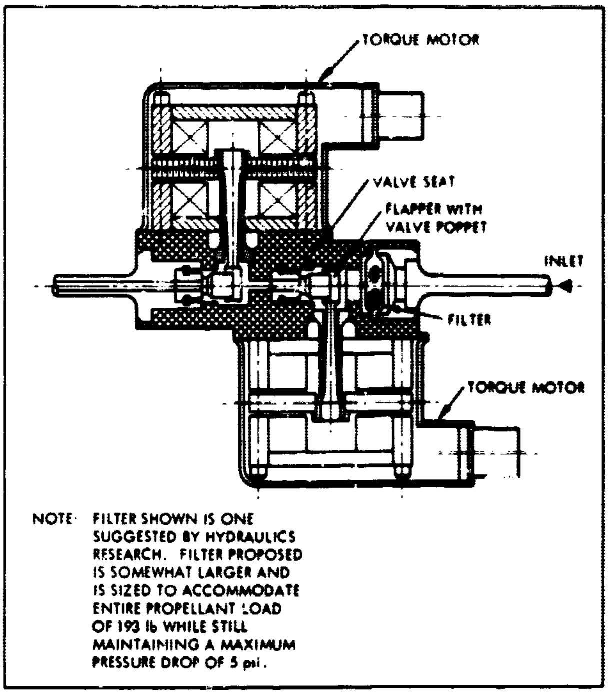

Figure 72. Cross Section of Hydraulic Research Valve

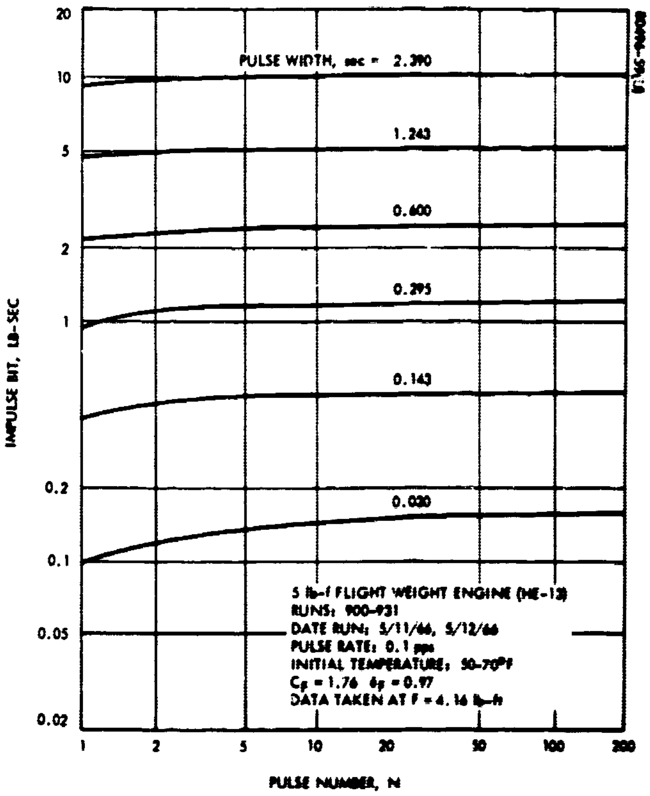

Figure 73. Effect of Pulse Number and Pulse Width on Impulse Bit

TABLE 15. SUMMARY OF VALVE CHARACTERISTICS

Valve type	Torque motor drive, flapper operated
Seat design	Metal-to-metal
Internal leakage	1.0 atm cc/hr GN_2 over range of 350 to 50 psig
Pressure ratings	350 psig operating, 700 psig proof, 1000 psig burst
Response time	2 to 4 milliseconds valve operating time
Flow rate	0.0224 lb/sec N_2H_4 at 20 psig maximum at 70°F
Weight	0.80 pound
Power requirements	40 watts maximum
Position discrimination	Microswitch
Major materials	CRES 304L, tungsten carbide

Another set of calibration curves would apply to the nominal spin of the module after separation from the lander. These calibration curves would govern the operation of the RCS during all phases of the mission and must cover the entire expected range of pressure and temperature.

The most important performance parameter for the RCS is the accuracy of the total impulse for any particular maneuver. This accuracy is a function primarily of the number of pulses (for pulse mode operation). For continuous firing, the accuracy is slightly better than the best accuracy attainable in the pulse mode. Table 16 summarizes the 3σ variation in total impulse accuracy for typical MSSM duty cycles. The accuracy is 4 percent for continuous firing, based on a duration of at least several spin periods.

In terms of actual maneuvers, the accuracy summarized in Table 17 means that any velocity maneuver or precession maneuver will be in error (3σ) by the indicated amount. In other words, using the parametric performance curves discussed previously under Re-orientation Maneuvers and Velocity Maneuvers, and the values of Tables 16 and 17, typical maneuver accuracies are shown in Tables 18 and 19.

The pulse train centroid location error does not mean that the final spin axis attitude will have the same error. A 1-degree re-orientation

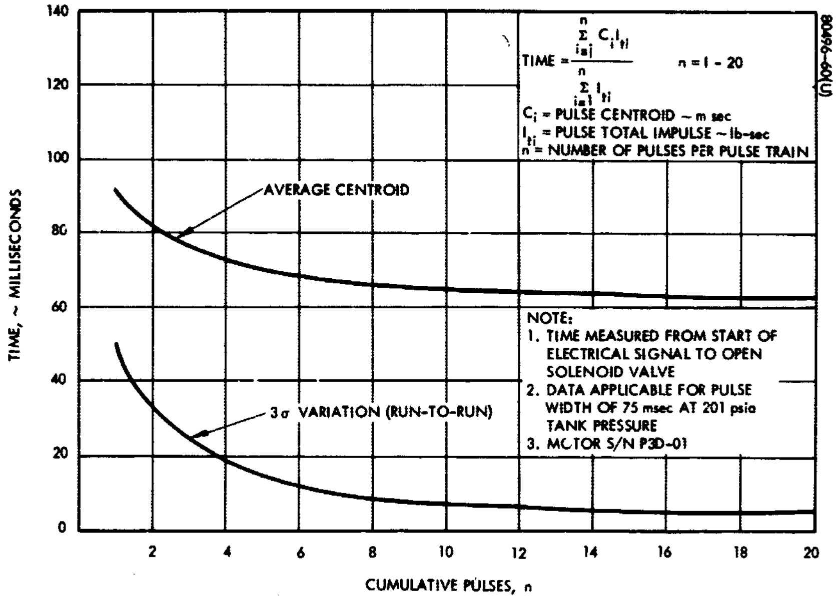

Figure 74. Time of Pulse Train Average Centroid Versus Number of Pulses Per Pulse Train

TABLE 16. ACCURACY OF PREDICTING IMPULSE BIT

Duty Cycle, milliseconds	Pulse Number in Pulse Train	Accuracy (3σ) of Predicting Average Impulse Bit of Pulse Train, percent
500 ON 1500 OFF	2 to 6 6 to 10	±20 ±10
(Typical for axial and radial jet 90-degree pulsing with lander and module together)	10 or over	±5
250 ON 1750 OFF	2 to 6 6 to 10	±30 ±15
(Typical for axial jet 45-degree pulsing with lander and module together)	10 and over	±5
250 ON 750 OFF	2 to 5 6 to 10	±30 ±15
(Typical for axial and radial jet 90-degree pulsing with module)	11 and over	±5
125 ON 875 OFF	2 to 10 11 to 50	±30 ±10
(Typical for axial jet 45-degree pulsing with module)	51 and over	±5

which takes off in the wrong direction by 4.5 degrees (Table 19) has a final attitude error of 1 x tan 4.5 degrees = 0.078 degree.

Typical test results on pulse centroid accuracy for a 5-pound hydrazine thruster are given in Figure 74. The data are for a 75-millisecond nominal pulse (i.e., 75 milliseconds between solenoid valve voltage "on" and "off"). Thus, for an ideal rectangular pulse, the nominal centroid time would be 37.5 milliseconds, indicating a significant lag of the actual centroid. This average shift in centroid is taken into account in the commanded start angle for pulse mode operation.

TABLE 17. ACCURACY OF PREDICTING IMPULSE BIT CENTROID LOCATION

Duty Cycle, milliseconds	Pulse Number in Pulse Train	Accuracy (3σ) of Predicting Average Centroid Location of Pulses in a Pulse Train, milliseconds
500 ON 1500 OFF	2 to 6 6 to 10 10 and over	±50 ±40 ±20
250 ON 1750 OFF	2 to 6 6 to 10 10 and over	±30 ±30 ±11
250 ON 750 OFF	2 to 5 6 to 10 11 and over	±30 ±30 ±11
125 ON 875 OFF	2 to 10 11 to 50 51 and over	±30 ±30 ±11

TABLE 18. 3σ ΔV ERRORS

Configuration	Maneuver	Amount, fps	3σ Error, fps
Combined	Axial ΔV	1 5 50	0.04 0.20 2.0
	Radial ΔV	1 5 50	0.05 0.25 2.5
MSSM	Axial ΔV	1 5 50	0.04 0.20 2.0
	Radial ΔV	1 5 50	0.05 0.25 2.5

TABLE 19. 3σ ERROR IN PULSE TRAIN CENTROID LOCATION

Configuration	Maneuver	Amount, degrees	3σ Pulse Centroid Error, degrees
Combined	Re-orientation	1	4.5
		5	4.5
		20	1.7
MSSM	Re-orientation	1	4.5
		5	4.5
		20	1.7

Reliability and Environmental Considerations

The positioning and orientation subsystem, as discussed above, has mechanical, but not propellant, redundancy. To preclude the trapping of unusable propellant in one system in the event of thruster valve closed failures, an interconnect line containing a normally closed, squib-acuated valve could be incorporated. In view of the inherently high reliability already demonstrated by the type of system proposed here, such an additional safeguard hardly appears warranted. It is being used in Intelsat IV because of the 7-year life requirement.

An extensive program for leakage measurement would be a part of the RCS test plan. With all-welded fabrication, leakage is minimized. Typical predicted leakage for the MSSM mission, extrapolated from Intelsat IV data, is indicated in Table 20.

The area of component reliability and failure modes for the RCS system has been and continues to be exhaustively treated at Hughes as a normal activity in the various hardware programs. A summary of various failure considerations and the preventive features employed is given in Tables 21 and 22.

Sterilization has been examined at length in the Voyager studies at Hughes, from which it was concluded that the entire hydrazine system could be sterilized in a loaded configuration.

TABLE 20. PREDICTED MAXIMUM LEAKAGE RATES

Component	Maximum Leak Rate, atm cc/hr of helium	1-Year Pressure Loss, percent
All gas-exposed surfaces	0.011	0.018
Axial solenoid valves	6	0.37
Radial solenoid valve	3	0.18
Tangential solenoid valves	6	0.37
Capped propellant fill valve	0.50	0.22
Rest of liquid-exposed surfaces	0.076	0.03
Maximum total subsystem pressure loss in 1 year		1.18

TABLE 21. PRIMARY FAILURES

Component	Failure Mode	Preventive Features
Thruster	Catalyst bed deterioration Catalyst bed powdering Retainer ring failure	1) Design considerations 2) Preconditioning of catalyst 3) Extensive qualification program featuring demonstration of twice required life over full environmental range
Propellant fill valve	Leakage	1) Cap with redundant seal 2) Gas leak test 3) Position valve to "see" liquid only
Filter	Passage of contaminant	1) Inspection 2) Flushing and purging subsystem manifolds
	Clogging shut	1) Flushing and purging subsystem manifolds
Tanks	Leakage	1) X-ray welds 2) Leak test
	Rupture	1) Surveyor-developed design consideration, proof pressure test, plus one-in-ten burst test
Pressure transducer	Mechanical/electrical failure	1) Design consideration 2) Previous history
	Leakage	1) X-ray welds 2) Leak test
Total subsystem	Manifold rupture	1) Hughes-developed fabrication and handling features
	Leakage	1) Use of all-welded design with minimum of mechanical seals 2) Position mechanical seals to be exposed to propellant during mission life
	Particulate contamination	1) Flush and purge tanks and manifolds

TABLE 22. PRIMARY FAILURE MODES OF THRUSTOR VALVES

Failure Mode	Preventive Features
Failure to open	1) Valve thermal control
	2) Use of compatible materials
	3) Filtration of contaminants
	4) Design of electrical connection
	5) Control of wire flexing
Failure to close	1) Spring design and material selection
	2) Series-redundant seat design
	3) Filtration of contaminants
Leakage	1) Filtration of contaminants
	2) Series-redundant seat design
	3) Leak test and X-ray inspection
	4) Use of hard seats and poppets

TELECOMMUNICATIONS

The Flyby-Video Data SM telecommunications subsystem provides for continuous SM communications with the NASA DSN during the 1973-74 Mars mission. This function is especially important during the Mars flyby phase when the SM relays 10^7 bits of lander video data at a nominal bit rate of 16,000 bits/sec. Prior to flyby, the SM accepts DSN commands and transmits SM and A/L telemetry data. These functions are all performed at S-band frequencies and allow for SM range and range rate determination by the DSN.

The SM telecommunications subsystem also receives A/L entry and video data at a frequency of 400 MHz, UHF, during the flyby phase. The video and entry data rates are 16,000 and 2000 bits/sec, respectively.

In addition, the telecommunications subsystem decodes DSN commands for the SM and A/L, encodes SM and A/L telemetry data, and converts the A/L UHF data into S-band data.

Video Data Link

The SM to DSN video data communications link uses a bit rate of 16,000 bits/sec. Since entry data also must be relayed, but at a lower rate of 2000 bits/sec, the video link capability is adequate for both functions. Trajectory analysis indicates the maximum SM to DSN range at flyby is no greater than 160×10^6 km for the direct entry mode arrival period.

The 1973 DSN configuration is expected to include two 210-foot antennas, one at Goldstone, California, and the other at Woomera, Australia, each with 400 kw radiated power capability. Since two DSN stations are not adequate for continuous communications with the SM, the 85-foot antenna systems also will be used. These and other significant DSN parameters are given in Table 23. In addition to the data in Table 23, a PCM/PSK/PM modulation technique is used because of its efficiency and wide acceptance, as indicated by its anticipated use for all future missions conducted from the NASA DSN.

The quality of the received video data, or its bit error rate (BER), is set at 10^{-3} based on present engineering practice. This value of BER implies a specific signal-to-noise ratio (SNR) that must be sustained by the video data transmission link. The determination of the SNR is based on the conservative design practice of directly adding all communication link tolerances to obtain a worst-case dB design margin.

Although the modulation technique has been specified, the coding technique must be decided upon. A convolutional encoding approach has been selected to minimize the SM telecommunications subsystem video link requirements. The video link performance is increased by approximately 4.8 dB, with acceptable SM hardware complexity, over a link using standard

TABLE 23. RF LINK ANALYSIS PARAMETERS
(FLYBY - VIDEO DATA)

Parameter	Down-Link MSSM – DSIF Telemetry	Up-Link DSIF – MSSM Commands	UHF-Link A/L – SM Telemetry, Video
Frequency	2295 MHz	2113 MHz	400 MHz
Carrier-pred. noise BW	5.0 Hz ±0.5 Hz	12.0 Hz ±1.2 Hz	8.5 kHz ±850 Hz[2]
Channel pred. noise BW	Bit rate in kHz ±10%	Bit rate in kHz ±10%	--
Carrier SNR threshold	7.0 dB ±1.0 dB	6.0 dB ±1.0 dB	10 dB ±0 dB
Channel SNR threshold	2.5 dB ±1.0 dB	11.0 dB ±1.0 dB	--
Support Module:			
RF output power	3 or 40 watts ±0.5 dBm	--	--
Circuit loss	-1.5 dB ±0.5 dB	-3.5 dB, +0 dB, -0.7 dB	-0.5 dB, +0 dB, -0.5 dB
Antenna gain	G_T dB, +0 dB, -0.5 dB	G_R dB, +0 dB, -6.5 dB	G_R dB, +0 dB, -0.5 dB
Pointing loss	0 dB, +0 dB, -PL dB	0 dB, +0 dB, -PL dB	0 dB, +0 dB, -PL dB
Polarization loss	--	-0.5 dB, ±0.3 dB	-0.5 dB ±0.3 dB
Noise temperature	--	500°K ±50°K	226°K ±23°K
210-foot diameter dish:			
RF output power	--	400 kw ±1 dBm	--
Circuit loss	-0.18 dB ±0.05 dB	-0.4 dB ±0.1 dB	--
Antenna gain	61.4 dB ±0.3 dB	59.8 dB ±0.5 dB	--
Pointing loss	0 dB	0 dB	--
Polarization loss	-0.5 dB ±0.3 dB	--	--
Noise temperature	33°K ±8.0°K	--	--
85-foot diameter dish:			
RF output power	--	100 KW ±1 dBm	--
Circuit loss	-0.18 dB ±0.05 dB	-0.6 dB ±0.2 dB	--
Antenna gain	53.5 dB ±0.6 dB	52.1 dB ±0.9 dB	--
Pointing loss	0 dB	0 dB	--
Polarization loss	-0.5 dB ±0.3 dB	--	--
Noise temperature	55°K ±10°K	--	--
Aeroshell/lander:			
RF output power	--	--	50 watts ±0.5 dBm
Circuit loss	--	--	-1.7 dB ±0.6 dB
Antenna gain	--	--	6 dB, +0, -0.5 dB
Pointing loss	--	--	0 dB, +0 dB, -6 dB

[2]Value shown is the amount necessary to support doppler shift and frequency instability, to this must be added the BW required for the information (example: 2 KDPS requires 10.5 KHz ±1.05 KHz).

coding. The DSN burden is increased because sequential decoding requires additional computational equipment. This approach also was considered in past Voyager studies. Should the selection prove unacceptable, the SM and Flyby trajectory design have adequate margin to absorb the redesign necessary to follow the standard coding technique.

Since it is desirable to isolate the required transmitter power and antenna gain for tradeoff studies, the SM communications parameters listed in Table 23 have been estimated. A -3 dB loss also is included in the video link to account for the use of a narrow-beam high gain antenna over its half power region of operation.

Figure 75 plots the required transmitter power-antenna gain product, in dB, as a function of bit rate and range. The corresponding modulation index (MI) of the data subcarrier on the carrier frequency is selected to minimize the total power-gain product consistent with satisfying carrier and channel thresholds. The MI is 1.84 radians for the bit rate range plotted. The link margin for generating the data is a worst-case sum of the individual link tolerances.

The data presented in Figure 75 have been replotted in Figures 76 and 77 for the nominal video and entry data bit rates. Figure 76 plots the transmitter-antenna product as a function of range, and Figure 77 plots the required transmitter power and antenna gain that will sustain the desired bit rates. These plots are in a convenient format for use in antenna and transmitter design and tradeoff studies.

Planar Antenna

The SM video data antenna is designed to produce its maximum gain in a direction along the SM spin axis. This allows the antenna to be firmly mounted to the SM structure and still maintain uninterrupted communications with the earth when the spin axis is directed at the earth. Also, since the antenna must radiate in the same direction the solar panels are viewing, it must not obscure the solar panels from the sun's solar energy. The inner diameter of the panels, therefore, determines one maximum antenna dimension. Also, since the minimum distance between the SM and A/L and canisters is of concern, the antenna dimension in the spin direction is minimized. These geometrical constraints along with the desire to maximize the antenna gain and maintain a beamwidth compatible with attitude control accuracy results in the selection of a planar antenna.

Figure 78 shows the relationship between gain, halfpower beamwidth (HPBW), and planar array surface area. The gain is computed by using

$$G = \eta (4\pi) A/\lambda^2$$

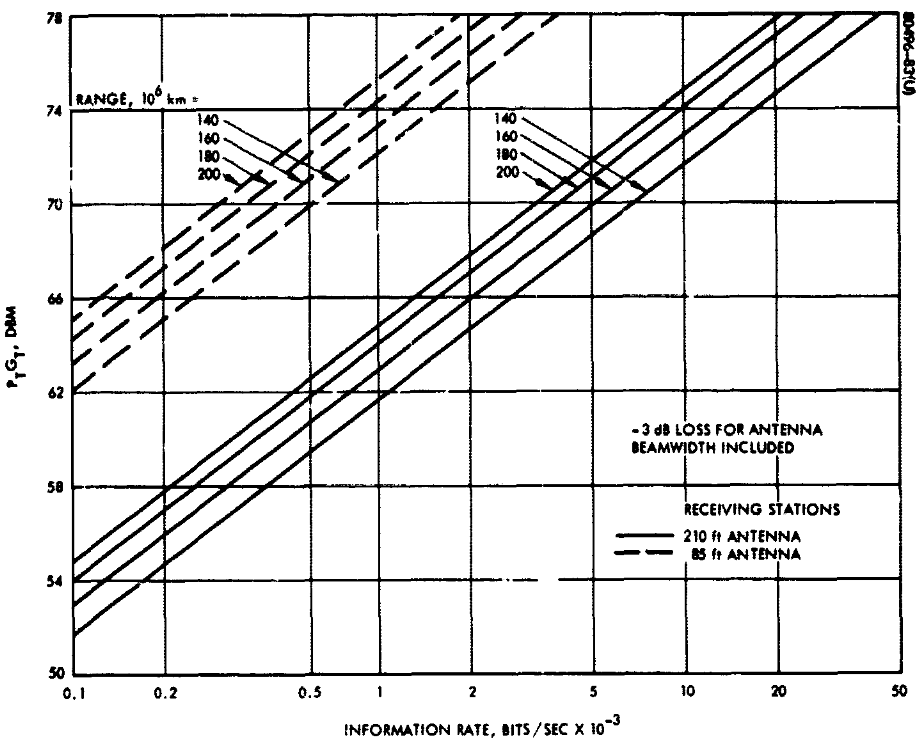

Figure 75. Transmitter Power Times Antenna Gain Versus Bit Rate

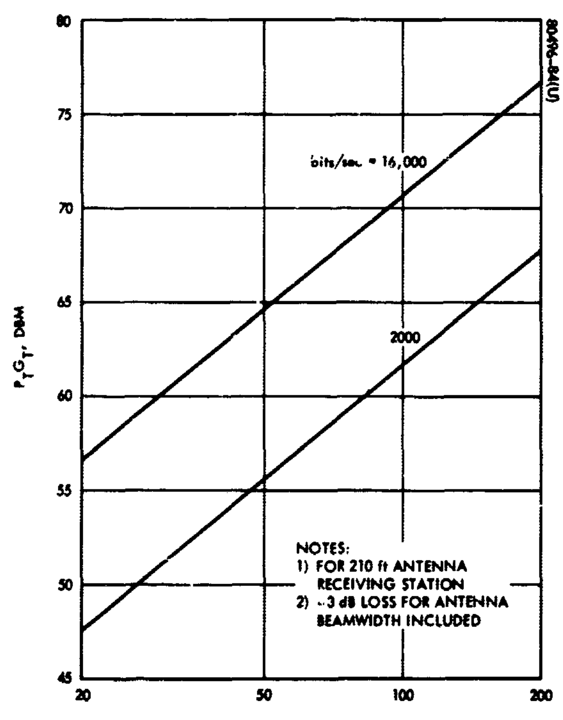

Figure 76. Transmitter Power Times Antenna Gain Versus Range

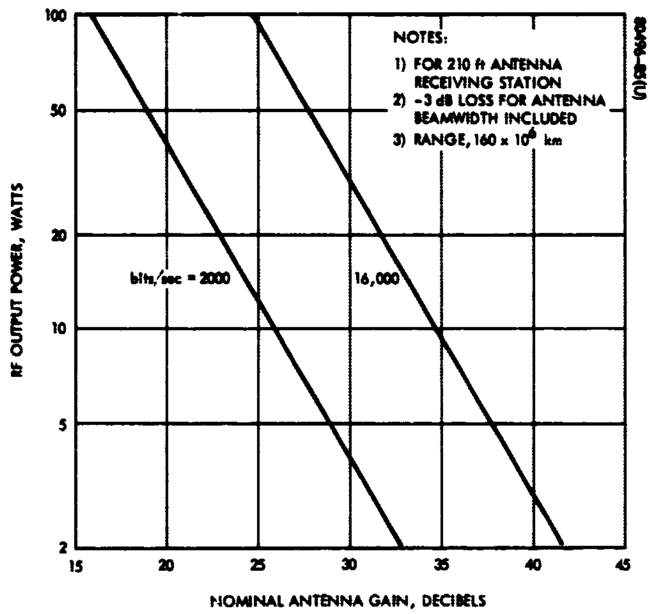

Figure 77. Transmitter Power Versus Antenna Gain

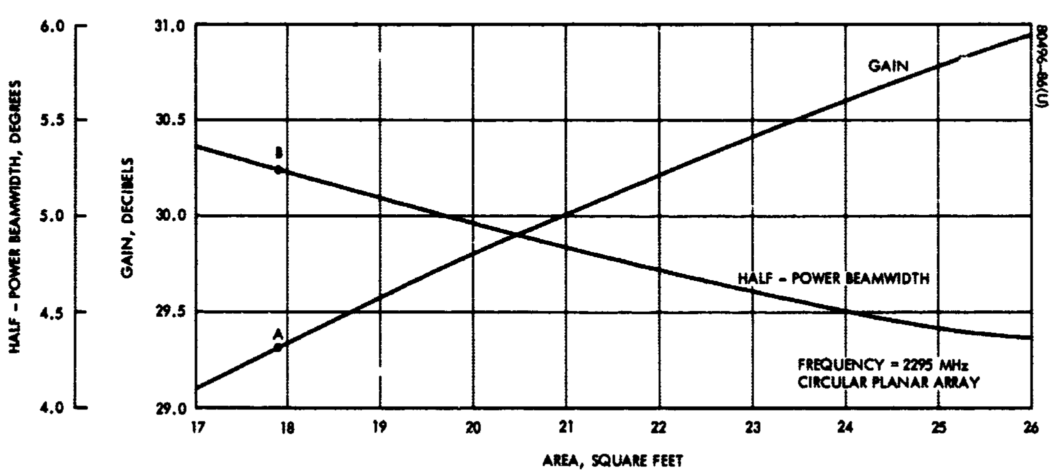

Figure 78. Gain and Half Power Beamwidth Versus Antenna Size for SM S-Band Planar Array

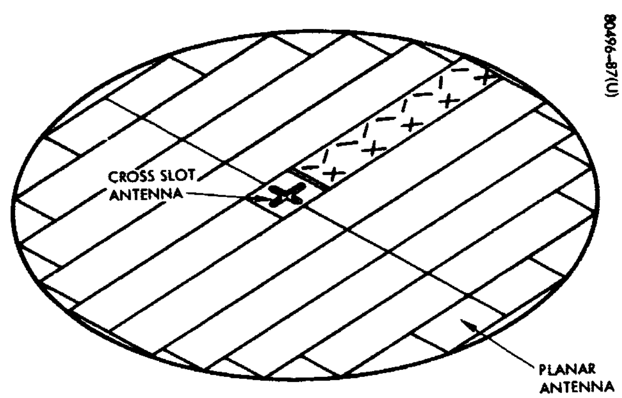

a)

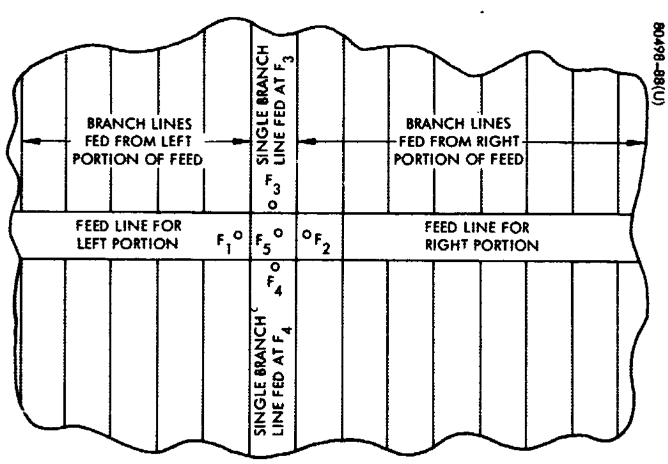

b)

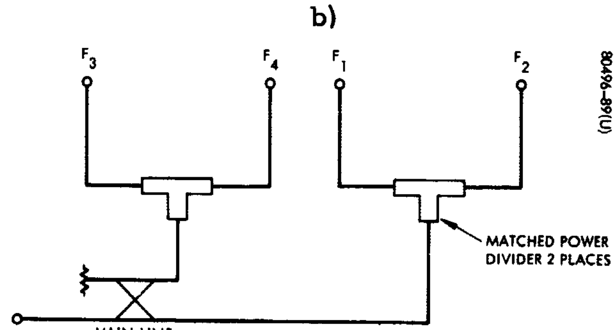

c)

Figure 79. Planar Antenna and Feed System

where

η = aperture efficiency (70 percent is used based on expected large diameter array performance)

A = actual surface area

λ = free space wavelength

The HPBW has been empirically found to be 58.4 $(\lambda/2a_m)$ where a_m is the mean radius, $(A/\pi)^{1/2}$. Using the Figure 78 data and stated constraints, the following planar antenna parameters have been selected:

Gain	29.2 dB, on axis
HPBW	5.2 degrees
Area	17.0 square feet
η	70 percent
Polarization	Right-hand circular

A general planar antenna sketch and a feed system are shown in Figure 79. A low-gain cross-slot antenna used during the mission cruise phase is an integral part of the planar antenna. F_1 and F_2 are tied together by a matched power divider, with F_3 and F_4 similarly coupled. A coaxial directional coupler is used to couple the proper amount of power from the main line and direct it to F_3 and F_4. F_5 is the cross-slot antenna terminal. Figure 80 is a Surveyor antenna constructed from rectangular cavity backed sections. Based on Surveyor weight, the Flyby - Video design antenna system is estimated to weigh 14 pounds.

High Power Transmitter

Figure 77 indicates that a transmitter with approximately 37 watts of power output suffices with the 29.2 dB antenna to satisfy the video data link requirements. A 40-watt transmitter is used for the SM subsystem because it can be readily implemented from Surveyor or Mariner type S-band equipment. Two Hughes 20-watt TWTs operating in parallel are included in the transmitter design. The transmitter weight is estimated to be 20.6 pounds, including a 3-watt transmitter used during the cruise phase of the mission. The margin of 3 watts provided by the 40-watt transmitter allows for a video transmission rate of 17,000 bits/sec at the Mars distance.

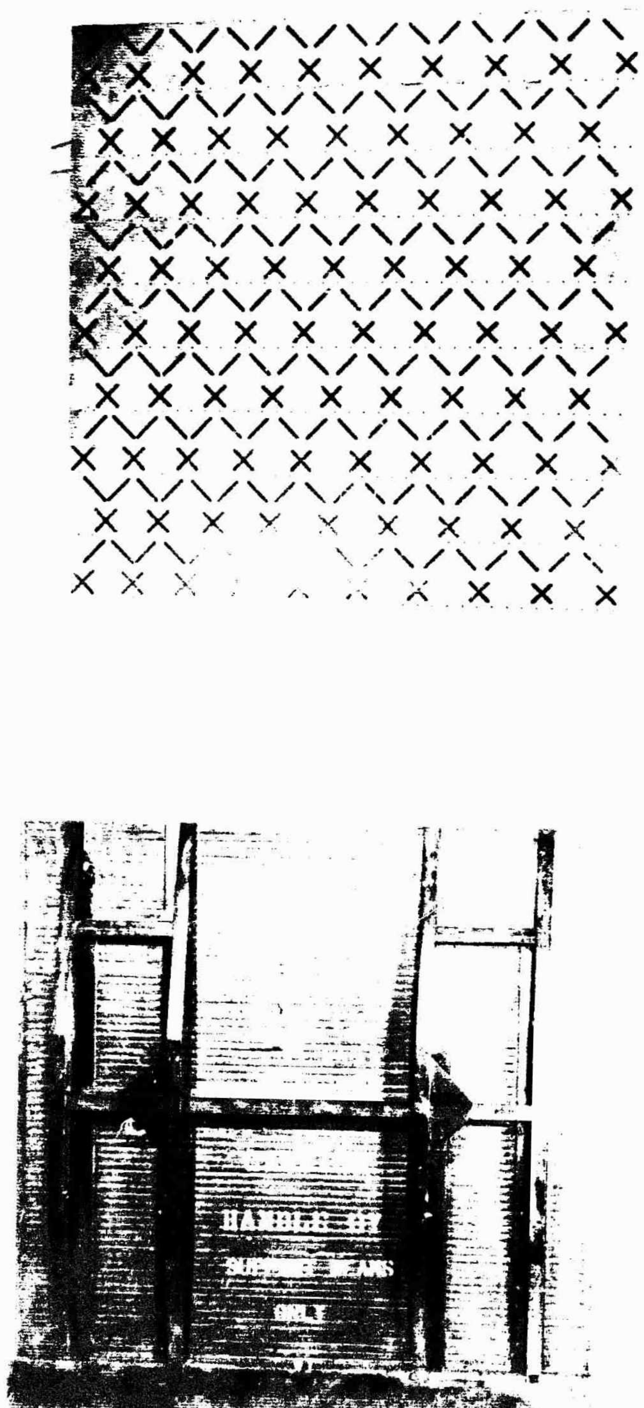

Figure 80. Productized Circularly Polarized Planar Array for Surveyor

Telemetry Link

The SM-to-DSN telemetry link is designed to relay A/L data at a rate of 1050 bits/hr, ≈ 0.3 bits/sec, plus SM subsystem data at a reasonable rate of at least 3 bits/sec during the entire mission. Also, during midcourse correction and pre-A/L separation, a rate as high as 2000 bits/sec is required. The planar antenna operating with a low power transmitter could perform this function, but the need for continuous spacecraft attitude corrections to direct the beam at the earth and loss of telemetry during encounter attitude maneuvers veto its use for the total mission. Instead, a wide beamwidth cross-slot antenna and low-power transmitter are used for this link during the first 90 days of the mission and the planar antenna used from 90 days to encounter except during the brief encounter maneuver period.

The particular mission geometry and required SM radiated power to sustain the telemetry link results in the selected cross-slot antenna and a 3-watt transmitter. The cross-slot antenna which weighs 0.5 pound is an integral part of the planar antenna having a hemispherical gain of at least -6 dB with a peak on-axis gain of approximately 3 dB and a gain which falls off to -1 dB 60 degrees off the axis. By placing the antenna flush with the surface and in the center of the planar antenna, it uses the planar antenna as a ground plane to increase its efficiency. The cross slot may cause more planar antenna energy to be transferred to the sidelobes, thereby slightly decreasing the planar antenna gain and beamwidth. A 3-watt S-band solid-state transmitter is presently under development at Hughes.

The SM-to-earth line nominally will be within 60 degrees of the spin axis, implying at least -1 dB is available with the cross-slot antenna. A link analysis yields the plot of telemetry bit rate capability versus range (Figure 81). The data are plotted for the 3 and 40-watt transmitters working with either the DSN 85-foot or 210-foot antenna. The plot indicates 3 to 4 bits/sec can be sustained to an SM-to-earth distance of approximately 70×10^6 km or 110 days of flight time using the 3-watt transmitter and 210-foot dish. Also, during the encounter maneuver phase of the mission, 24 bits/sec is available if the 40-watt transmitter and 210-foot dish are employed. Figure 82 is a plot of the required cross-slot gain versus range required to support telemetry or DSN commands at a rate of 3 bits/sec. Various combinations of SM transmitter power and DSN transmitter and receiving antenna sizes are also shown. This figure allows the acceptable SM attitudes and therefore cross-slot gains to be studied as a function of the designated parameters.

To maintain the telemetry link after 110 days, the planar antenna is used. A series of four SM attitude maneuvers may be required to keep the antenna pointing at the earth if 90 days after earth injection is assumed as discussed in the Trajectory/Navigation section. Figure 83 plots the planar bit rate capability as a function of range for various dish sizes, DSN-to-SM planar electrical boresight angles, and SM transmitters.

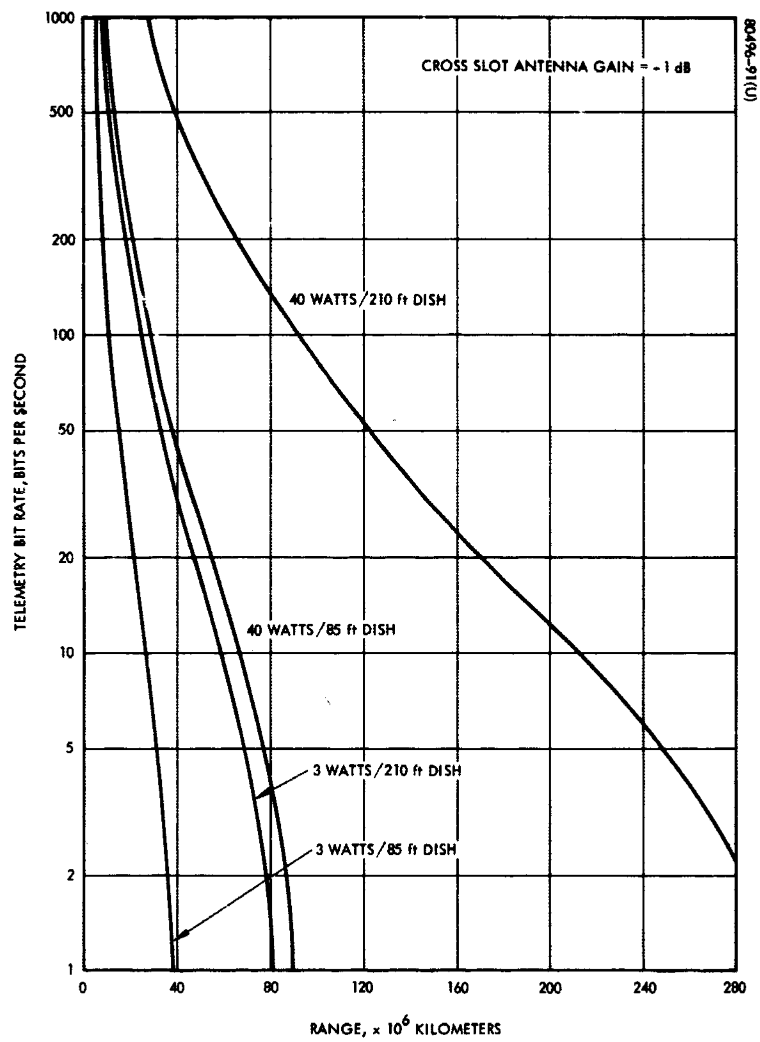

Figure 81. Telemetry Bit Rate Versus Range for Several Values of SM RF Level and DSIF Antenna Diameter

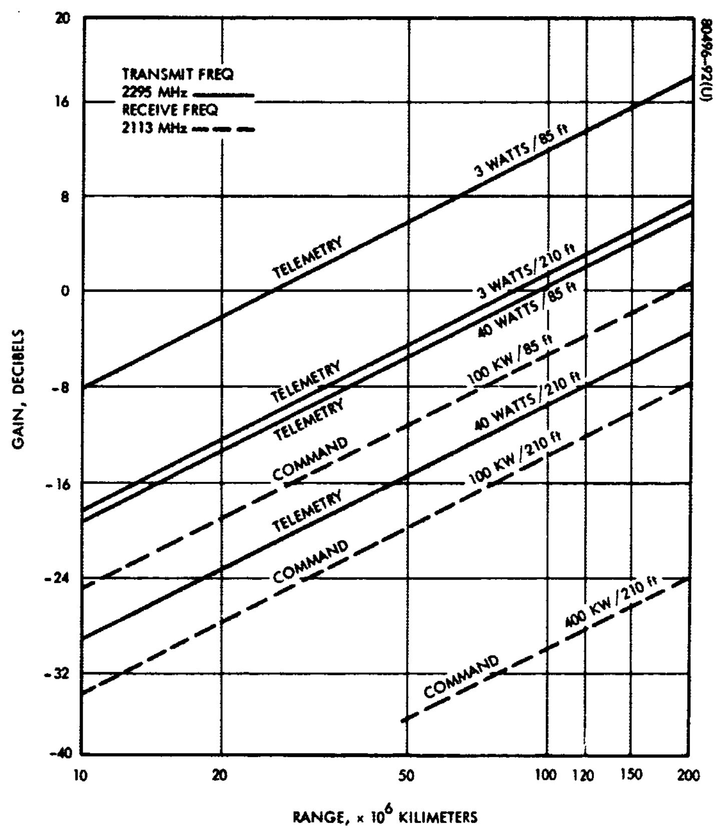

Figure 82. Support Module Antenna Gain Required to Support 3 bps Telemetry or Command Rate

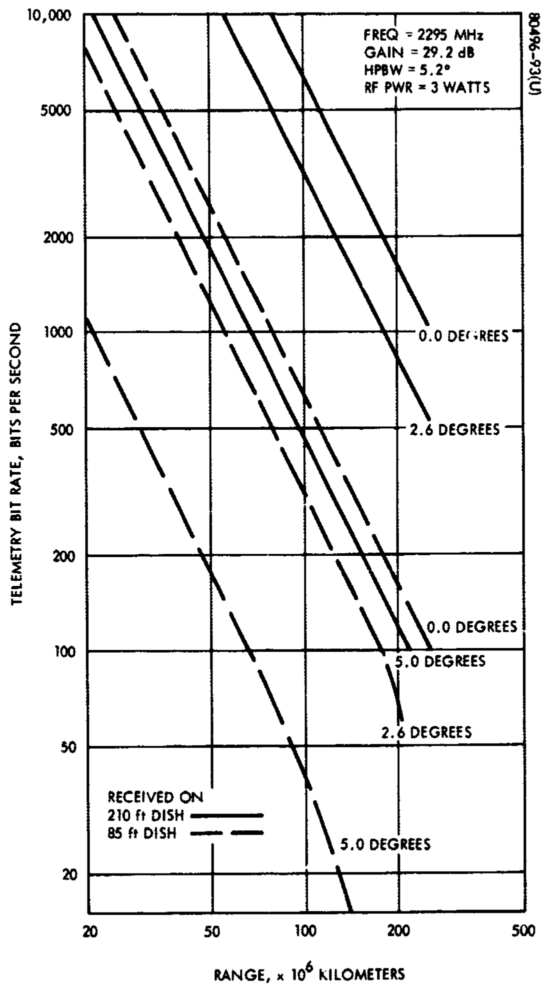

a) RF Power = 3 watts

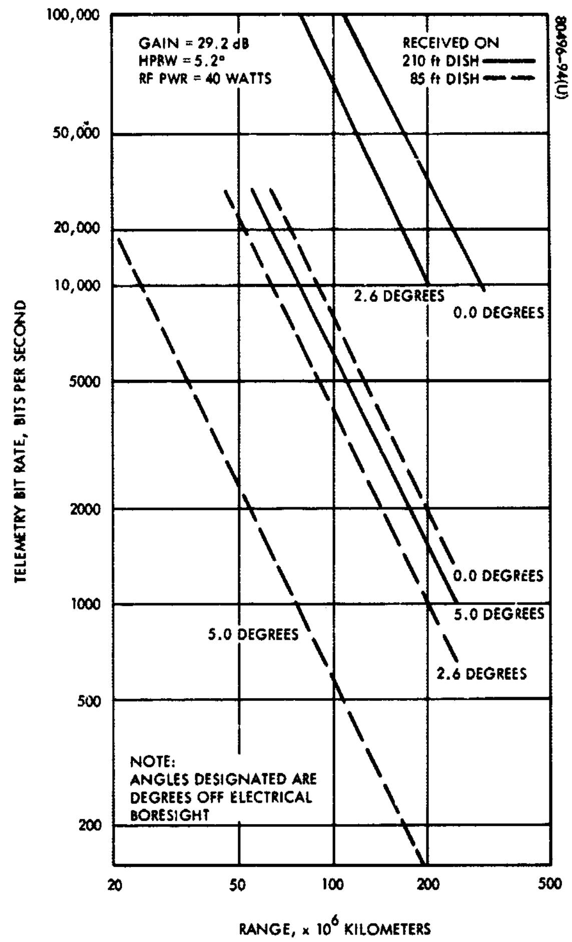

b) RF Power = 40 watts

Figure 83. Telemetry Bit Rate Versus Range for High-Gain Antenna (Planar Array)

Two Surveyor-type turnstile antenna are placed on the SM extending arms and used as backups in the event a nonstandard attitude or equipment failure occurs. Their composite gain pattern provides a sphere of coverage ranging from 0 to -9 dB. Figure 82 can be used to study the semi-omni antenna performance, just as the cross slot was used as a function of the indicated parameters. Figure 84 plots the omni antenna bit rate capability versus range for various SM transmitters and DSN antenna. A typical omni gain of -6 dB has been selected. Use of the SM 40-watt transmitter and DSN 210-foot dish provides for telemetry via the omni out to Mars encounter. The omni antennas are estimated to weigh 1.0 pound.

The use of an omni antenna may result in significant frequency and amplitude modulation on the links due to SM spin. This effect is minor if the planar or cross-slot antennas are used because of gain symmetry about the spin axis. In the worst case, two-way tracking and continuous communications could not be maintained via the omni antenna, but commands could be input to the SM and telemetry received on an intermittent basis. A telecommunications system dynamic switching arrangement would have to be effected to provide complete capability.

Command Link

The DSN-to-SM command link must be maintained throughout the mission. A command bit rate of 1 bit/sec and BER of 10^{-5} are assumed acceptable. The SM cross-slot antenna feeding a typical Surveyor-type receiver is adequate to sustain a bit rate of 960 bits/sec out to a range of 200×10^6 km. This value is based on usage of the 210-foot dish. The omni antenna system will maintain 304 bits/sec. Using the 85-foot dish, 3.3 bits/sec can be sustained via the cross-slot antenna at Mars encounter. The planar antenna has not been coupled to a receiver; therefore, SM commands cannot be received via the planar antenna. The command link analysis is based on the nominal values and tolerances presented in Table 23. Table 24 gives additional command link data.

Tracking

The SM telecommunications subsystem must function as a transponder to provide the DSN with range and range rate information for determining the spacecraft flight path. Nominally the cross-slot-receiver-transmitter loop provides this function during the early mission phases. These plus the planar antenna are used later in the mission. A Mariner type coherent two-way range and range rate system is envisioned.

A pseudo-random noise (PRN) code is phase-modulated on the uplink, phase demodulated and phase modulated on the down link, and correlated with the original PRN up-link code. The correlation process yields the round-trip propagation time used to determine range. The previous link analyses did not include the effects of ranging. Approximately 1dB of loss in the link margin is expected, based on the use of a ranging channel, 0.45 radian MI, and loss proportional to $\cos^2$ MI. The critical video link margin plus minor SM redesign will accommodate this effect. Range rate presents no additional channel requirements.

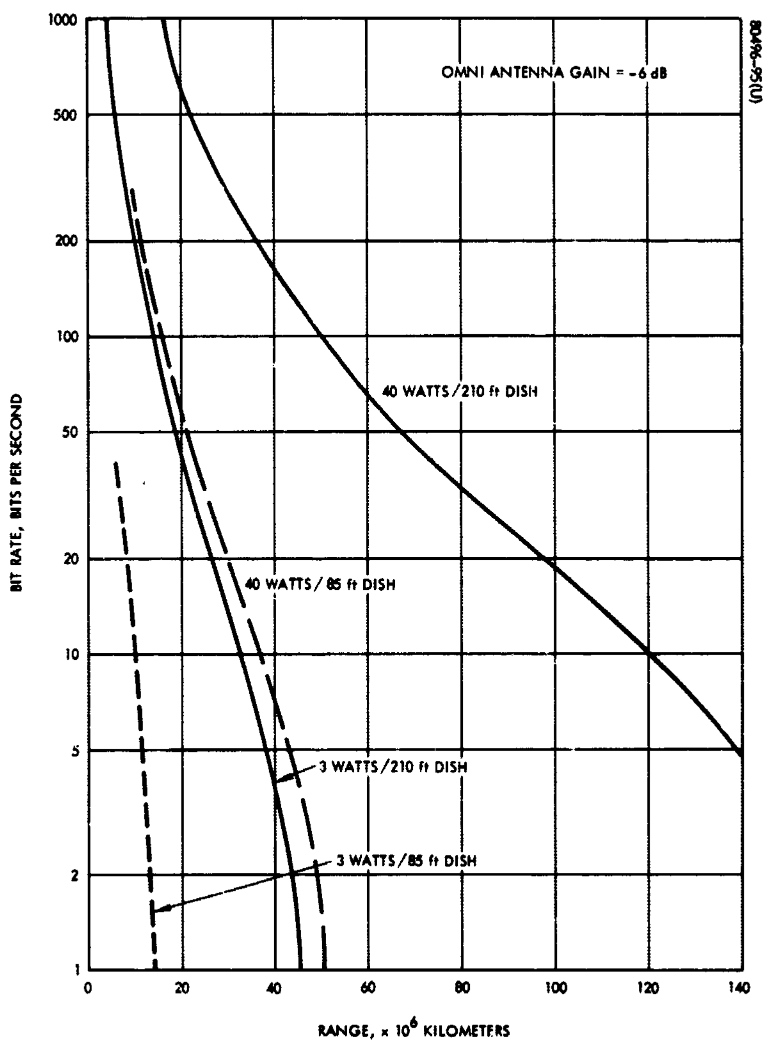

Figure 84. Telemetry Bit Rate Versus Range for Several Values of SM RF Level and DSIF Antenna

S-band communication link performance is summarized in Table 24.

A/L to SM UHF Link

The SM receives entry and video data from the A/L during the descent and postlanding mission phases, respectively. As in the case of the SM-to-DSN video link, the nominal video data transmission rate of 16,000 bits/sec is a bounding design requirement. Using the data from Table 23 and assuming PCM/FSK/FM is satisfactory with respect to A/L encoding and modulation and SM receiving equipment design simplicity, the plots in Figure 85 have been generated. Shown are the A/L plus SM antenna gain as a function of relative range required to sustain the selected bit rates.

Since the A/L transmitter and antenna gain are given, the SM antenna/receiver must be designed to sustain the required gain during the variable geometry descent and postlanding phase. The A/L transmitter power is 50 watts and the antenna gain is symmetrical about its roll axis and approximated by

$$\text{GAIN} = 6 - \log_{10} (1 + \cos \theta)^{3.5} \text{ dB}$$

The SM UHF antenna consists of a circular array of sixteen half-wave length, 7.38 inches, center-fed elements. The elements are spaced around the circumference of the solar panels at a distance of 56.5 inches from the spin axis. This arrangement yields a simple fixed array which provides adequate gain and clearance between SM and canister.

A radiation pattern formed by a single half-wave dipole in free space has a theoretical maximum gain of 2.14 dB. A 2 dB loss can be expected, due to the proximatey of the antenna elements to the spacecraft, reducing the maximum gain to about 0 dB. When fed in phase progression, a multielement circular array will produce a pattern which is a circularly polarized on-axis but becomes linearly polarized with phase and amplitude cancellation at right angles to the array. Such a pattern resembles a cardioid in shape with the gain falling off by 6 dB at 90 degrees. In addition, the finite number and spacing of the elements will cause a ripple effect on the pattern, which becomes more pronounced at angles of lower gain. The ripple is difficult to estimate, but it was assumed that allowing for a worst-case loci of exponential form with a -2 dB effect at 90 degrees was pessimistic but reasonable.

When all the elements are fed simultaneously, in phase, the standard half-wave dipole pattern is formed. Since this pattern is linearly polarized, there will be a 3 dB attenuation for receiving circularly polarized signals. The worst-case ripple, due to element spacing, is approximated by an exponentially increasing attenuation with angle with about 2 dB loss at 50 degrees off boresight.

Provisions can be made via a "phasing network" to feed the elements in phase progression or in equal phase. In Figure 86 both patterns are

TABLE 24. MSSM S-BAND LINK PERFORMANCE SUMMARY

Support Module to DSN, 2295 MHz

	Maximum Allowable Information Rate, bits/sec															
	Receive on 210-Foot Dish								Receive on 85-Foot Dish							
	Cross-Slot Antenna		Omni Antenna		High-Gain Antenna (Gain = 29.2 dB)				Cross-Slot Antenna		Omni Antenna		High-Gain Antenna (Gain = 29.2 dB)			
	Gain = -1 dB		Gain = -6 dB		Boresight ±2.6 degrees (Gain = 26.2 dB)		Boresight ±5 degrees (Gain = 17.7 dB)		Gain = -1 dB		Gain = -6 dB		Boresight ±2.6 degrees Gain = 26.2 dB		Boresight ±5 degrees (Gain = 17.7 dB)	
Range (km x 10^6)	3w	40w	3w	40w	3w	40w	3w	40w	3w	40w	3w	40w	3w	40w	3w	40w
10	520	-	200	2.58k	-	-	-	-	150	790	10.7	250	-	-	-	-
40	310	470	4	160	-	-	-	-	0.9	43	0	7.3	1.95	-	276	-
80	1.3	130	0	33	5.12k	-	735	9.6k	0	4	0	0	490	6.5k	63	915
120	0	53	0	10	2.27k	-	321	4.26k	0	0	0	0	217	2.88k	23	407
160	0	23	0	1.8	1.28k	17.0k	181	2.4k	0	0	0	0	122	1.62k	9.1	228
175	0	18	0	0	1.07k	14.2k	151	2.0k	0	0	0	0	102	1.35k	6.1	190
200	0	12	0	0	820	10.85k	116	1.53k	0	0	0	0	73	1.04k	2.6	146

DSN to Support Module, 2113 MHz

Maximum Allowable Command Rate, bits/sec

Transmit on 210-Foot Dish (400 kw RF)				Transmit on 85-Foot Dish (100 kw RF)			
Cross-Slot Antenna (Gain = -1 dB)		Omni Antenna (Gain = -6 dB)		Cross-Slot Antenna (Gain = -1 dB)		Omni Antenna (Gain = -6 dB)	
Range (km x 10^6)	Bit Rate	Range (km x 10^6)	Bit Rate	Range (km x 10^6)	Bit Rate	Range (km x 10^6)	Bit Rate
160	1500	160	475	160	3.3	92.3	3
200	960	200	304	200	1.2	116.3	1

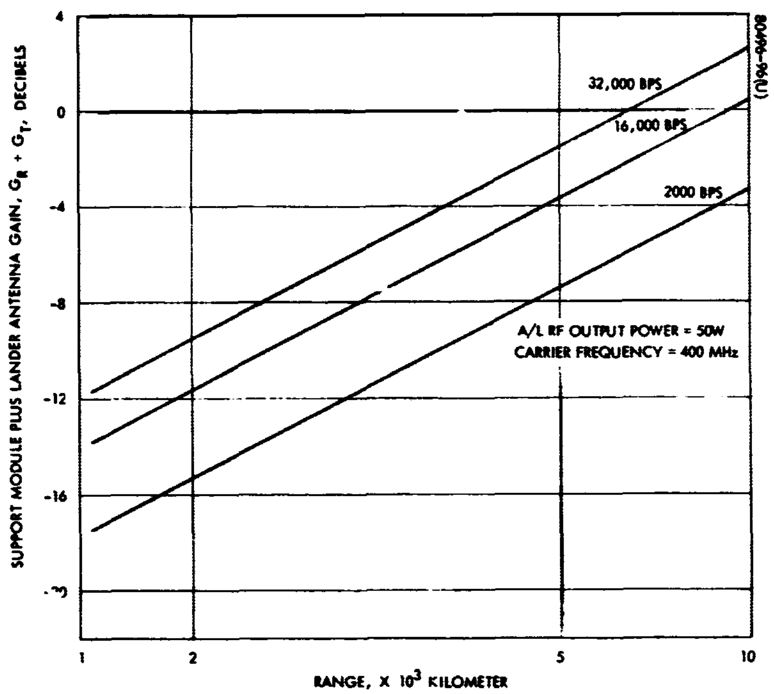

Figure 85. UHF Link Antenna Gain Requirements to Support Given Data Rates

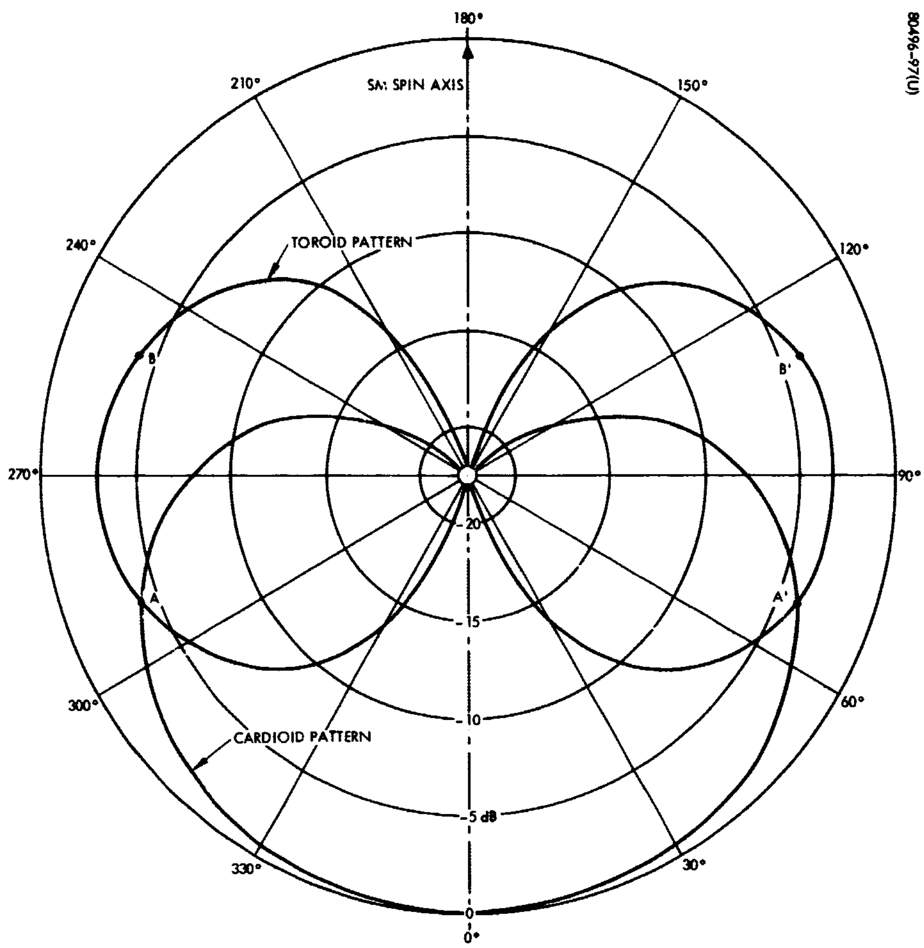

Figure 86. MSSM Receive Antenna Composite Pattern Gain in dB Versus Angle From Spin Axis

displayed. Using the previously mentioned considerations, the patterns were plotted according to the following formulas:

$$\text{Cardioid pattern} = \left[20 \log_{10} .25(1 + \cos \theta)\right] e^{(3.17)(10^{-3})(\theta)} \text{ dB}$$

$$\text{Toroid pattern} = \left[20 \log_{10} \left(\frac{\cos (\pi/2)(\cos \theta)}{\sin \theta}\right) - 3\right] e^{(4.5)(10^{-3})(\theta)} \text{ dB}$$

A standard UHF receiver completes the SM UHF antenna/receive unit.

Using the relative range and angle data from the video data phase, the data shown on Figure 87 are plotted. The SM plus lander gain is plotted as a function of the range from the start, t_o, to the end, t_f, of video transmission for the cardioid and dipole antenna patterns. This is done for the range of expected A/L entry angles, γ_e. Also shown is the gain required to support 16,000 bits/sec. The use of the dipole antenna will yield continuous video data for the range of anticipated situations, whereas the cardioid will not because the total gain falls below requirements at the steeper entry angles. This analysis also includes the effect of the lander on a 15-degree slope producing the lowest A/L antenna gain.

During the entry phase, the maximum slant range is 5300 km, which requires approximately -7 dB to sustain 2000 bits/sec (Figure 85). Since the A/L gain is greater than 0 dB because the A/L-to-SM line with respect to the A/L axis is within 70 degrees, and the SM gain can be maintained above -4.2 dB over the expected angle range B to B' (Figure 86), the entry data link gain is more than adequate. The -4.2 dB may have to be obtained by switching patterns, at points A or A' (Figure 86). Even though the cardioid pattern may be acceptable during the entry phase, the dipole must be used during the video phase.

The UHF antenna system is estimated to weigh 3.0 pounds. Two UHF receivers weigh 4.7 pounds.

As in the case of the S-band link, the SM will spin modulate the UHF carrier. In addition, the relative range rate between A/L and SM will produce a doppler shift. Since no carrier tracking is provided in the FM UHF link, the RF predetection bandwidth must be sized to include the doppler effects. The total frequency excursion for a complete rotation of the SM is twice the value of peak doppler shift, Δf, defined by

$$\left|\Delta f\right| = \frac{2\pi r}{\lambda} \frac{\omega s}{60} \left|\sin \theta_s\right| \left|\sin \theta_o\right|$$

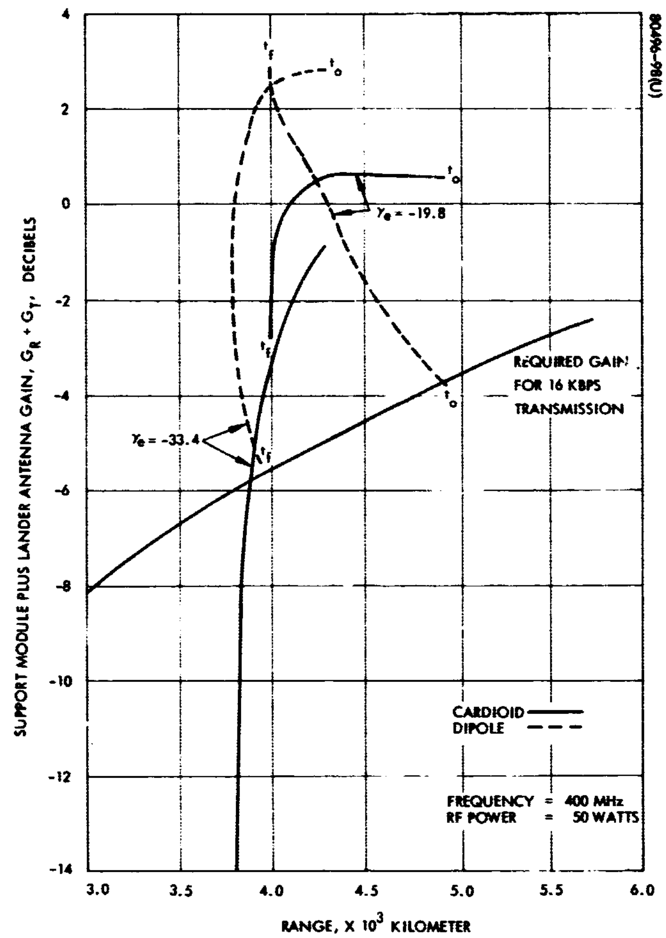

Figure 87. SM Plus A/L Antenna Gain Required to Support 16 kbps and Actually Available in UHF Relay Link

where

θ_o = angle between A/L-SM line and spin axis of the SM

θ_s = angle between spin axis and line drawn through the antenna and cg of SM

r = distance from cg to antenna, inches

λ = free space wavelength of signal, inches

ω_s = frequency or rate of rotation of SM, rpm

The largest doppler shift occurs when $|\sin \theta_s||\sin \theta_o| = 1$.

In the longitudinal case where the transmitting or receiving antenna is moving in a straight line toward or away from the point of observation, the doppler shift is related to antenna velocity by the following expression:

$$f = \frac{V}{\lambda}$$

where

f = doppler shift, Hz

V = velocity of antenna, ips

The maximum doppler rotation and longitudinal shifts are 24 Hz and 11.2 kHz, respectively. The parameter values used are ω_s = 60 rpm, r = 56.5 inches, V = 4.2 km/sec, and λ = 29.5 inches.

A sample calculation showing the relationship of the doppler frequency shift to predetection bandwidth sizing in the PCM/FSK UHF link is given below. Let

B_{IF} = RF predetection bandwidth, Hz

Δf_c = RF carrier peak deviation, Hz

f_B = bit rate frequency, Hz = bit rate (BPS)/2, for proposed NRZ PCM data, $\approx \Delta f_c$

Δf_i = carrier frequency deviation due to oscillator instability, Hz

Δf_D = carrier frequency deviation due to doppler shift, Hz

The RF predetection bandwidth may be specified as

$$B_{IF} \cong 2\left[\Delta f_c + \Delta f_i + \Delta f_D\right] \tag{70}$$

For f_B = 16,000/2 = 8 kHz, Δf_D has been computed previously as 11.2 kHz, worst case.

If an oscillator stability of 10^{-6} is assumed,

$$\Delta f_i = 10^{-6} f_c = 400 \text{ Hz}$$

Thus, for a worst-case predetection sizing,

$$B_{IF} \geq 2[8 + 11.2 + .4] \text{ kHz}$$

$$\geq 39.2 \text{ kHz} \tag{71}$$

Note that this specification is perhaps unduly confining since the doppler shift is worst case and for predetection filters typical of the linear phase variety the skirt attenuation has a gentle slope. Thus, movement of the PCM modulated carrier spectrum within the RF bandwidth by an amount equal to even the maximum doppler shift is not disastrous (in fact, the portion of the modulated carrier spectrum which is thus moved away from the filter's band edge will be attenuated less than for perfect alignment with the carrier). In any case, the RF bandwidth that can realistically be used is somewhat less than the computed worst-case estimate.

Signal Processing

The telecommunications subsystem signal processing includes decoding of DSN commands for the SM and A/L, encoding SM and A/L telemetry data, and transforming UHF to S-band data.

Commands and Telemetry

Table 25 lists the SM command and telemetry channels based on anticipated requirements.

The telemetry channels are based on the use of three commutators:

Commutator I	General Support Module Data
Commutator II	Attitude Data
Commutator III	Aeroshell/Lander Data

TABLE 25. TELEMETRY AND COMMAND REQUIREMENTS FOR SUPPORT MODULE

Subsystem	Commands		Telemetry Channels	
	Basic	Spares	Basic	Spares
Flight control	30	6	40	8
Telecommunication	30	6	20	4
Signal processing	20	4	6	2
Propulsion	20	4	22	4
Vehicle and mechanisms	20	4	30	6
Power	20	4	20	4
Subtotal	140	28	138	28
Total	168		166	

Each commutator has 64 frame positions. Synchronization will take three positions, and identification will take one. Sixty frame positions are available for spacecraft data.

It is assumed that second and fourth level subcommutation is permitted.

It had been assumed earlier that there are 8 bits/word. Therefore, there are 512 bits/frame.

Commutator I - General Support Module Data

Primary cruise mode commutator

Subsystem Telemetry

FC Flight control

18 words in 6 frame positions
16 words subcommutated to fourth level; four positions
2 words single commutation; two positions

TCM Telecommunications (RF and Command)

22 words in 16 frame positions
8 words subcommutated to fourth level, two positions
14 words single commutation; 14 positions

SP Signal processing (Telemetry)

8 words in 5 frame positions
4 words subcommutated to fourth level; one position
4 words single commutation; four positions

PR Propulsion

10 words in 4 frame positions
8 words subcommutated to fourth level; two positions
2 words single commutation; two positions

VM Vehicle and Mechanisms

36 words in 11 frame positions
32 words subcommutated to fourth level; eight positions
2 words subcommutated to second level; one position
2 words single commutation; two positions

PO Power

24 words in 15 frame positions
12 words subcommutated to fourth level; three positions
12 words single commutation; 12 positions

A/L Aeroshell/Lander
12 words in 3 frame positions
12 words subcommutated to fourth level; three positions.

Commutator II - Attitude Data

Subsystem Telemetry

FC: 40 words in 40 positions
8 words subcommutated to fourth level; two positions
26 words single commutation; 26 positions
6 words supercommutated (2X); 12 positions

PR: 20 words in 14 positions
8 words subcommutated to fourth level; 2 positions
12 words single commutation; 12 positions

TCM: 4 words in 1 position
4 words subcommutated to fourth level; one position

SP: Same as TCM

VM: Same as TCM

PO: Same as TCM

A/L: Same as TCM

One spare frame position

Commutator III - Aeroshell/Lander Data

Subsystem Telemetry

A/L: 54 positions, number of words unknown

FC, TCM, SP, PO, PR, VM: 4 words in 1 position, subcommutated to fourth level for each subsystem

The two command decoders and signal processor which mechanize the telemetry and command functions are estimated to weigh 5.7 and 10.0 pounds, respectively. They are assumed to be similar to existing Hughes equipment.

A star data processing unit is used to convert the signals from the star sensor into forms suitable for telemetry to earth. This information is used to help determine the attitude of the spacecraft. The processor measures the amplitude of the star pulses and converts these signals into digital form. The angle of the star pulse from the sun reference is also measured and stored to be transmitted to earth later via telemetry. The star sensor will produce two pulses per star. Data from four stars (eight star signals) can be stored. In order to simplify spacecraft equipment, no attempt is made to identify pulse pairs in the spacecraft. This processing can easily be done on the ground. The processor has selectable threshold levels, so that only stars of a given magnitude are observed. An angle gate is also provided to limit the angles over which stars will be detected. The star processor unit will be constructed from space-qualified integrated circuits and discrete components which have been proven on other space programs. The unit will weigh about 3.0 pounds and require about 2.5 watts of power. A block diagram of the star processor is shown in Figure 88.

The pulses from the star sensor go to a peak detector which converts the pulse amplitude to an analog signal. The analog-to-digital converter converts the analog signal to a 4 bit (32 state) digital signal representing the star magnitude. The pulses from the star sensor also go to a threshold circuit which provides a signal to the star detector only for star pulses above a specified amplitude. One of several (e.g., four) amplitudes can be specified by command. The star detector will produce a logic signal, synchronized with the basic clock of the unit on the trailing edge of the star pulse.

The angle increments into the angle counter represent 512 counts per revolution or 0.7 degree per count. The counter is reset by the sun reference signal. Thus, the content of the counter represents the angle from the sun. The gate counter allows the processor to be operated on segments of the revolution. The gate start angle and gate width will be inserted into two registers by ground command. The sun reference signal will transfer the start angle to the counter. At completion of the count, the gate will be set to 1, allowing detected star pulses to set the control flip-flop. The gate width will then be counted and the gate set to 0 at completion of the count.

When a star above the specified magnitude and within the specified sampling interval has been detected, the star magnitude and angle will be transferred in parallel to an eight-word (13 bits/word) storage register. This register will hold data from four stars since each star will be viewed twice. The stored data will be serially transferred to the telemetry subsystem on command.

UHF To S-Band

The specific means of providing the data transfer from the UHF relay link to the S-band DSIF link is a proper trade study. Conceivably (although not attractive from a minimal SM power standpoint), two subcarriers could be used to effect the transmission of data from both the SM and the A/L with their data streams uncorrelated with each other. Alternately, a single digital data stream can be constructed from demodulated relay link PCM, combined appropriately with the SM digital data and subsequently transmitted on a single subcarrier via the S-band carrier. The latter approach, which is more efficient, has been assumed for this study. In this configuration, the SM hardware must frequency demodulate the relay link FSK data, condition it, suitably interleave it with the locally generated SM digital data, and phase modulate the composite PCM stream onto a subcarrier for subsequent phase modulation of the carrier S-band down-carrier. The subcarrier/carrier modulation index must be compatible with the PRN code which can be simultaneously modulating this carrier.

Command Storage and Sequencer

The terminal sequence commands will be loaded into the command storage and sequencer unit approximately 3 days before encounter and executed automatically when initiated by ground command. A block diagram of a command storage and sequencer unit for controlling the terminal sequence is shown in Figure 89. A ground command will start the sequence counter which will generate the commands in proper sequence at the specified times. Commands in the sequence which can be specified during spacecraft development will be prewired as part of the output matrix controlled by the sequence counter. Magnitudes and discrete commands which will be determined after launch, such as the parameters for the attitude maneuvers, will be loaded into a serial shift register approximately 3 days prior to encounter to be executed later at the proper time in the sequence.

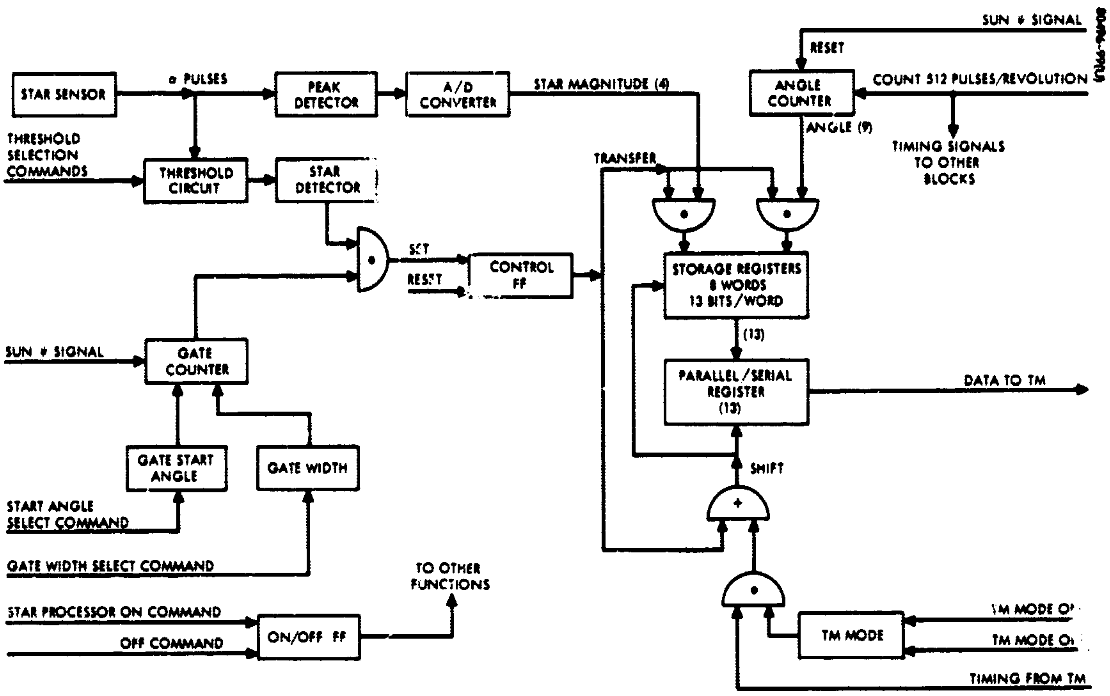

Figure 88. Block Diagram of Star Processor

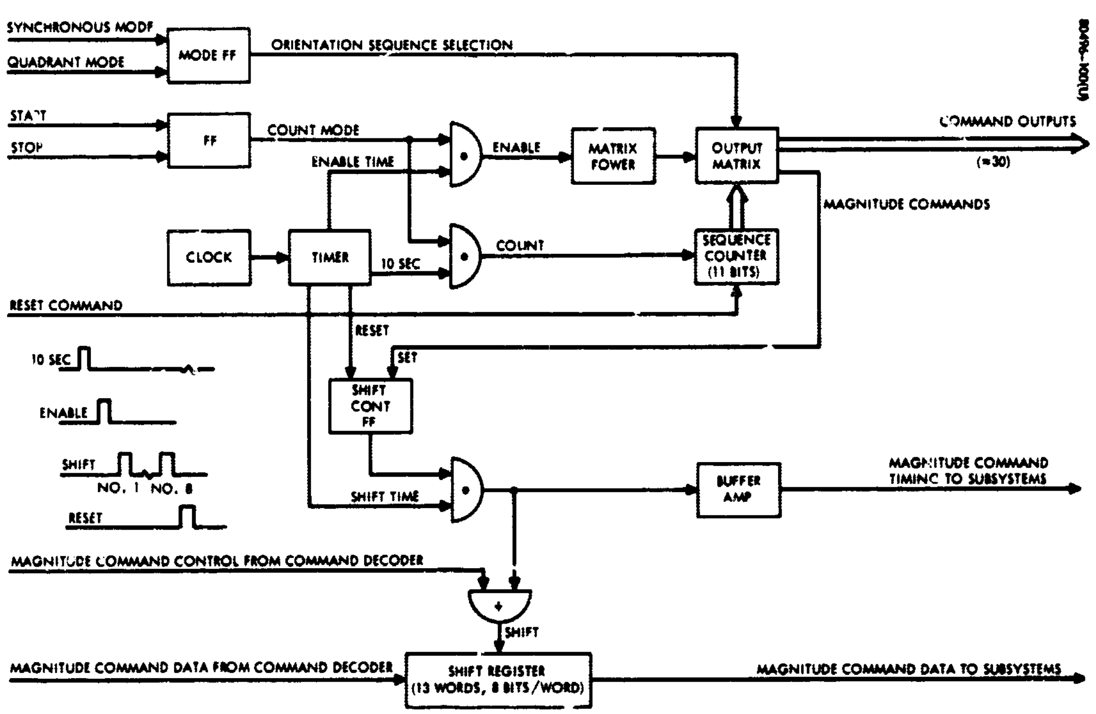

Figure 89. Block Diagram of Command Sequencer

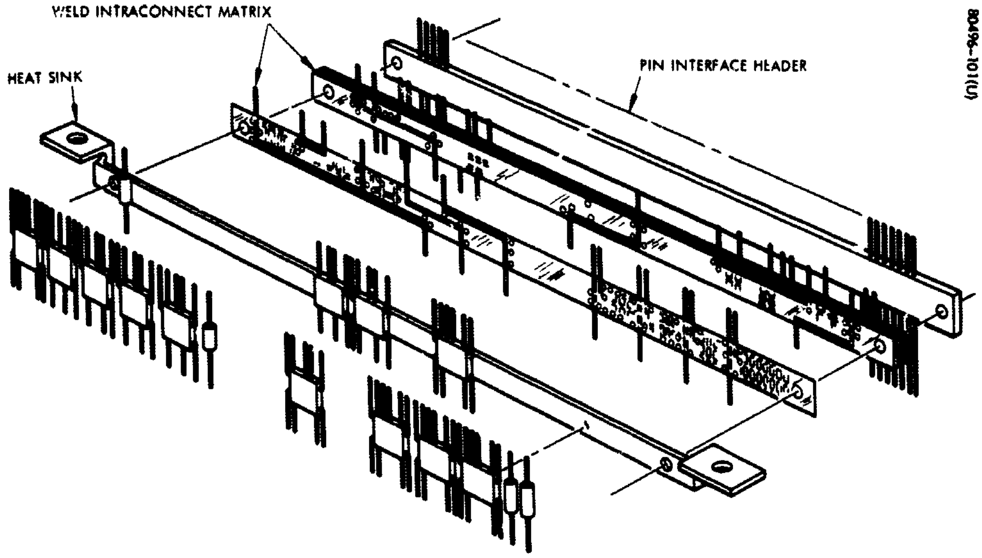

Figure 90. MICAM Subassembly

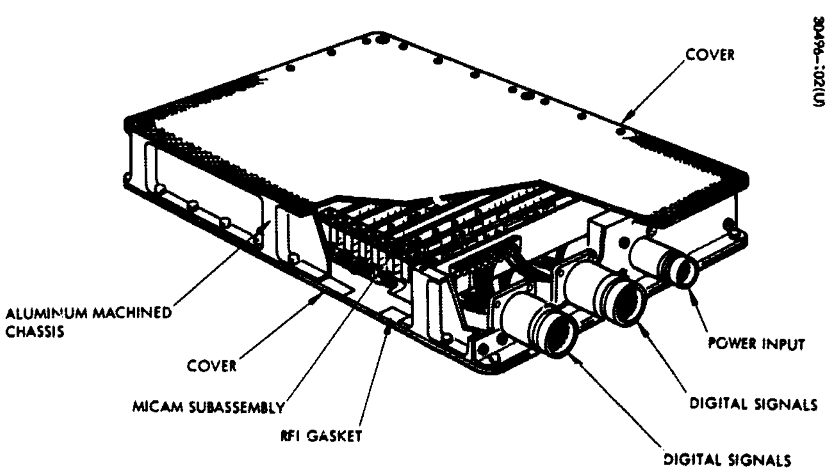

Figure 91. Decoder Packaging

The initial conditions for the command sequencer will be determined well in advance of the time for the terminal sequence. Attitude maneuver parameters and other variable commands will be read into the shift register and verified via telemetry. The orientation mode (synchronous or quadrant) will be selected and the sequence counter reset to its initial value. At the time for initiation, a start command will be sent to begin the sequence. Ten-second count pulses will be generated by a crystal oscillator and timer. The timer will also generate other timing signals required by the sequencer. When the sequence counter reaches the time specified for a given command, a command pulse will be generated and sent to the associated subsystem.

Any given command output can be energized several times in the sequence. If the sequence counter indicates that a magnitude command is to be executed, the shift control flip flop will be set and one word (8 bits) will be shifted out of the shift register into the associated subsystem. The sequence counter will continue to count until the last command in the sequence has been executed, and then the counter will stop. If desired, the sequence can be stopped and later restarted by ground command.

The command sequencer unit can be constructed of space-qualified integrated circuits and discrete components that have been proven on other space programs. Packaging techniques for command decoders and other electronics units used on various satellites can be used on the command sequencer. One such technique uses a dual packaging approach for the integrated circuits and major discrete components. The integrated circuits are packed on a "stick" termed MICAM (Micro Connection Assembly Method), as shown in Figure 90, and the major discrete components are housed in welded modules. Use of the MICAM circumvents the need for soldered interconnections at the integrated circuit and component level. Consequently, components contained both in cordwood welded modules and in MICAM subassemblies are not thermally stressed during assembly.

The command sequencer can be packaged into a unit similar to that shown in Figure 91. The unit will weigh about 2.5 pounds and require about 3.0 watts of power.

The total telecommunications subsystem is shown in block diagram form in Figure 92. In addition to the redundant omni antenna and command decoders previously discussed, backup transmitter, receivers, and transponders are provided. A dpdt commandable switch allows either transmitter to be connected to any antenna. An sp, three-position switch, provides the transmission path to the desired low gain antenna. An spdt switch connects either omni to receiver A. Receiver B is permanently connected to the cross-slot antenna. It also may be desirable to provide a path from the cross slot to to receiver A. Selector logic, similar to that used on Surveyor, allows for various receiver/decoder paths. Diplexers are included to allow for simultaneous receive/transmit. Weight allowances of 1.5, 5.5, and 1.3 pounds are provided for RF switches, cables/clips, and diplexers, respectively.

80495-10(U)

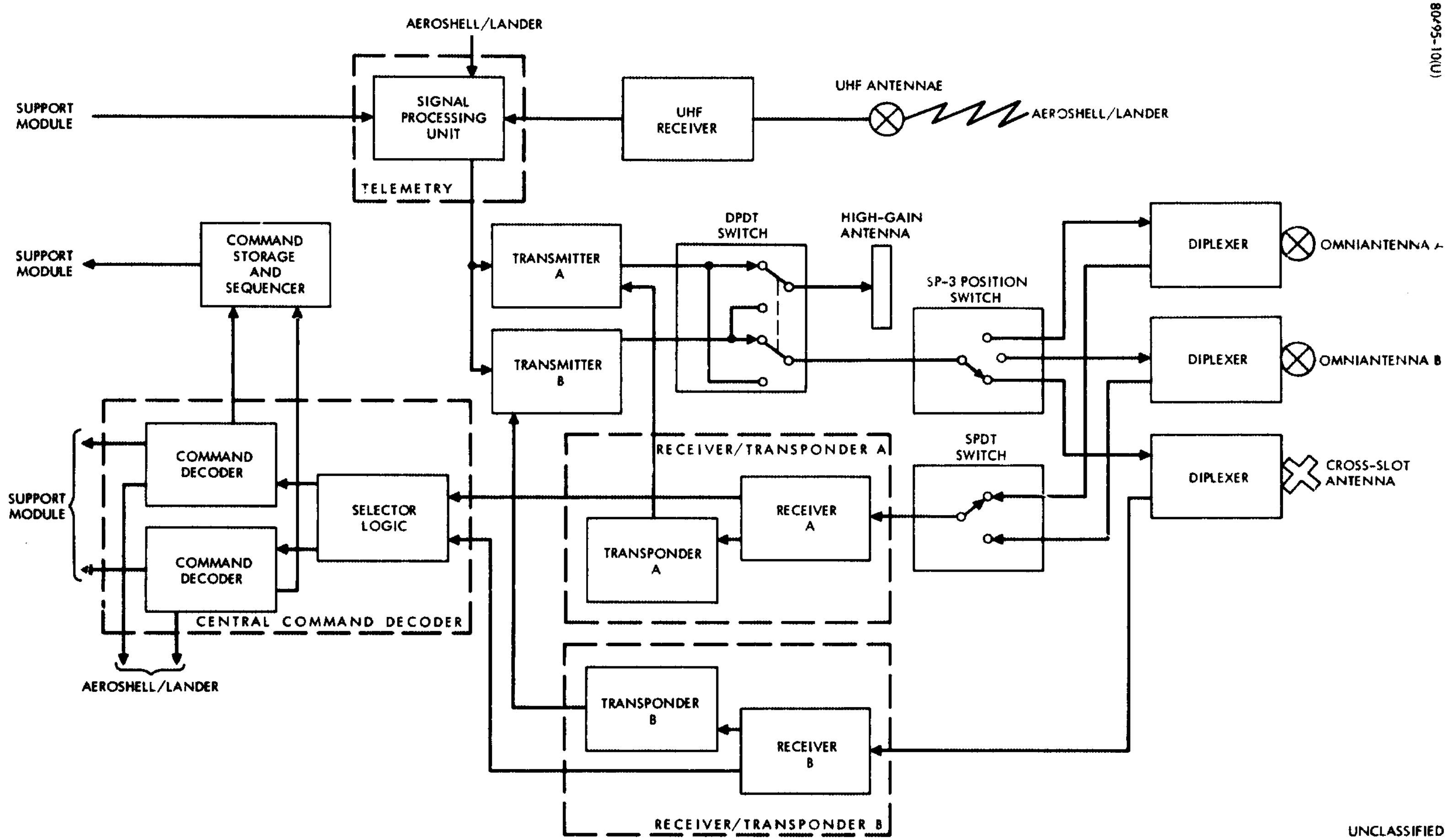

UNCLASSIFIED

Figure 92. Telecommunications Subsystem

POWER/THERMAL

Power

General Requirements

The SM must supply approximately 15 watts of continuous power to the A/L during the mission and sustain its own subsystems during low-power cruise and high-power terminal phases of the mission. In keeping with the state of the art, solar panels and batteries are selected for solar energy conversion and electrical storage, respectively. The panels are used primarily for low power, and the batteries supply the high power.

Solar Panels

Table 26 lists the steady-state cruise mode power requirements, with a total of 85 watts being the required panel output power. The maximum SM-to-sun range is fixed as Mars aphelion, approximately 250 x 10^6 km. This is greater than the 232 x 10^6 km obtained from trajectory analysis; therefore, a conservative design results. Also, since the SM spin axis is directed toward earth at Mars encounter to maintain communications, the sun's energy makes an angle of approximately 40 degrees with respect to the spin axis. Weight of the panels is minimized for this design by attaching them to the SM cylindrical section in a plane normal to the spin axis. Based on a solar cell conversion factor of 3.30 watts/ft^2, 15 percent radiation degradation and voltage mismatch, and 90 percent area utilization factor, 37.4 square feet of panel area is required to supply 85 watts of power. Eight trapezoidal panels are used to generate the total power. This number is a reasonable balance between weight and dimension constraints, manufacturing, and assembly. This arrangement of the panels on the SM structure allows for a wide range of acceptable spin-axis orientations with respect to the sun, especially early in the mission. Figure 93 illustrates the use of this flexibility in designing the mission sequence. The solar panel power output is plotted as a function of SM-to-sun distance for various solar incidence angles. The data do not include losses due to voltage mismatch. If properly designed, the power subsystem would have the highest mismatch near earth and virtually none near Mars. The dotted line in Figure 93 represents the panel power capability based on the atttiude control history presented in the trajectory/navigation section. The minimum power output is 96 watts, well above the 85 watts required to sustain the steady-state power level. It is anticipated that an n/p type solar cell, similar to those used on Hughes satellites, will be used for constructing the panels. The cells have glass cover slides. The panels are estimated to weigh 36.8 pounds.

Batteries

Battery capacity requirements are dictated by the system loads during the encounter minus 12 hours through the flyby phase of the mission. A detailed command/ time sequence was generated for this phase and used to generate a power and energy histogram. The results appear in Table 27. These results are conservative because the sequence was started 5 rather

TABLE 26. CRUISE MODE STEADY-STATE LOADS

Unit	Power Required, watts Unregulated	Regulated
Transmitter (low power, 3 watts)		
Assume 15 percent efficient	----	20.0
Flight control	----	10.0
Telemetry and command	----	6.5
S-band receivers	3.0	----
Aeroshell/lander	25.0	----
SM thermal control	5.0	----
Battery charge regulator*	1.5	----
Boost regulator		
Assume 75 percent efficient	9.0	----
Subtotals	43.5	36.5
Totals	80.0	
Contingency and high power operation	5.0	
Total	85.0	
Solar panel power to be supplied	85.0	

*Assumes that the battery will be disconnected from the bus (after being fully charged) for most of transit.

TABLE 27. ENERGY REQUIREMENTS FOR TERMINAL SEQUENCE

Unit	Power, watts		Pre-Encounter Phase		Fly-By Phase	
	Regulated	Unregulated	Time, minutes	Energy, watt-hrs	Time,* minutes	Energy, watt-hrs
Transmitter						
40 watts RF, 25 percent efficient	160.0		63.3	168.7	53.7	143.3
3 watts RF, 15 percent efficient	20.0		120.8	40.3	-	-
Flight control						
Cruise mode	10.0		38.0	6.3	53.7	8.9
Thrusting mode	15.0		146.0	36.5	-	-
Telemetry and command decoder	6.5		184.1	19.9	53.7	5.8
Command storage and sequencer	3.0		184.1	9.2	-	-
UHF receivers	2.5		183.9	7.7	53.7	2.2
S-band receivers		3.0	184.1	9.2	53.7	2.7
Battery charge regulator		4.5	184.1	13.8	53.7	4.0
Boost regulator						
P_{reg} = 187 watts (87 percent efficient)		24.3	26.0	10.5	-	-
P_{reg} = 182 watts (87 percent efficient)		23.6	37.3	14.7	-	-
P_{reg} = 46.5 watts (77.5 percent efficient)		10.4	120.0	20.8	-	-
P_{reg} = 41.5 watts (77 percent efficient)		9.5	0.8	0.1	-	-
P_{reg} = 179 watts (87 percent eificient)		23.3	-	-	53.7	20.8
Thermal control		5.0	184.1	15.3	53.7	4.5
Subtotals				373.0		192.2
Solar panel		85.0	184.1	260.5	53.7	76.0
Battery energy required				112.5		116.2

*Times are based on 30 minutes total visibility after lander touchdown.

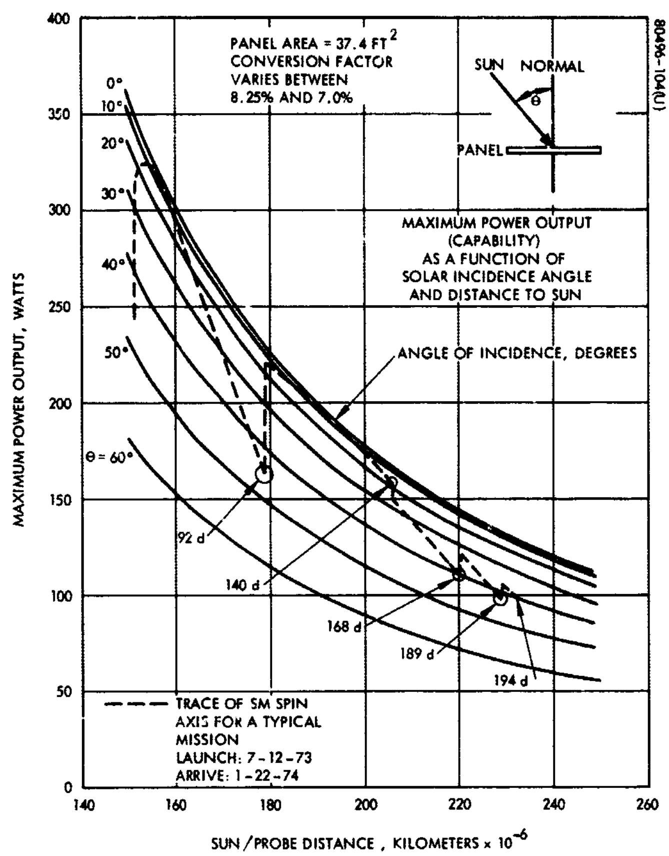

Figure 93. Maximum Power Output (Capability) as Function of Solar Incidence Angle and Distance to Sun

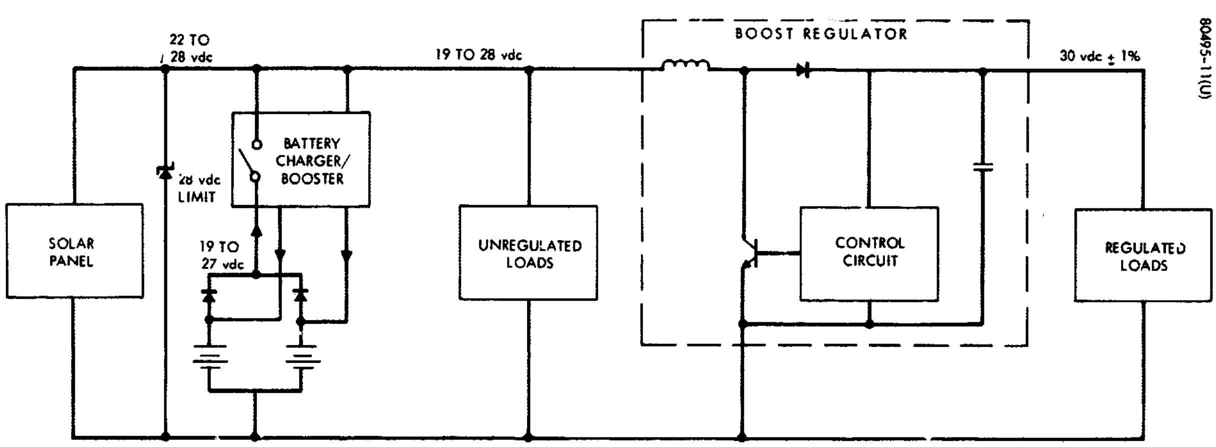

Figure 94. Power Subsystem Functional Block Diagram

than 12 hours before encounter, based on earlier studies. The reduction in battery size and weight using 12 hours is insignificant because of the very low charging rate, 1.7 w-hr/hr, in the additional available time. To enhance system reliability, two batteries are used, each sized such that the mission can be completed on a single battery if necessary. Additional safety is provided by the use of isolating diodes between each battery and the bus, (Figure 94). In this way, failure of a single battery during the mission will disconnect it from the line, thereby preventing a rapid discharge of the remaining battery.

In determining battery size, a minimum period of 1.5 hours between the end of the SM deflection maneuver and the start of flyby, a battery charging rate of 6 percent and a discharge limited to 80 percent of capacity are assumed. Under these conditions, the battery can be sized as shown below for the flyby case:

Battery energy used = 112.5 + 116.2 = 228.7 w-hr

Battery charge rate for a battery of approximately 285 w-hr is 1.7 w-hr/hr.

Recharge energy	= 1.5 x 1.7	= 2.6 w-hr
Battery energy required	= 228.7 - 2.6	= 226.1 w-hr
Battery capacity per battery	= 226.1 ÷ 0.80	= 282 w-hr

Two batteries with a capacity of 283 w-hr each, totaling 566 w-hr, satisfy the requirements. Power calculations indicate that the maximum current drain on a battery will be on the order of 5 amperes, assuming single battery operation. Since the capacity of each battery is approximately 12 amp-hr, the maximum discharge rate will be approximately 40 percent of capacity. Although detailed functional performance characteristics of sterilizable batteries are not known presently, the discharge rate indicated appears to be approximately 50 percent of the anticipated maximum discharge capability.

The energy-to-weight ratio for a sterilizable silver-zinc battery of this capacity is approximately 20 w-hr/pound; therefore, the total battery weight is 28.3 pounds. Although no fully operational sterilizable batteries exist presently, the development of fully sterilizable (prolonged soak at 135°C) silver-zinc primary and secondary batteries is in an advanced stage. The studies under way at JPL of battery cells provided by Electrical Storage Battery, Inc., are well documented.

Battery Charger/Booster

Overcharging the batteries will be prevented by the battery charger booster, which will contain a charge current limiting function. It is anticipated at this time to essentially disconnect the batteries from the bus after being fully charged. Although a thorough knowledge of sterilizable silver-zinc battery characteristics does not presently exist, it is felt that a long period of float charging could prove detrimental. When the solar panel output is insufficient to sustain system loads, the batteries will automatically be connected to the bus. This procedure is similar to that followed on the Mariner spacecraft.

Boost Regulator

The boost regulator provides regulated power to the transmitters, UHF receivers, and the command storage and sequencer, as well as the flight control and telemetry subsystems. The concept of a central regulator was chosen primarily on the basis of minimizing overall cost, weight, thermal, and electrical dissipations. Additional advantage of the existing redundancy of the transmitter can be realized by having separate regulators with current limiting for each transmitter. In this way, a short circuited transmitter could be removed from the bus and the system could continue operating on the remaining transmitter. However, there would be attendant penalties in the areas previously mentioned.

The steady-state regulated power requirements for cruise mode operation is 36. 5 watts. Assuming a regulated bus voltage of 30 v ±1 percent, the boost regulator output current is approximately 1. 2 amperes. The maximum regulated load requirement is expected to be 6 or 7 amperes. It is estimated that an efficiency of 75 percent is reasonable at the lower output, while 85 to 90 percent can be achieved at the higher output. The boost regulator weight is 8. 5 pounds.

Figure 94 is a block diagram of the power subsystem.

Although not part of the SM power subsystem, two A/L battery chargers are incorporated into the SM design. The SM and A/L battery charge regulators weigh 10. 5 pounds.

Thermal

The SM equipment compartment temperature must be maintained between 40° to 100° F to prevent freezing of the hydrazine propellant and maintain reasonable equipment operation, especially the batteries. Also, materials and equipment mounting must include a consideration of heat energy conduction and radiation. In addition, equipment outside the SM cylindrical section and A/L-SM interfaces must include a thermal design.

Louvers/Equipment Mounting

Table 28 displays the estimated thermal power dissipations used to develop the thermal subsystem design for the SM. Data are shown for steady-state conditions as well as critical peak power modes. Also shown are the solar incidence angles and intensities anticipated throughout the mission. To keep the SM compartment temperature below 100° F, six active

TABLE 28. THERMAL ENVIRONMENTAL PARAMETERS

	Thermal Power Dissipations, watts			
	Steady-State Cruise[1] Min.	Steady-State Cruise[1] Max.	Titan Separation through DSN Lock[2]	Maximum High Power with Thrusting[3]
Transmitter (3 watts/ 40 watts RF)	17.0	17.0	120.0	120.0
Flight control	10.0	10.0	10.0	15.0
Central command decoder	2.5	2.5	2.5	2.5
S-band receivers	3.0	3.0	3.0	3.0
UHF receivers	0	0.0	0.0	2.5
Battery charger/booster	1.0	4.5	4.5	4.5
Boost regulator	8.5	9.3	23.0	24.0
Signal processing unit	4.0	4.0	4.0	4.0
Command storage/sequencer	0.0	3.0	0.0	3.0
Lander battery charger 1 *	0.0	10.0	0.0	0.0
Lander battery charger 2	0.0	0.0	0.0	0.0
Lander sequencer	0.0	2.0	0.0	0.0
Thermal control heaters	0.0	5.0	0.0	5.0
Battery	0.0	0.5	1.0	4.0
Total thermal dissipation	46.0	70.8	168.0	187.5
Solar incidence angle	0° to 45°		40° to 50°	30° to 40°
Solar intensity	140 to 51 $\frac{mw}{cm^2}$		140 $\frac{mw}{cm^2}$	60 to 58 $\frac{mw}{cm^2}$

*Only one lander battery is charged at a time.

Durations:

1. Steady State Cruise
   a. Minimum. This is the primary thermal dissipation mode and is prevalent throughout transit.
   b. Maximum. This thermal dissipation mode will exist for several hours at a time during transit.

2. Titan Separation through DSN Lock
   The mode is initiated by separation and continues until the support module is commanded off. Duration is approximately 60 minutes.

3. Maximum High Power With Thrusting
   This thermal dissipation mode occurs near the final portion of the mission and lasts for approximately 2 hours.

Thermal louvers are used. Four are mounted to the equipment shelf and planar antenna and transfer heat energy between the two. The antenna doubles as an electrical and thermal radiator. The other two louvers are attached to the side of the SM. The high heat energy transmitters and associated TWTs are mounted directly behind them. The electronic equipment bolt-down area requirements for adequate heat transfer to the shelf and side louvers are listed in Table 29. The estimates are based on the physical characteristics of similar Hughes equipment. It is estimated that 15 square feet of louver area is adequate using designs comparable to those used on the Mariner spacecraft (bimetallic construction to affect shutter response to temperature changes). The Flyby - Video Data louver weight is 15. 6 pounds. Another attractive louver system configuration is to mount all equipment and louvers about the SM central cylinder.

Thermal Blanket

To prevent the SM compartment temperature from dropping below 40° F, a thermal blanket surrounds the equipment and is attached to the inside of the cylinder. The blanket weight is estimated as 6. 5 pounds assuming the use of thin aluminized mylar (or its equivalent) sheets with possibly some insulating material in its construction.

Propellant Lines

The propellant lines that feed the axial jets may need heaters to prevent propellant freezing. It is estimated that the temperature between the A/L and SM may stabilize at approximately 160° F. If so, heaters may not be required.

SEQUENCE OF EVENTS

Introduction

In order to examine in detail the subsystem requirements imposed by the system mission requirements, a typical mission profile was generated. This was used as a basis to construct a mission sequence of events which would include considerations of telecommunications link requirements, scheduling of midcourse and attitude maneuvers, as well as electrical power and energy requirements. This was done for the case of launch on 12 July 1973 and encounter on 22 January 1974. The scheduling and magnitude of attitude maneuvers was based on the analysis presented in the Trajectory/Navigation section, power and thermal considerations as discussed in the Power-Thermal section, and communication aspects presented in the Telecommunications section.

Scheduling of attitude and midcourse corrections during transit was based primarily on two considerations:

1) The period between the last attitude and midcourse maneuver occurring at approximately E-5 days and the maneuver before

TABLE 29. PHYSICAL CHARACTERISTICS OF ELECTRONIC UNITS

	Approximate Volume, cubic inches	Approximate Weight, pounds	Required Bolt-down Area, square inches	As Designed Bolt-down Area, square inches
Battery 1	180	14.2	30	30
Battery 2	180	14.2	30	30
Battery charger booster	100	3.5	20	20
Boost regulator	180	8.5	46	46
Transmitter 1	510	20.6	100	120
Transmitter 2	510	20.6	100	120
S-band receiver 1	100	4.0	20	24
S-band receiver 2	100	4.0	20	24
UHF receiver 1	75	3.0	18	21
UHF receiver 2	75	3.0	18	21
Signal processing unit	160	10.0	23	32
Central command decoder	150	5.7	18	30
Command storage and sequencer	125	5.0	25	30
Flight control unit	440	17.5	50	84

the last one should be maximized. In this way, the longer tracking period prior to the last midcourse correction would permit a higher accuracy for the final stages of the trajectory.

2) By maintaining the earth within 5 degrees of the true boresight of the high-gain antenna, the down-link transmission rate can be maintained above 200 bits/sec using the 3-watt output of the transmitter and receiving on the 210-foot dish. The pertinent capabilities were presented in the Telecommunications section.

3) The spin-axis attitude with respect to the sun direction must be greater than 10 to 15 degrees for proper operation of the sun and star sensors.

Using similar techniques, the attitude correction magnitudes and their optimum scheduling within the mission can be optimized for any mission.

Typical Detailed Sequence of Events

The following information contains a typical detailed sequence of events for the cruise and terminal phases of the mission and the attitude/velocity control subsystem.

Cruise Sequence

Pre-Launch Status of Support Module

Flight control on.

Transmitter low power on.

Transmitter high power TWT filaments on.

Transmitter to cross-slot (or possibly omni) antenna.

Commutator 1 (SM cruise) selected.

Star sensor off.

200/bits/sec bit rate selected.

*Launch.

*Boost.

*Parking orbit. Separate forward canister.

*Injection to Mars trajectory. Support module, aeroshell/lander, aft canister, adapter, and Titan last state still connected.

*Titan last stage engine cutoff.

*Attitude rotation with Titan last stage. Align SM spin axis parallel to ecliptic (±5 degrees) and approximately 45 degrees to the sunline (toward earth).

*Verify attitude.

*Transmitter to high power.

*Separate payload from Titan last stage. Aft canister goes with Titan. Impart $\Delta V \approx 2$ fps, $\theta \approx 2$ deg/sec.

(A) Spinup to 25 rpm (Subsequence C).

(A) Enable squib circuits for axial jet/omni antenna mechanisms.

(A) Extend axial jets and omni antennas.

Acquisition by DSN. Establish two-way link.

- Transmitter to cross-slot antenna.
- Transmitter to low power.
- Aeroshell/lander to cruise mode.
- Select commutator 2 (attitude data).
- Select commutator 3 (aeroshell/lander data).
- Select commutator 1 (SM general data).
- Wait approximately 1 day.
- Turn on star sensor.
- Transmitter to high power.
- Select 2000 bits/sec bit rate.
- Select commutator 2 (attitude data).

  Star data received in real time. Data storage not required at this time; however, the data can be stored and recalled if desired.

- Select 200 bits/sec bit rate.
- Transmitter to low power.

- Turn off star sensor.
- Select commutator 1 (SM general data).
- Reorient to desired cruise attitude if necessary. The maneuver would be done according to Subsequence A with commutator 2 selected. After maneuver completion, attitude verification using sun and star sensor would be made.
- Establish transponder mode to get tracking data.
- Wait half day to several days.
- Select commutator 3 (A/L data).
- Activate A/L for thorough checkout. (It may be possible to activate the UHF link and perform the checkout through it if the SM and A/L are designed in this way).
- Transmitter to high power.
- Select 200 bits/sec bit rate.
- Return A/L to cruise mode.
- Select Commutator 2 (attitude data).
- Select commutator 1 (SM general data).
- Select 10 bits/sec bit rate.
- Transmitter to low power.
- Continue to evaluate A/L data.
- Cruise. Continue acquiring tracking data.

First midcourse correction maneuver at approximately I + 5d. Sun incidence angle at approximately 40 degrees. Range approximately 1.5 million km.

- Select commutator 3.
- Select commutator 2.
- Turn on star sensor
- Turn off star sensor.

- Wait for attitude verification before thrusting. Star data probably cannot be received in real time, even using transmitter high power. Star data will be stored on board and transmitted to DSN for evaluation.

- Axial jet thrusting continuous (Subsequence D).

- Radial jet thrusting (Subsequence E).

- Turn star sensor on.

- Turn star sensor off.

- Select commutator 3.

- Select commutator 1.

Star data will be stored on board and transmitted back to DSN for evaluation.

- Cruise. Continue tracking.

<u>Second midcourse correction maneuver at approximately I + 30d.</u> Sun incidence angle approximately 15 degrees. Range approximately 10 million km.

- Same steps as for first midcourse correction.

- Cruise. Continue tracking.

There will be no sun sensor data from approximately I + 30d to I + 60 d. At approximately I + 30d, the bit rate may have to be lowered from 200 to 10 bits/sec in order to maintain good data quality while in low power.

<u>First attitude rotation to point planar antenna at earth ≈ I + 92d.</u> Rotation to be approximately 60 degrees. Center of antenna beam to be approximately 4.5 degrees away from earth center. Sun incidence angle, i, to be approximately 15 degrees.

- Select commutator 2.

- Turn on star sensor.

- Turn off star sensor.

  Wait for attitude verification before thrusting. Star data will be stored on board and transmitted to DSN for evaluation.

- Reorientation maneuver using Subsequence A.
- Transmitter to high power.
- Select 500 bits/sec rate.
- Transmitter to planar antenna.

  Verify receipt of good data at 500 bits/sec.

- Turn on star sensor.
- Turn off star sensor.
- Select commutator 1.

  Star data will be stored on boa and transmitted to DSN for evaluation.

- Cruise. Continue tracking.

Check out 16,000 bits/sec bit rate capability at approximately I + 106d. Center of planar antenna beam to be on earth center. Sun incidence angle, i, to be approximately 10 degrees.

- Transmitter to high power.
- Select 16,000 bits/sec bit rate.
- Select commuator 2.
- Select commutator 3.
- Select commutator 1.
- Select 500 bits/sec bit rate.
- Transmitter to low power.
- Cruise. Continue tracking.

<u>Second attitude rotation to point planar antenna at earth at approximately I + 140d.</u> Rotation to be approximately 9 degrees. Center of antenna beam to be approximately 4.5 degrees away from earth center. Sun incidence angle, i, to be approximately 25 degrees.

- Same steps as for first attitude rotation.
- Cruise. Continue tracking.

- Load command storage and sequencer with terminal sequence commands at approximately E-3d.
- Activate aeroshell/lander for final checkout at approximately E-36 hours.
- Transmitter to high power.
- Select 16,000 bits/sec bit rate.
- Select commutator 3.
- Select commu...tor 2.
- Select commutator 1.
- Transmitter to low power.
- Select 500 bits/sec bit rate.

  Verify readiness of aeroshell/lander and support module for encounter phase. Verify data quality in all commutators at 16,000 bits/sec bit rate.

Terminal sequence:

Commands	Time Executed E = Encounter minutes
Pre-Encounter Phase (see Note B)	
Aeroshell/lander to internal power	E - 300:00
Turn on UHF receivers	E - 299:50
Command storage and sequencer on	E - 299:40
Select 30 bits/sec bit rate	E - 299:30
Transmitter to high power	E - 299:20
Execute terminal sequence (starts counter storage and sequencer. Following commands are automatically executed).	E - 299:00
Reorient to entry attitude (Subsequence A).	E - 298:30
Activate aeroshell/lander	E - 283:30

Despin to 5 rpm (Subsequence B).	E - 282:30
Wait 30 minutes for status evaluation.	
Separate.	E - 252:30
Spinup to 60 rpm (Subsequence C).	E - 252:00
Reorient to cruise attitude (Subsequence A).	E - 251:00
Transmitter to planar antenna.	E - 236:00
Transmitter to low power.	E - 235:50
Select 2000 bits/sec bit rate.	E - 235:40
Deflection ΔV thrusting (Subsequence D, axial jets, and Subsequence E, radial jet).	E - 235:30
Select commutator 1.	E - 115:30
Command storage and sequencer off. This completes the automatic sequence.	E - 115:20

<u>Encounter Phase</u>

Transmitter to high power.	E - 23:30
Select 16,000 bits/sec bit rate.	E - 23:20
Select Commutator 3.	E - 23:10
Encounter (Touchdown)	E - 0
Select 500 bits/sec bit rate.	E + 30:00
Transmitter to low power.	E + 30:10

NOTES:

* Events performed by Titan programmer.

A. Events automatically commanded.

B. The terminal sequence - pre-encounter phase is shown starting at E-5 hours. The complete pre-encounter phase can be moved to an earlier or slightly later time if desired. For example, if the initial command of the pre-encounter phase were moved to E-24 hours, the phase would be completed approximately 3 hours later. The encounter phase would still be initiated at the same time.

Subsequences

Subsequence A: Reorientation

1) Synchronous Mode

    a) Select firing angle magnitude.

    b) Select pulse width.

    c) Select number of pulses.

    d) Select thruster number.

    e) Enable axial jet.

2) Quadrant Mode

    a) Quadrant select command.

    b) Select number of pulses.

    c) Select thruster number.

    d) Enable axial jet quadrant mode.

    e) Quadrant select command.

    f) Select thruster number.

    h) Enable axial jet quadrant mode.

Subsequence B: Despin

a) Select spin/despin duration.

b) Enable despin jets.

c) Stop despin (backup).

Subsequence C: Spinup

a) Select spin/despin duration.

b) Enable spinup jets.

c) Stop spinup (backup).

Subsequence D: Continuous Thrusting

1) Synchronous

   a) Select number of spin periods x 100.

   b) Select number of spin periods.

   c) Jet continuous command.

   d) Polarity control command.

   e) Enable axial jets.

2) Quadrant

   a) Select number of quarter spin cycles x 100.

   b) Select number of quarter spin cycles.

   c) Jet continuous command.

   d) Polarity control command.

   e) Enable axial jets quadrant mode.

Subsequence E: Radial Jet Thrusting

1) Synchronous Mode

   a) Select firing angle · ›gnitude.

   b) Select number of pulses x 100.

   c) Select number of pulses.

   d) Enable radial jet.

2) Quadrant Mode

   a) Quadrant select command.

   b) Select number of pulses x 100.

   c) Select number of pulses.

   d) Enable radial jet quadrant mode.

   e) Quadrant select command.

f) Select number of pulses x 100.

g) Select number of pulses.

h) Enable radial jet quadrant mode.

3. FLYBY-ENTRY DATA DESIGN

The Flyby-Entry Data SM design was studied prior to the Video design, and growth provisions were made to accommodate the Video design. This resulted in many common elements in the two designs; therefore, only the differences are presented in this section. The primary differences are in the planar antenna and high-power transmitters (reduction in size because the Mars encounter goal is only the relaying of entry data at 2000 bits/sec) and associated reduction in Entry Data design weight. Most of the analysis for the Video design is applicable to the Entry design.

TRAJECTORY/NAVIGATION

The Flyby-Entry Data design uses the same direct entry mode of mission delivery and launch and arrival periods as the Video SM design. The only difference in the trajectory and navigation aspects of the mission is the spin-axis correction strategy used to maintain SM-to-DSN communications approximately 90 days after injection. The larger planar antenna beamwidth, 11.5 degrees, allows for fewer corrections. The pointing strategy for the Entry design is based on the techniques presented in the Trajectory/Navigation section (Spacecraft Attitude Corrections).

VEHICLE CONFIGURATION/WEIGHTS

The Entry Data SM design canister, adapter, A/L, upper cylinder, solar panels, equipment shelf, axial jet arms and control jets, sensors, UHF antennas, thermal blanket dimensions, weight, and locations are identical to those of the Video design. The differences between the two designs are described in the following paragraphs. Figure 75 is an inboard profile of the Entry Data design.

Planar Antenna

The S-band high-gain (21.2 dB) planar antenna consists of cavity sections which form a 23-inch square that is mounted against the thermal louvers. A frustum cover coated with a high emissivity material, such as quartz mirror used on Surveyor, to enhance radiation surrounds the planar antenna. The cross-slot antenna is mounted alongside the planar antenna but could be made an integral part of the planar as in the Video design. The planar antenna weighs 4 pounds, and the cover weighs 4.2 pounds.

Equipment Shelf

The Entry design transmitters (3 and 20 watts) are mounted to the equipment shelf; therefore, the general arrangement of equipment differs from that of the Video design. Also, the propellant tanks are slightly smaller in diameter, 13.9 inches, allowing for other arrangements. All the thermal control louvers are mounted to the shelf opposite the equipment.

Peripheral Equipment

The Entry design radial jets are shown in Figure 95 with their axes directed through the spacecraft cg. Later studies indicated that one jet directed through the spacecraft cg and the other through the SM, as in the Video design, has significant advantages and is, therefore, recommended. The Entry Data SM harness weighs 10 pounds.

Mass Properties

The Entry Data SM weights, listed in Table 30, yield a total of 521 pounds. The new weights indicated, plus primarily the reduced transmitter and propulsion subsystem weights, account for the Entry design weight being less than that of the Video design, 558 pounds. Table 31 shows an SM, adapter, and canister contingency allotment of 138 pounds. Table 32 lists the moment of inertia estimates.

ATTITUDE/VELOCITY/REACTION CONTROL

The lighter weight Entry Data SM design requires less propellant for mission attitude, velocity, and spin control, 109 pounds, and smaller propellant tanks, 13.9-inch diameter (18 pounds), than the Video design. The less than 10 percent weight difference between the two designs implies a conservative Entry design performance if the values presented in the Video design section are applied directly to the Entry Data design. Since the Entry design planar antenna beamwidth is greater than that of the Video design, the final attitude maneuver accuracy, 2.6 degrees, after A/L separation, is much better than required.

TELECOMMUNICATIONS

The Entry Data SM telecommunications subsystem relays only entry data at a rate of 2000 bits/sec from the A/L to the DSN; therefore, a small square planar antenna, 22.2 dB and 11.5-degree beamwidth, and a 20-watt transmitter are adequate. The entry data link was designed in a manner similar to that presented in the Video Data telecommunications section. A DSN receiver temperature of 25°K, receive gain of 61.0 ± 1 dB, and a transmit gain of 60.0 ± 0.8 dB were used for the 210-foot antenna. The remaining S-band link parameter values and tolerances are identical to those listed in Table 23. Figure 96 shows the SM transmitter power - antenna gain product as a function of bit rate capability and range. Also plotted are the corresponding optimum MIs. A product of approximately 65 dB will

Page 186 Blank

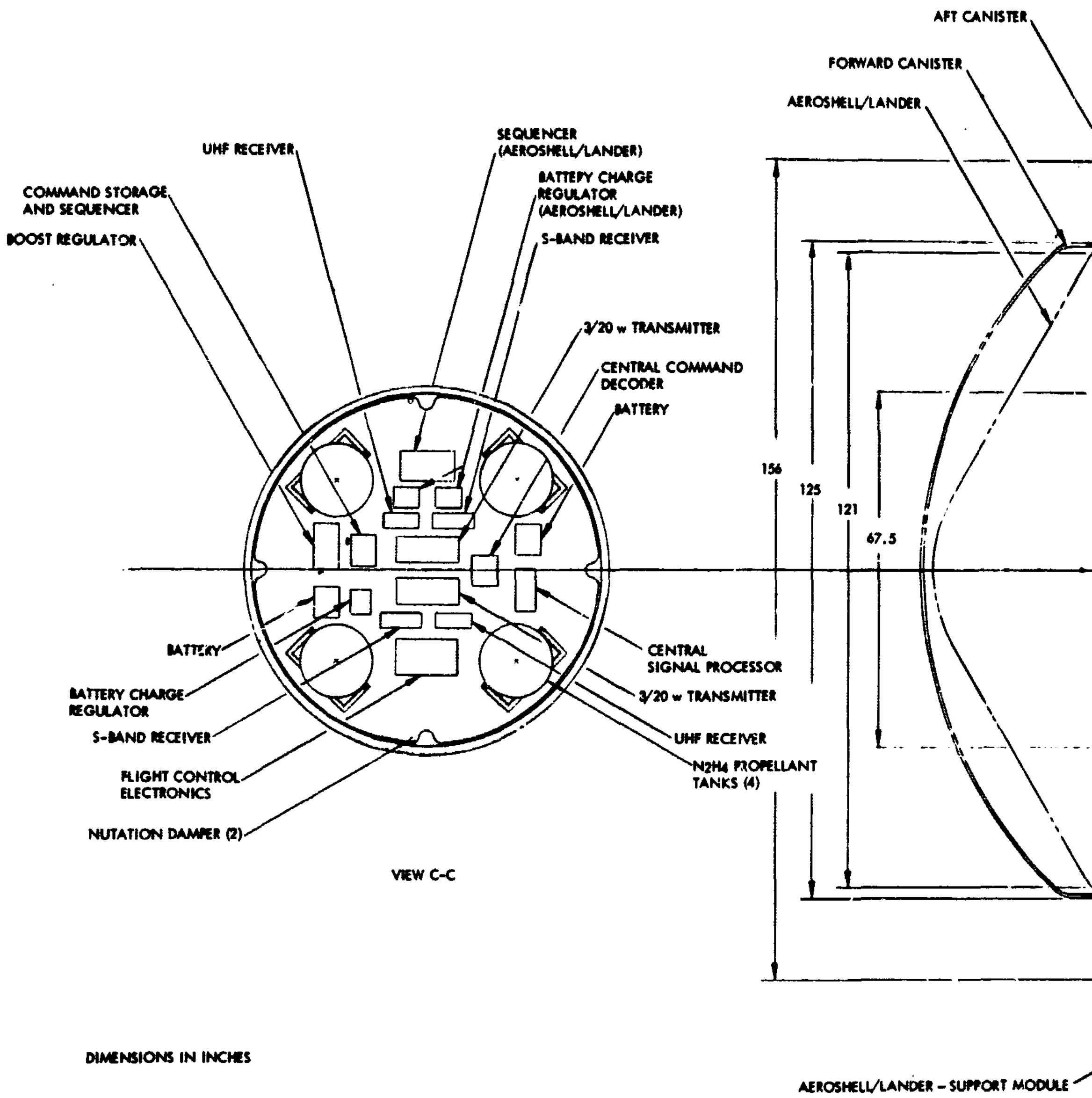
AFT CANISTER
FORWARD CANISTER
AEROSHELL/LANDER
UHF RECEIVER
SEQUENCER
(AEROSHELL/LANDER)
BATTERY CHARGE
REGULATOR
(AEROSHELL/LANDER)
COMMAND STORAGE
AND SEQUENCER
BOOST REGULATOR
S-BAND RECEIVER
3/20 w TRANSMITTER
CENTRAL COMMAND
DECODER
BATTERY
156
125
121
67.5
BATTERY
BATTERY CHARGE
REGULATOR
S-BAND RECEIVER
FLIGHT CONTROL
ELECTRONICS
NUTATION DAMPER (2)
CENTRAL
SIGNAL PROCESSOR
3/20 w TRANSMITTER
UHF RECEIVER
N2H4 PROPELLANT
TANKS (4)
VIEW C-C
DIMENSIONS IN INCHES
AEROSHELL/LANDER – SUPPORT MODULE

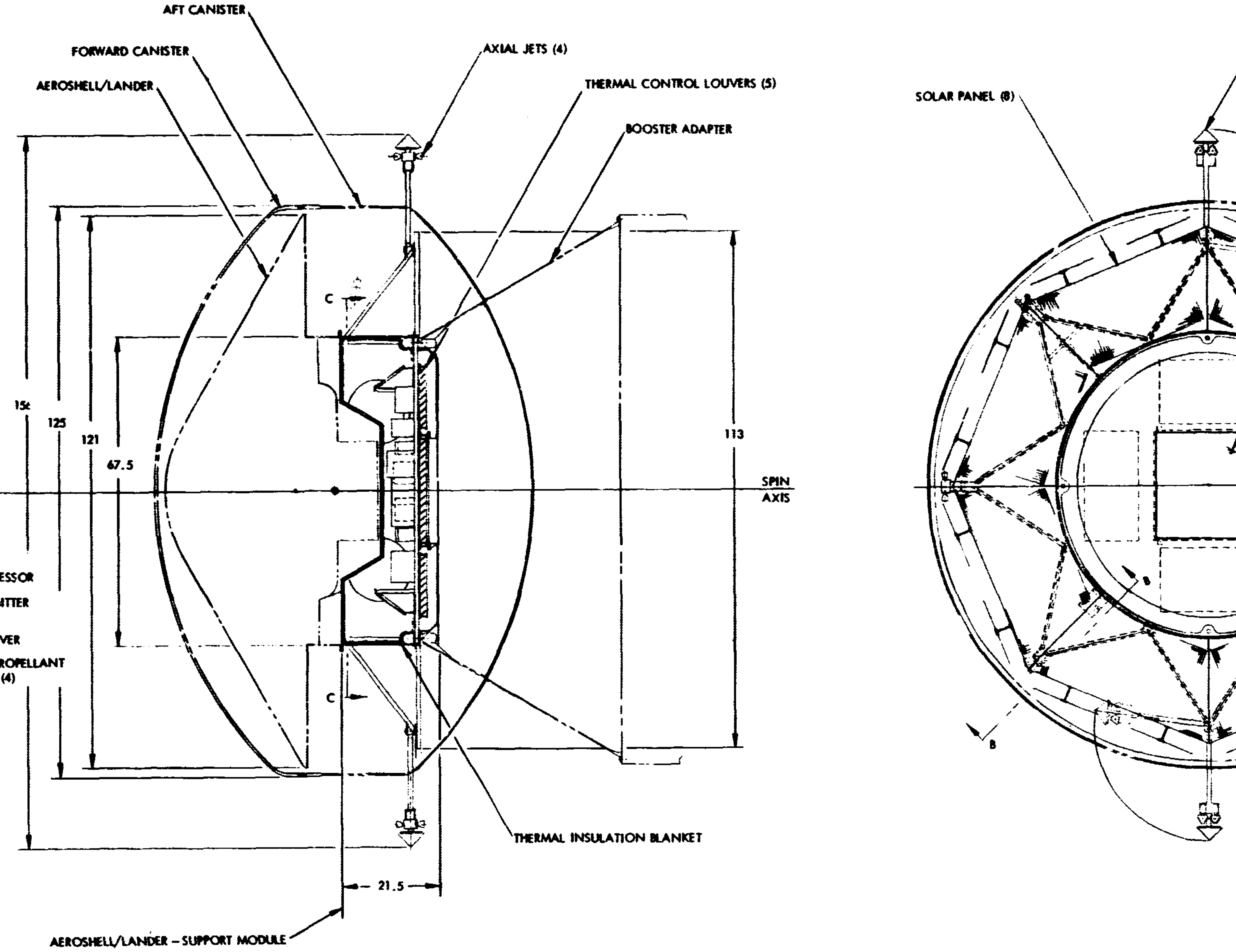
AFT CANISTER
FORWARD CANISTER
AEROSHELL/LANDER
AXIAL JETS (4)
THERMAL CONTROL LOUVERS (5)
BOOSTER ADAPTER
SOLAR PANEL (8)
125
121
67.5
113
SPIN AXIS
C
B
THERMAL INSULATION BLANKET
21.5
AEROSHELL/LANDER – SUPPORT MODULE

Fi

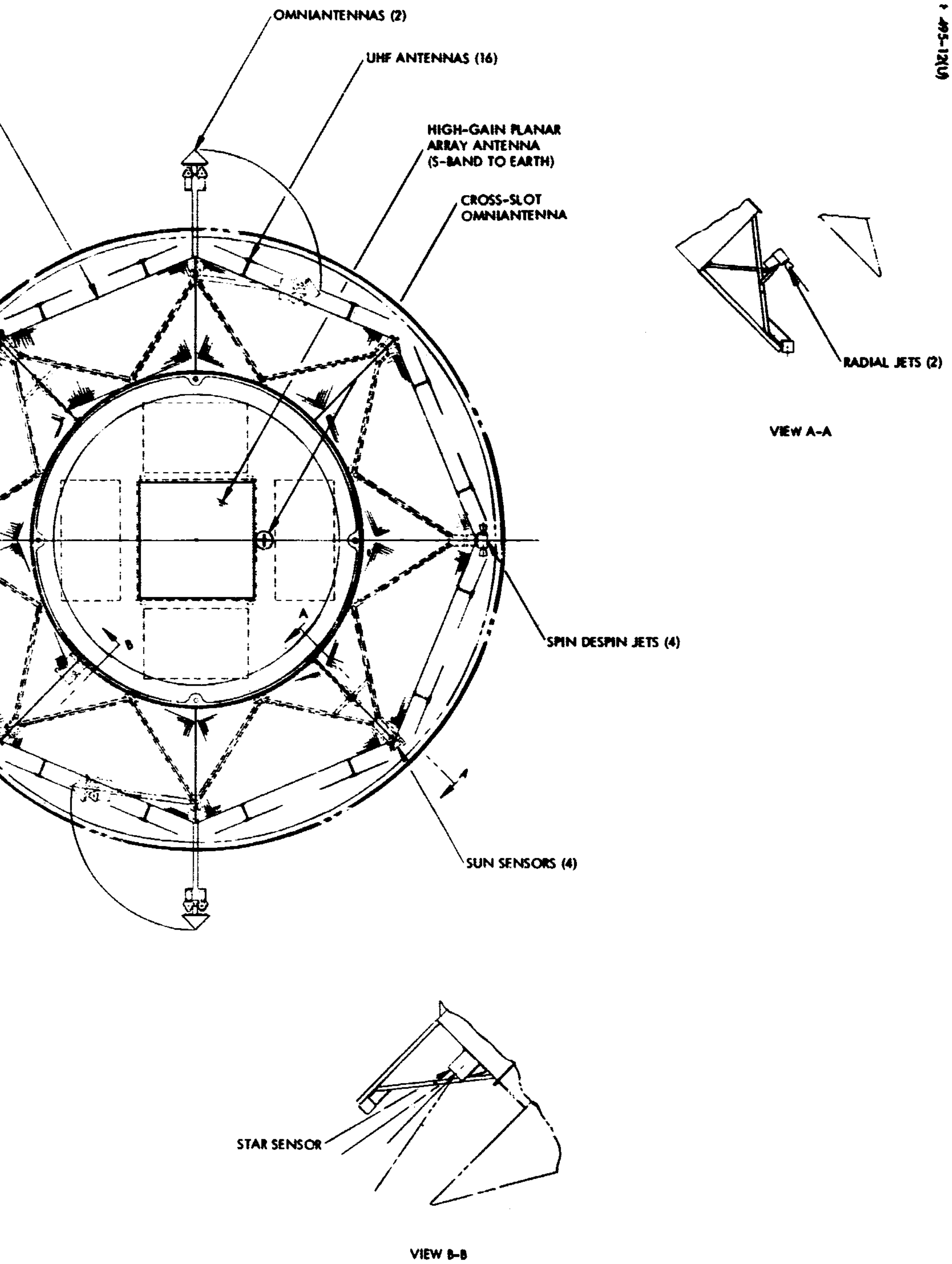

Figure 95. Flyby - Entry Data SM Inboard Profile

PRECEDING PAGE BLANK NOT FILMED.

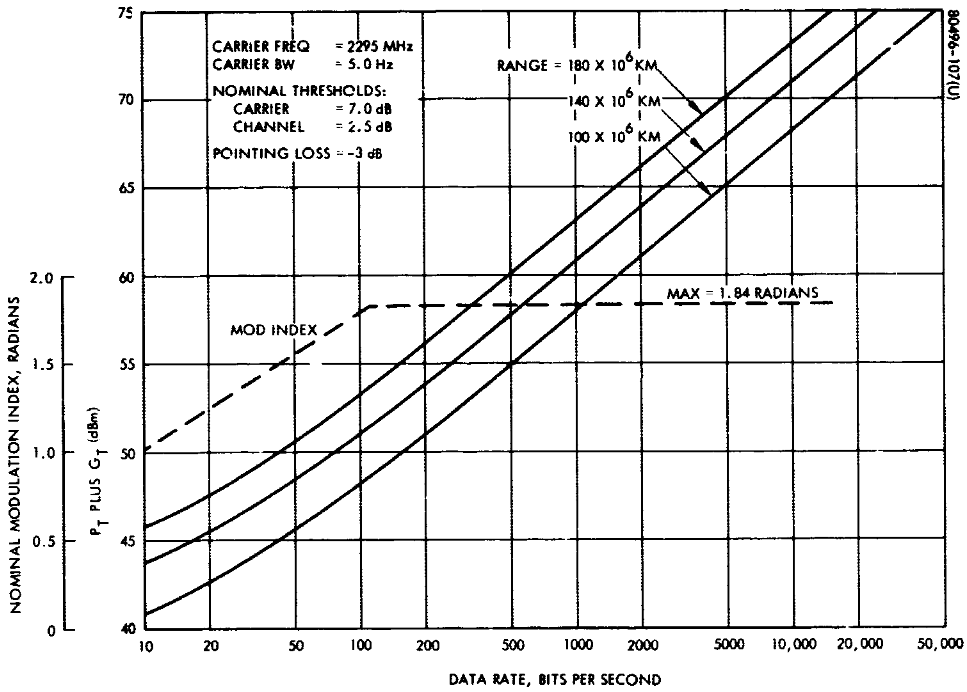

Figure 96. P_t (dBm) + G_c (dB) Versus Bit Rate

TABLE 30. MSSM SUBSYSTEM WEIGHT ALLOTMENT, FLYBY DESIGN – ENTRY DATA

Item	Weight, pounds	
RF Subsystem		51.5
3-watt transmitter (2)	22.0	
20-watt transmitter (2)		
High-gain antenna (1)	4.0	
UHF antennas (16)	3.0	
Turnstile antenna (2)	1.0	
S-band receiver (2)	8.0	
UHF receiver (2)	4.7	
RF switches (3)	1.5	
Coaxial cables and attach clips	5.5	
Cross slot omni	0.5	
Diplexer (3)	1.3	
Signal Processing		30.7
Central command decoder (2)	5.7	
Central signal processor	10.0	
Command storage and sequencer (S/M)	5.0	
Sequencer (A/L)	10.0	
Propulsion		146.0
5-pound thrusters (10)	11.0	
13.9-inch diameter tanks (4)	18.0	
Valves, lines, filters, and pressurant	8.0	
Propellant/pressurant (2 pounds)	109.0	
Flight Control		30.0
Flight control electronics	17.0	
Star sensors (1)	5.1	
Sun sensors (4)	1.0	
Local cables, connectors, and clips	3.4	
Nutation damper	2.5	
Accelerometer and acceleration switch	1.0	
Structure		116.4
Upper ring	11.7	
Upper cylinder	21.1	
Central ring	11.6	
Lower frustum	4.2	
Equipment shelf	21.0	
Thermal blankets and tie downs	4.5	
Lower thermal blanket support	6.5	

TABLE 30. MSSM SUBSYSTEM WEIGHT ALLOTMENT, FLYBY DESIGN - ENTRY DATA - Concluded

Item	Weight, pounds	
Harness	10.0	
Solar panel support tubes	7.0	
Balance weights	4.0	
Thermal control louver (5)	13.6	
Radial jet supports (2)	1.2	
Mechanisms		14.8
Separation mechanism	11.6	
SM/lander 4.8		
SM/adapter 6.8		
Axial jet deployment (2)	3.2	
Electrical Power		84.1
Solar panel (substrate, cells, interconnections)	36.8	
Boost regulator	8.5	
Battery charge regulator (1 S/M, 2 A/L)	10.5	
Battery (2) 40 percent discharge	28.3	
SM weight	473.5	
Contingency	47.5	
Total	521.0	

TABLE 31. MSSM - LAUNCH WEIGHT DISTRIBUTION, FLYBY-ENTRY DESIGN

Item	Weight, pounds	
Aeroshell/lander		1100.0
SM weight (includes 47 pounds contingency)		521.0
SM/booster adapter		117.2
Structure	77.2	
Umbilical	35.0	
Pyrotechnic separation logic	5.0	
Aft canister		181.8
Structure	128.8	
Pressure and vent.	50.0	
Separation harness	3.0	
Forward canister		69.0
Launch weight		1989.0
Titan payload	2080	
Total contingency for SM, adapter and canister		138

TABLE 32. MOMENTS OF INERTIA, FLYBY-ENTRY DESIGN

Vehicle State	Slug – ft^2
A/L and SM	
Full fuel	
I_{Roll}	380
I_{Pitch}	287
40 percent fuel	
I_R	374
I_P	283
SM	
40 percent fuel	
I_R	67
I_P	35
Zero percent fuel	
I_R	61
I_P	32

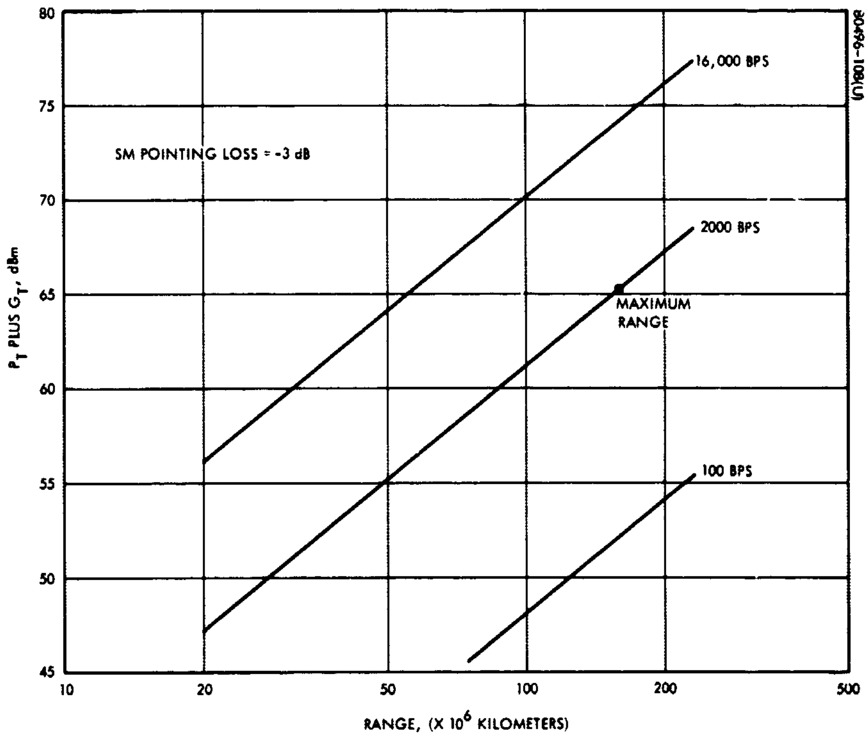

Figure 97. RF Power Plus Antenna Gain Versus Range for Baseline Bit Rates

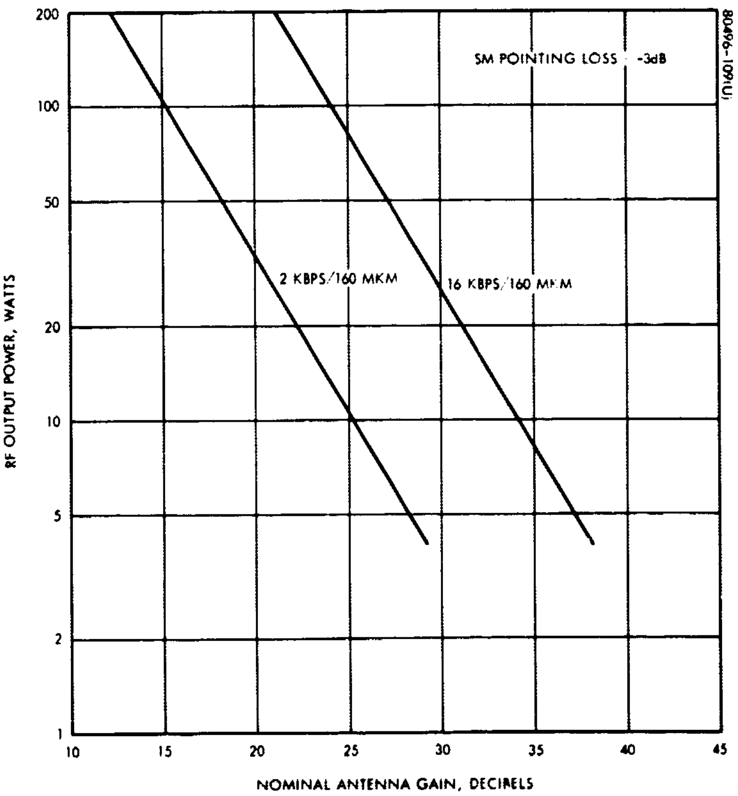

Figure 98. High-Gain Antenna Power Versus Gain for Baseline Bit Rates

will sustain 2000 bits/sec at 160×10^6 km SM-to-earth range. Figures 97 and 98 are plotted for study purposes using the data of Figure 96.

Using the results of preliminary studies, a scaled down Surveyor type planar antenna 23 inches square, with 22.2 dB gain and 11.5 degrees beamwidth was selected. As shown on Figure 98, a 20-watt transmitter working with this planar antenna supports 2000 bits/sec. A readily available Hughes 20-watt TWT is included in the transmitter design. A larger planar antenna can be accommodated by the SM structure and a smaller transmitter used. No attempt was made to optimize the SM design along these lines because the Video Data design was anticipated.

The use of a parabolic antenna also was considered as an alternate, but it presented no particular advantages over the planar antenna. Figure 99 show planar and parabolic antenna gains and beamdwidths as a function of the parabola diameter or planar side length. Figure 100 plots their corresponding weights. The gains are computed from

$$G' = \eta \, 4\pi \frac{A}{\lambda^2}$$

where

G = gain ratio (gain, dB = $10 \log_{10} G'$)

η = aperture efficiency (efficiency is proportional to size. The η for the planar array varies from 63 percent at L = 20 inches to 70 percent at L = 60 inches. The η of a parabolic reflector was taken to vary from 53 percent at P = 20 inches to 62 percent at 0 = 72 inches)

λ = wavelength (5.15 inches at 2295 MHz)

A = aperture area

The HPBW of a parabolic antenna is calculated by:

$$HPBW = \frac{70,000}{f\,D}$$

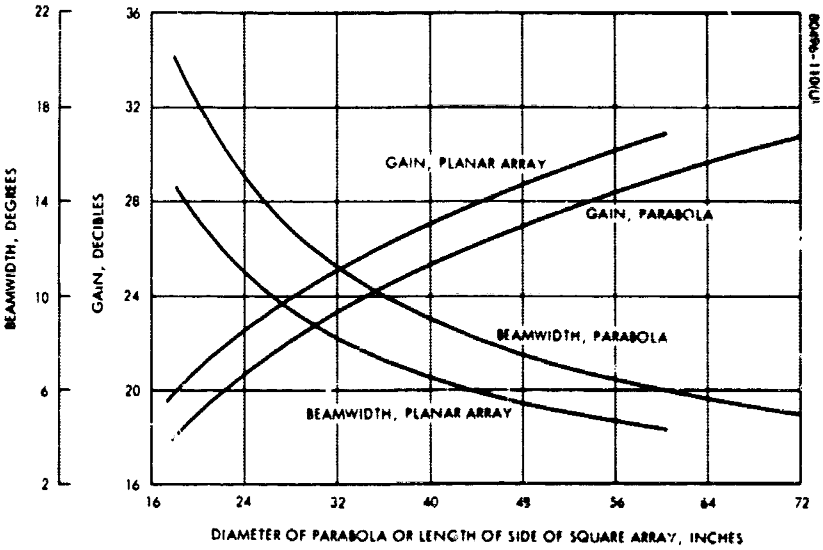

Figure 99. Gain and Beamwidth for Planar Array and Parabola

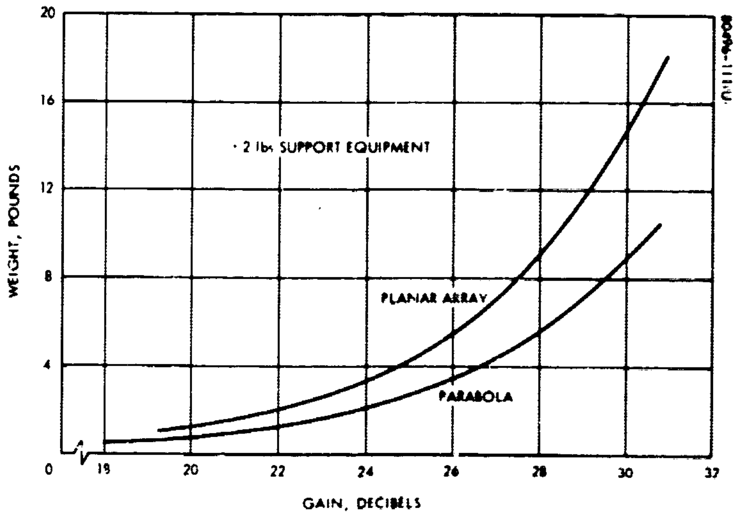

Figure 100. Weight Versus Gain for Planar Array and Parabola

where

$$HPBW = \text{half power beamwidth, degrees}$$

$$f = \text{frequency, MHz}$$

$$D = \text{diameter, feet}$$

The HPBW for a square array is calculated by:

$$HPBW = 51 \frac{\lambda}{D}$$

where

$$HPBW = \text{half power beamwidth, degrees}$$

$$\lambda = \text{wavelength } (\approx 5.15 \text{ inches at } 2295 \text{ MHz})$$

$$D = \text{diameter, inches}$$

The weight of either a planar array or a parabolic antenna grows larger at a slightly greater rate than the area because of the need to use thicker structures to meet stiffness and rigidity requirements.

Figure 101 gives bit rate versus range for various angles off the electrical boresight of the planar or parabolic antenna. 20 and 3-watt transmitters are considered. As in the Video design, the 3-watt transmitter is used primarily during the mission cruise phase. These data are used to determine the planar antenna pointing strategy after the SM cross-slot antenna range is exceeded.

A cross slot is used early in the mission and near encounter just as in the Video design, but it was not integrated with the planar antenna. Also, backup omni antennas are included in the Entry design. Figures 102 and 103 indicate the telemetry bit rate which can be achieved for various ranges and SM transmitters. Table 33 summarizes the telemetry and entry link performance for the Entry Data SM design. The command link performance is identical to that of the Video Data design, Table 24.

An A/L transmitter power of 35 watts is used to sustain the UHF link for the Entry Data design concept. Figure 104 is a plot of the SM antenna gain required as a function of range to sustain 2000 bits/sec. As the Video Data study indicates, the maximum range during the entry phase is 5300 km.

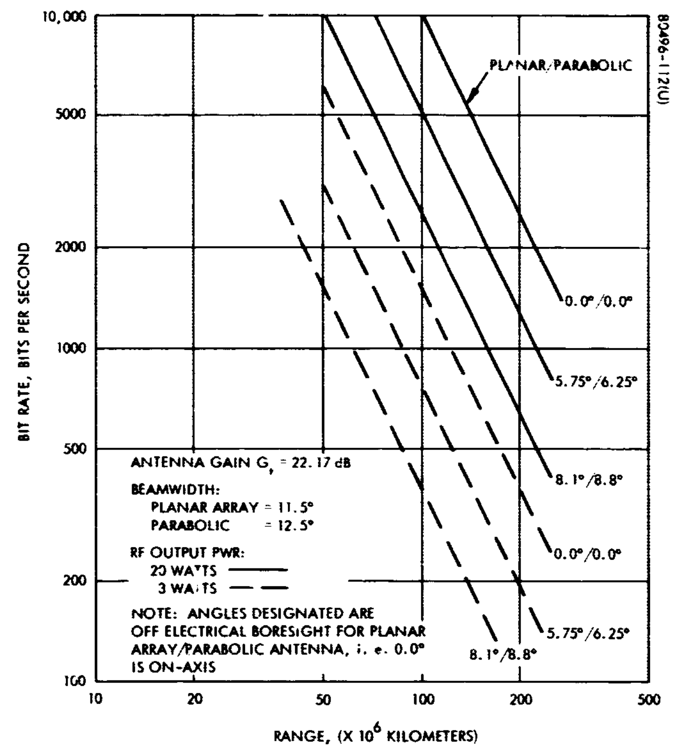

Figure 101. Bit Rate Versus Range for Various Angles Off Electrical Boresight of Planar or Parabolic Antenna

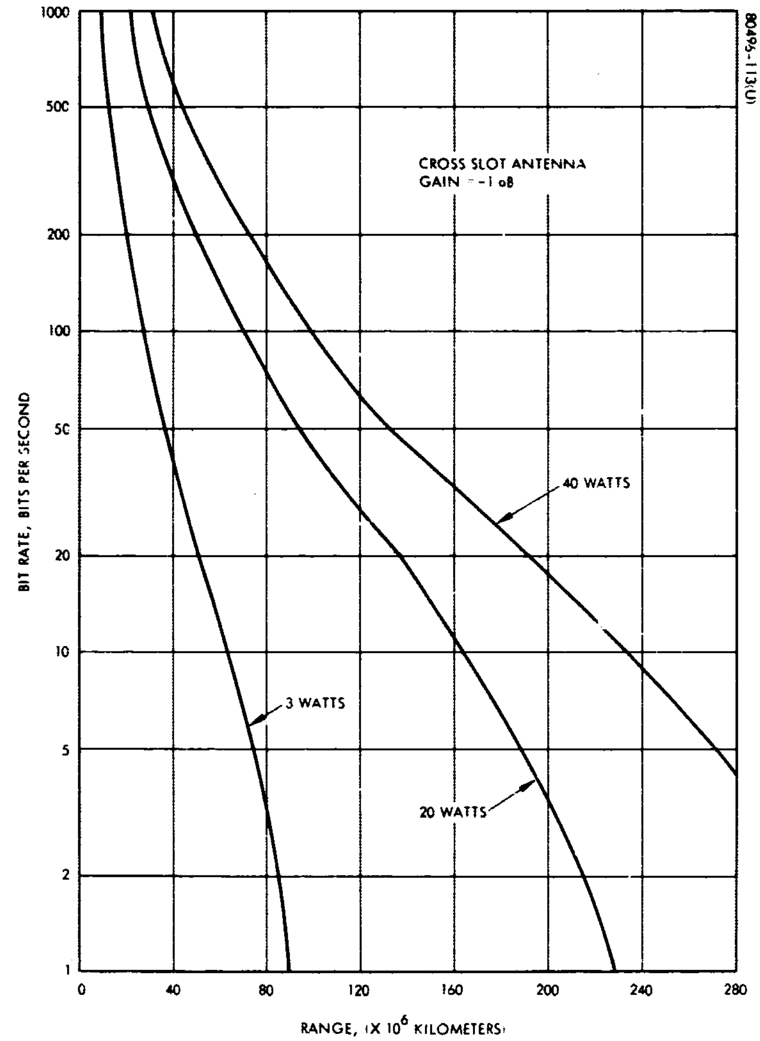

Figure 102. Telemetry Bit Rate Achievable for Cross-Slot Antenna

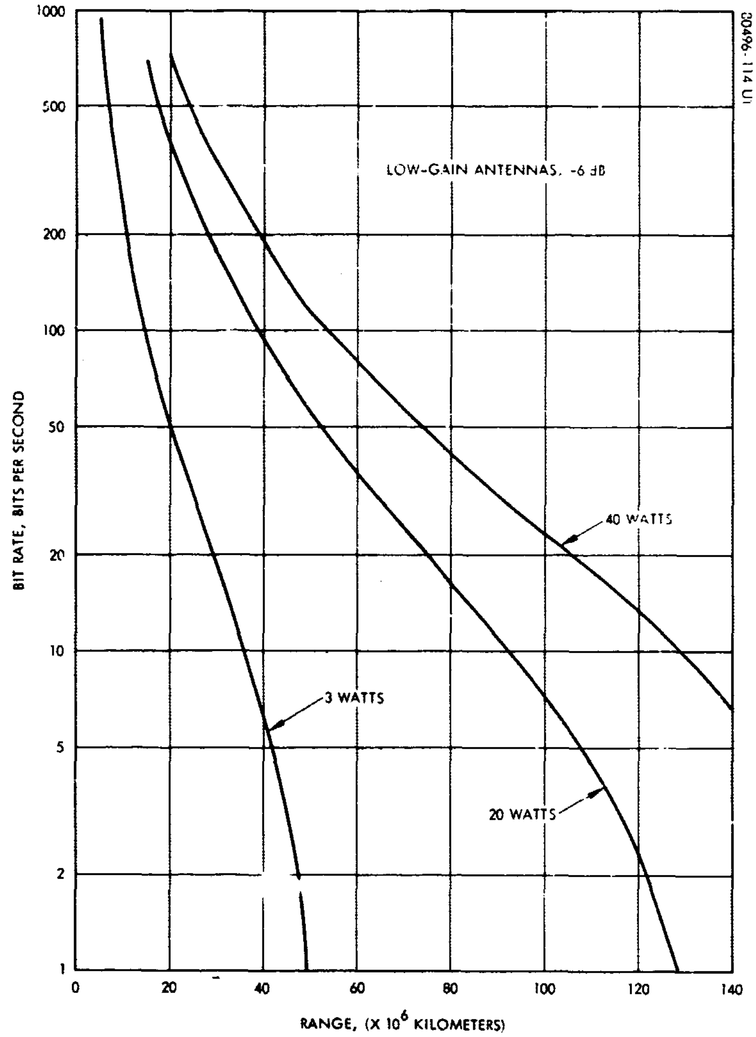

Figure 103. Telemetry Bit Rate Achievable for Low-Gain Antenna

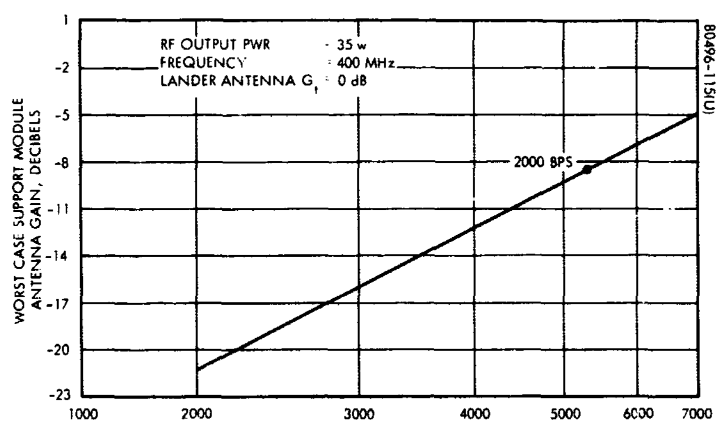

Figure 104. SM Antenna Gain Required as Function of Range to Sustain 2000 Bits/Sec

TABLE 33. MSSM TELEMETRY LINK PERFORMANCE SUMMARY

Mission Phase	Range ($\times 10^6$ km)	Maximum Allowable Information Rate, bits/sec					
		S-Band Link to DSIF (Approximately 2295 MHz)					
Antenna Gain and RF Output Power Conditions		Low-Gain Antennas[1] (-6 dB worst case)			High-Gain Antenna (22.17 dB on-axis)		
		3 watts RF	20 watts	40 watts	3 watts	20 watts	40 watts
Transit I	≤10	240	1600				
First Midcourse	10	240	1600				
Transit II	≤100		43[2]/7	98[2]/23	640	4280	
Second Midcourse	100		43[2]/7	98[2]/23	640	4280	
Transit III	≤160		11[2]	31[2]/3.7	250	2000	
Descent	160				250	2000	4000

[1] Either cross-slot or boom-mounted omni antennas, over the earth-directed hemisphere.

[2] Assumes that gain of cross-slot antenna is always ≥ -1 dB in look angle cone.

A gain of approximately -8 dB is required, which is more than satisfied by an antenna system identical to the Video design VHF antenna system.

With the exception of the planar antenna weight, 4.0 pounds, and the transmitter weight, 22.0 pounds, all Entry design telecommunications weights are identical to those of the Video design.

POWER/THERMAL

The Entry Data SM power subsystem is identical to that of the Video design. This implies a large margin in the battery design because only 20-watt transmitters and entry data must be considered. If it is desired, the battery weight can be reduced. The solar panels are designed to satisfy the anticipated cruise phase loads which are identical for both Flyby designs. The discussion presented in the Video design power section is directly applicable to the Entry data power system.

The use of 20-watt transmitters and a small planar antenna allows all the equipment to be mounted on the equipment shelf and heat energy to be transferred, via five louvers above the shelf, from the equipment to the antenna and lower frustum. The antenna and frustum that is coated with a high emissivity material provide for heat radiation to outer space. There are no louvers mounted about the cylindrical section as in the Video design. The five louvers weigh 13.6 pounds. All other aspects of the Entry Data thermal control subsystem are identical to those presented in the Video design thermal section.

SEQUENCE OF EVENTS

The Entry Data design mission sequence of events is similar to that of the Video design through the entry data phase.

4. ORBITER DESIGN

The Orbiter SM design was studied after the Flyby-Video Data design study was concluded. It incorporates many of the Video design features but differs primarily because of the orbit insertion, nonsterilization, and increased communication range requirements. The design was not studied to the depth of the Video design because of the short study period.

TRAJECTORY/NAVIGATION

The Orbiter design uses the flyby mode of mission delivery whereby the spacecraft is placed initially on a nonimpacting earth-to-Mars trajectory; and, near Mars encounter, the A/L is deflected (rather than the SM as in the Flyby SM design) and placed on a landing course. After relaying video data, the SM performs a braking maneuver to attain a Mars orbit. Data are relayed from the SM once per day while in orbit for the minimum lander lifetime of 3 days.

Trajectory Characteristics

The launch and arrival dates considered are shown in Table 34 along with the resulting range of approach velocities corresponding to the range of launch dates.

Approach velocities of 3.0 and 3.3 km/sec were considered for this study, thereby bounding the range of launch and arrival dates.

TABLE 34. LAUNCH DATES, ARRIVAL DATES, AND APPROACH VELOCITIES

	Spacecraft 1	Spacecraft 2
Launch date	13 July to 10 August 1973	2 July to 12 August 1973
Arrival date	30 January 1974	9 February 1974
Approach velocity V_∞ range	3.2 to 3.3 km/sec	3.0 km/sec

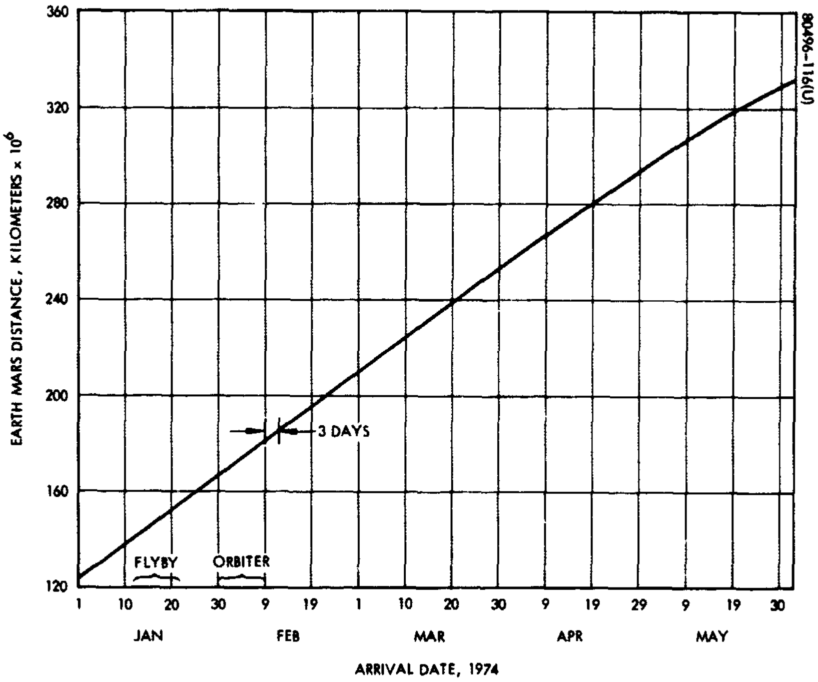

Figure 105. 1974 Earth - Mars Distance

The earth-Mars distance is plotted in Figure 105 as a function of SM arrival at Mars in 1974. Shown are the possible Orbiter arrival distances and the distance 3 days after the last arrival date, 183×10^6 km. This value is used to design the SM communications subsystem. Also shown for comparison are the Flyby SM design distances and dates.

The attitude maneuver strategy employed for the Orbiter design to keep the planar antenna directed at the earth will be similar to that used for the Video Data design because of comparable planar antenna beamwidth.

The flyby mode of mission delivery requires the initial trajectory to be targeted for a 99 percent Mars miss. If this biasing is done in a direction along the minor axis of the expected miss region, no significant midcourse requirement change results; therefore, the guidance analysis done for the Video design is applicable to the Orbiter study.

Encounter/Orbit Characteristics

The A/L maneuver will be similar in magnitude to the SM maneuver in the Flyby design mission. In addition, if the periapsis radius of the Orbiter SM design is similar to the periapsis radius of the Flyby SM design, then the descent communication geometry, lander location, and postlanding visibility will be similar for both designs provided V_∞ is the same. Therefore, for purposes of analysis, it is assumed that the lander true anomaly at touchdown (with respect to the SM periapsis, defined positive before periapsis and negative after periapsis passage) is approximately 20 degrees and that an SM periapsis radius of approximately 7093 km (3700 km periapsis altitude) will satisfy descent communication geometry postlanding visibility constraints for an adverse lander slope of 15 degrees. Previous studies indicated that decreasing V_∞ decreases the required SM periapsis altitude. Since V_∞ for the Orbiter design is less than V_∞ for the Flyby design, an SM periapsis altitude of 3700 km represents an upper bound on the required periapsis altitude for the Orbiter design.

If the postlanding visibility time constraint is relaxed (for example, an increased data transmission rate from the lander to SM would decrease the required postlanding visibility time), a lower SM periapsis altitude would be acceptable. Therefore, in order to assess the pertinent tradeoffs, the analysis was performed for periapsis altitudes of 2000 and 3700 km.

After lander touchdown and lander-to-SM data transmission, the SM is injected from the hyperbolic flyby trajectory into an elliptic Mars synchronous orbit to perform as a data relay for an extended period of time. In addition to being Mars synchronous, periapsis of the ellipse nominally is constrained to be aligned directly over the lander so that lander-to-SM data transmission opportunities will occur near periapsis when the lander-to-SM range is at or near minimum.

Requirements for injection into a Mars synchronous orbit (ΔV magnitude and direction) and the resulting ellipse periapsis altitude are a function of the position on the hyperbolic flyby trajectory at which the injection maneuver is performed. Figure 106 presents ΔV magnitude versus hyperbola true anomaly at injection (with hyperbola true anomaly defined as positive before periapsis and negative after periapsis passage) for hyperbola periapsis altitudes of 3700 and 2000 km. Results are shown for the bounding approach velocities of 3.0 and 3.3 km/sec. The figure indicates that higher hyperbola periapsis altitudes require larger ΔV magnitudes and that, for a given hyperbola periapsis altitude and approach velocity, there is an injection true anomaly that minimizes the required ΔV magnitude.

Direction of the ΔV maneuver is presented in Figure 107 for the indicated hyperbola periapsis altitudes and approach velocities.

Although the orbit is constrained to be Mars synchronous, the ellipse periapsis altitude will vary depending on the hyperbola periapsis altitude, approach velocity, and hyperbola true anomaly at injection. This variation is shown in Figure 108 for hyperbola periapsis altitudes of 3700 and 2000 km. Higher hyperbola periapsis altitudes result in higher ellipse periapsis altitudes; and, for a given hyperbola periapsis altitude and approach velocity, there is an injection point which minimizes the resulting ellipse periapsis altitude.

A constraint must be placed on the hyperbola true anomaly at injection. It has been noted that a hyperbola periapsis altitude of 3700 km (or 2000 km for increased lander data transmission rates) will satisfy postlanding visibility time constraints for adverse lander slopes of 15 degrees. For these conditions, injection into the ellipse must not occur before the end of postlanding visibility. In addition, 3 to 5 minutes must be allowed for orientation of the SM to the required attitude for injection. Therefore, the hyperbola true anomaly at injection must be constrained such that, for adverse lander slopes of 15 degrees, 3 to 5 minutes past the end of postlanding visibility is allowed for SM orientation. Figure 109 presents, for an approach velocity of 3.3 km/sec and hyperbola periapsis altitudes of 3700 and 2000 km, time past end of postlanding visibility versus hyperbola true anomaly at injection for various lander slopes. Curves for an approach velocity of 3.0 km/sec are not significantly different. For a given hyperbola true anomaly at injection, time past the end of postlanding visibility decreases as the lander slope decreases. However, as the lander slope decreases from +15 degrees (assumed maximum adverse slope), the postlanding visibility time increases from the required minimum of 12 minutes. Therefore, although the time past the end of postlanding visibility for a given hyperbola true anomaly may be less for a lander slope of -15 degrees, the postlanding visibility time is greater for the -15 degree slope. The required constraint is that the hyperbola true anomaly at injection allows 3 to 5 minutes orientation time past the end of postlanding visibility for a lander slope of +15 degrees.

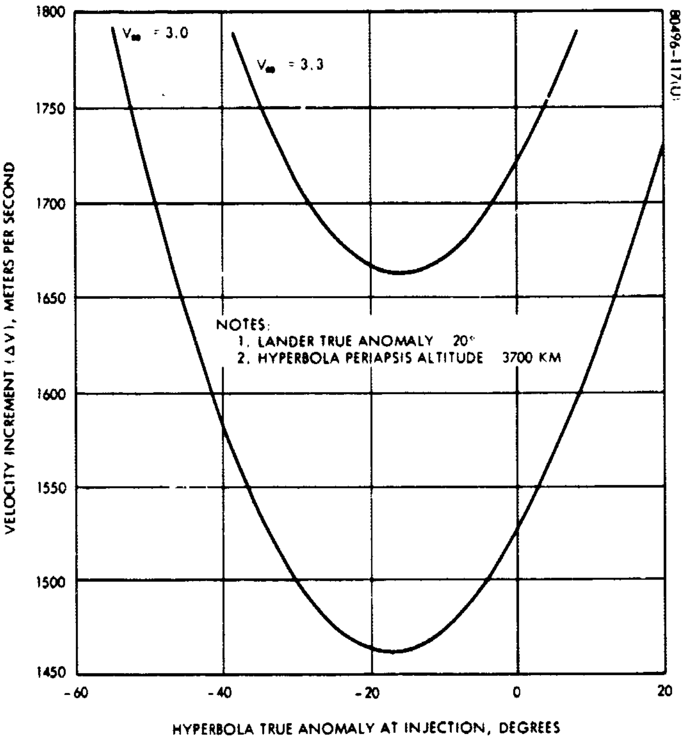

a) Hyperbola periapsis altitude = 3700 km

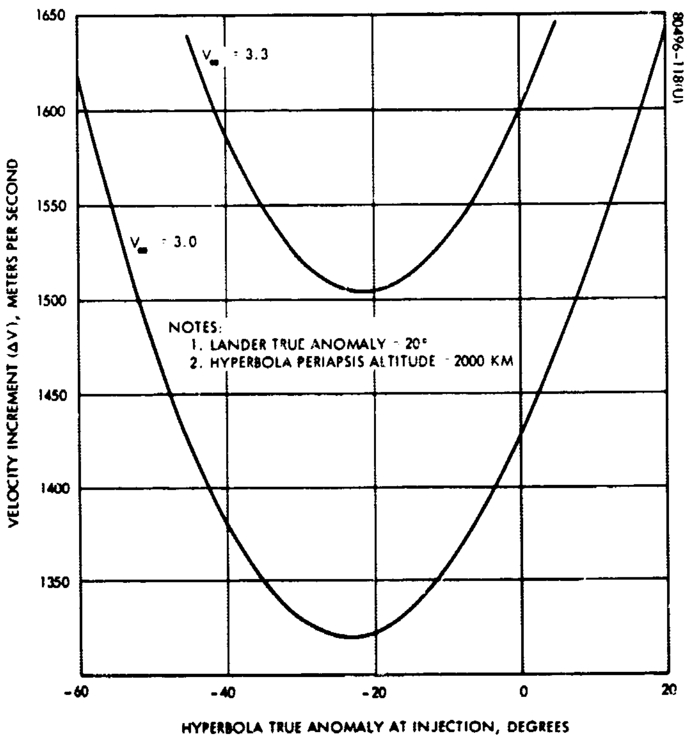

b) Hyperbola periapsis altitude = 2000 km

Figure 106. Velocity Increment Magnitude

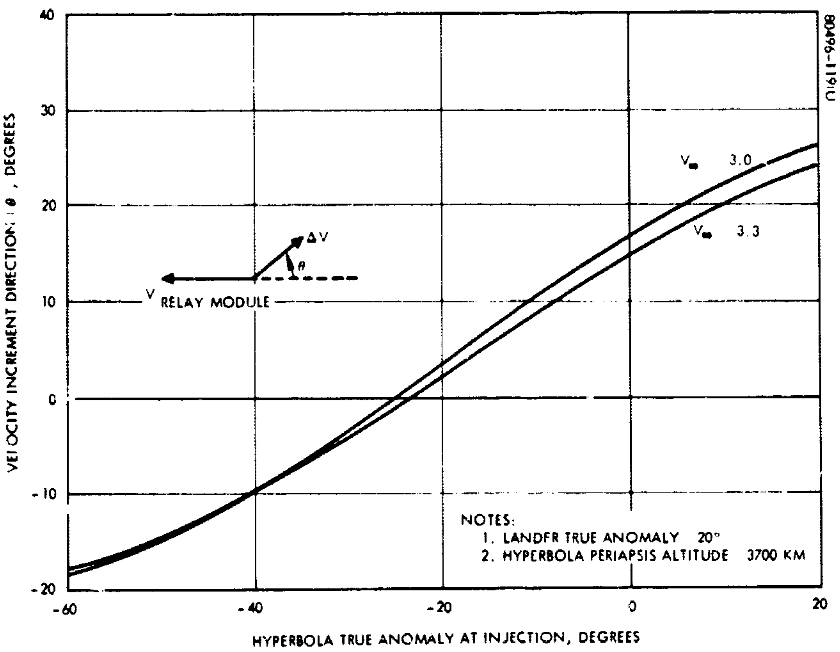

a) Hyperbola periapsis altitude 3700 km

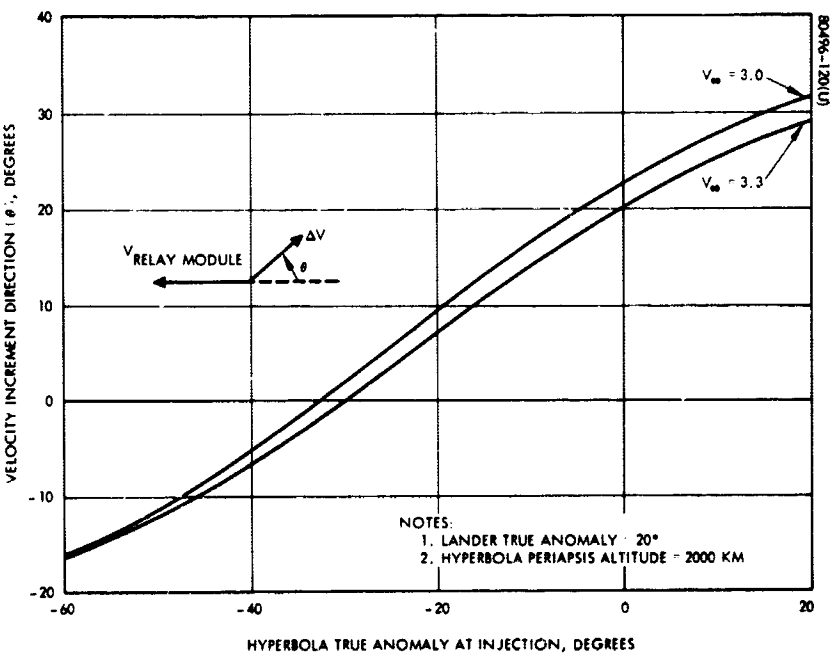

b) Hyperbola periapsis altitude = 2000 km

Figure 107. Velocity Increment Direction

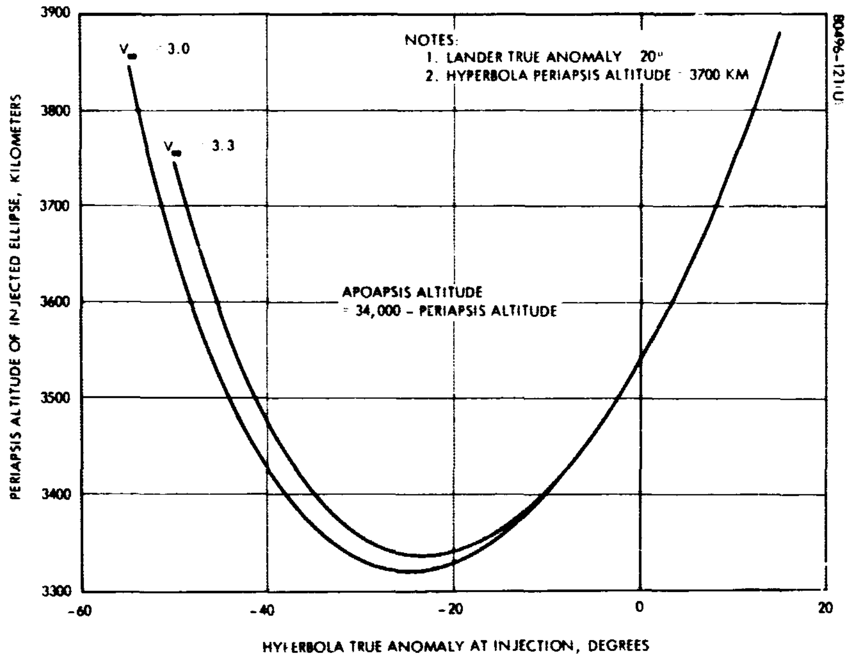

a) Hyperbola periapsis altitude = 3700 km

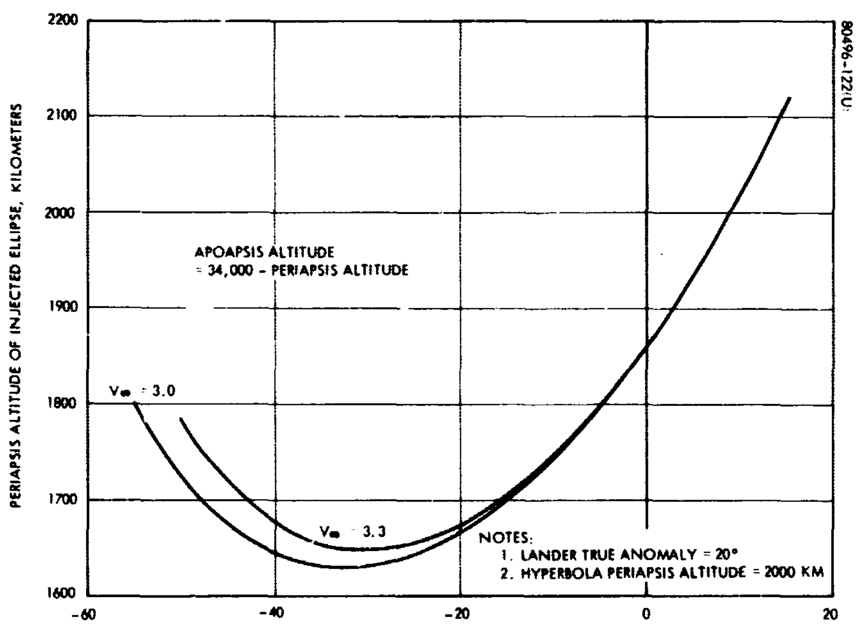

b) Hyperbola periapsis altitude 2000 km

Figure 108. Ellipse Periapsis Altitude

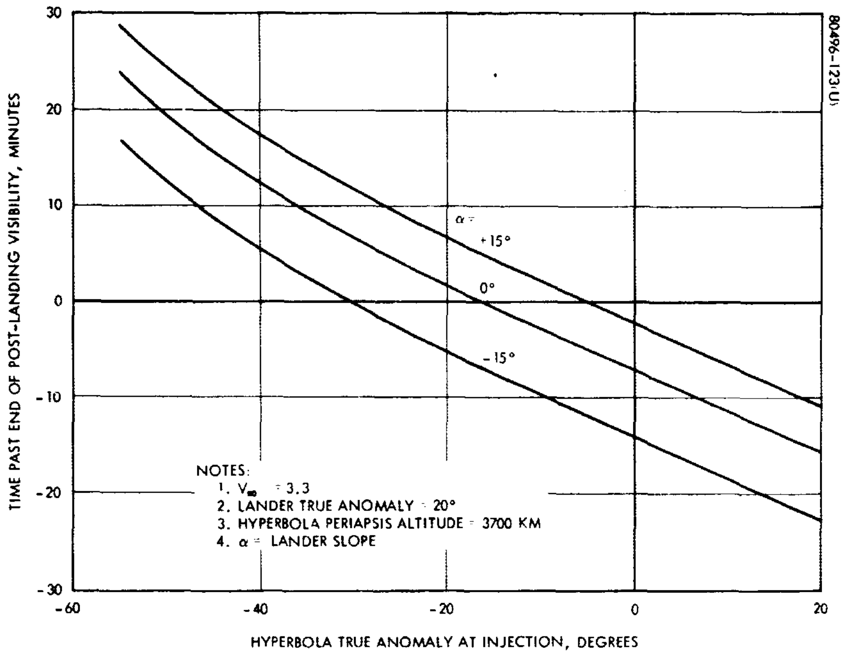

a) Hyperbola periapsis altitude = 3700 km

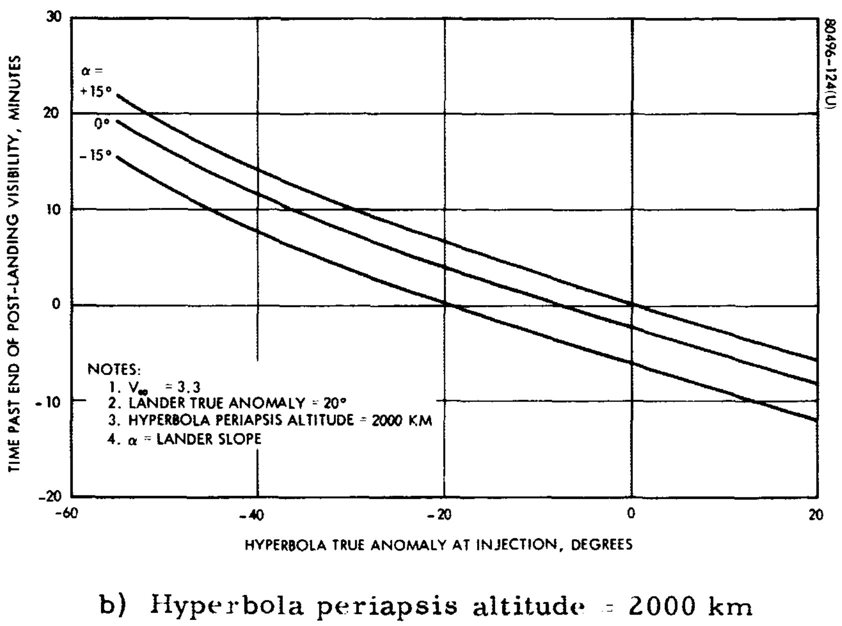

b) Hyperbola periapsis altitude = 2000 km

Figure 109. Time Past End of Postlanding Visibility

Figure 109 may also be used to determine the injection point required to take advantage of the possibility of a -15 degree lander slope and the resulting increase in postlanding visibility time available for lander data transmission. For example, to allow for the contingency of a -15 degree lander slope and 5 minutes for SM orientation, Figure 109b indicates that the injection maneuver should occur at a hyperbola true anomaly of approximately -33.5 degrees if the hyperbola periapsis altitude is 2000 km and the approach velocity is 3.3 km/sec. However, Figure 106b indicates that the ΔV magnitude is approximately 35 m/sec greater for this hyperbola true anomaly than the minimum of 1504 m/sec which occurs at a true anomaly of approximately -21 degrees.

Figure 110 shows a typical geometry indicating the SM approach trajectory and Mars synchronous ellipse. This figure is for a hyperbolic approach trajectory with an approach velocity of 3.3 km/sec and a periapsis altitude of 2000 km. Injection into the Mars synchronous ellipse occurs at the minimum ΔV point or a hyperbola true anomaly of approximately -21 degrees. The injection requirements, ellipse periapsis altitude, and time past end of postlanding visibility may be found from Figures 106b through 109b and are listed in Table 35.

The foregoing orbiter analysis has assumed a nominal approach trajectory and injection maneuver resulting in a nominal Mars synchronous ellipse with periapsis aligned directly over the lander. However, a complete analysis requires the determination of the effect on the synchronous orbit of errors in the approach trajectory and uncertainties in the magnitude and direction of the injection maneuver. Table 36 lists in-plane errors in the miss parameter, b, ΔV magnitude error, and ΔV direction (θ) error. The values listed are considered 3σ. Two values of the miss parameter error were used to determine the effect of variations in this error, while the errors in ΔV and θ were assumed to be constant.

TABLE 35. TYPICAL INJECTION MANEUVER (REPRESENTED IN FIGURE 110)

Hyperbola True Anomaly at Injection	ΔV Magnitude	ΔV Direction	Ellipse Periapsis Altitude	Time Past End of Postlanding Visibility at Injection (Lander Slope = 15 degrees)
-21 degrees	1504 m/sec	6.3 degrees	1670 km	7 minutes

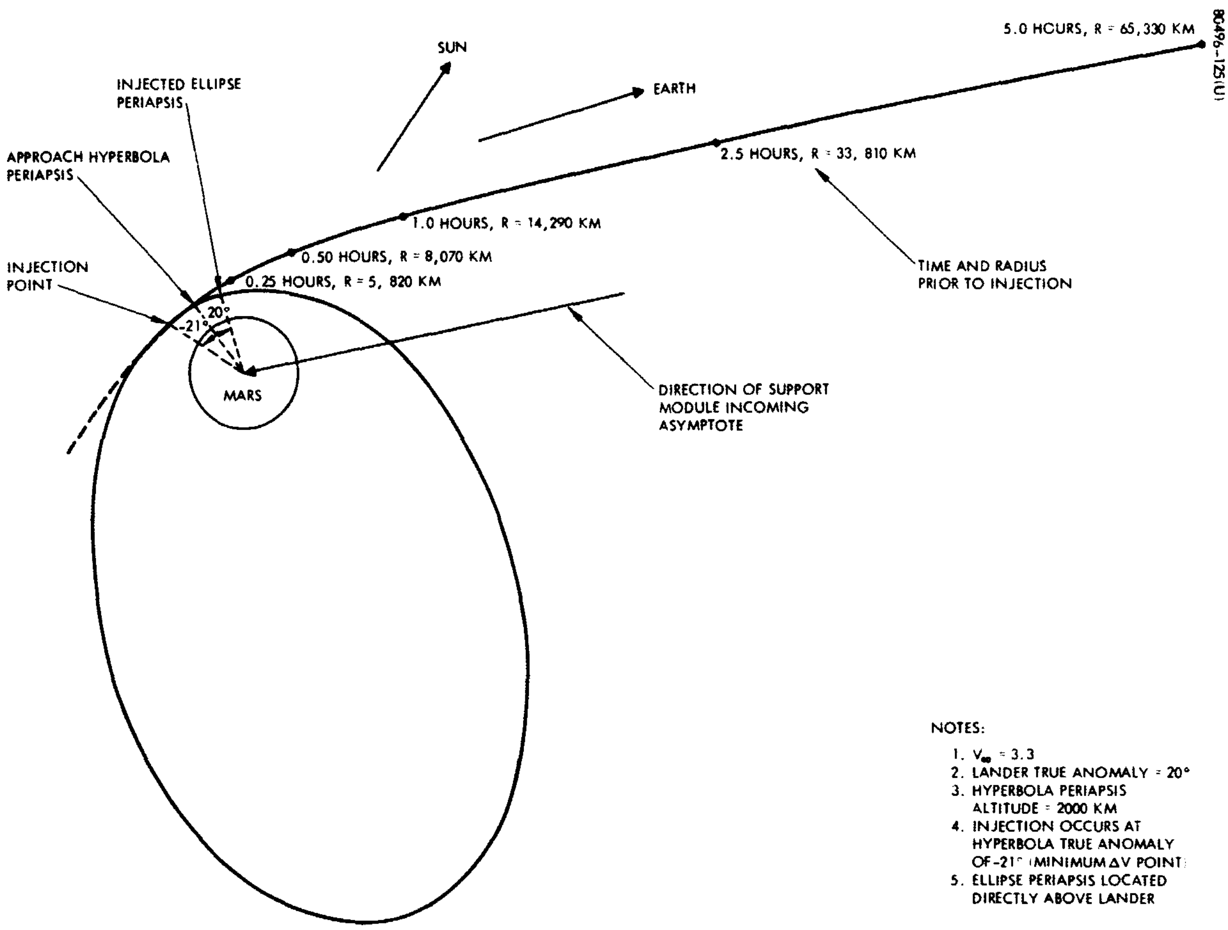

Figure 110. Approach Trajectory and Injection Geometry

TABLE 36. 3σ MISS PARAMETER AND INJECTION ERRORS

Miss Parameter Error, δb	ΔV Magnitude Error	ΔV Direction, Error, $\delta\theta$
±300 and ±50 km	±1 percent	±1 degree

Error analysis results indicate that dispersions in the period of the Mars nominally synchronous orbit are of primary importance. Figure 111 presents deviation in orbit period versus hyperbola true anomaly at injection for hyperbola periapsis altitudes of 3700 and 2000 km. A decrease in δb from ±300 km to ±50 km substantially decreases the period deviation, while an increase in hyperbola periapsis altitude from 2000 to 3700 km also decreases the period deviation but to a smaller degree. For example, Figure 111b indicates that, for a hyperbola periapsis altitude of 2000 km, V_∞ = 3.3 km/sec and a true anomaly at injection of -21 degrees, a decrease in δb from ±300 to ±50 km decreases the period deviation from 272 to 123 minutes. A comparison of Figures 111a and b for V_∞ = 3.3 km/sec and true anomaly at injection = -21 degrees indicates that increasing the hyperbola periapsis altitude from 2000 to 3700 km decreases the period deviation from 272 to 203 minutes. Figure 111 also indicates that, for the range of injection true anomalies considered, the minimum period deviation is nearly the same for hyperbola periapsis altitudes of 3700 or 2000 km and ranges from 97 to 104 minutes, respectively.

Figure 112 presents deviations in ellipse periapsis altitude, and Figure 113 presents deviations in ellipse apoapsis altitude for the indicated combinations of V_∞, δb, and hyperbola periapsis altitude. Deviations in ellipse periapsis altitude are small, indicating that communication during periapsis passage will not be hampered by large uncertainties in the lander-to-SM communication range. Deviations in ellipse apoapsis altitude are substantially larger. However, communications are not required at apoapsis. The primary effect of apoapsis altitude deviation is the translation of this deviation into orbit period deviation. This is evidenced by the fact that Figure 111 (period deviation) is similar in shape to Figure 113 (apoapsis altitude deviation).

Orientation of the ellipse line of apsides will also be affected by errors in b, ΔV, and θ. Nominally, the ellipse line of apsides is coincident with a radius vector from the center of Mars to the lander since the ellipse periapsis is nominally aligned directly over the lander. Figure 114 presents the deviation of the ellipse line of apsides from nominal in terms of the angle between the nominal and perturbed lines of apsides. These figures indicate that the line of apsides orientation error is small and approaches a minimum of approximately 2.3 to 2.5 degrees for hyperbola periapsis altitudes of 2000 and 3700 km, respectively.

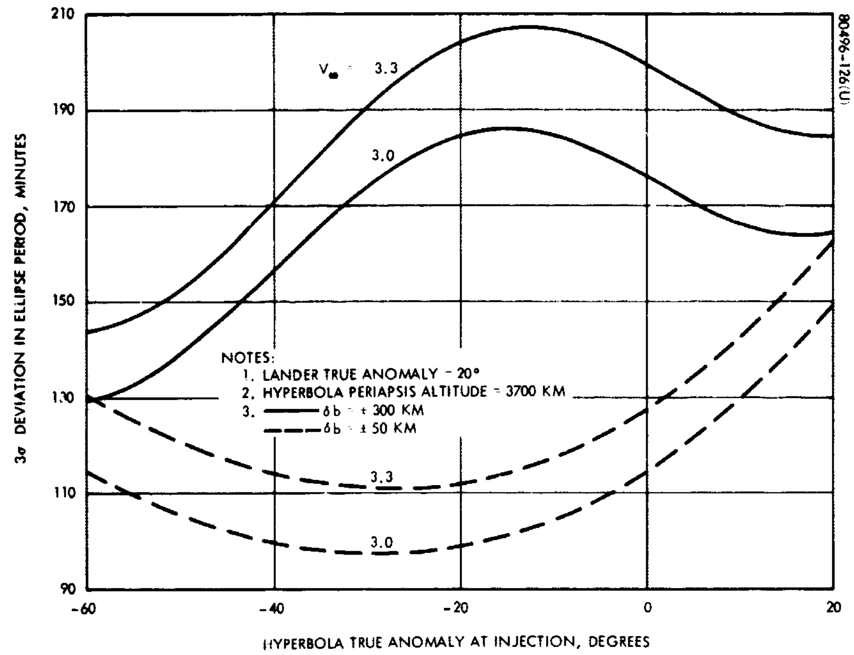

a) Hyperbola periapsis altitude = 3700 km

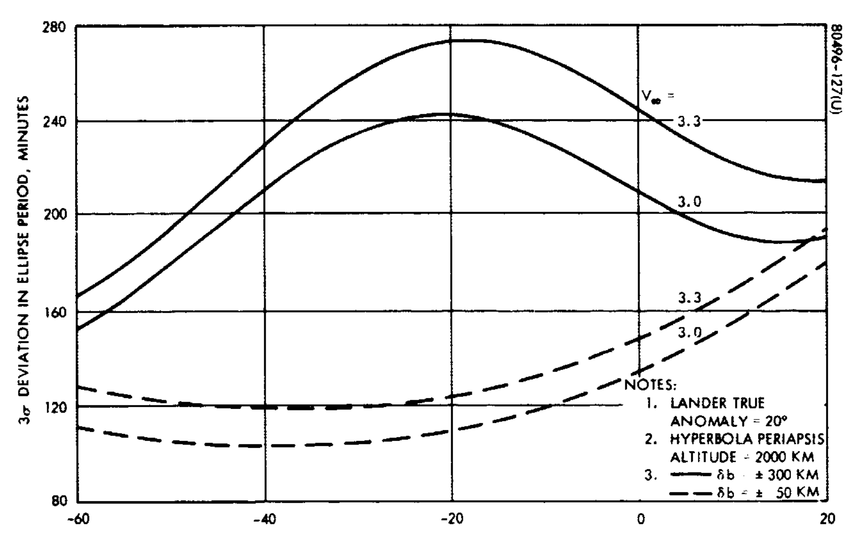

b) Hyperbola periapsis altitude = 2000 km

Figure 111. Ellipse Period Deviation

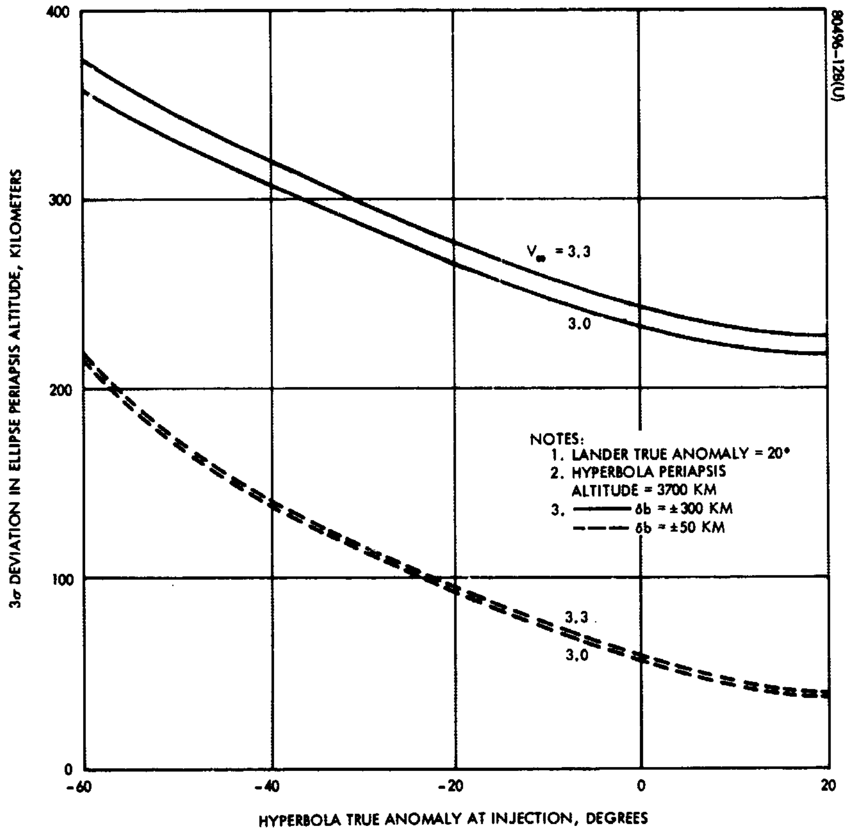

a) Hyperbola periapsis altitude = 3700 km

Figure 112. Ellipse Periapsis Altitude Deviation

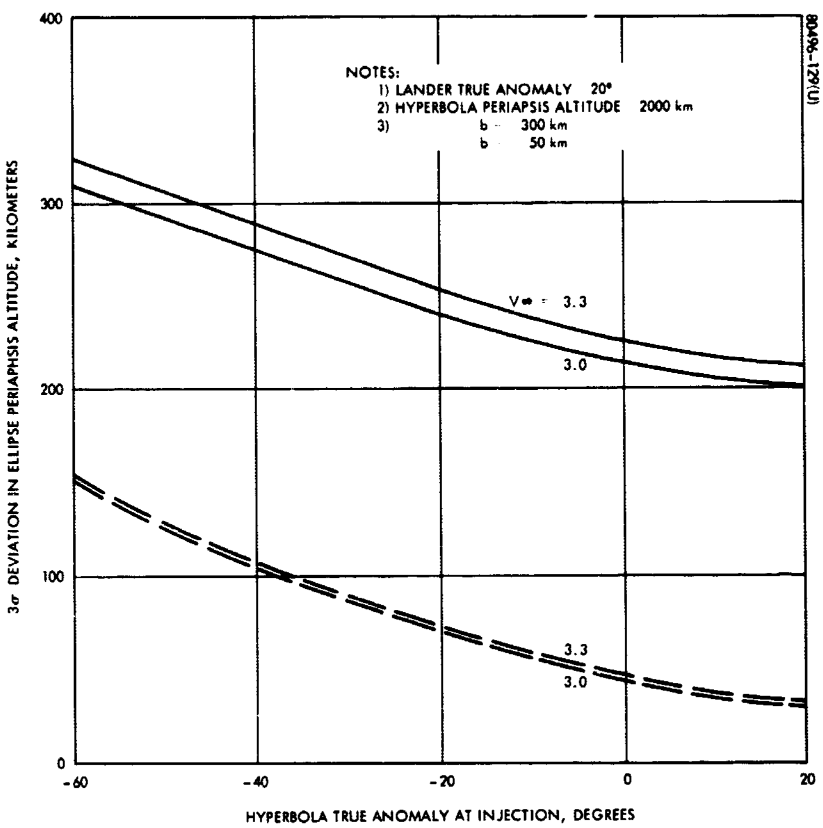

b) Hyperbola periapsis altitude = 2000 km

Figure 112. Ellipse Periapsis Altitude Deviation (continued)

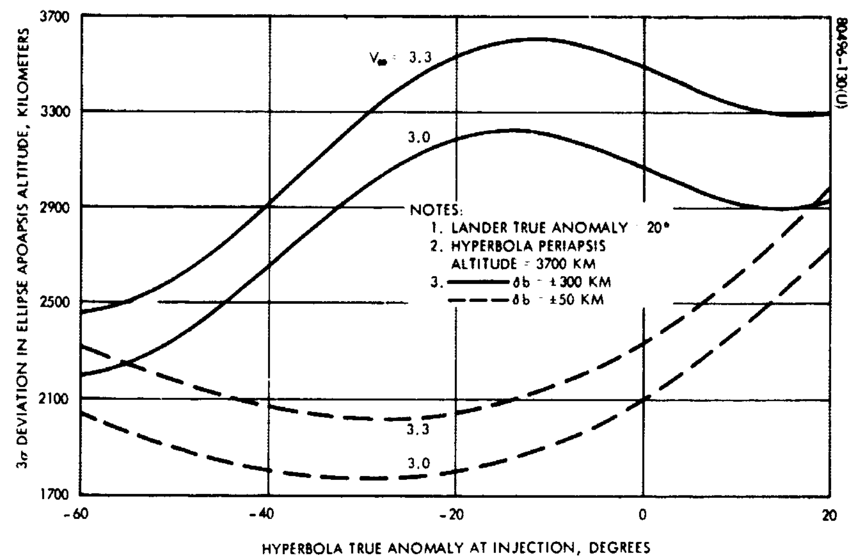

a) Hyperbola periapsis altitude = 3700 km

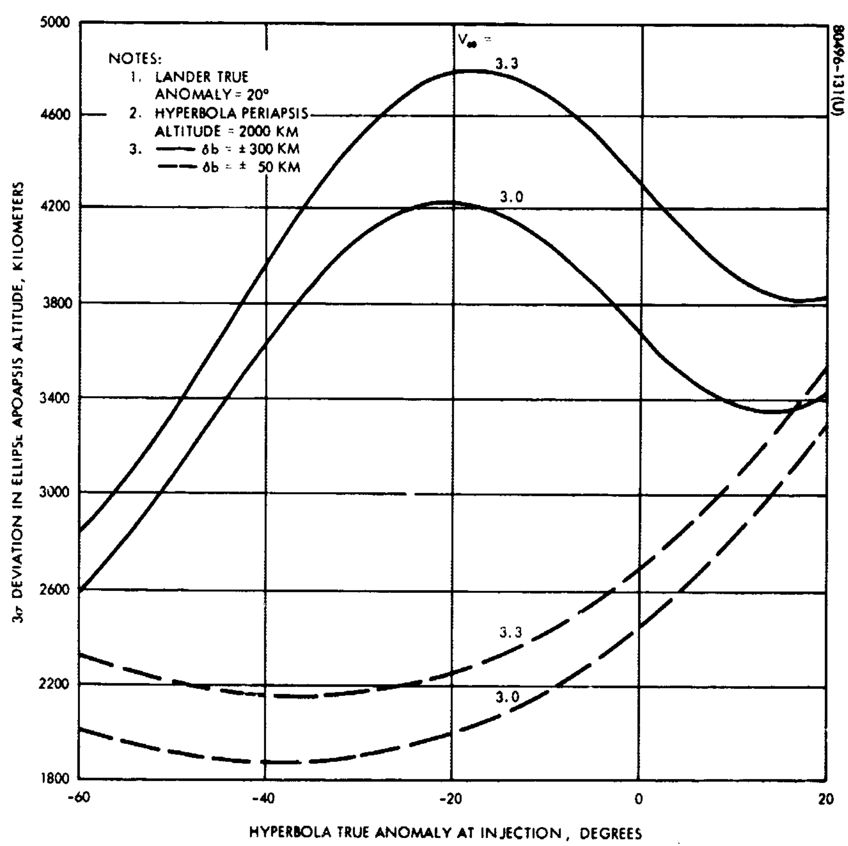

b) Hyperbola periapsis altitude = 2000 km

Figure 113. Ellipse Apoapsis Altitude Deviation

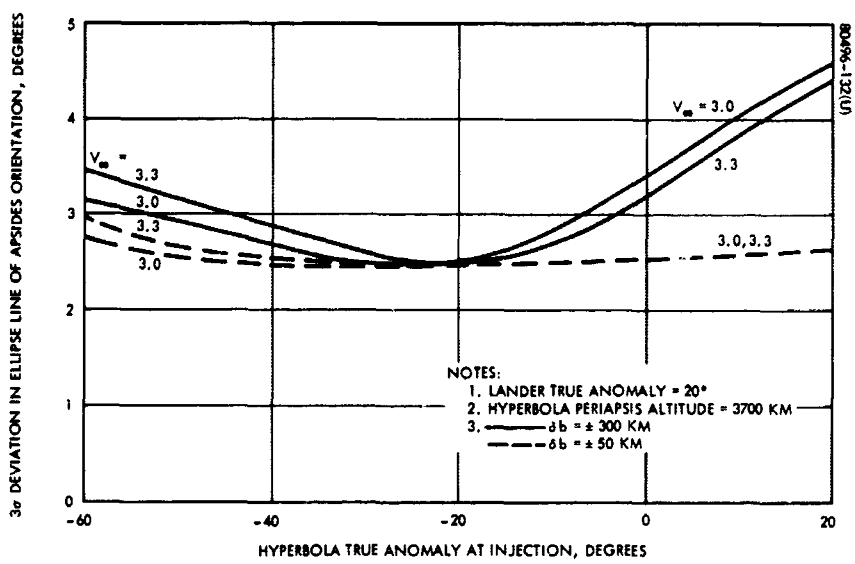

a) Hyperbola periapsis altitude 3700 km

Figure 114. Ellipse Line of Apsides Orientation Deviation

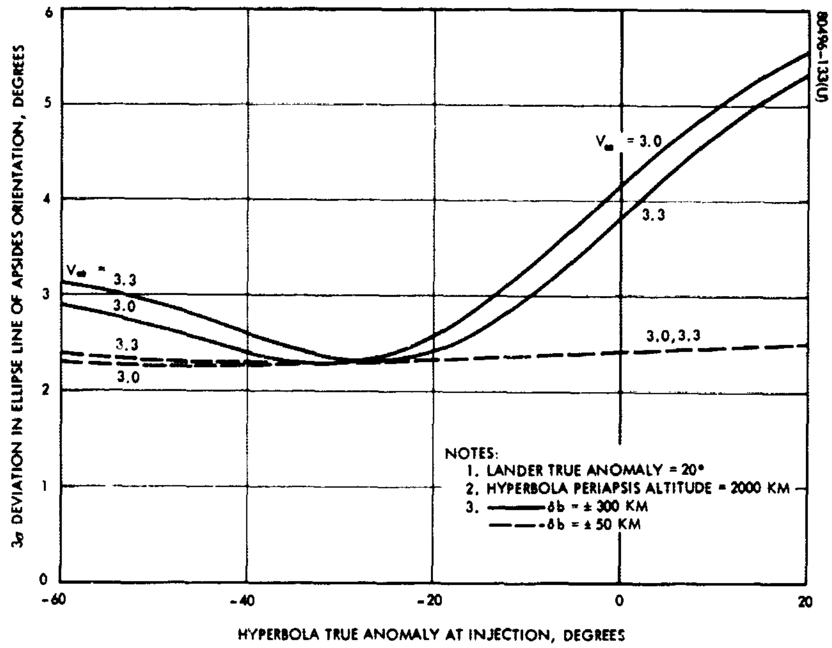

b) Hyperbola periapsis altitude 2000 km

Figure 114. Ellipse Line of Apsides Orientation Deviation (continued)

The significance of the orbital insertion errors, especially the period error, requires further detailed studies of such aspects as DSN orbit determination, SM orbit trim capability, and lander-to-Orbiter geometry and communications requirements.

VEHICLE CONFIGURATION/WEIGHTS

The A/L and canister inboard profile shown in the Video design section is used with the Orbiter SM design. The A/L and canister diameter changes are still in order for the Orbiter design, but the solid deflection engine and heavier interface structure are retained. The A/L weight is 1186 pounds, which includes 86 pounds for the solid engine and interface structure. The forward canister weight remains the same, 69 pounds, but the aft canister weight is reduced to 150 pounds because the SM is outside the canister, thereby allowing for a shortened canister. The adapter is increased to 125 pounds because of the heavier load it supports.

The Orbiter inboard profile is shown in Figure 115. This version of the Orbiter has a solid propellant engine. Since this drawing was completed, a few small dimensional changes have been made to accommodate a slightly larger planar antenna. The new dimensions are: upper cylinder, 72.8 inches, and solar panel outer diameter, 117.6 inches. The adapter and A/L interface diameter are equal to the cylinder diameter. The discussion that follows uses the latest design values.

The Orbiter design upper cylinder has an increased length, 40 inches, to provide for the solid retro engine length. The equipment shelf has been eliminated, and all equipment is attached to the inner cylinder wall. Heat energy from the equipment is transferred to louvers mounted outside the cylinder. The planar antenna is attached to the cylinder via a ring. A frustum section encloses one end of the cylinder and is mated with a ring to the solid engine. This section is designed to transfer loads produced by the engine. Directly surrounding the engine is an inner cylinder which is ring-attached to the planar array.

The solar panels still have 37.4 square feet of area, but the outer diameter is 117.6 inches. The increase was necessary to allow for a greater planar antenna area, 21.2 square feet, required because of greater SM-to-earth distance. The outer diameter is limited by the shroud diameter plus an allowance for clearance. All other Orbiter SM configuration features are similar to those of the Video design.

Table 37 lists the basic Orbiter weights that yield the total weight of 1120 pounds; 90 pounds is allowed for contingencies. The maximum amount of solid propellant was designed into the Orbiter after allowance had been made

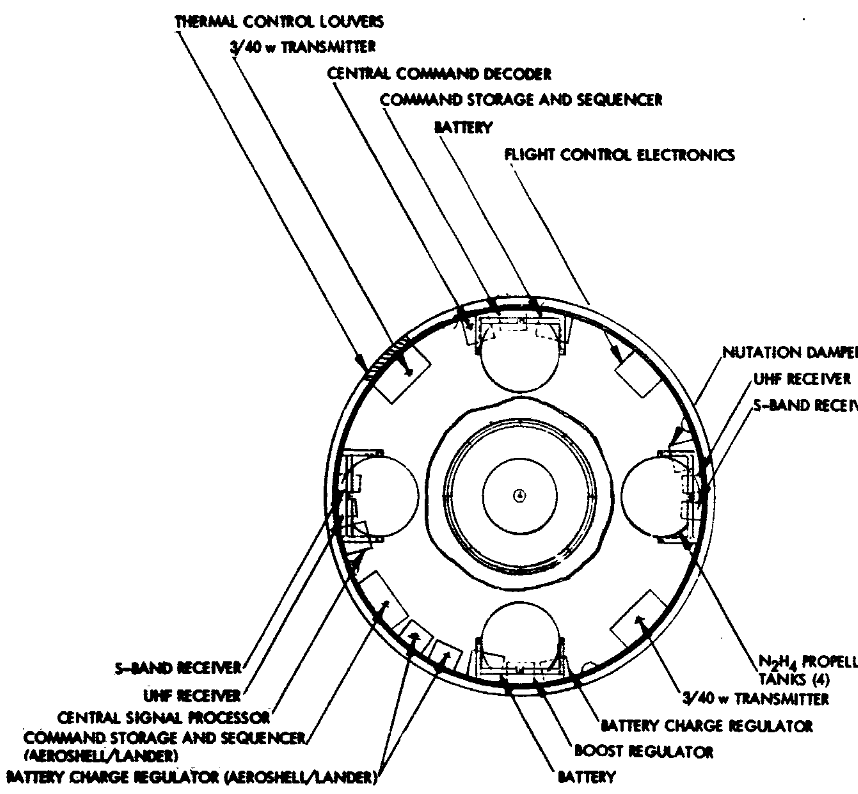

VIEW B-B

DIMENSIONS IN INCHES

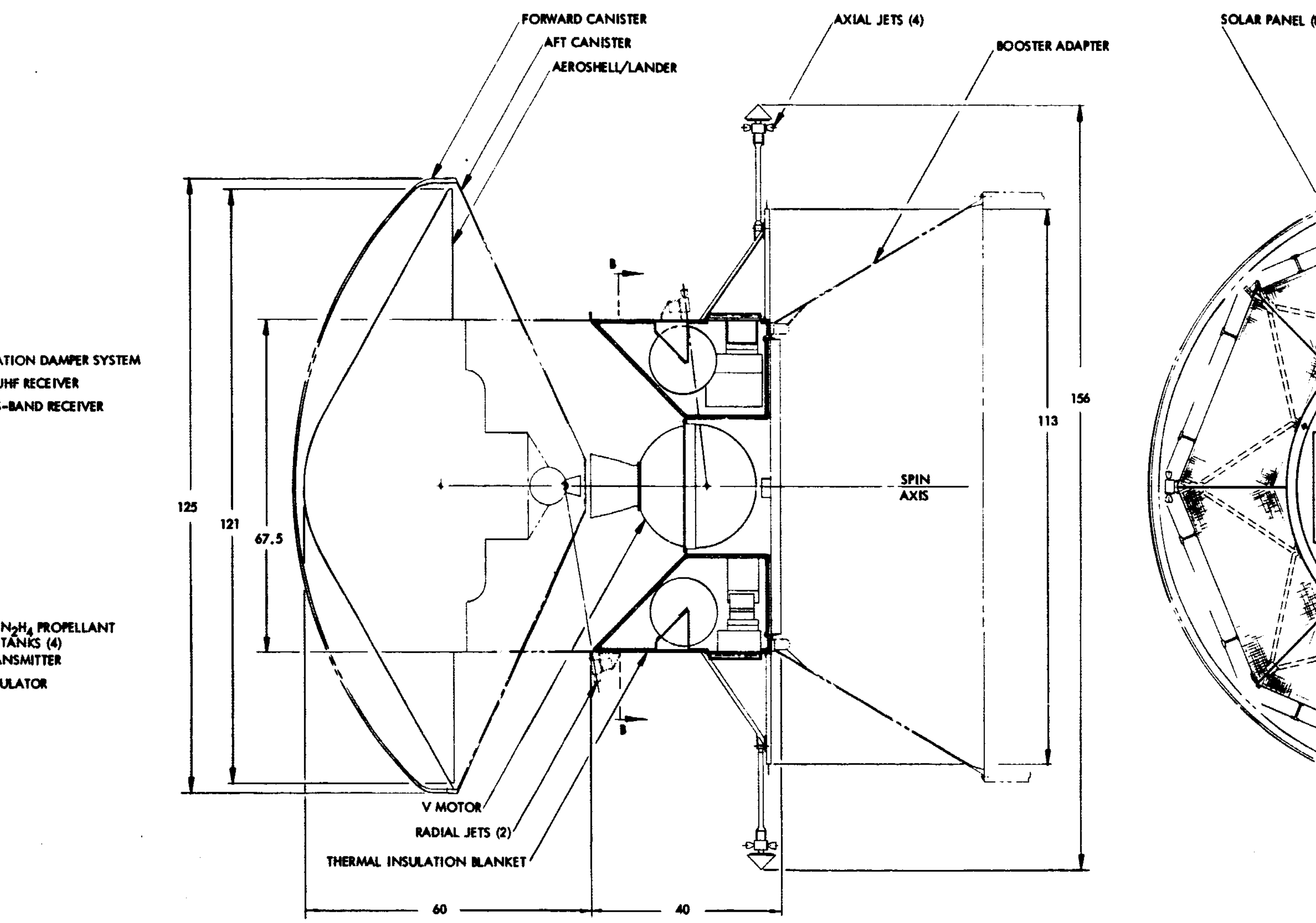

FORWARD CANISTER
AFT CANISTER
AEROSHELL/LANDER
AXIAL JETS (4)
BOOSTER ADAPTER
SOLAR PANEL (
ATION DAMPER SYSTEM
UHF RECEIVER
S-BAND RECEIVER
N_2H_4 PROPELLANT TANKS (4)
NSMITTER
ULATOR
125
121
67.5
156
113
SPIN AXIS
B
B
V MOTOR
RADIAL JETS (2)
THERMAL INSULATION BLANKET
60
40

Figure

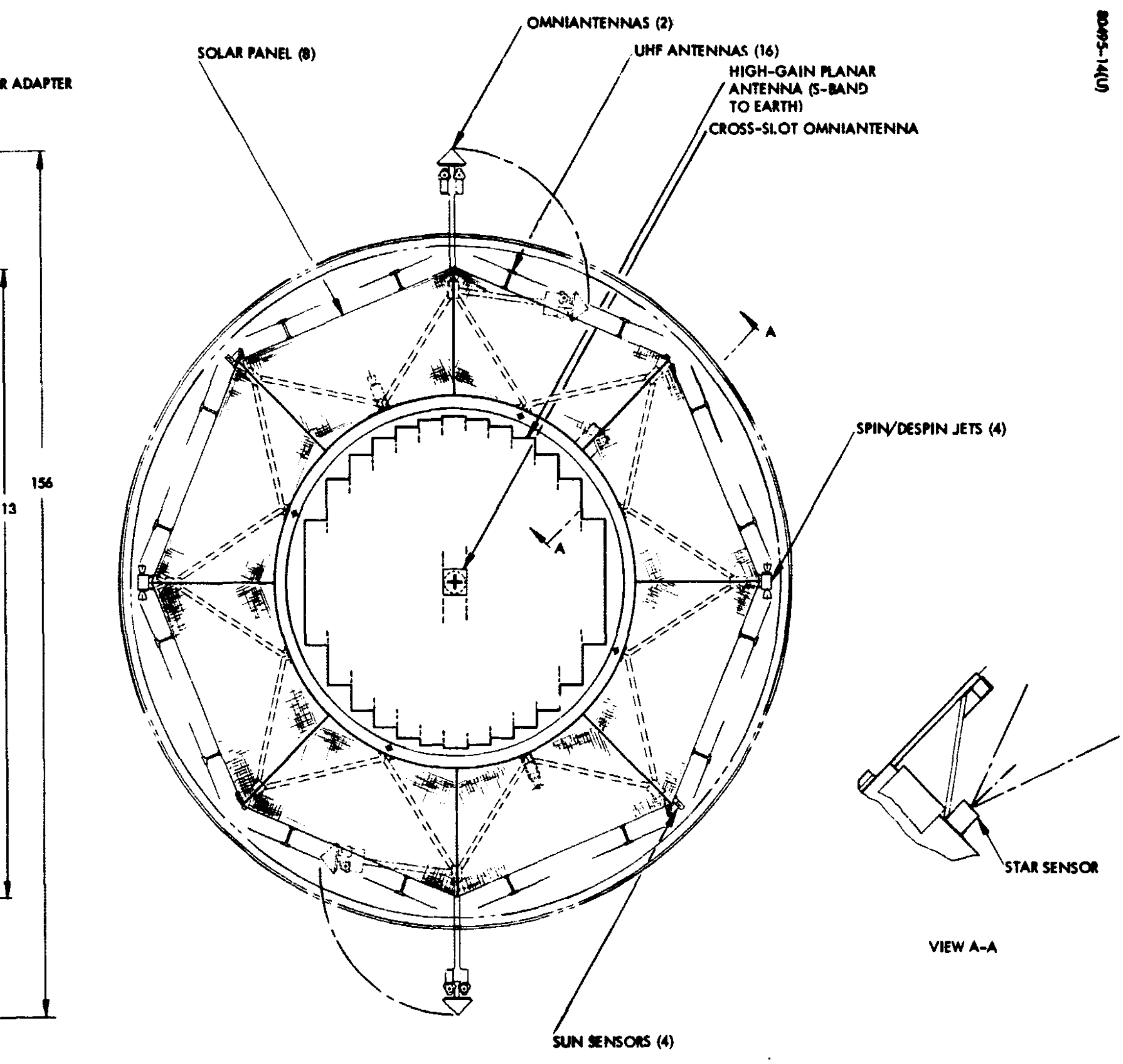

Figure 115. Solid Propellant Orbiter SM Inboard Profile

PRECEDING PAGE BLANK NOT FILMED.

TABLE 37. ORBITER (SOLID) SUBSYSTEM WEIGHT ALLOTMENT

Item		Weight, pounds	
RF Subsystem			83.3
3-watt transmitter (2)		41.2	
40-watt transmitter (2)			
High-gain antenna (1) (21.2 ft^2)		16.6	
UHF antennas (16)		3.0	
Turnstile antenna (2)		1.0	
S-band receiver (2)		8.0	
UHF receiver (2)		4.7	
RF switches (3)		1.5	
Coaxial cables and attach clips		5.5	
Cross slot omni		0.5	
Diplexer (3)		1.3	
Signal Processing			30.7
Central command decoder (2)		5.7	
Central signal processor		10.0	
Command storage and sequencer (S/M)		5.0	
Sequencer (A/L)		10.0	
Propulsion			632.7
5-pound thrusters (10)		11.0	
14.2-inch diameter tanks (4)		20.7	
Valves, lines, filters, and pressurant		8.0	
N_2H_4 propellant		115.0	
Solid propellant		430.0	
Case and inerts		48.0	
Flight Control			37.5
Flight control electronics		17.0	
Star sensors (1)		5.1	
Sun sensors (4)		1.0	
Local cables, connectors, and clips		3.4	
Nutation damper (2) (active)		10.0	
Accelerometer and acceleration switch		1.0	
Structure			149.2
Upper ring		12.7	
Upper cylinder		4.0	
Engine frustum and ring		27.4	
Inter cylinder and ring		5.1	
Lower ring		9.2	
Thermal blankets and tie downs		5.5	
Thermal blanket support		6.1	
Harness		15.0	
Solar panel support tubes		7.0	
Balance weights		4.0	
Thermal control louver (15 square feet)		12.0	
Radial jet supports (2)		1.2	
Equipment support brackets and hardware		4.0	
Mechanisms			14.8
Separation mechanism		11.6	
SM/lander	4.8		
SM/adapter	6.8		
Axial jet deployment (2)		3.2	
Electrical Power			81.8
Solar panel (substrate, cells, interconnections)		45.8	
Boost regulator		8.5	
Battery charge regulator (1 S/M 2 A/L)		10.5	
Battery (2) 40 percent discharge		17.0	
Subtotal			1030.0
Contingency			90.0
Total			1120.0

for the subsystem and contingency. The resultant retro velocity capability is approximately 1.7 km/sec. This assumes approximately 80 percent propellant usage and a retro specific impulse of 290 seconds. This retro capability more than satisfies the requirements, see Encounter/Orbit section. Table 38 lists the weights that determine the total launch weight of 2650 pounds.

Table 39 presents the Orbiter moments of inertia and indicates the spacecraft is not passively stable about the spin axis. A single active nutation damper is included in the design to maintain stability about the spin axis.

An alternate Orbiter design using a liquid braking system was considered. The inboard profile is shown in Figure 116. A weight breakdown is given in Table 40. Due to study limitations, the system was not pursued in detail. The system is envisioned using a monopropellant for all preorbiting maneuvers and then adding an oxidizer to produce a high specific impulse for the orbital insertion phase. Two fuel and two oxidizer tanks, plus a gas bottle for pressurant, are required. In addition to the low thrust jets, two 200-pound thrust engines are mounted outside the SM cylindrical section. The design allows a closer attachment to the A/L and possibly a more stable spacecraft. The flexibility of the liquid design may warrant further study.

ATTITUDE AND VELOCITY CONTROL

The configuration of the MSSM-Orbiter is somewhat different from the Flyby discussed in depth previously. The new spacecraft mass and moments of inertia are of most concern in assessing the velocity and attitude control capabilities and performance.

For the sake of brevity, the performance curves and tables are presented with little explanation because they are analogous to the ones discussed earlier for the Flyby study.

The following pages give the result of the nutation study done for spinup and despin. These cases are presented: 1) spinup after booster separation, 2) despin prior to lander separation, and 3) spinup after lander separation. The despin prior to A/L separation is not required, but the analysis is included in the event a despin is required.

Tables 41 through 43 present the velocity and attitude control performance summary for 1) support module attached to aeroshell/lander, 2) support module only before orbit injection, and 3) support module only after orbit injection. Figure 117 presents the reorientation time of the vehicle for the three conditions above. Figures 118 through 124 are velocity control performance curves for the axial and radial control mode. Table 44 presents the propellant budget for the hydrazine system.

TABLE 38. ORBITER (SOLID) LAUNCH WEIGHT DISTRIBUTION

Item	Weight, pounds	
Aeroshell/lander		1186
SM weight (including contingency of 90 pounds)		1120
SM/booster adapter		125
Structure	85.0	
Umbilical	35.0	
Pyrotechnic separation logic	5.0	
Aft canister		150
Structure	97.0	
Pressure and vent	50.0	
Separation harness	3.0	
Forward canister		69
Launch weight		2650
Titan payload	2650	
Total contingency for SM, adapter, and canisters		90

TABLE 39. ORBITER (SOLID) MOMENTS OF INERTIA

Vehicle State	Slug-ft^2
A/L and Orbiter	
Full Fuel	
I_{Roll}	471
I_{Pitch}	730
Midcourse, fuel removed	
I_R	454
I_P	720
Orbiter alone at separation	
I_R	84
I_P	58.3
Orbiter-liquid and solid fuel used	
I_R	67
I_P	50.0

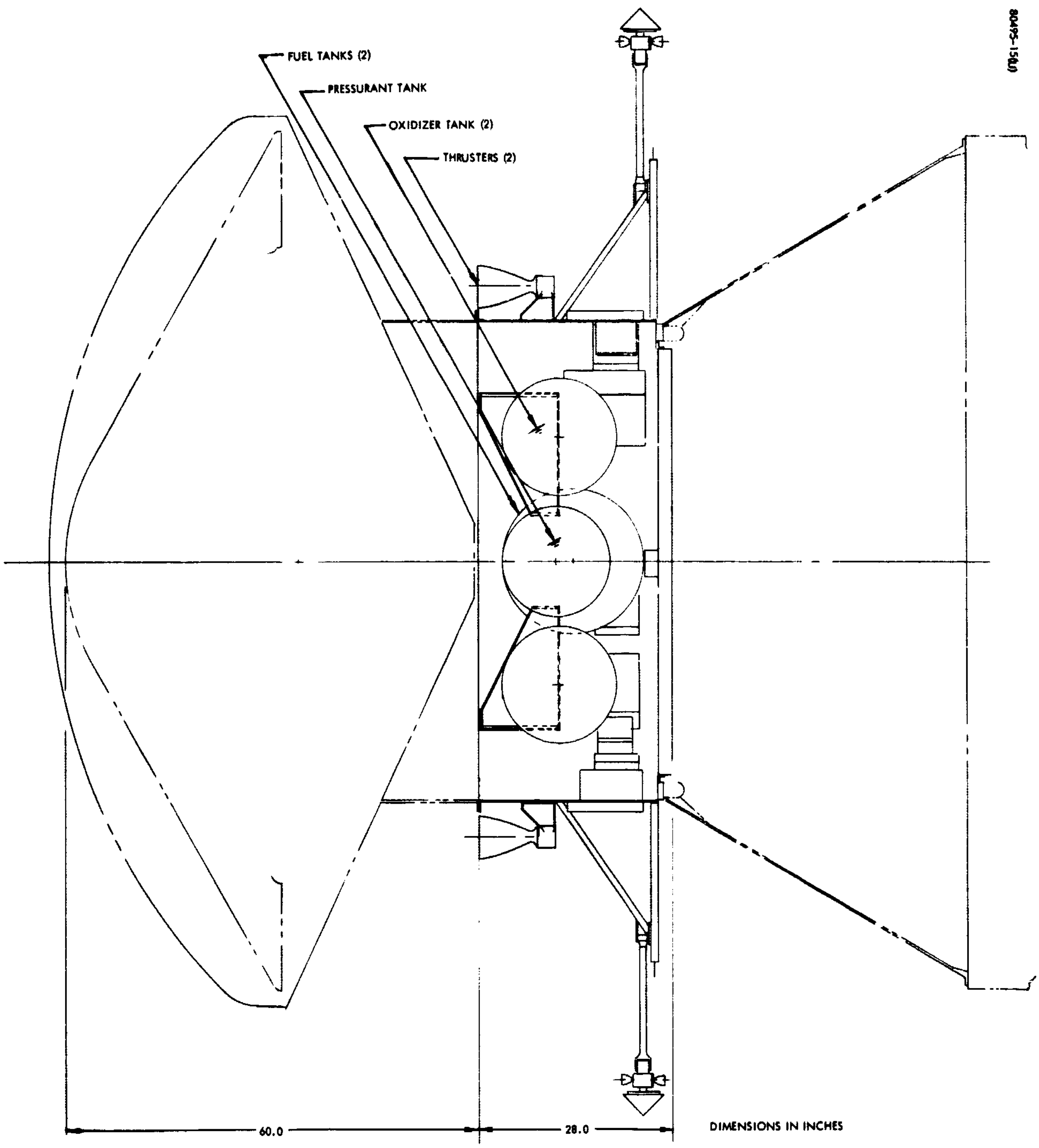

Figure 116. Liquid Braking System Orbiter SM Design

TABLE 40. ORBITER (LIQUID) SUBSYSTEM

Item	Weight, pounds	
RF Subsystem		83.3
3-watt transmitter (2)	41.2	
40-watt transmitter (2)		
High-gain antenna (1)	16.6	
UHF antennas (16)	3.0	
Turnstile antenna (2)	1.0	
S-band receiver (2)	8.0	
UHF receiver (2)	4.7	
RF switches (3)	1.5	
Coaxial cables and attach clips	5.5	
Cross slot omni	0.5	
Diplexer (3)	1.3	
Signal Processing		30.7
Central command decoder (2)	5.7	
Central signal processor	10.0	
Command storage and sequencer (S/M)	5.0	
Sequencer (A/L)	10.0	
Propulsion		609.0
5-pound thrusters (10)	11.0	
Tanks (2 oxidizer, 2 fuel, 1 pressurant), regulator, valves, lines, filters, and pressurant	61.7	
200-pound thrusters (2)	536.3	
Midcourse and attitude		
ΔV_R		
N_2H_4 fuel		
N_2O_4 oxidizer		
Flight Control		37.5
Flight control electronics	17.0	
Star sensors (1)	5.1	
Sun sensors (4)	1.0	
Local cables, connectors, and clips	3.4	
Nutation damper (2) (active)	10.0	
Accelerometer and acceleration switch	1.0	
Structure		146.1
Upper ring	12.7	
Upper cylinder	28.0	
Engine and tank support structure Inner support structure	32.0	
Lower ring	9.2	
Thermal blankets and tie downs	6.0	
Thermal blanket support	15.0	
Harness	15.0	
Solar panel support tubes	7.0	
Balance weights	4.0	

TABLE 40. ORBITER (LIQUID) SUBSYSTEM - Concluded

Item		Weight, pounds	
Thermal control louver (15 square feet)		12.0	
Radial jet supports (2)		1.2	
Equipment support brackets and hardware		4.0	
Mechanisms			14.8
Separation mechanism		11.6	
SM/lander	4.8		
SM/adapter	6.8		
Axial jet deployment (2)		3.2	
Electrical Power			81.8
Solar panel (substrate, cells, interconnections)		45.8	
Boost regulator		8.5	
Battery charge regulator (1 S/M 2 A/L)		10.5	
Battery(2) 40 percent discharge		17.0	
Subtotal			1003.2
Contingency			98.1
Total			1101.3

TABLE 41. VELOCITY AND ATTITUDE CONTROL (NOMINAL PERFORMANCE) FOR SUPPORT MODULE ATTACHED TO AEROSHELL LANDER

1)	ΔV per continuous axial jet firing per spin period (one jet)	0.14 fps/revolution (25 rpm, 4.5 pounds thrust)
2)	Axial jet continuous firing time per fps ΔV	16.9 sec/fps (one jet) 8.45 sec/fps (two jets)
3)	Weight of propellant per fps ΔV	0.365 lb/fps
4)	Attitude change per pulse	1.56 degrees/pulse* (90 degree pulse) 0.842 degree/pulse* (45 degree pulse)
5)	Propellant weight per degree of attitude change	0.016 lb/deg
6)	ΔV per 90 degree pulse of radial jet	0.032 fps/pulse
7)	Propellant weight per radial jet pulse (90 degree pulse)	0.014 lb/pulse
8)	Number of radial jet pulses per fps	31.4 pulses/fps
9)	Propellant weight per fps (radial)	0.40 lb/fps
10)	Time required per fps (radial jet)	74 sec/fps (one jet) 37 sec/fps (two jets)
11)	Spacecraft ΔV per degree of attitude change	0 (nominally, using two axial jets)
12)	Maximum nutation angle during reorientation	2.0 degrees

*Using two axial jets to produce pure couple.

TABLE 42. VELOCITY AND ATTITUDE CONTROL (NOMINAL PERFORMANCE) FOR SUPPORT MODULE ONLY BEFORE ORBIT INJECTION

1)	ΔV per continuous axial jet firing per spin period (one jet)	0.138 fps/revolution (60 rpm, 4.5 pounds thrust)
2)	Axial jet continuous firing time per foot per second ΔV	7.19 sec/fps (one jet) 3.59 sec/fps (two jets)
3)	Weight of propellant per fps ΔV	0.176 lb/fps
4)	Attitude change per pulse	3.14 degrees/pulse* (90 degrees pulse) 1.69 degrees/pulse* (45 degrees pulse)
5)	Propellant weight per degree of attitude change	0.008 lb/deg
6)	ΔV per 90 degree pulse of radial jet	0.0315 fps/pulse
7)	Propellant weight per radial jet pulse (90 degrees pulse)	0.00483 lb/pulse
8)	Number of radial jet pulses per fps	31.8 pulses/fps
9)	Propellant weight per fps (radial)	0.179 lb/fps
10)	Time required per fps (radial jet)	31.8 sec/fps (one jet) 15.9 sec/fps (two jets)
11)	Spacecraft ΔV per degree of attitude change	0 (nominally, using two axial jets)
12)	Maximum nutation angle during reorientation	1.5 degrees

*Using two axial jets to produce pure couple.

TABLE 43. VELOCITY AND ATTITUDE CONTROL (NOMINAL PERFORMANCE) FOR SUPPORT MODULE ONLY AFTER ORBIT INJECTION

1) ΔV per continuous axial jet firing per spin period (one jet)	0.266 fps/revolution (60 rpm, 4.5 pounds thrust)
2) Axial jet continuous firing time per foot per second ΔV	3.73 sec/fps (one jet) 1.87 sec/fps (two jets)
3) Weight of propellant per fps ΔV	0.0809 lb/fps
4) Attitude change per pulse	5.86 degrees/pulse* (90 degrees pulse) 3.14 degrees/pulse* (45 degrees pulse)
5) Propellant weight per degree of attitude change	0.0043 lb/deg
6) ΔV per 90 degree pulse of radial jet	0.06 fps/pulse
7) Propellant weight per radial jet pulse (90 degrees pulse)	0.00483 lb/pulse
8) Number of axial jet pulses per fps	16.5 pulses/fps
9) Propellant weight per fps (radial)	0.093 lb/fps
10) Time required per fps (raidal jet)	16.5 sec/fps (one jet) 8.25 sec/fps (two jets)
11) Spacecraft ΔV per degree of attitude change	0 (nominally, using two axial jets)
12) Maximum nutation angle during reorientation	1.5 degrees

*Using two axial jets to produce pure couple.

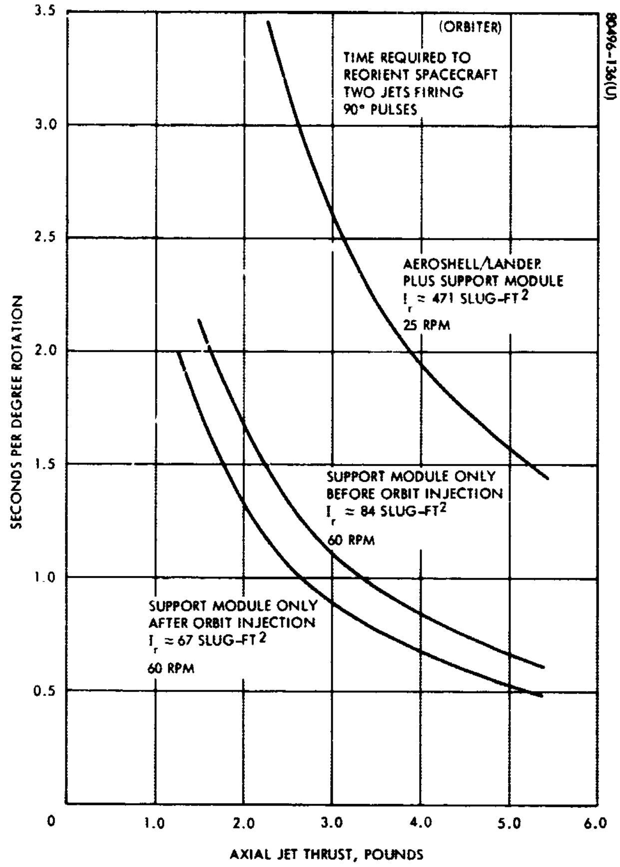

Figure 117. Time Required to Reorient Spacecraft

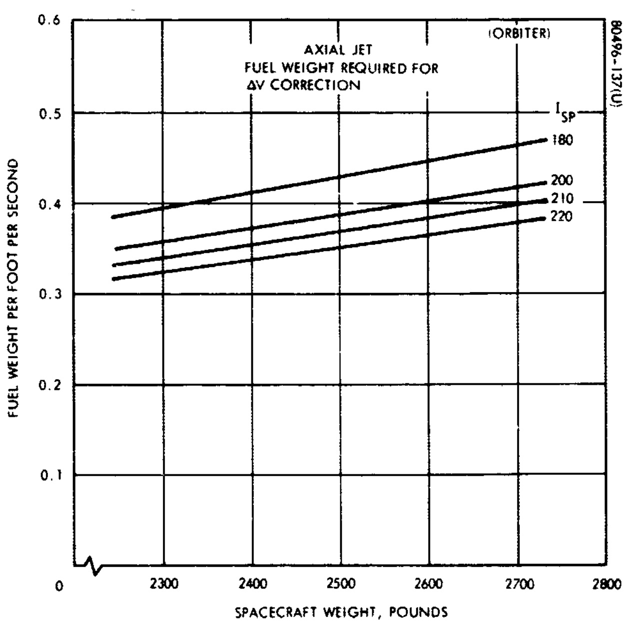

Figure 118. Axial Jet Fuel Weight Required for ΔV Correction

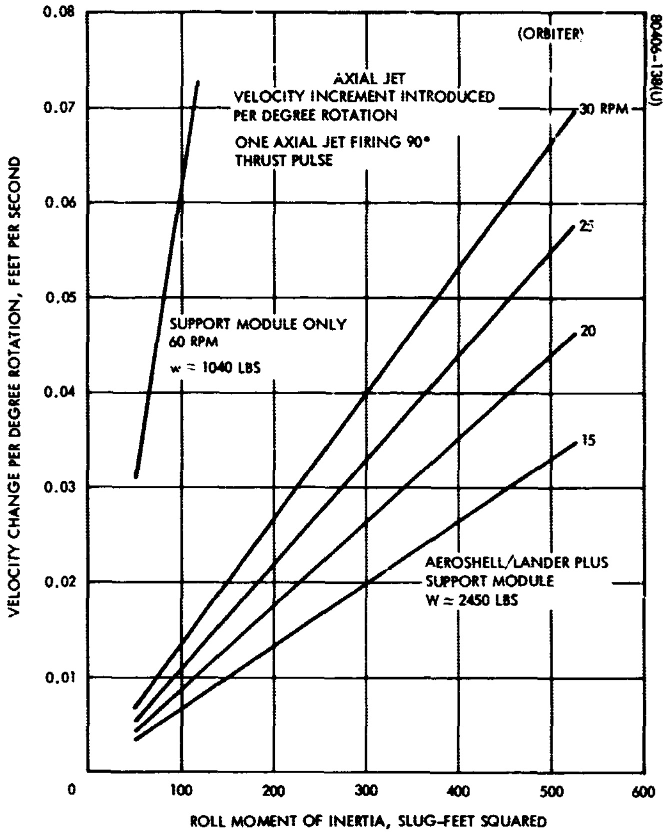

Figure 119. Axial Jet Velocity Increment Introduced Per Degree of Rotation

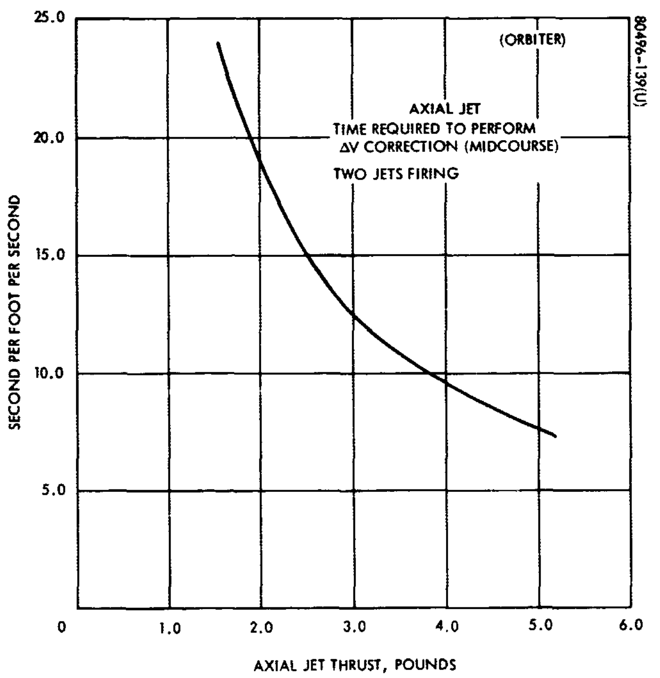

Figure 120. Axial Jet Time Required to Perform ΔV Correction (Midcourse)

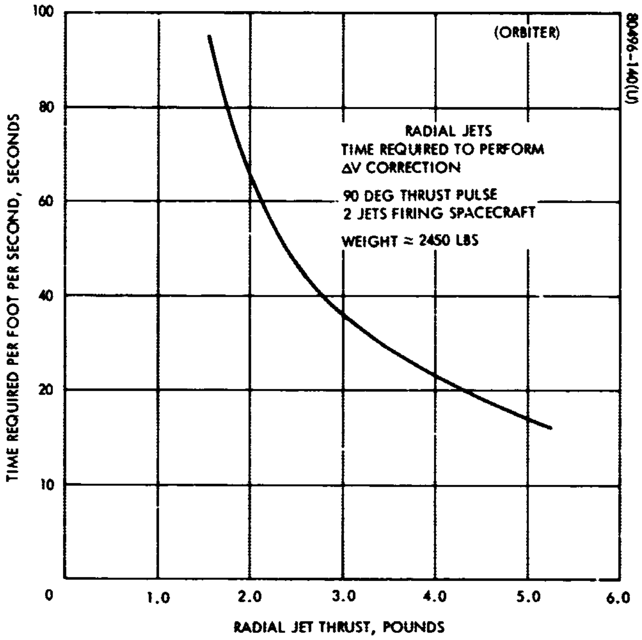

Figure 121. Radial Jet Time Required to Perform ΔV Correction

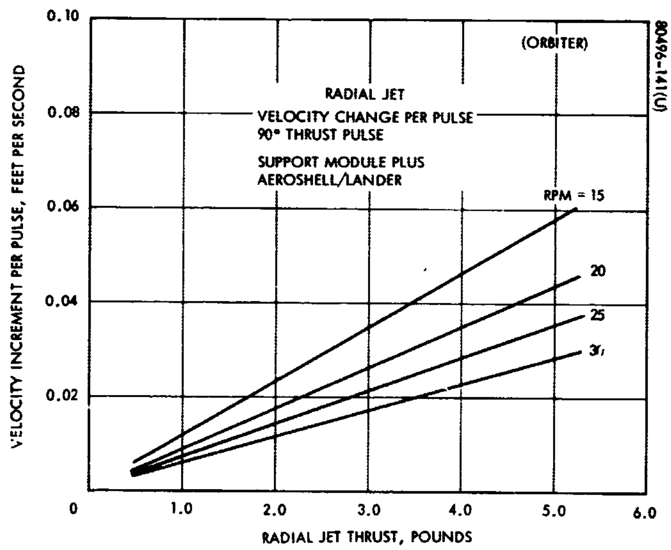

Figure 122. Radial Jet Velocity Change Per Pulse

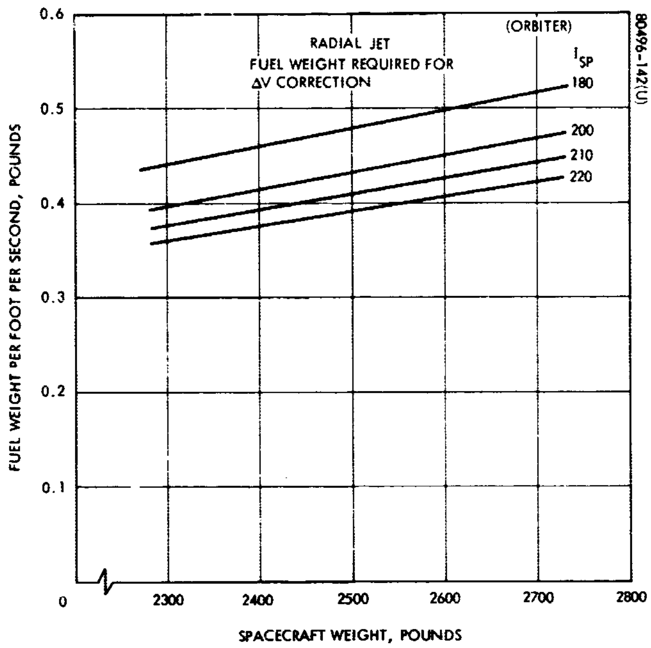

Figure 123. Radial Jet Fuel Weight Required for ΔV Correction

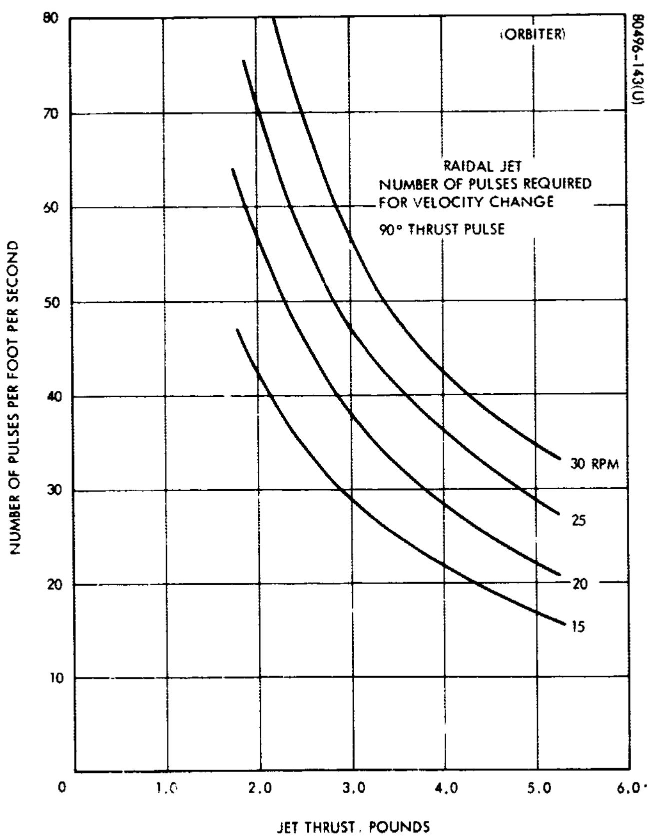

Figure 124. Radial Jet Number of Pulses Required for Velocity Change

TABLE 44. RCS PROPELLANT BUDGET ORBITER DESIGN

Maneuvers	Velocity Increment, mps	Propellant Weight, pounds
1) Initial spinup to 25 rpm	-	1.12
2) Midcourse correction	(65)	107.50
a) First midcourse	60	99.31
b) Second midcourse	3	4.95
c) Third midcourse	0.6	1.08
d) Fourth midcourse	1.2	2.16
3) In-transit attitude corrections to maintain proper angle between HGA boresight and earth (≈90 degrees)	-	1.48
4) Attitude maneuver to align lander (≈90 degrees)	-	1.48
5) Spindown of lander + module to ≈ 5 rpm	-	0.90
6) Spinup of module to ≈ 60 rpm	-	0.51
7) Attitude maneuver to align antenna to earth (≈90 degrees)	-	0.73
8) Reorient to orbit injection attitude (≈45 degrees)	-	0.37
9) Reorient to align antenna to earth (≈45 degrees)	-	0.20
Total RCS propellant required		114.29 pounds

Mars Lander and Module Spinup After Booster Separation

Typical Parameters

A = roll MOI = 471 slug-ft^2

B = pitch-yaw MOI = 730 slug-ft^2

N = number of nozzles = 2

β = principal axis tilt = 1 degree

L = distance from nozzles to cg = 42 inches

ΔL = tolerance on L = 0.1 inch

D = nozzle position diamter = 108 inches

ϕ = angular nozzle misalignment normal to roll plane = 0.25 degree

γ = angular nozzle misalignment in the roll plane = 0.25 degree

ω_t = initial tipoff rate = 1.4 deg/sec

F = thrust level per nozzle = 5 pounds

ΔF = thrust tolerance per nozzle = 4 percent

RSS body fixed transverse torque (due to various error sources above) as a percentage of the available spinup torque ≈ 2 percent

Nutation angle resulting from spinup ≈ 1.2 degree (body nutation rate = 8.82 rpm)

Attitude error resulting from spinup ≈ 8.1 degree (inertial nutation rate = 16.2 rpm)

Time delay between separation start and spinup start ≈ 2 sec.

Attitude error resulting from time delay and tipoff rate ≈ 2.8 degree

Spinup (thrusting) interval ≈ 27.5 seconds

Spin rate at end of spinup ≈ 25 rpm

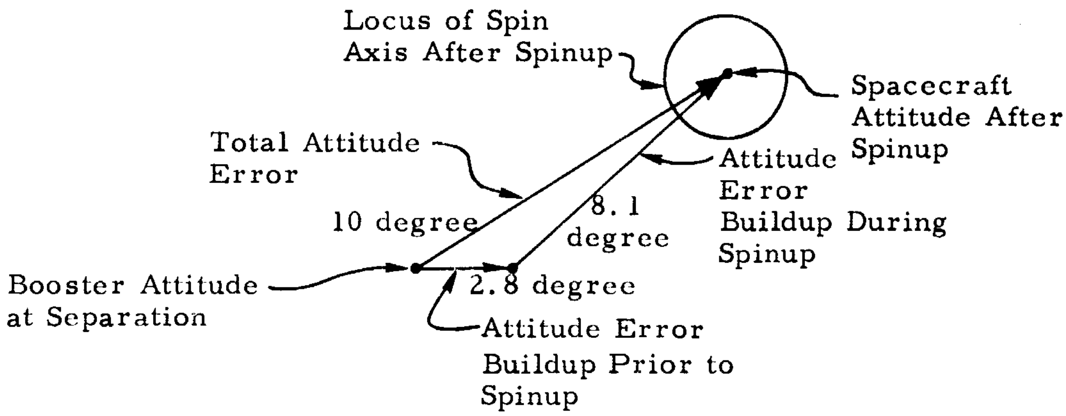

<u>Mars Lander and Module Despin Prior to Separation</u>

<u>Typical Parameters</u>

A = roll MOI = 454 slug-ft^2

B = pitch-yaw MOI = 720 slug-ft^2

N = number of nozzles = 2

β = principal axis tilt = 1 degree

L = distance from nozzles to cg = 42 inches

ΔL = tolerance on L = 0.1 inch

D = nozzle position diamter = 108 inches

ϕ = angular nozzle misalignment normal to roll plane = 0.25 degree

γ = angular nozzle misalignment in the roll plane = 0.25 degree

ω_s = initial spin rate = 25 rpm

θ_o = initial nutation angle 0.9 degree

F = thrust level per nozzle = 4.5 pounds

ΔF = thrust tolerance per nozzle = 0.16 pound (14 percent)

Spindown (thrusting) interval $\approx$ 23.5 seconds

Spin rate at end of spindown $\approx$ 5 rpm

RSS body fixed transverse torque (due to various error sources above) as a percentage of the available spindown torque ≈ 2 percent

Nutation angle resulting from spindown ≈ 9.0 degree (body nutation rate = 9.2 rpm)

Attitude change resulting from despin ≈ 1.7 degree (inertial nutation rate = 15.8 rpm)

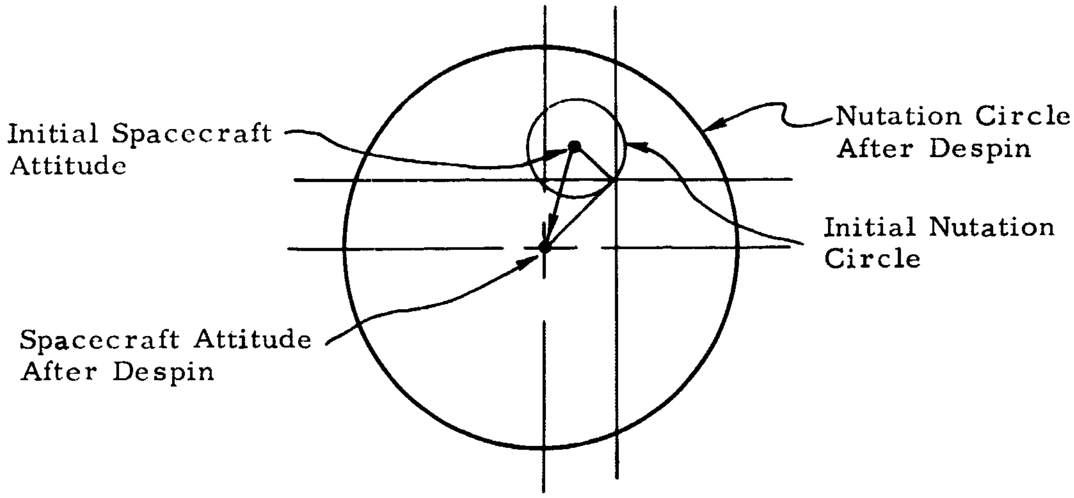

Mars Support Module Spinup After Lander Separation

Typical Parameters

A = roll MOI = 84 slug-ft^2

B = pitch-yaw MOI = 58.3 slug-ft^2

N = number of nozzles = 2

β = principal axis tilt = 0.5 degree

L = distance from nozzles to cg = 12.5 inches

ΔL = tolerance on L = 0.1 inch

D = nozzle position diameteı = 108 inches

ϕ = angular nozzles misalignment normal to roll plane - 0.25 degree

γ = angular nozzle misalignment normal to roll plane = 0.25 degree

ω_s = initial spin rate - 5 rpm

θ_o = initial nutation angle = 1 degree

F = thrust level per nozzle = 4 pounds

F = thrust tolerance per nozzle = 0.16 pound (4 percent)

Spinup (thrusting) interval = 12.0 seconds

Spin rate at end of spinup = 60 rpm

RSS body fixed transverse torque (due to various error sources above) as a percentage of the available spin torque = 1.1 percent

Nutation angle after spinup = 0.18 degree (body nutation rate = 26.7)

Attitude change resulting from spinup = 1.6 degree (inertial nutation rate = 86.5 rpm)

Nutation Control for Orbiter Configuration

As a result of the addition of a solid propellant rocket for injecting the MSSM into orbit, the spacecraft combination and possibly MSSM alone are nutationally unstable — that is, in the presence of energy dissipation arising from nutational motion, the nutation continues to increase until the spacecraft reaches "flat spin" about an axis of maximum moment of inertia. Three approaches are available, in general, for coping with nutation control in unstable spinning spacecraft (i.e., spacecraft which spin about an axis of minimum moment of inertia). First, there is the Gyrostat* approach which provides a despin platform on which to mount a tuned passive damper. A second approach is the active nutation control system employing an accelerometer as a nutation sensor for supplying appropriate signals for activating an axial jet which operates in a pulsed mode to reduce the nutation. Both of the above approaches were rejected for the MSSM orbiter mission — the first because of problems associated with integrating a small despun platform on the spacecraft spin axis and the second because of the potential problems of propellant consumption and attitude perturbation during the relatively long mission duration. A third approach to nutation control, and the one selected for the MSSM orbiter mission, was devised at Hughes for effecting spin axis search patterns without disturbing the angular momentum vector. In this technique for nutation control, a

*Patent applied for.

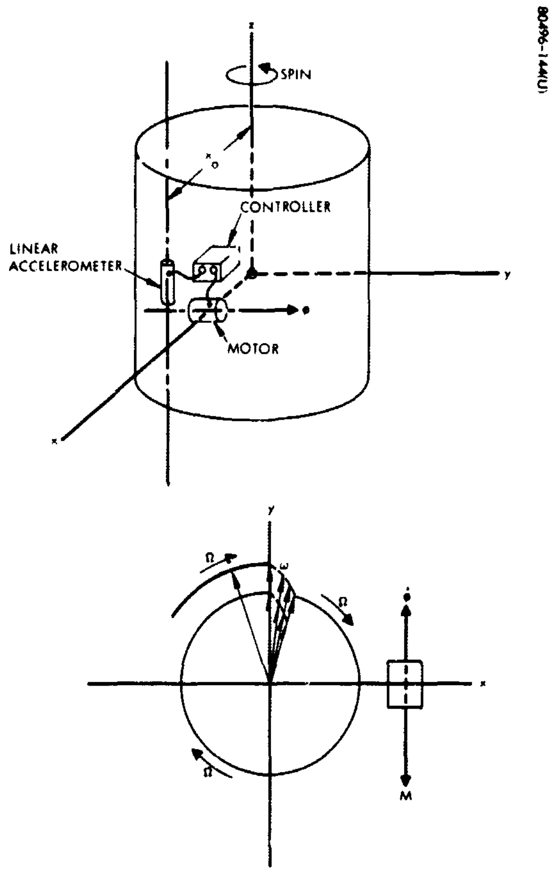

Figure 125. Active Nutation Damper

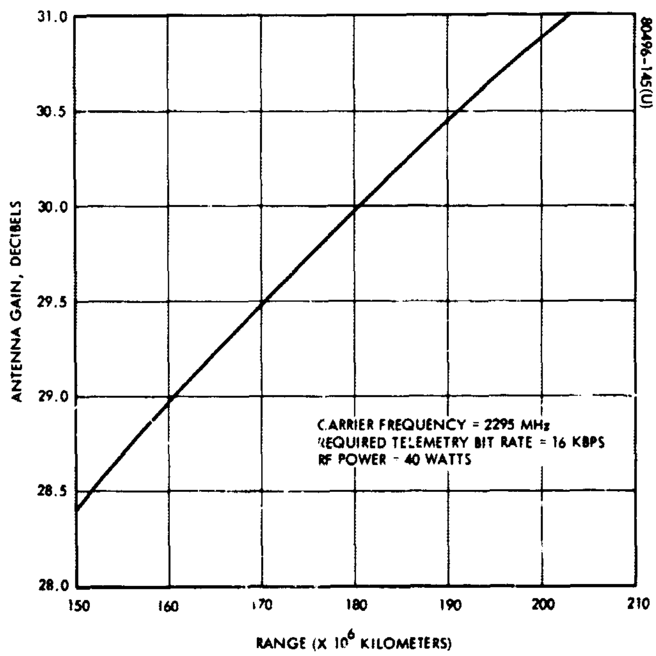

Figure 126. SM S-Band Antenna Requirements as Function of Range

sensor is required for detecting the nutation levels of interest as well as an amplifier and a small hermetically sealed motor. The schematic arrangement is indicated in Figure 125. The relative positions of the system elements are not significant, the important requirement being the relative alignment of the control motor spin axis and the accelerometer axis. All elements may be assembled in a single package weighing roughly 2 pounds and consuming an average power of several milliwatts although the peak power requirement may be on the order of 8 watts. Two units may be used for redundancy.

The system does not function until the nutation builds up to a maximum allowable level at which point the motor, under the control of the accelerometer and amplifier, is alternately accelerated, stopped, and reversed to reduce the nutation to an acceptably low level. All control action then ceases until the nutation again builds up to the maximum allowable level.

The lower portion of Figure 125 indicates the relative position of the transverse angular velocity vector, ω, and the motor torque and speed during a nutation control "pulse."

This system has one definite advantage over the despun damper approach, namely, it has practically no constraint on integration with the MSSM. The use of redundancy, as well as hermetic sealing of the lubricated component, essentially eliminates reliability as a consideration.

TELECOMMUNICATIONS

The increased SM-to-earth range requires the addition of a slightly larger planar antenna to the telecommunications subsystem. Figure 126 is a plot of the antenna gain required to sustain 16,000 bits/sec as a function of range. Approximately 30 dB of gain is required at the Orbiter distance of 182×10^6 km. The performance of the Orbiter communication subsystem is slightly better than that presented for the Video design.

POWER/THERMAL

The Orbiter power subsystem is functionally identical to that of the Video design. The weight of the solar panels is 45.8 pounds. The battery weight has been reduced to 17 pounds because sterilization is not required.

Since all equipment is attached around the inner cylinder wall, the louvers are also mounted to the cylinder. The louvers provide 15 square feet of surface area and weigh 12 pounds. The retro engine will require a thermal blanket and heaters.

SEQUENCE OF EVENTS

Aside from the orbit insertion events, the primary mission event difference is the separation of the aft canister near encounter. The orbit insertion and orbital sequence of events have not been detailed.

PRECEDING PAGE BLANK NOT FILMED.

5. ALTERNATE DESIGNS

During the initial phase of the MSSM study, several SM concepts were evaluated before selecting the Flyby-Entry Data concept for detailed consideration. The primary mission objective of these concepts was to relay entry data at 2000 bits/sec from the A/L to the DSN during the Mars flyby. The concepts were categorized as spinning parallel or normal to the ecliptic plane during the mission cruise phase. The SM with its spin axis in the ecliptic plane was selected as a result of this study. Figure 127 is an inboard profile of this SM design. It is similar to the Flyby-Entry Data design.

A SM patterned after the Hughes Gyrostat is shown in Figure 128. The spin axis is nominally perpendicular to the ecliptic plane. A cylindrical section surrounded by solar cells is the spinning element and mounted inside is the despun platform section. The platform is mounted to the spinning section via a rotating joint. The high-gain antenna is mounted to the stationary platform and has mechanical arms which allow the antenna to be directed as desired. Aside from the RF equipment which is mounted on the platform to avoid lossy RF joints, all equipment is attached to the inside of the spinning section. Although a parabolic antenna is shown on Figure 128, a planar antenna could have been used.

Table 45 is a list of the basic weights for the design shown in Figures 127 and 128. The increased structural and solar panel weights primarily account for the heavier SM which has its spin axis normal to the ecliptic plane.

Table 46 is a list of the basic launch weights for both configurations. Although a weight difference of approximately 200 pounds is shown, both designs can be accommodated by the Titan III-C. The longer Gyrostat type SM requires a significantly heavier aft canister.

Although the two concepts satisfy the mission requirements and have similar subsystem performance, significant differences exist and they resulted in selection of the concept with the spin axis parallel to the ecliptic for further studies. Table 47 lists the selection criteria and the preferred choice.

In addition to the antenna systems indicated, two other general types were considered. One was an electronically despun antenna which eliminated the need for the despun platform or allows the spin axis to be directed other than at the earth for the selected design. To achieve the desired performance, the structural volume, weight, power usage, and reliability become major problems; therefore, the electronically despun antenna was eliminated. Also considered was a simpler mechanically despun antenna similar to that used on ATS-C. Since the weight, power, and volume problems also exist with this design, in addition to a rotating joint consideration, the concept was eliminated. Table 48 lists further details for these and the planar and parabolic antenna designs.

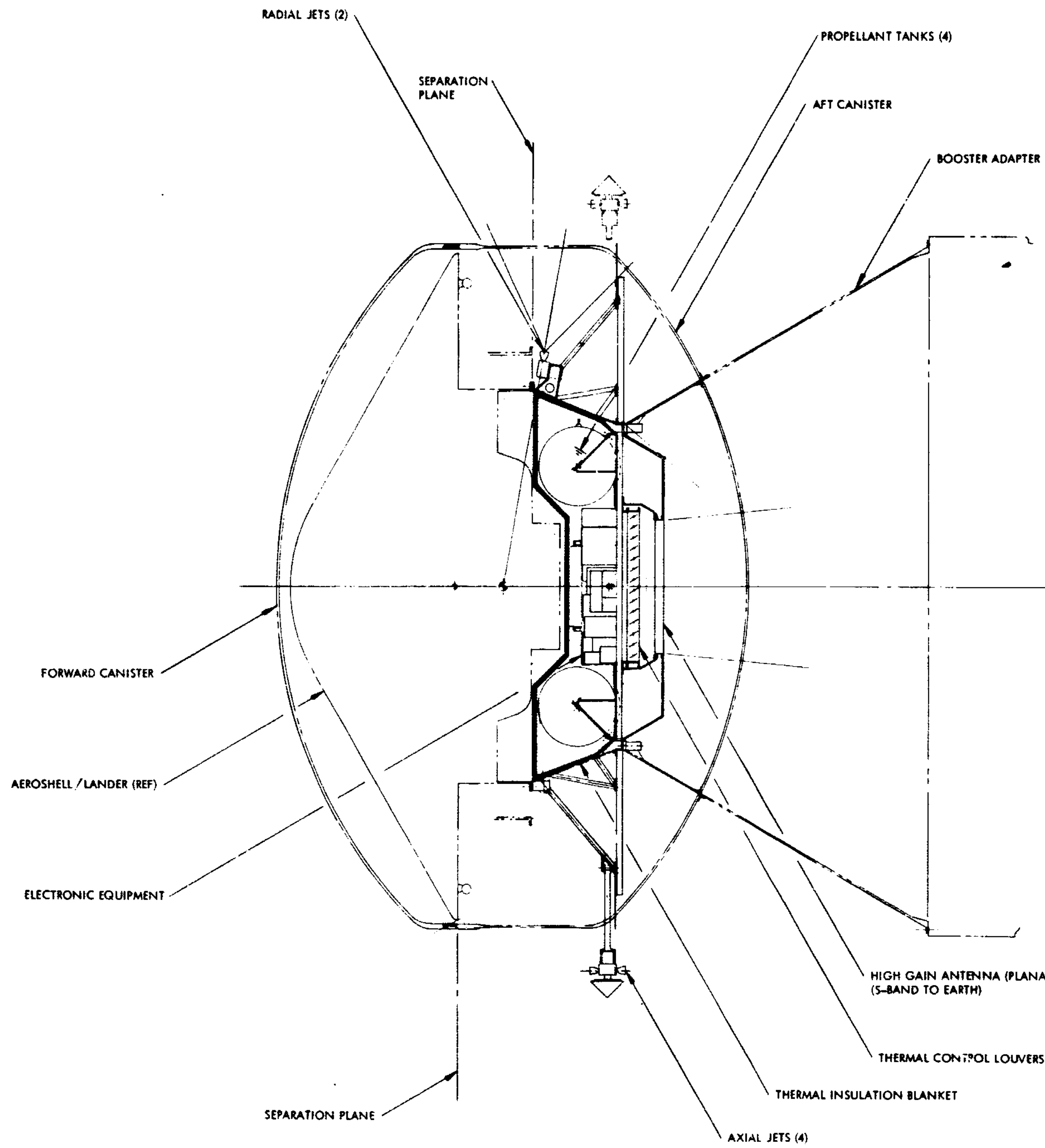
RADIAL JETS (2)
PROPELLANT TANKS (4)
SEPARATION PLANE
AFT CANISTER
BOOSTER ADAPTER
FORWARD CANISTER
AEROSHELL / LANDER (REF)
ELECTRONIC EQUIPMENT
HIGH GAIN ANTENNA (PLANA
(S-BAND TO EARTH)
THERMAL CONTROL LOUVERS
THERMAL INSULATION BLANKET
SEPARATION PLANE
AXIAL JETS (4)

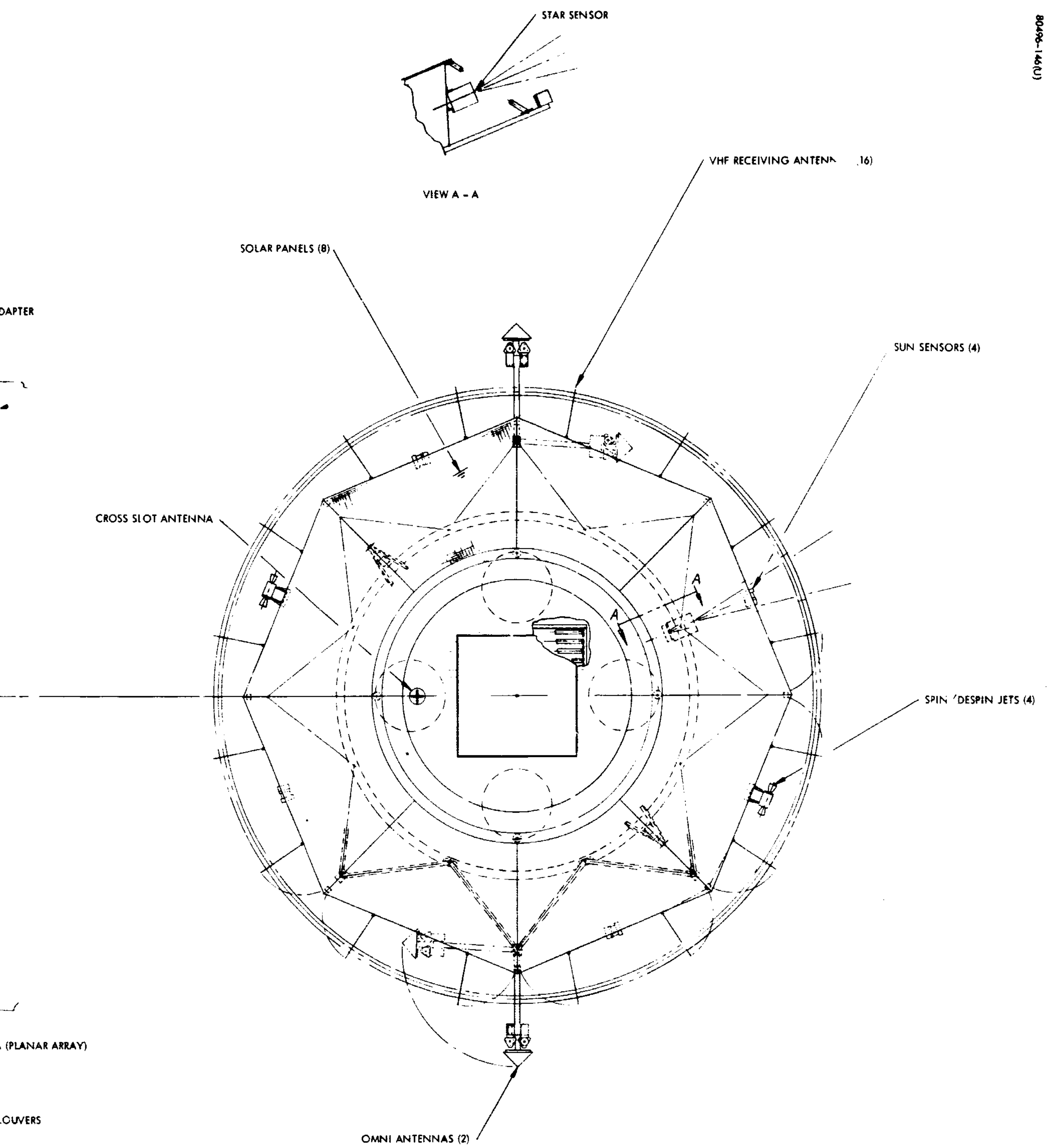

Figure 127. MSSM With Spin Axis in Plane of Ecliptic

PRECEDING PAGE BLANK NOT FILMED.

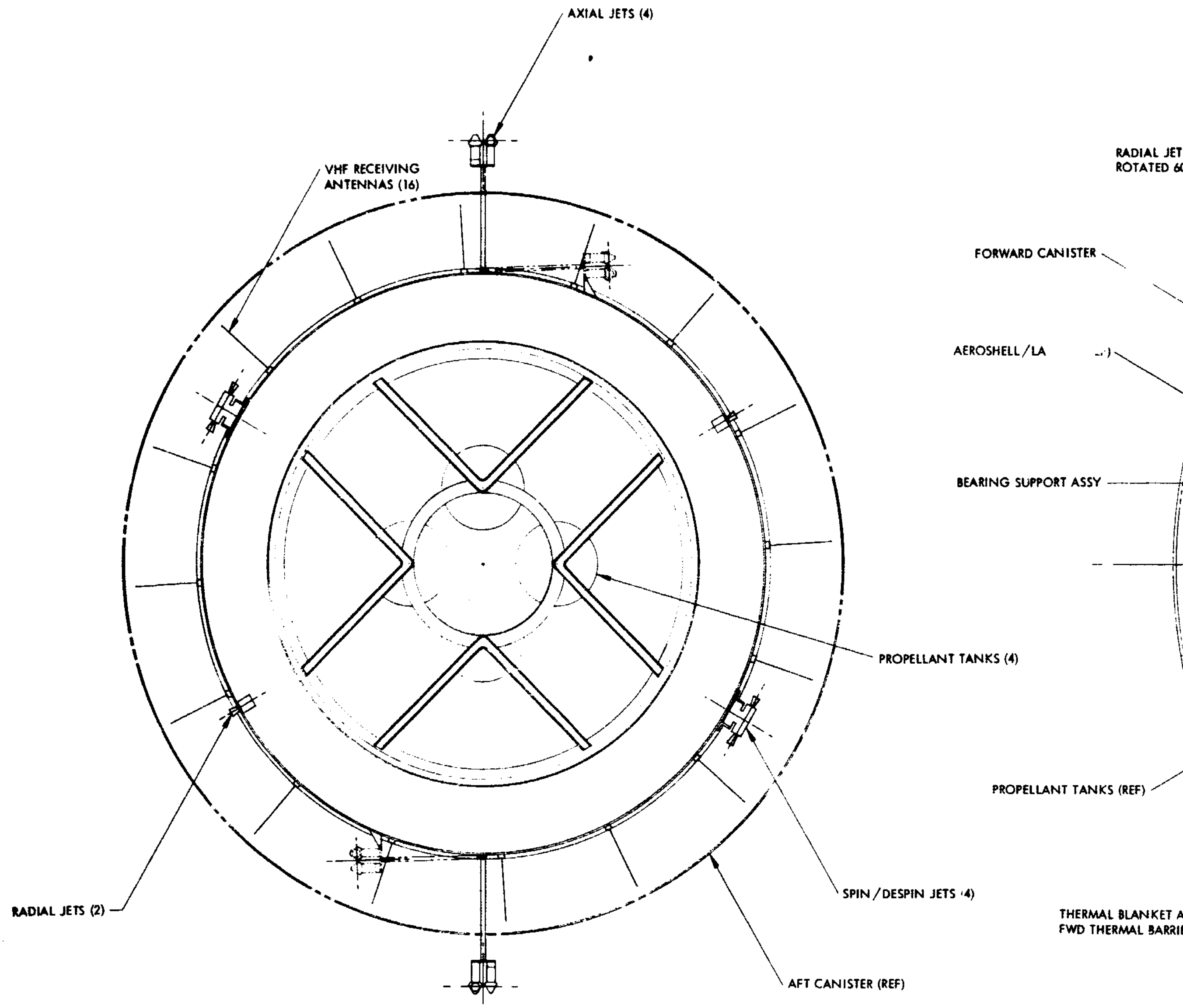

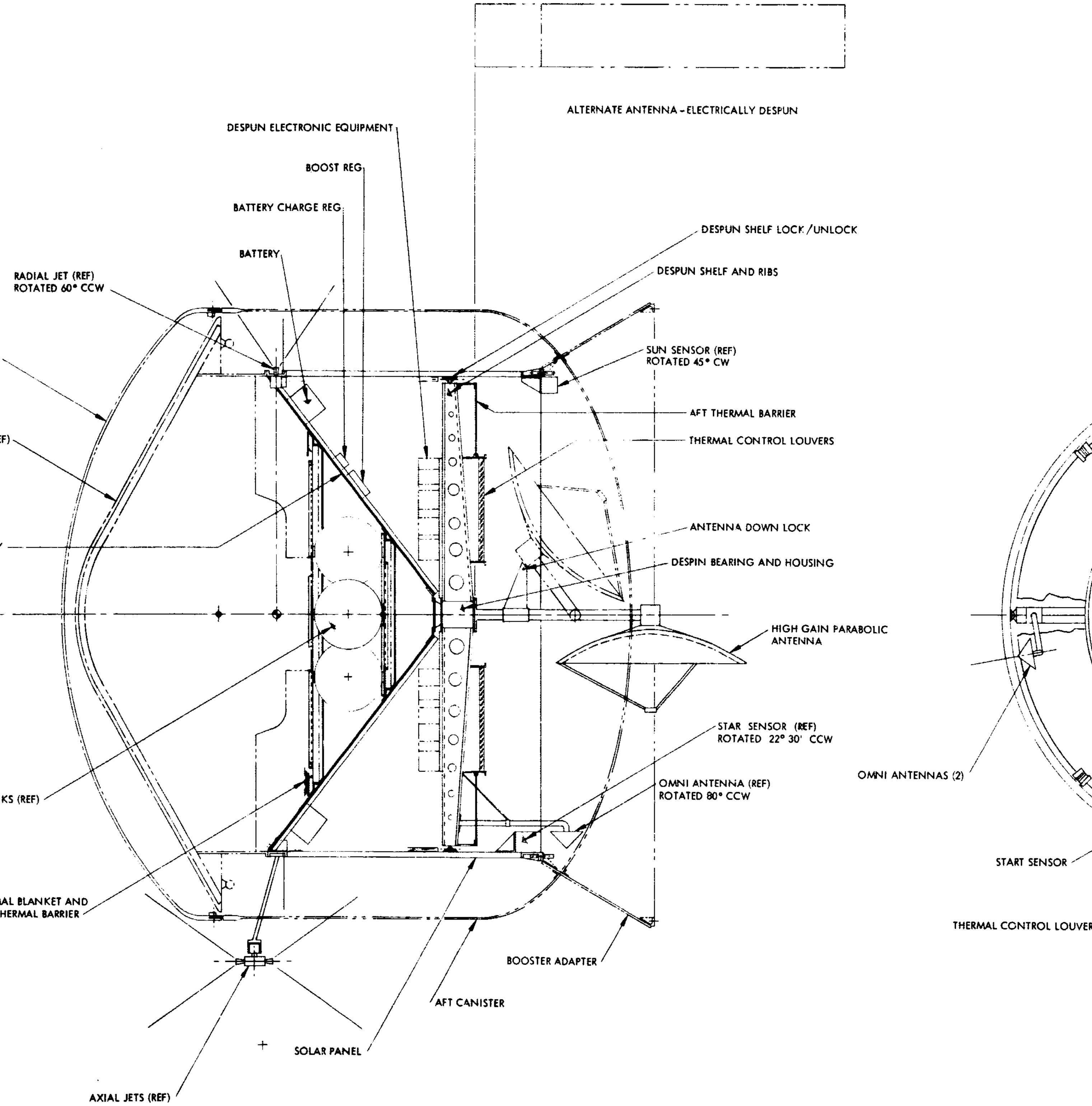

Figure 128. MSSM W

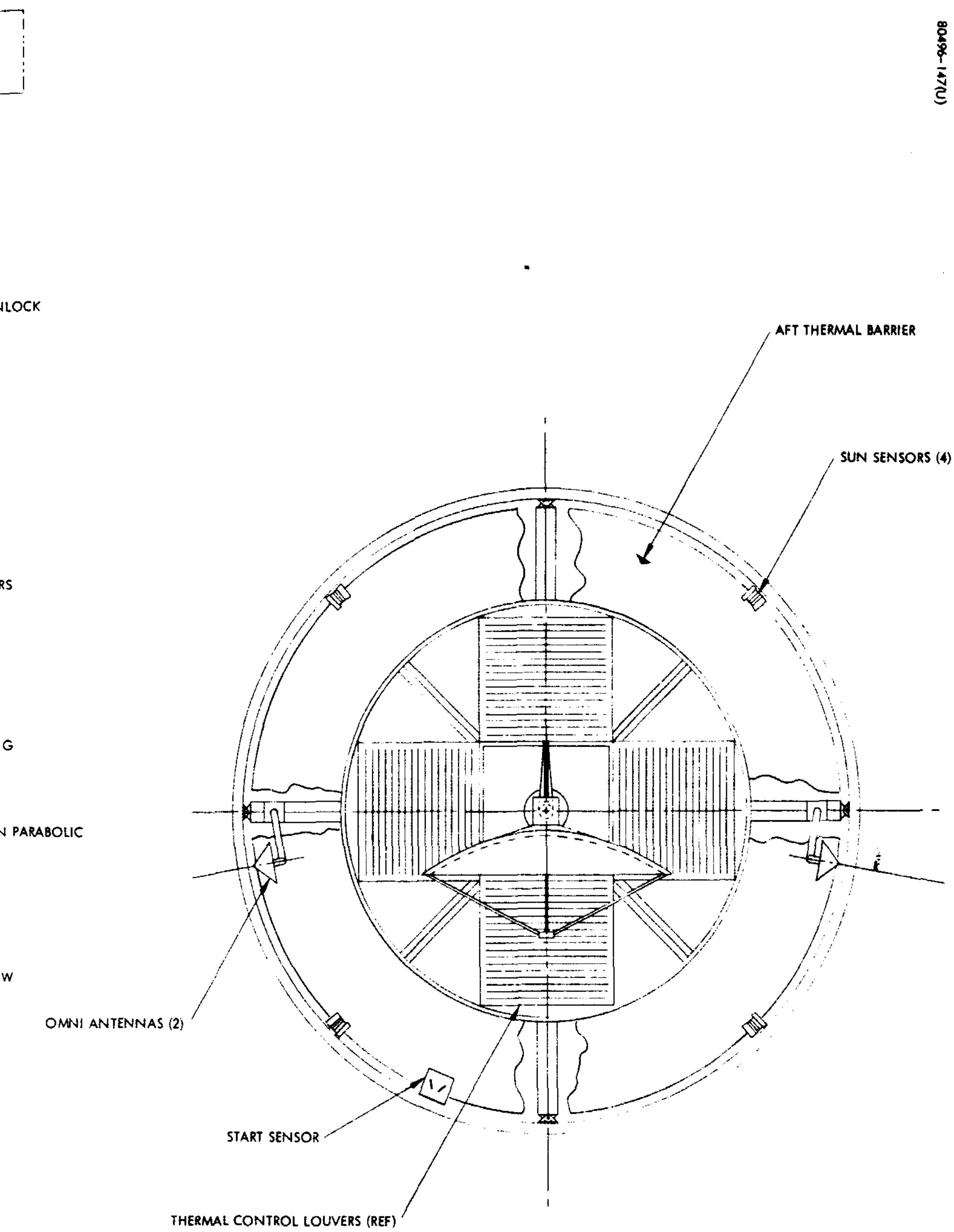

Figure 128. MSSM With Spin Axis Perpendicular to Ecliptic

PRECEDING PAGE BLANK NOT FILMED.

TABLE 45. MSSM WEIGHT ALLOTMENT

	In Ecliptic		Perpendicular to Ecliptic	
RF Subsystem				
3-watt transmitter (1)	22.0	50.5	22.0	48.5
20-watt transmitter (2)				
High-gain antenna (1)	4.0		2.5	
VHF antennas (16)	2.0		2.0	
Turnstile antenna and diplexer (2)	2.5		2.5	
S-band receiver (2)	8.0		8.0	
VHF receiver (2)	6.0		6.0	
RF switches (3)				
Cables	5.5		5.5	
Cross-slot omni antenna	0.5		—	
Signal Processing		20.0		29.5
Central command decoder	5.0		5.0	
Central signal processor	10.0		10.0	
Command storage and sequencer	5.0		5.0	
Despin electronics	—		9.5	
Propulsion		125.0		139.4
5-foot thrusters (10)	11.0		11.0	
13.4 inch diameter tanks (4)	16.0		18.4	
Valves, lines, filters and pressurant	8.0		8.0	
Propellant	90.0		102.0	
Flight Control		30.0		30.0
Flight control electronics	17.5		17.5	
Star sensors (1)	5.1		5.1	
Sun sensors (4)	1.0		1.0	
Cables and brackets	3.4		3.4	
Nutation damper	3.0		3.0	
Structure		89.5		165.1
Upper ring	10.4		16.0	
Upper frustum	18.5		—	
Central ring	8.5		—	
Lower frustum	4.2		—	
Spinning equipment shelf	14.0		4.0	
Thermal blankets	4.5		10.8	
Thermal barrier (lower)	5.0		5.0	
Harness and RF cable	10.0		13.0	
Solar panel support tubes	7.0		—	
Balance weights	4.0		4.0	
Thermal control louver	3.4		6.5	
Despin bearing and housing (BAPTA)	—		24.7	
Despun shelf and ribs	—		26.5	
Forward thermal barrier	—		2.0	
Bearing support assembly	—		32.5	
Aft ring	—		17.5	
Antenna mast	—		2.6	
Mechanisms		15.8		16.8
Separation mechanism	11.6		11.6	
SM/lander 4.8				
SM/adapter 6.8				
Axial jet deployment (2)	3.2		3.2	
Antenna deployment (8), (1)	1.0		1.0	
Despin system unlock (4)			1.0	
Electrical Power		79.8		123.8
Solar panel (substrate, cells, interconnections)	44.0		88.0	
Boost required	9.3		9.3	
Battery charge required	3.5		3.5	
Battery (50 percent discharge)	23.0		23.0	
SM total	410.6		553.1	
Contingency	39.4		54.9	
Total	450.0		608.0	

TABLE 46. MSSM - LAUNCH WEIGHT DISTRIBUTION

	In Ecliptic		Perpendicular to Ecliptic	
Aeroshell/Lander		972.0		972.0
SM weight		450.0		608.0
SM/booster adapter		118.5		92.0
Structure	83.5		57.0	
Umbilical	35.0		35.0	
Aft canister		161.8		236.3
Structure	111.8		176.3	
Pressure and vent.	50.0		60.0	
Forward canister		62.0		62.0
Launch weight		1764.3		1970.3

TABLE 47. SUMMARY

Criterion	Preferred	1. In Ecliptic	2. Perpendicular to Ecliptic
Simplicity	1	Pure spinner	• Despun section • Antenna mechanism
Sterilizability	1	Star sensor Battery	• Star sensor • Battery • Rotating joint
Relibility	1		• Rotating joint • Antenna mechanism • Joint interface
Weight Margin, 1250 maximum	1	519 pounds	314 pounds
Cost	1	Structure	• Rotating joint • Solar panels • Shroud
Flexibility	1		• Loss of high gain if antenna mechanism or joint fails

TABLE 48. MSSM ANTENNA SYSTEM TRADE STUDY

2 kb/sec 160 MKM 20 watts (43 dBm)	In-Ecliptic Earth Pointing Case			In-Ecliptic Sun-Pointing, or Out-of-Ecliptic Plane Case - Despin Technique				
	Planar Array			Electronic		Mechanical		
	Square	Circular	Parabolic	Phased Array	Phased Array	Square Planar	Parabola	ATS-C
				16 linear elements	Switched beam 16 elements			Parabolic cylinder
EIRP, dBw	65	65	65	65	65	65	65	
Gain, dB	22	22	22	22	22	22	22.	12.5
-3 dB Beamwidth, degrees	11.5	11.5	13	20 x 3.6	20 x 5.6	11.5 conical	13 conical	25 x 8.25
Weight, pounds	2	2.2	1.2	27	16	2.4	1.6	25
Required Prime Power, watts	NA	NA	NA	5	9	≈5	≈5	9.46
Dimension, inches	23 (side)	25 (diameter)	28 (diameter)	73 (length) 12 (diameter)	48 (length) 18 (diameter)	23 (side)	28 (diameter)	28 (length) 18 (diameter)